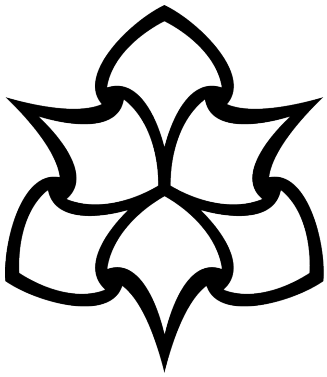

# Development of Signal Amplification By Reversible Exchange (SABRE) towards biological and forensic applications

T B R ROBERTSON

PhD 2019

# Development of Signal Amplification By Reversible Exchange (SABRE) towards biological and forensic applications

THOMAS BENJAMIN RUNNACLES ROBERTSON

A thesis submitted in partial fulfilment of the requirements of Manchester Metropolitan University for the Degree of Doctor of Philosophy

Department of Natural Sciences

Manchester Metropolitan University

2019

# Abstract

Work presented in this thesis focuses on the application of signal amplification by reversible exchange (SABRE) to the hyperpolarisation of small molecules. The aim of this work was to develop the technique towards future biologically relevant applications through resolution of barriers currently preventing clinical relevance. Furthermore, applications to forensics were also investigated.

SABRE currently almost exclusively utilises iridium-based catalysts, however, there are reports of the utilisation of cobalt and one mixed iridium/rhodium system. A range of rhodium based complexes, [Rh(IMes)(COD)Cl] (**6**), [Rh(Im*N*Pr$^{i}_{2}$)(COD)Cl] (**7**), [Rh(I$^{t}$Bu)(COD)Cl] (**8**) and [Rh(ICy)(COD)Cl] (**9**), were synthesised and evaluated for SABRE activity. Testing demonstrated that these species were unable to form stable dihydride species at room temperature and therefore the iridium complex [Ir(IMes)(COD)Cl] (**4**) was utilised for the remainder of the work.

$^{19}$F SABRE provides a versatile route for measurements *in vivo* due to the low background present within the body. This work assessed the hyperpolarisation of 2-, 3-, 4-, 3,5- and pentafluoropyridine (**L$_2$** – **L$_6$**), that have been interrogated by SABRE to establish a theoretical understanding of their efficacy with respect to polarisation transfer. However, hyperpolarisation of **L$_3$**, which yielded the highest enhancement, resulted in an antiphase signal which may lead to internal cancelation within a biological imaging context. Thus, Signal Amplification By Reversible Exchange in shield enables alignment transfer to heteronuclei (SABRE-SHEATH) was employed to generate an in-phase absorptive hyperpolarised signal.

Recent studies have demonstrated **4** is cytotoxic, therefore the mounting of the catalyst on silica or polymer derived supports was evaluated for the generation of a HET-SABRE catalyst and hyperpolarisation reported for a heterogeneous system. The solids proved effective at scavenging the metal from solution, therefore, an evaluation of their potential efficacy for production of a biocompatible bolus following homogenous SABRE is presented. 2-(2-pyridyl)ethyl - functionalised silica gel (**S$_5$**) is reported to be the most effective

metal scavenger utilised, with results suggesting ~1g of **$S_5$** is capable of reducing the iridium content of a bolus from ~1005ppm to below background levels within 2 minutes.

The hyperpolarisation of a range of fentanyl derivatives is **$F_1$-$F_5$**, including Mirfentanil (**$F_5$**), a derivative with known biological activity. Both **$F_2$** and **$F_5$** have been detected within an excess of heroin. **$F_5$** was detected at a concentration of 81 μM in ~5 seconds when ~145 mM of heroin was present. Further to this, the $^{19}F$ SABRE of a world health organisation essential medicine, voriconazole, is reported at a concentration ~4 times below current dosing guidelines.

# Abbreviations

| | |
|---|---|
| AAS | Atomic Absorption Spectroscopy |
| ALTADENA | Adiabatic Longitudinal Transport After Dissociation Engenders Net Alignment |
| API | Active Pharmaceutical Ingredient |
| BPS | Bathophenanthrolinedisulphonic acid disodium salt |
| CASH-SABRE | CAtalyst Separated Hyperpolarisation-Signal Amplification By Reversible Exchange |
| COD | 1,5-Cyclooctadiene |
| CODDA | 1,2-Dihydroxy-3,7-cyclooctadiene |
| COSY | COrrelated SpectroscopY |
| DLS | Dynamic Light Scattering |
| DNP | Dynamic Nuclear Polarisation |
| eNOS | endothelial Nitric Oxide Synthase |
| EPR | Electron Paramagnetic Resonance |
| EXSY | EXchange SpectroscopY |
| HET-SABRE | HETerogeneous Signal Amplification By Reversible Exchange |
| ICP | Inductively Coupled Plasma |
| IDEG | 1,3-bis(3,4,5-tris(diethyleneglycol) benzyl)imidazole-2-ylidene |
| IMes | 1,3-bis(2,4,6-trimethylphenyl)imidazole-2-ylidene |
| Itome | 1,3-bis(3,4,5-trimethoxybenzyl)imidazole-2-ylidene |

| | |
|---|---|
| IR | InfraRed spectroscopy |
| LAC | Level Anti-Crossing |
| LC | Liquid Chromatography |
| L-NOHA | $N^{\omega}$–hydroxy-L-arginine |
| MANDRAKE | MANchester DRug And Knowledge Exchange |
| MRI | Magnetic Resonance Imaging |
| MS | Mass Spectrometry |
| MTF | Magnetisation Transfer Field |
| NHC | *N*-Hetrocyclic Carbene |
| NK | Natural Killer cells |
| NMR | Nuclear Magnetic Resonance |
| NOESY | Nuclear Overhauser Effect SpectrometrY |
| NOS | Nitric Oxide Synthase |
| NPS | New Psychoactive Substance |
| o/n | Over Night |
| OTf | trifluoromethanesulfonate |
| PASADENA | *Para*hydrogen And Synthesis Allow Dramatically Enhanced Nuclear Alignment |
| PHIP | *Para*Hydrogen Induced Polarisation |
| PMAA | Poly(methacrylic acid) |
| PVP | Polyvinylpyridine |
| SABRE | Signal Amplification By Reversible Exchange |

| | |
|---|---|
| SABRE-RELAY | Relayed Signal Amplification By Reversible Exchange |
| SABRE-SHEATH | Signal Amplification By Reversible Exchange in SHield Enables Alignment Transfer to Heteronuclei |
| SQUID | Superconducting QUantum Interference Device |
| TLC | Thin Layer Chromatography |
| UV | UltraViolet spectroscopy |
| WHO | World Health Organisation |
| XPS | X-ray Photoelectron Spectroscopy |

# Contents

# Table of Figures

# Table of Tables

# Table of Equations

# Acknowledgements

I would like to thank my supervisory team for their help and support throughout my project. Firstly, my director of studies, Dr Ryan Mewis, who has constantly been on hand to offer help, encouragement and pragmatic advice both within an academic context and with other stepping stones along my research journey. I would particularly like to thank him for his help whilst writing up my thesis (including teaching me more word shortcuts than I knew existed) and his constant support for my future career aspirations. I would like to thank Dr Lindsey Munro for her support as my supervisor for the last 5 years. Finally, I would like to thank my advisor Dr Leon Clarke for his support, particularly for the utilisation of the ICP-OES and subsequent data interpretation.

I would like to thank all of the technical staff within the chemistry department for their help and assistance in obtaining analytical data. In particular I would like to thank David McKendry, Dr Hayley Andrews and Paul Warren for their support with ICP, SEM/EDX and NMR respectively.

My thanks also go to Dr Oliver Sutcliffe who has enabled my work to utilise new psychoactive substances and has been an invaluable mentor throughout my PhD. I would also like to express my thanks to the other MMU PhD's, in particular Lysbeth Antonides and Nicolas Gilbert of the Sutcliffe research group whom have synthesised fentanyl analogues utilised within this work. I would like to thank the MChems and Erasmus students for company in the lab. I would also like to thank Robert Martin for putting up with me in the office and with my constant request of 'can you just give this a read over please?'

I am very grateful to all those who have volunteered to read over elements of this thesis, in particular my parents whom have supported and encouraged me with patience, love and questions of 'is it almost done then?' throughout this journey and continue to support my future career aspirations. Finally, a big thank you is owed to Amy for her continued support, understanding and reassurance, going a long way to making the completion of this thesis possible.

For Vince and Grandma.

# 1. Introduction

## 1.1. NMR

A wide range of techniques are available in the field of sample analysis, however, while techniques such as infrared (IR) and ultraviolet (UV) spectrometry are useful for sample identification, these rely on a response factor. Therefore, the same concentration of two different samples may elicit different integrals. However, nuclear magnetic resonance (NMR), first reported in 1938 by Rabi *et al.*,[1] eliminates this response factor meaning NMR may be used as a qualitative technique. The first bulk NMR samples were run in 1946, followed by the publication of the first spectrum, shown in Figure 1, by Arnold *et al.* in 1951.[2, 3]

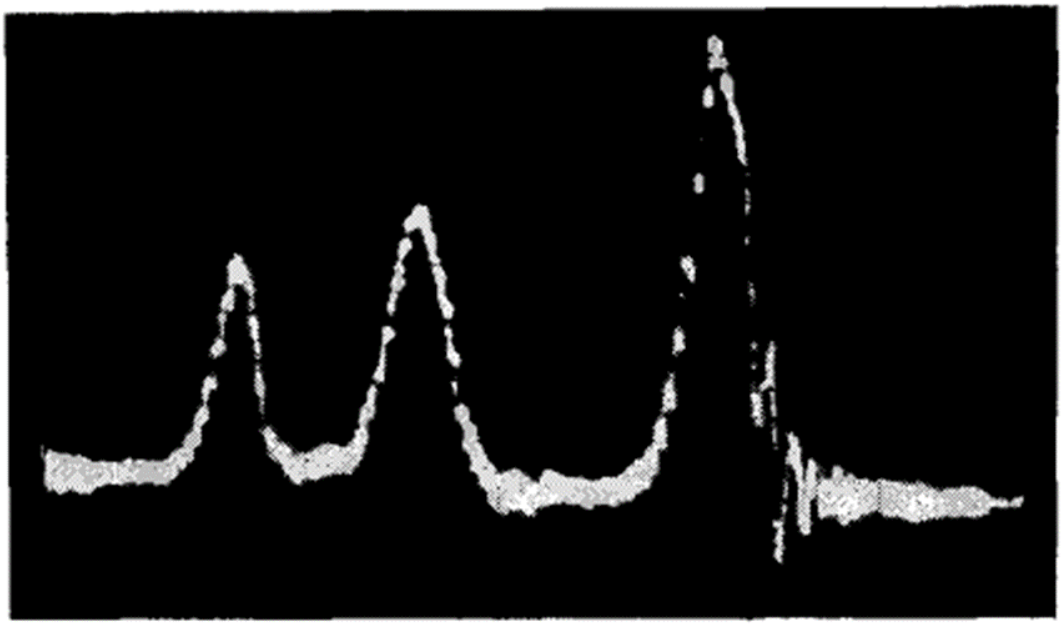

Figure 1. First published NMR spectrum by Arnold *et al.* showing the $^{1}H$ spectrum of ethanol.[2]

Development of NMR in the decades since has led to the discovery of chemical shift,[4] as well as the ability to interrogate a range of nuclei including $^{13}C$ and $^{19}F$. However, despite magnet and probe improvements, the main limitation of NMR remains the inherent insensitivity of the technique.

The primary nuclei examined in the course of this work ($^{1}$H, $^{13}$C and $^{19}$F) are all spin ½ nuclei meaning that, when placed within an external magnetic field, two discrete energy levels of +½ and -½ are generated. The population of each energy level is defined by the Boltzmann distribution. The number of nuclei populating each energy level is influenced by the strength of the external field, leading to an overall thermal polarisation level, which may be described utilising Equation 1.

$$P = \frac{\gamma h B_0}{2 k_B T}$$

Equation 1. Expression for calculating thermal polarisation. $\gamma$ is the gyromagnetic ratio, $h$ is Planck's constant, $B_0$ is the magnetic field to which nuclei are exposed to, $T$ is the temperature and $k_B$ is the Boltzmann constant.

In the course of an NMR experiment the populations of these energy levels oppose each other, meaning the signal observed is effectively based on the small excess in population of one of the energy states. This problem is exacerbated in nuclei such as $^{13}$C, which have a gyromagnetic ratio significantly smaller than that of $^{1}$H. Table 1 demonstrates the effect of field, gyromagnetic ratio and temperature on overall polarisation of a range of nuclei.

Table 1. Polarisation values for $^{1}$H, $^{13}$C, $^{15}$N and $^{19}$F nuclei at different magnetic fields and temperatures.[5]

| Nucleus | $B_0$ = 1.4 T, T = 273 K | $B_0$ = 1.4 T, T = 298 K | $B_0$ = 9.4 T, T = 273 K | $B_0$ = 9.4 T, T = 298 K |
|---|---|---|---|---|
| $^{1}$H | 5.24 x10$^{-6}$ | 4.80 x10$^{-6}$ | 3.52 x10$^{-5}$ | 3.22 x10$^{-5}$ |
| $^{13}$C | 1.32 x10$^{-6}$ | 1.21 x10$^{-6}$ | 8.85 x10$^{-6}$ | 8.10 x10$^{-6}$ |
| $^{19}$F | 4.93 x10$^{-6}$ | 4.51 x10$^{-6}$ | 3.31 x10$^{-5}$ | 3.03 x10$^{-5}$ |

## 1.2. Hyperpolarisation

Hyperpolarisation methods attempt to overcome the inherent low sensitivity of NMR through an increase in the population of one energy state relative to the other in order to obtain a greater observed signal. A range of techniques may achieve this, which are described herein.

### 1.2.1. Brute force

Brute force, first reported by Abragam *et al.* in 1958,[6] centres around manipulating the terms of Equation 1, rather than attempting to create a non-Boltzmann spin distribution. This technique maximises the Boltzmann distribution through low temperature and high field measurement. For example, for $^{1}H$ nuclei at 4 K and 9.4 T the polarisation is $2.4 \times 10^{-3}$, which is two orders of magnitude larger than at 298 K. Increasing the field strength to 20 T results in a ~50% increase in polarisation to $P = 5.11 \times 10^{-3}$.

Brute force polarisation also takes a long time for polarisation to develop as at low temperatures nuclear relaxation is significantly slowed due to the loss of molecular motion.[7] However, this limitation may be overcome by making use of low field thermal mixing in order to transfer polarisation from briskly relaxing nuclei such as $^{1}H$ to slower relaxing nuclei such as $^{13}C$. This obstacle may also be negated with the addition of relaxing agents into the sample. However, there are practical and cost limitations to the application of this technique. For example, superconducting magnets required to generate strong fields are expensive and low temperatures may not be applied to *in vivo* magnetic resonance imaging (MRI) measurements due to patient wellbeing. Resultantly, brute force techniques have largely been superseded by other hyperpolarisation techniques that show greater potential for biological measurement.

### 1.2.2. Dynamic Nuclear Polarisation

Dynamic Nuclear Polarisation (DNP) was first proposed by Overhauser in 1953.[8] This technique involves the transfer of polarisation from a radical species to the substrate of interest *via* microwave irradiation near the electron

paramagnetic resonance (EPR) transition.[9] This process takes place at a relatively low temperature, typically between 2 K and 100 K, with an efficiently vitrified sample ideal for polarisation transfer.[10] Following polarisation transfer, the sample is briskly thawed and transferred to a suitable measurement field where the hyperpolarised state may be interrogated. Care must be taken during the dissolution of the vitrified state that the process occurs faster than the nuclear relaxation process. Relaxation may be exacerbated by high levels of radicals present in the sample, meaning sample design is a trade-off between high polarisation levels and longevity of the hyperpolarised state. Polarisation transfer takes a significant length of time, traditionally taking hours, though recent work has demonstrated polarisation transfer times of under an hour.[11]

Although very high signal enhancements, in excess of 10,000 times, may be attained utilising DNP, the technique is very expensive as it requires specialised equipment and high cryogen usage while only allowing low sample throughput. In contrast, the more recently discovered *para*hydrogen techniques require less infrastructure and allow for faster sample preparation.

### 1.2.3. *Para*hydrogen techniques

*Para*hydrogen techniques are used to create a non-Boltzmann distribution of spins in the sample. The two main techniques are *para*hydrogen induced polarisation (PHIP) and the focus of this work, signal amplification by reversible exchange (SABRE). Both of these techniques make use of polarisation derived from one of the spin isomers of hydrogen, *para*hydrogen.[10]

$^1$H is a spin-½ nucleus and has two spin-states, +½ or −½, written as α or β respectively. As hydrogen is found as dihydrogen ($H_2$), these states may combine in four possible combinations as αα, (αβ - βα), (αβ + βα) and ββ; of these states three do not represent a change in the sign of the overall wavefunction and can be considered symmetric: these are αα, (αβ + βα) and ββ. These symmetric forms of $H_2$ are referred to as *ortho*hydrogen and hence this is the triplet spin isomer. This spin isomer can be observed in the NMR

experiment. The remaining state, (αβ - βα), is antisymmetric with respect to sign change and may be referred to as *para*hydrogen. *Para*hydrogen is not observable in the NMR experiment. At room temperature roughly 75% of $H_2$ is found as *ortho*hydrogen with the remaining 25% being *para*hydrogen.

*Para*hydrogen is the more stable of the spin isomers due to Pauli's exclusion principle stating that the overall wavefunction (Ψ) of $H_2$ must be antisymmetric. This wavefunction is a combination of translational, electronic, vibrational, rotational and nuclear contributions:

$$\Psi = \psi(\text{translational})\psi(\text{electron})\psi(\text{nuclear})\psi(\text{rotational})\psi(\text{vibration})$$

Equation 2. Expression of the wave function of $H_2$.

The translational, electronic and vibrational elements of this wavefunction are always symmetric, therefore, for the overall expression to be antisymmetric the nuclear and rotational functions must have different symmetry. Due to its symmetrical rotational states *ortho*hydrogen must have an antisymmetric nuclear state, J = 1, 3, 5… conversely *para*hydrogen with its antisymmetric rotational function must be found in a symmetrical nuclear state represented by J = 0, 2, 4… As *para*hydrogen may access the more stable J = 0 nuclear state, this is demonstrated in Figure 2.

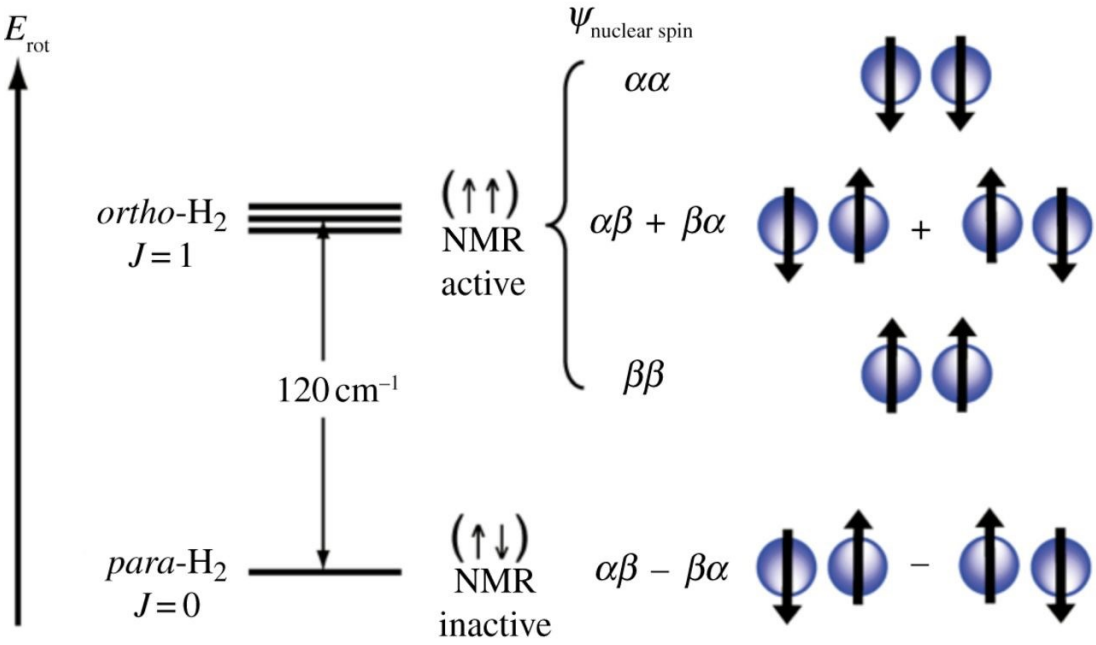


Figure 2. The spin combinations of *ortho* and *para* hydrogen demonstrating that *para*hydrogen occupies a lower energy.[12]

As *para*hydrogen is more stable it is, therefore, found in a higher proportion at lower temperatures, this trend has been evaluated experimentally by Duckett *et al.* and is demonstrated in Figure 3.

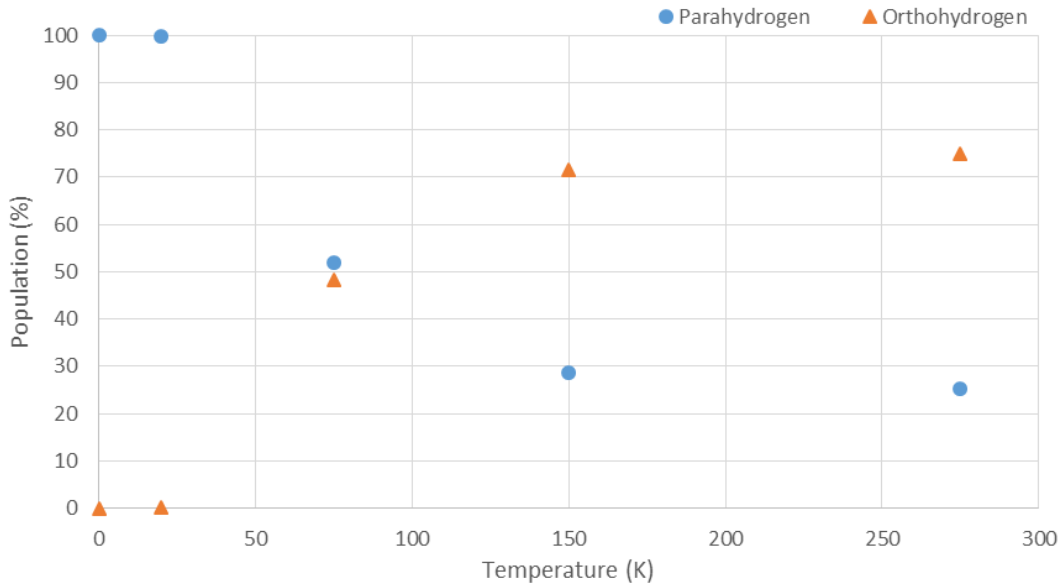


Figure 3. The proportion of *para*hydrogen and *ortho*hydrogen over a range of temperatures based on data collected by Duckett *et al.*[13]

Unfortunately changing two states within the wavefunction is spin forbidden, meaning that an interconversion catalyst such as $Fe_2O_3$,[14] charcoal,[15] or silica/$FeCl_3$,[16] is required in order to generate *para*hydrogen at low temperatures.[17] However, this transition being forbidden means once *para*hydrogen is generated it may be stored at room temperature, provided it is isolated from any suitable interconversion catalyst.[18]

### 1.2.4. *Para*hydrogen induced polarisation (PHIP)

Proposed in 1986 by Bowers *et al.*, PHIP makes use of *para*hydrogen in a hydrogenation reaction targeting an olefin containing substrate to achieve a non-Boltzmann hyperpolarised state.[19] The same group demonstrated this effect the following year making use of Wilkinson's catalyst ([$RhCl(Ph_3)_3$]) with *para*hydrogen added to the sample within the magnetic field used for measurement. This approach to PHIP became known as PASADENA (*Para*hydrogen And Synthesis Allow Dramatically Enhanced Nuclear Alignment) and generated a mixture of in and out of phase signals in the acquired spectra.[20] In the same year another report conducted *para*hydrogenation at low field before rapid transport to a higher field for measurement; this process resulted in in-phase signals and was therefore differentiated from PASADENA and instead termed ALTADENA (Adiabatic Longitudinal Transport After Dissociation Engenders Nuclear Alignment). PHIP is used as a general term to describe both approaches.

Despite enhancement levels of several hundred times being demonstrated,[21] the requirement for a suitable hydrogen acceptor presents an important limitation of PHIP. This limitation has led to the need to develop a *para*hydrogen technique which could allow substrate polarisation without hydrogenation.

### 1.2.5. Signal amplification by reversible exchange (SABRE)

First reported by Adams *et al.* in 2009, SABRE demonstrated that the simultaneous reversible binding of *para*hydrogen and the substrate of interest to a metal could facilitate polarisation transfer onto the substrate.[22] This

hyperpolarisation method means there was no chemical modification of the substrate as polarisation is transferred from *para*hydrogen derived hydrides to the analyte *via* a *J*-coupling network at low magnetic fields. This effect was first demonstrated making use of $[Ir(H)_2(PCy_3)(substrate)_3]$ which is formed following the reaction of the pre-catalyst, $[Ir(COD)(PCy_3)(MeCN)][BF_4]$, where COD is 1,5-cyclooctadiene, with *para*hydrogen in the presence of a suitable substrate. As the binding of both hydrides and substrate is reversible, this allows a build-up of polarised substrate molecules free in solution as shown in Figure 4; this means that for maximum polarisation build-up a commensurate hydride/substrate exchange rate with the SABRE active catalyst is ideal.

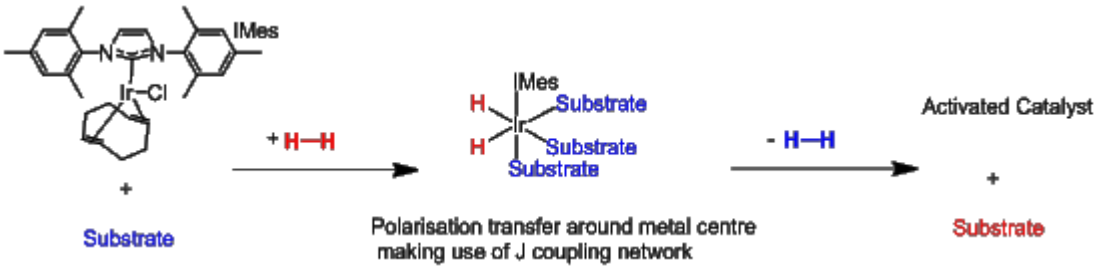


Figure 4. Mechanism of polarisation transfer from *para*hydrogen to a metal bound substrate molecule when [Ir(IMes)(COD)Cl] is utilised as the pre-catalyst. Hyperpolarised species are shown in red.

However, overly fast exchange rates may decrease the observed substrate polarisation due to insufficient time for polarisation transfer to occur before the substrate dissociates from the active species. SABRE experiments are practically undertaken by the bubbling of *para*hydrogen through the sample or the shaking of a Young's capped NMR tube with an atmosphere of *para*hydrogen. Since this first report, SABRE has been demonstrated on a wide range of molecules; a near exhaustive list is provided by Barskiy *et al.*[23]

## 1.3. SABRE catalyst optimisation

After the initial report of SABRE, the first generation of pre-catalysts continued to make use of iridium phosphine complexes, of these it was discovered that the most sterically hindering and electron donating ligand provided the best polarisation transfer to pyridine. These pre-catalysts do not themselves facilitate polarisation transfer, however, in the presence of a suitable substrate

and $H_2$, an active species is formed. For instance [Ir($PCy_3$)(COD)Cl] forms the active species [Ir($PCy_3$)(substrate)$_3$($H_2$)]. Having established that sterically demanding and electron donating phosphines optimised polarisation transfer, the development of catalysts was expanded to examine *N*-heterocyclic carbenes (NHCs) to establish if further polarisation enhancement could be gained.

An NHC containing catalyst, [Ir(IMes)(COD)Cl] (IMes=1,3-*bis*(2,4,6-trimethylphenyl) imidazole-2-ylidene) was synthesised.[24] The exchange rates of both pyridine and hydrides were measured for both the SABRE active catalysts [Ir(IMes)(py)$_3$($H_2$)]$^+$ and [Ir($PCy_3$)(py)$_3$($H_2$)][$BF_4$] making use of exchange spectroscopy (EXSY). These exchange rates may be experimentally investigated making use of a modified nuclear Overhauser effect spectrometry (NOESY) pulse sequence known as exchange spectroscopy or EXSY.[25] This sequence selectively pulses a spin transfer catalyst-bound peak, of either the hydride or ligand, then allows magnetisation transfer over a range of mixing times into the free species. Modelling the relative integrals of the free and bound peaks over a range of known mixing times allows the calculation of the rate of exchange for either the substrate or hydride (depending on which species was irradiated) for a given temperature. Conducting this experiment at a range of temperatures allows the construction of an Eyring-Polanyi plot.[26, 27]

The use of an Eyring-Polanyi plot allows determination of ΔH, ΔS and ΔG values for a given exchange, enabling multiple ligand systems to be directly compared in energetic terms, as well as through inspection of the exchange rates.

The exchange rate of pyridine with [Ir(IMes)(py)$_3$($H_2$)]$^+$ at 300 K was shown to be 11.7 $s^{-1}$ and 9 $s^{-1}$ for pyridine and hydride ligands respectively.[24] This may be compared with an analogous pyridine exchange rate making use of $PCy_3$ as the electron donating ligand of 1.9 $s^{-1}$.[28] An increase in observed polarisation, when [Ir(IMes)(COD)Cl] was used as the pre-catalyst, was attributed to this faster, yet more commensurate, ligand and hydride exchange. This investigation also demonstrated that an increase in pyridine concentration

leads to a decrease in hydride exchange, supporting the mechanism of hydride loss following pyridine dissociation, as shown in Figure 7.

In order to further optimise polarisation, a series of pre-catalysts with the general formula [Ir(NHC)(COD)Cl] were synthesised making use of the range of NHC's shown in Figure 5.[29]

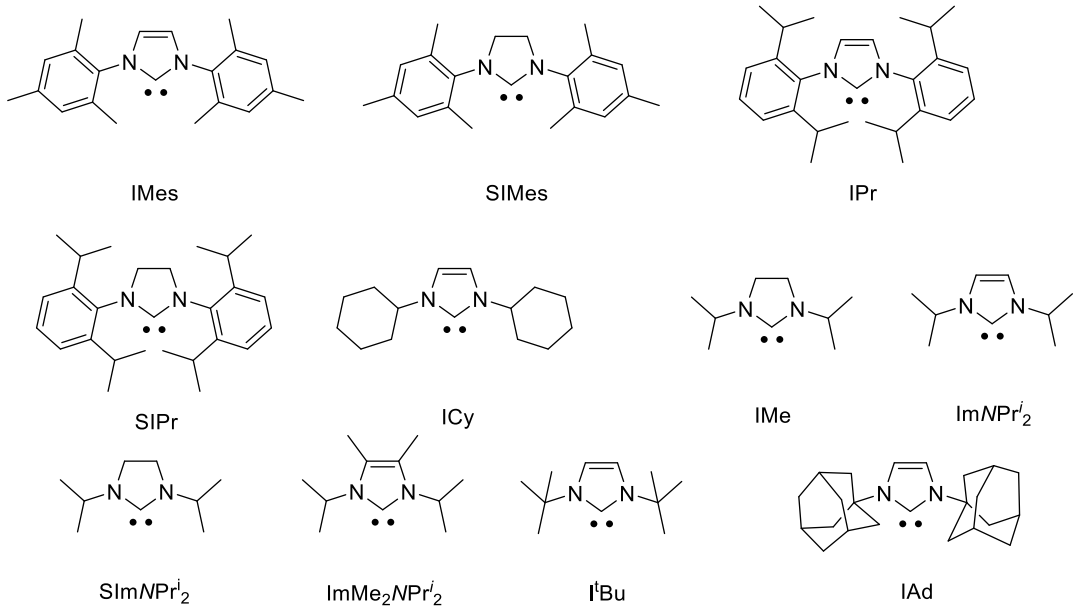


Figure 5. Carbenes evaluated as potential SABRE pre-catalyst ligands.[29]

It was noted that the exchange rates of both pyridine and hydrides increase with steric bulk of the NHC due to weaker binding to iridium. In both cases, IMes was near the middle of the range of NHCs in terms of exchange rate but led to the largest overall signal enhancement for pyridine. This suggests that an optimal exchange rate exists. This has led to [Ir(IMes)(COD)Cl] being used in the majority of reports since this study.[27, 30-32] Additional studies into the modification of structures similar to IMes have further examined complexes with modification of substituent groups in the *ortho*, *meta* and *para* positions of the phenyl rings of the imidazole backbone as shown in Figure 6.[33] Asymmetric carbenes have additionally been examined and demonstrate potential for the polarisation of more sterically encumbered substrates.[34, 35]

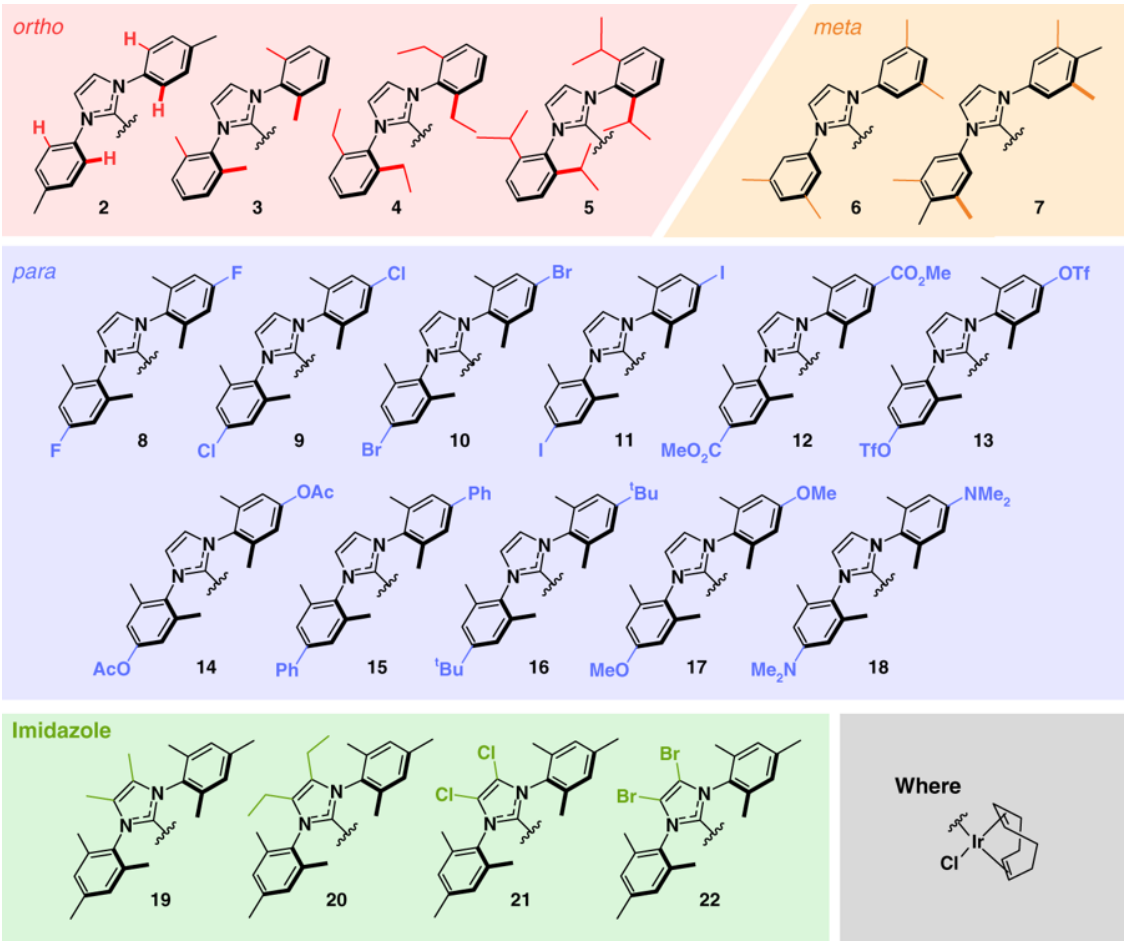


Figure 6. NHC structures initially evaluated by Rayner *et al.*[33]

Of the structures examined by Rayner *et al.* in Figure 6, IMes was shown to yield the highest polarisation levels when the [Ir(NHC)(COD)Cl] was exposed to 4,6-$d_2$-nicotinate as the substrate and 3 bar of *para*hydrogen. Though Rayner *et al.* went on to demonstrate higher polarisation levels could be attained by the deuteration of IMes, this is due to a reduction in 'dilution' of polarisation with no protons present to potentially be polarised within the carbene.

In general [Ir(IMes)(COD)Cl] is utilised within this work in order to allow comparison with the bulk of existing literature. This does, however, mean that polarisation levels reported here may be further optimised through the utilisation of a deuterated NHC.

### 1.3.1. Exchange Rates

The mechanism of polarisation transfer to a reversibly bound ligand, typically an *N*-heterocycle such as pyridine, is shown in Figure 7.[23] The rate at which the *para*hydrogen derived hydrides and the analyte exchange with the spin transfer catalyst have a major impact on polarisation transfer efficiency. Ideally these exchange rates would be commensurate, in order to enable the formation of a scalar coupling network between each pair of *para*hydrogen derived hydrides and each ligand pair, before dissociation and turnover to facilitate efficient build-up of a hyperpolarised bolus in solution.

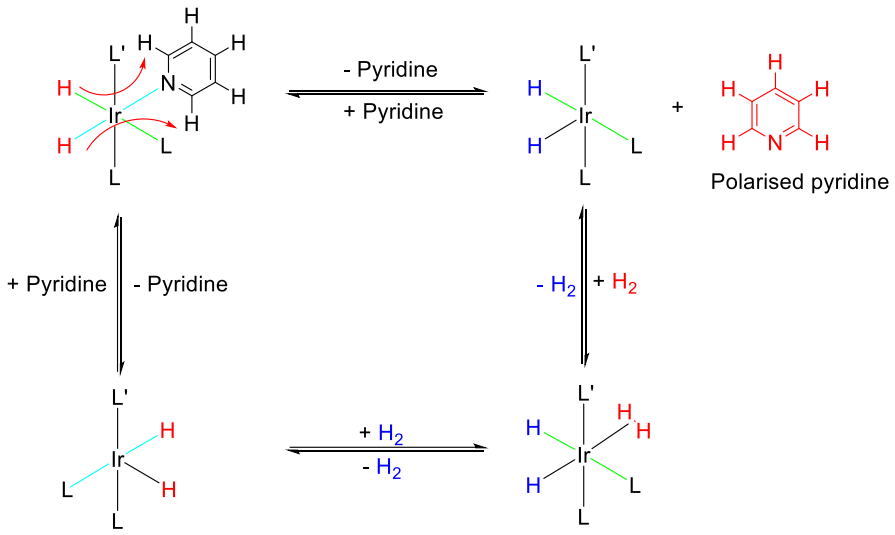


Figure 7. SABRE mechanism of polarisation exchange to a reversibly bound ligand (in this case pyridine (L)). L' is a carbene, typically IMes. Hyperpolarised species are shown in red. Ligands *trans* to hydrides are shown with cyan and/or green bond pairs.

The ligand *trans* to the NHC has been reported not to exchange which means the ligands *trans* to *para*hydrogen derived hydrides are the primary contributors to polarisation build-up.[36, 37] This is fortunate as polarisation transfer is preferential to the ligands *trans* to a hydride (shown by cyan/green bond pairs in Figure 7) due to the scalar couplings present in this case (*cis* couplings are ~0 Hz).[38]

Catalyst design may play a major role in the speed of these exchanges – in particular the identity of substituent L', typically an NHC, from Figure 7 has an

impact on the speed of exchanges as a L' with a significant buried volume increases steric encumberment, resulting in faster exchange.

## 1.4. Metals utilised for the formation of SABRE-based catalysts

As discussed in 1.3 the majority of recent SABRE reports make use of the iridium complex [Ir(IMes)(COD)Cl], however, other metals have been used to facilitate the SABRE process.

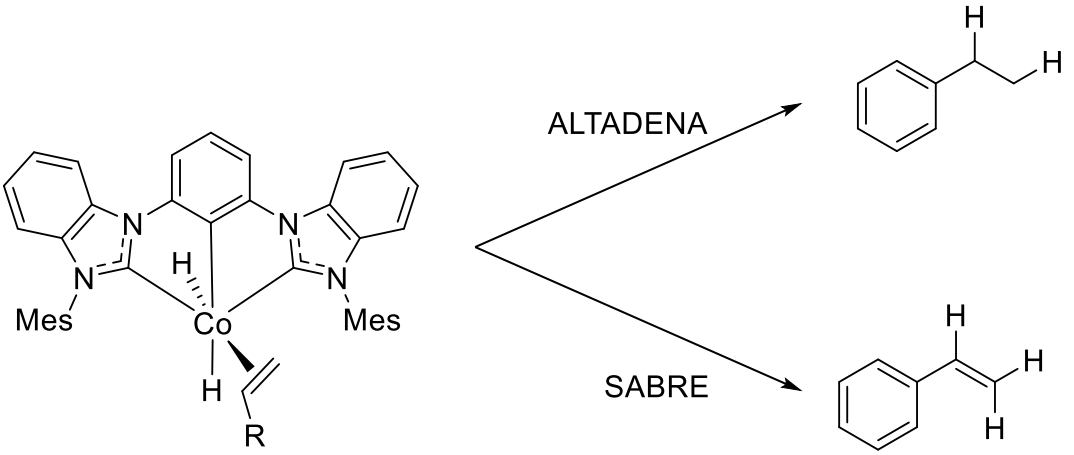


Figure 8. Styrene products identified when the indicated cobalt catalyst, in conjunction with parahydrogen, was utilised. R = Ph and Mes = 1,3,6-trimethylphenyl.

Cobalt has been used to facilitate simultaneous SABRE and ALTADENA polarisation using a [($Mes^{CCC}$)Co($N_2$)($PPh_3$)] ($Mes^{CCC}$ = (*bis*(mesityl-benzimidazol-2-ylidene)phenyl)) pre-catalyst, as shown in Figure 8.[39, 40] The bulky strongly electron donating tridentate ligand means the SABRE active form of this species has been proposed as [($Mes^{CCC}$)Co($H_2$)(substrate)]. Therefore, polarisation transfer may occur *via* a different mechanism when compared to the iridium-based complexes.

Despite its common use in PHIP, there is only a single literature source for the use of rhodium in SABRE. This comes from a mixed [Rh(DPPB)(COD)]$BF_4$ (DPPB = 1,4-*bis*(diphenylphosphino)butane) and [Ir($PCy_3$)(COD)(Py)]$PF_6$ pre-catalyst system used to achieve $^{31}P$ polarisation.[41] However, the authors note

that, due to a complex equilibrium of multiple species within the sample, they were unable to assign polarisation transfer to a particular species.

## 1.5. Nuclei used in SABRE

SABRE has been applied successfully to a range of spin ½ nuclei utilising a range of substrates. Each NMR active nucleus SABRE has currently been applied to are discussed within this section.

### 1.5.1. Proton

A focus of extant literature has been the application of SABRE to acquire $^{1}H$ NMR data. One of the key steps for $^{1}H$ SABRE was the optimisation of the polarisation transfer field; for pyridine optimisation, an automated reaction setup was used which would conduct a SABRE experiment inside a variable field coil.[27] This demonstrated optimal polarisation transfer in a field of 65-70 G as shown in Figure 9.

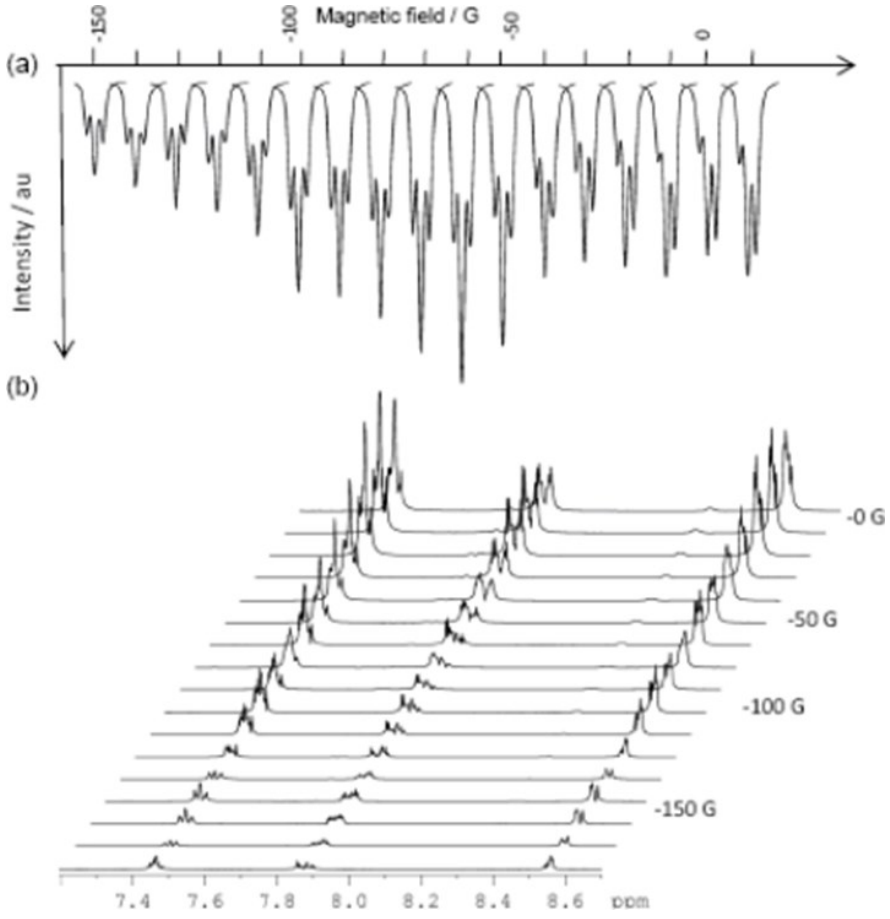


Figure 9. Field dependency of polarisation transfer to pyridine.[27]

Additional investigation made use of the same experimental setup but instead focused on the biologically relevant substrates isoniazid and pyrazinamide. Again a 65 G field was found to be optimal for the SABRE process. This study also demonstrated that polarisation is temperature and solvent dependent.

$^{1}$H polarisation has been successfully applied to a range of applications including detection and quantification of analytes at nanomolar concentrations.[42] This high sensitivity means that SABRE is still highly effective at low detection fields (*circa* 1.4 T) such as those found in benchtop NMR instruments. This has been exemplified for $^{1}$H NMR reaction monitoring and in the acquisition of natural abundance $^{13}$C NMR spectra in a single scan.[43-45]

Recently hyperpolarised signals equating to an overall polarisation of 50% in an optimised system have been demonstrated by Rayner *et al.*[46] In order to achieve high polarisation levels Rayner *et al.* have deuterated all sites on IMes except the imidazole ring, partially deuterated the substrate (4,6-$d_2$-nicotinate) to reduce polarisation acceptors and utilised 5.5 bar of *para*hydrogen which was enriched at 30 K for a very high *para*hydrogen content. This signal could be detected for ~2 mins demonstrating significant steps towards *in vivo* application.

Work towards the application of SABRE *in vivo* has explored polarisation of amino acids as well as two small peptides.[47] This work demonstrated it is possible to hyperpolarise all proteinogenic amino acids, in addition to two small peptides tested, though the authors note that water soluble catalysts would be ideal to undertake studies of amino acid and peptide analytes as they have poor solubility in organic solvents such as $d_4$-methanol. This work was expanded upon by Ratajczyk *et al.*[48] who have successfully demonstrated the hyperpolarisation of a range of SABRE labelled (using nicotinamide or isonicotinamide) peptides shown in Figure 10, though hyperpolarised signals were only observed for the label rather than the peptide chain.

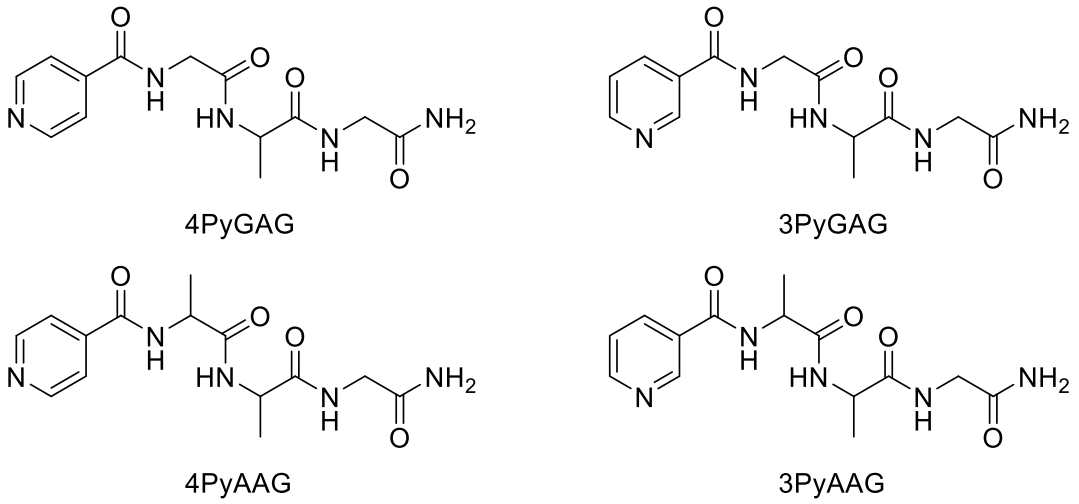


Figure 10. Labelled peptides hyperpolarised by Ratajczyk *et al.*[48]

A small number of low molecular weight drugs have also been polarised, such as pyrazinamide and isoniazid.[49] Optimisation of the polarisation conditions for both drugs supported $^{1}H$ polarisation being most efficient in a 65 G field with the largest enhancements being observed in $d_4$-methanol as opposed to methanol, ethanol and DMSO (polarisation was observed to be inversely proportional to solvent viscosity). The polarisation was further optimised at greater than room temperature, with a temperature of 46.1°C showing optimal transfer for both drugs in all solvents tested except pyrazinamide when ethanol was used as a solvent which was optimised at 37.5°C. The polarisation optimisation at high temperature for these drug molecules, shown in Figure 11, demonstrates a faster exchange rate is desirable in these systems to achieve the build-up of hyperpolarised free substrate in solution.

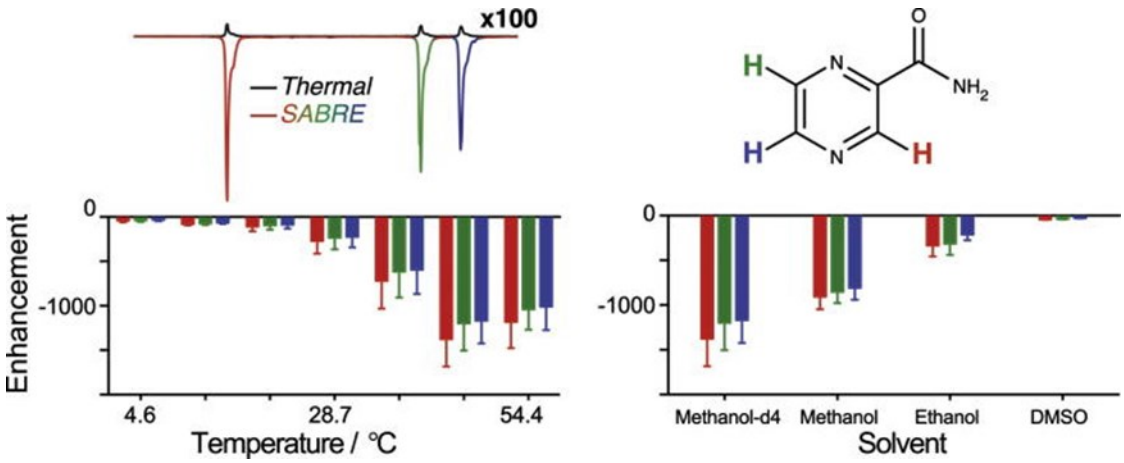


Figure 11. Effects of temperature and solvent on the hyperpolarisation of isoniazid.[49]

### 1.5.2. Nitrogen

$^{15}$N labelled substrates have been successfully polarised, primarily making use of SABRE-SHEATH (SABRE in shield enables alignment transfer to heteronuclei). SABRE-SHEATH utilises a μ-magnetic shield to conduct SABRE experiments within a microtesla magnetic field.[50] This technique created ~24% polarisation in metronidazole, an antibiotic.[30] Combined with the relatively long relaxation times of $^{15}$N, this is an attractive approach for biological imaging with hyperpolarised signals detectable for over an hour in some applications.[51] A theoretical basis for the effectiveness of SABRE-SHEATH has been presented to support the increased $^{15}$N polarisation generated when SABRE is conducted within a magnetic shield.[52]

The application of SABRE-SHEATH has been shown to increase enhancements measured for $^{15}$N,[53-55] though studies have shown that short $T_1$ values in this field regime may limit the efficiency of polarisation build up when traditional iridium-based SABRE pre-catalysts are utilised.[56] Despite this, SABRE-SHEATH has been shown to provide an efficient mechanism for the polarisation of long lived singlet states ($^{13}C_2$) due to the relative size of $J_{CC}$ compared to the hydride $J_{HH}$ in a micro-tesla field.[57] Therefore, with rational substrate design, it seems likely that short relaxation times could be overcome. A selection of substrates that SABRE-SHEATH has been reported for is demonstrated within Figure 12.

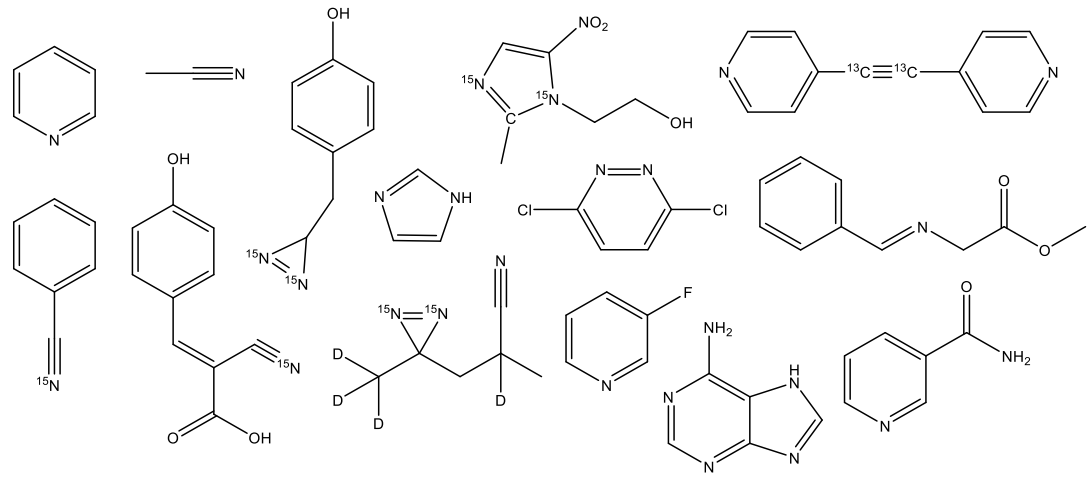

Figure 12. Range of molecules hyperpolarised by SABRE-SHEATH.[52-54, 57-59]

### 1.5.3. Carbon

$^{13}$C SABRE was included within the first report of SABRE by Duckett *et al.* in 2009.[22] Though enhancements reported have been lower than those reported for heteronuclei such as $^{15}$N, with polarisation levels of ~4.4% being reported,[60] $^{13}$C has still been shown to be an effective tool for the detection of all carbon environments within a substrate such as nicotinamide within a single scan.[61] The effectiveness of $^{13}$C SABRE for the rapid acquisition of carbon NMR data has recently been exemplified for 4-methylpyridine with carbon present at natural abundance within a detection field of 1 T as shown in Figure 13.[44]

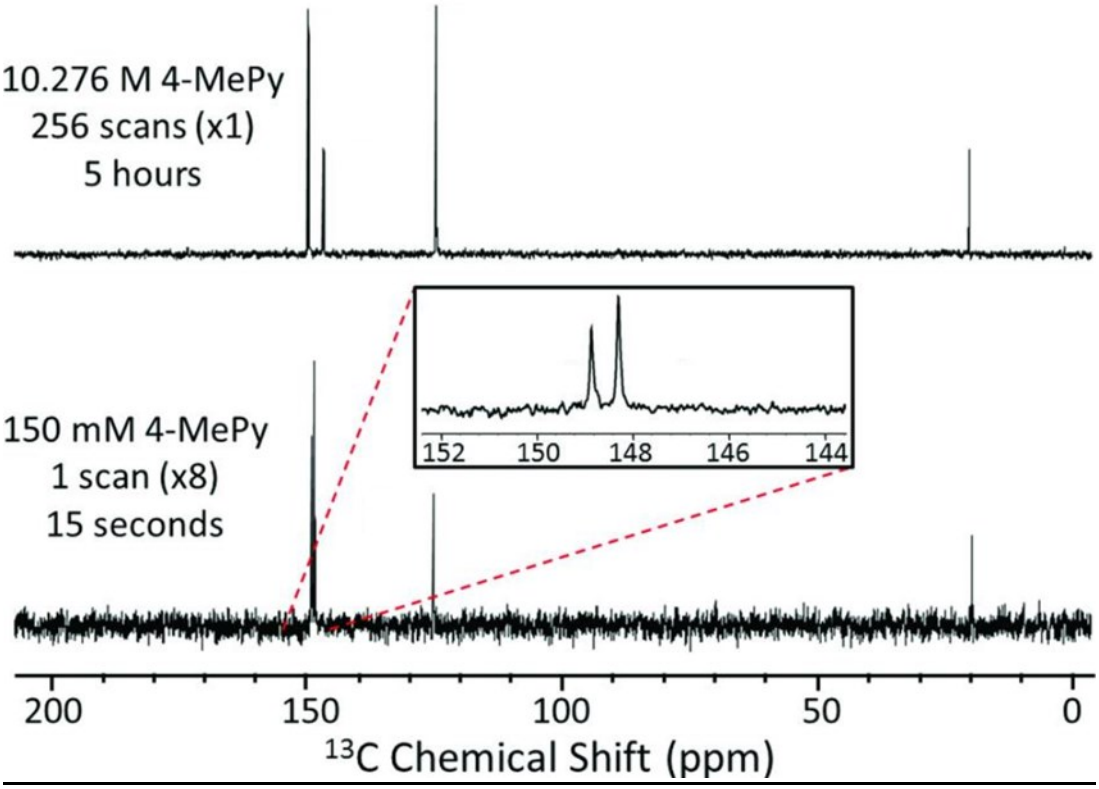


Figure 13. Spectra of 4-methylpyidine after 256 scans under thermal conditions (top) and after a single scan under SABRE conditions (bottom, scaled by x8). The SABRE sample is ~70 times less concentrated than the sample used for thermal data collection.[44]

Duckett *et al.* have demonstrated that $^{13}C$ polarisation levels of ~0.5% may be observed for $T_1$'s of 186 ± 18 seconds within a ~10 mT field when substrate design is utilised in order to integrate $^{13}C$ spin pairs within the substrate of interest.[62]

### 1.5.4. Phosphorus

$^{31}P$ SABRE was first reported in 2013.[36] In this report triphenylphosphine and tricyclohexylphosphine were utilised as ligands. The complexes formed with these phosphines favoured acetonitrile and pyridine coligands *trans* to the hydrides with the phosphine bound *trans* to carbene due to the high buried volume of the ligand. The ligand being bound *trans* to the carbene, however, appears to have precluded ligand exchange with no exchange rate for $PR_3$ being reported in the complexes $[Ir(IMes)(PR_3)(Py)(Acetonitrile)(H)_2]$ where $PR_3$= triphenylphosphine or tricyclohexylphosphine. The ligand bound *trans* to

the carbene not exchanging has also been reported for other ligand systems.[29] This led to a relatively modest $^{31}P$ enhancement of 30-fold when measured at a 9.4 T or 11.7 T field.

A further report by Koptyug *et al.* did not utilise a carbene in order to enable $PPh_3$ binding *trans* to hydrides.[63] Instead, a polarisation transfer species $[Ir(PPh_3)_3(H)_2Cl]$ was generated in solution which enabled a 260 times enhancement for $^{31}P$ when measured at 7 T. While this represents a significant increase in enhancement due to the enabling of ligand reversible exchange, the authors note that EXSY interrogation of the species does not show $PPh_3$ exchange at sites *cis* to the *para*hydrogen derived hydrides within the relaxation time of $^{31}P$ magnetisation.

Pyridine based ligands with phosphorous containing substituents were tested by Duckett *et al.* and demonstrated a $^{31}P$ enhancement of up to 860 times at a 9.4 T or 11.7 T field for 3,5-*bis*(diethoxyphosphoryl)pyridine.[64] Deuteration of the substituent ethyl chains resulted in this enhancement being further increased to 3588 times the thermal signal. Notably these substrates were characterised to form the traditional SABRE polarisation transfer species of $[Ir(IMes)(L)_3(H)_2]$.

### 1.5.5. Silicon and Tin

The low gyromagnetic ratios of $^{29}Si$ and $^{119}Sn$, -8.47 and -15.97 MHz $T^{-1}$ respectively, compared to 42.58 MHz $T^{-1}$ for $^{1}H$, lead to low sensitivity for these nuclei due to polarisation being proportional to γ (Equation 1). This low sensitivity is further exacerbated by a low natural abundance of 4.7% and 8.6% respectively for $^{29}Si$ and $^{119}Sn$, leading to typical measurement times in the tens of hours for high signal-to-noise spectra of these nuclei.

Olaru *et al.* have reported an investigation into the applicability of SABRE to these spin ½ nuclei.[65] This has been conducted through the utilisation of pyrimidine labelled with a $^{29}Si$ or $^{119}Sn$ heteronucleus in the form of 5-(tributylstannyl)pyrimidine (**$L_{Sn}$**) for tin and 5-(trimethylsilyl)pyrimidine (**$L_{Si}$**) for silicon as shown in Figure 14.

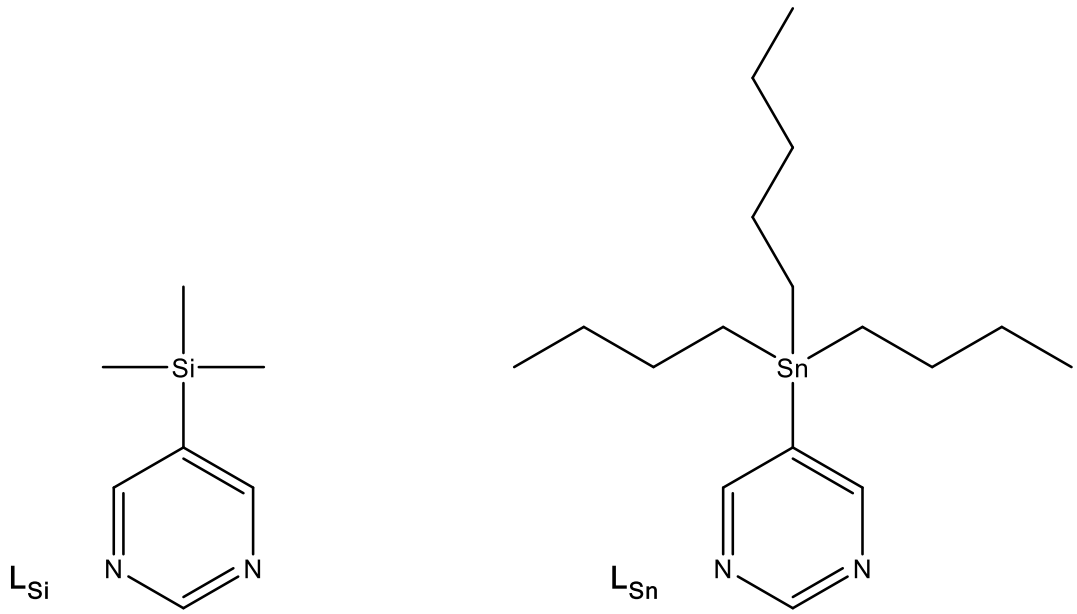


Figure 14. Structures of 5-(tributylstannyl)pyrimidine (**$L_{Si}$**, left) and 5-(trimethylsilyl)pyrimidine (**$L_{Sn}$**, right) utilised for demonstrating the applicability of SABRE to $^{29}$Si and $^{119}$Sn.

When [Ir(IMes)(COD)Cl] was utilised as the polarisation transfer pre-catalyst and exposed to **$L_{Si}$** and **$L_{Sn}$** the complexes $[Ir(IMes)(\mathbf{L_{Si}})_3(H)_2]^+$ and $[Ir(IMes)(\mathbf{L_{Sn}})_3(H)_2]^+$ were formed with hydrides present in their $^1$H NMR spectra at -22.44 and -22.06 ppm respectively. $^{29}$Si SABRE was observed making use of **$L_{Si}$** and demonstrated a 200-fold increase in signal-to-noise compared with thermal conditions.

$^{119}$Sn SABRE was observed making use of **$L_{Sn}$** and optimised when a substrate loading of 17:1 substrate:[Ir(IMes)(COD)Cl] was utilised. This optimised system was responsible for a 772-fold enhancement which equates to a time saving of over 400 hours when compared to obtaining the same signal intensity under Boltzmann conditions.

EXSY was utilised to give insight into the speed of hydride loss for these complexes with a hydride exchange rate at 295 K of 1.44 and 0.57 $s^{-1}$ reported for $[Ir(IMes)(\mathbf{L_{Si}})_3(H)_2]^+$ and $[Ir(IMes)(\mathbf{L_{Sn}})_3(H)_2]^+$ respectively. Notably, this is far slower than the equivalent exchange speed utilising pyridine as the substrate. The rate of hydride exchange may be increased through the usage of a carbene with a higher buried volume such as SIMes, which increases the

exchange rate at 295 K for hydride loss from 0.57 $s^{-1}$ in $[Ir(IMes)(\mathbf{L_{Sn}})_3(H)_2]^+$ to 2.29 $s^{-1}$ in $[Ir(SIMes)(\mathbf{L_{Sn}})_3(H)_2]^+$. Increasing the exchange rate was, however, observed to be detrimental to observed polarisation levels which is postulated by Olaru *et al.* to suggest scalar coupling in this system between substrate and hydride is smaller in magnitude than in an analogous pyridine system.

### 1.5.6. Fluorine

Due to the high gyromagnetic ratio of $^{19}F$ (94% compared to proton) and its 100% natural abundance, this nucleus presents an attractive prospect for MR studies.[66] $^{19}F$ is particularly attractive for *in vivo* imaging applications as there is minimal biological background signal and clinical MRI equipment may be easily adapted to detect $^{19}F$. This has led to the development of a range of $^{19}F$ containing contrast agents, which are already detectable at millimolar levels when thermally polarised.[67] The application of hyperpolarisation is hoped to potentially lower this detection limit by an order of magnitude.

The application of SABRE to fluorinated molecules was first demonstrated by Duckett *et al.* in their 2009 initial report of SABRE.[22] This report demonstrated a complicated antiphase signal which was polarised compared to thermal polarisation when 3-fluoropyridine was used as a substrate. It has been proposed that polarisation transfer occurs *via* a coupling system with $J_{HF}$ being similar to $J_{HH}$. It is likely that a range of fluorine substrates could be polarised. However, Hovener *et al.* were unsuccessful in attempts to polarise pentafluoropyridine as a substrate when both [Ir(IMes)(COD)Cl] and Crabtree's catalyst were used as the pre-catalyst.[68]

Theis *et al.* have recently demonstrated $^{19}F$ polarisation of ~0.3% (compared to ~50% demonstrated for $^{1}H$) for 3-fluoropyridine,[46, 69] though Theis notes that only 50% *para*hydrogen was used, meaning that if 100% had been used this could lead to an effective polarisation of ~0.85%. While it is noted this polarisation is significantly lower than $^{1}H$ and other heteronuclei, such as $^{15}N$,[52] it is hypothesised that this is due to the significantly lower $T_1$ of $^{19}F$ leading to signal loss during sample transfer prior to magnetisation read-out.

Theis *et al.* demonstrated that $^{19}F$ SABRE results in an antiphase signal when conducted at earth's magnetic field. Previous heteronuclei studies have demonstrated this due to intramolecular couplings;[50] an antiphase signal would be less suitable for MR imaging as a smaller observation window may result in effective observed signal cancellation, negating some of the hyperpolarisation effect. However, SABRE-SHEATH has been applied to fluorine systems which, just like when SABRE-SHEATH is applied to $^{15}N$, results in an absorptive signal. In addition to 3-fluoropyridine, pentafluoropyridine and 2-fluoropyridine were also tested as substrates, however, both failed to demonstrate the SABRE effect. This is suggested to be due to steric effects.

The application of $^{19}F$ SABRE-SHEATH to MRI imaging has been successfully demonstrated as shown in Figure 15. Finally, the application of hyperpolarised $^{19}F$ to pH detection was demonstrated. This is noted to be similar in capability to $^{15}N$ while demonstrating a sensitivity >30 times larger than $^{1}H$ NMR for changes in local pH.

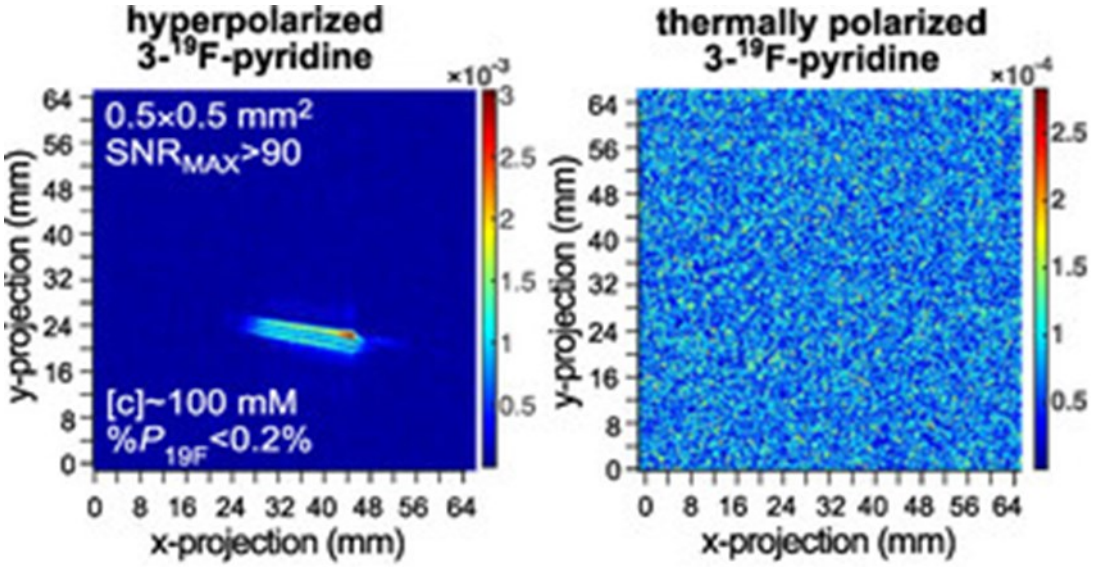


Figure 15. MRI imaging of $^{19}F$ hyperpolarised 3-fluoropyridine compared to a thermally collected image under the same conditions at the same concentration.[69]

The combination of low background, high gyromagnetic ratio and relative ease of conversion for existing hardware to detect fluorine makes $^{19}F$ an attractive prospect going forwards. In 2010 it was estimated that 20% of approved drugs contain fluorine and novel application of $^{19}F$ SABRE to a drug currently on the market in addition to a new psychoactive substance (NPS) is presented in section 6.3.[70] The relatively short $T_1$ of these species currently presents a barrier to *in vivo* applications, however, methods for lengthening the relaxation time of SABRE substrates have been previously reported in literature.[31]

### 1.5.7. Relaxation Rates

Approaches have been reported which may enable the lengthening of relaxation time – in particular, it is important to note that the polarisation transfer catalyst (typically $[Ir(IMes)(L)_3(H)_2]^+$) increases the speed of relaxation, known as $T_1$.[29] $T_1$ or longitudinal relaxation describes the process by which magnetisation returns to thermal polarisation within an external magnetic field. Within the context of SABRE this process therefore describes how long the hyperpolarised state survives after polarisation transfer.

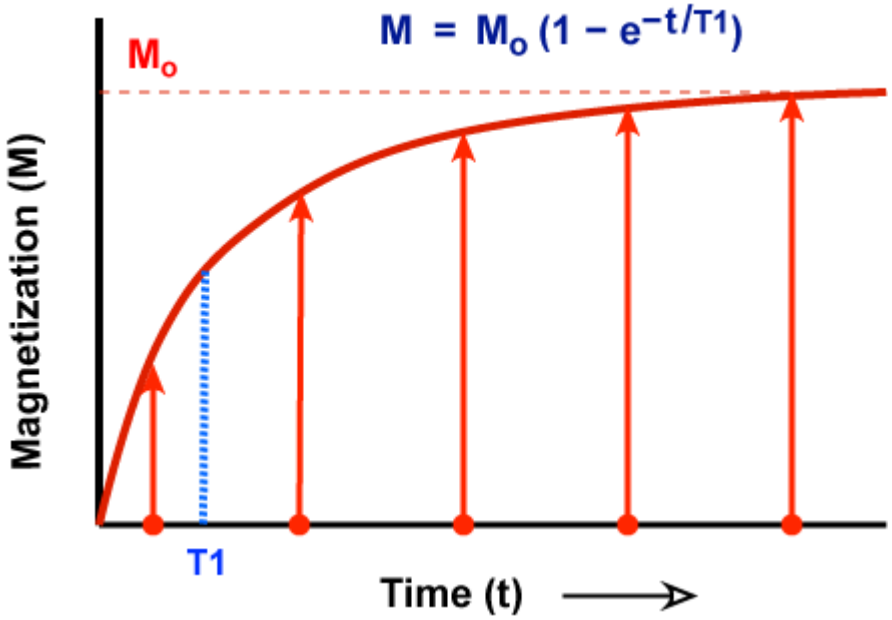


Figure 16. $T_1$ relaxation may be modeled as an exponential growth back to thermal equilibrium within an external magnetic field following the application of a 90º pulse.

As shown in Figure 16 $T_1$ may be described by the magnetisation (M) compared to the initial or thermal magnetisation ($M_o$) after a period of time t.

This means that after $T_1$ 63% of the hyperpolarised signal has relaxed back to thermal polarisation therefore a short $T_1$ requires rapid interrogation of the hyperpolarised state.

As the polarisation transfer catalyst facilitates $T_1$ relaxation through spin lattice interactions the addition of a chelating agent, such as bipyridine (bpy) led to the formation of the species $[Ir(IMes)(bpy)(H)_2(L)]^+$, with nicotinamide being the ligand (L) in this report.[31] This species was formed in ~1.2 s for a 97% conversion from $[Ir(IMes)(L)_3(H)_2]^+$ meaning this method would be viable for rapid 'quenching' of SABRE after generating a hyperpolarised bolus. In this report 2,2'-bipyridine is bound bidentate *trans* to the hydride ligands and the remaining nicotinamide is bound *trans* to the carbene. Comparison of nicotinamide $T_1$ values when the catalyst is not present, before catalyst deactivation and following catalyst deactivation demonstrated that deactivating the catalyst results in relaxation times comparable to that of nicotinamide without catalyst present as shown in Table 2. It is worth noting, however, that 4,4'-bipyridine has been SABRE hyperpolarised without any reported deactivation, meaning the binding mode of the ligand is important for deactivation.[71]

Table 2. Nicotinamide relaxation rates without catalyst present, before and after catalyst deactivation (at 9.4 T).

| | $T_1$ (s) | | |
|---|---|---|---|
| **Proton** | No catalyst | $[Ir(IMes)(L)_3(H)_2]^+$ | $[Ir(IMes)(bpy)(H)_2(L)]^+$ |
| **H-2** | 43.1 | 7.0 | 38.0 |
| **H-4** | 11.3 | 6.1 | 11.5 |
| **H-5** | 13.5 | 3.7 | 14.0 |
| **H-6** | 6.6 | 4.3 | 6.8 |

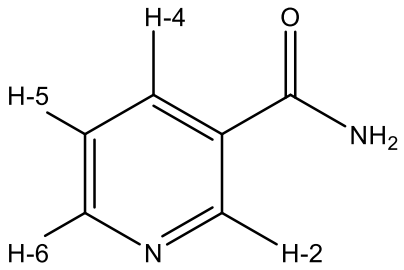


Figure 17. Nicotinamide with proton environments labelled, $T_1$ values for each environment are shown in Table 2.

In addition to 2,2'-bipyridine, deactivation has been demonstrated making use of 1,10-phananthroline,[31] bathophenanthrolinedisulphonic acid disodium salt (BPS),[72] and with silica-based scavengers.[73, 74] The deactivation and removal of the catalyst making use of silica scavengers is further discussed in 1.7.6.

## 1.6. SABRE Reproducibility

The SABRE process has a high degree of irreproducibility, in particular the 'shake and drop' approach utilised within this work involves manual shaking of a Young's capped NMR tube after the head space has been charged with *para*hydrogen. However, though this approach does not require specialised equipment, slight variations in height, angle and speed of shaking, in addition to the variable time of transfer before acquisition, may lead to a high degree of inconsistency. A variation of ±20% has been reported for the 'shake and

drop' approach.[61] This may be alleviated through bubbling of *para*hydrogen through the solution which may yield a significant increase in reproducibility at the cost of polarisation level due to the reduced vigour of interactions and the potential for line broadening if flow continues during the acquisition time.[61, 75, 76]

The traditional approach of utilising the stray field of a high-field NMR magnet in order to conduct polarisation transfer in a heightened magnetic field e.g. 65 G has led to issues with being unable to regulate the polarisation transfer field closely. Recently this has been alleviated through the use of handheld permanent magnet arrays,[77] or, as utilised herein, a tuneable electromagnetic coil where the polarisation transfer field may be set and controlled accurately.

## 1.7. Towards *in vivo* application

There are currently multiple challenges to be overcome before SABRE may be applied to *in vivo* imaging, amongst these are the need for polarisation to occur in a biologically compatible solvent and the expense/potential toxicity of catalyst injection. *Para*hydrogen hyperpolarisation techniques have recently been applied *in vivo* with PHIP being applied to 1-$^{13}$C-phospholactate *in vivo* to successfully obtain hyperpolarised MR images of a mouse brain.[78]

### 1.7.1. Progress towards aqueous SABRE

Though SABRE has been optimised and found to be most efficient in $d_4$-methanol, this solvent is unsuitable for use in *in vivo* imaging.[27, 33, 72, 79] Solvents, such as $D_2O$ or ideally $H_2O$, are better suited for biological applications. Progress has been made in making use of methanol/water mixtures to demonstrate SABRE; this has shown some activity for a limited range of analytes in mixtures of up to 90% water.[80] This has been improved though the pre-activation of the pre-catalyst [Ir(IMes)(COD)Cl] in the presence of pyridine or nicotinamide and $H_2$ in methanol or ethanol.[81] Once activated in the presence of a suitable substrate and $H_2$, the active species [Ir(IMes)(substrate)$_3$(H)$_2$] could be isolated and reconstituted in $H_2O$ – this yielded SABRE enhancements of roughly half of what could be achieved in $d_6$-

ethanol for nicotinamide, although this did demonstrate that SABRE in pure water solvent system was feasible.

### 1.7.2. Water soluble catalysts

In order to better study aqueous systems making use of SABRE, the synthesis of aqueous pre-catalysts has been a priority for several research groups. Fekete *et al.* successfully synthesised the pre-catalyst shown in Figure 18,[82] which facilitated a 750-fold enhancement of the proton environments in pyridine in $d_4$-methanol after polarisation transfer at 60 G. In a partially aqueous media (67% $D_2O$, 3% DMSO and 30% ethanol) an enhancement of 9.4-fold was observed under the same conditions. DMSO was included to increase the solubility of $H_2$. Enhancements for 4-hydroxypridine (22-fold) and oxazole (2.7-fold) were observed when making use of this catalyst in 70% $D_2O$ and 30% ethanol.

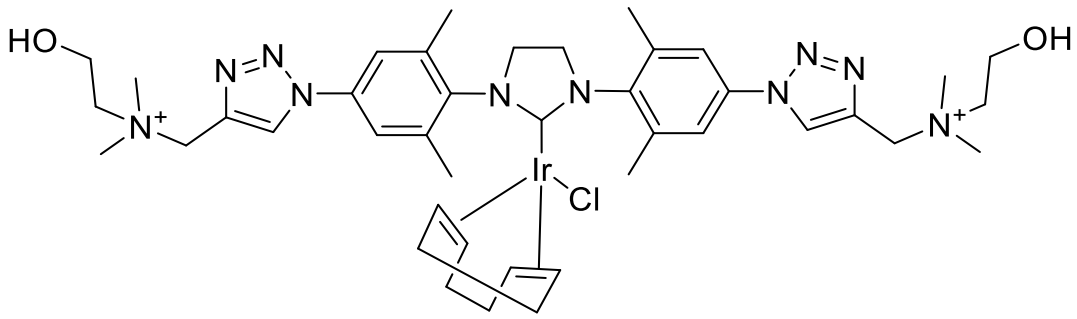


Figure 18. Water soluble pre-catalyst synthesised by Fekete *et al.*[82]

Other groups have also opted to modify the NHC of the pre-catalyst in order to include water-solubilising groups. In particular Spannring *et al.* have attempted to synthesise a water soluble pre-catalyst, [Ir(Itome)(COD)Cl], (Itome = 1,3-*bis*(3,4,5-trimethoxybenzyl)imidazole-2-ylidene) with the addition of methoxy groups to the NHC, demonstrated in Figure 19, however, this catalyst proved to be insoluble in $D_2O$.[83] The addition of the more sterically bulky 3,4,5-tri(diethyleneglycol)benzyl groups instead of the mesityl groups to give the pre-catalyst [Ir(IDEG)(COD)Cl], (IDEG = 1,3-*bis*(3,4,5-tris(diethyleneglycol) benzyl)imidazole-2-ylidene), resulted in a 64-fold enhancement of pyridine in $D_2O$ with polarisation transfer in an 80 G field and

measurement in a 300 MHz field. This demonstrated that, despite the low solubility of $H_2$ in water, SABRE may occur.

No SABRE is observed for [Ir(IMes)(COD)Cl] in $D_2O$, unless the catalyst is activated in an organic solvent and then isolated prior to reconstituting in water. Despite this, it has been demonstrated that replacing COD with a suitable diol such as CODDA (CODDA=1,2-dihydroxy-3,7-cyclooctadiene) allows catalyst activation and SABRE in an aqueous environment, forming the same catalytic $[Ir(IMes)(substrate)_3(H)_2]^+$ species.[84]

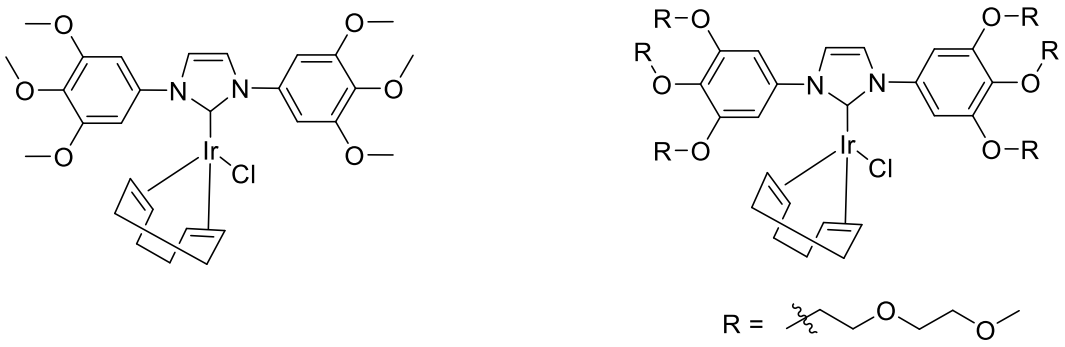


Figure 19. Structures of the pre-catalysts [Ir(Itome)(COD)Cl] and [Ir(IDEG)(COD)Cl].[83]

### 1.7.3. SABRE-RELAY

SABRE-RELAY was first reported in 2018 by Duckett *et al.* and demonstrated a route for the hyperpolarisation of previously inaccessible substrates, such as alcohols, carboxylic acids and amines.[85] Figure 20 shows the SABRE-RELAY mechanism compared to the traditional SABRE approach, in SABRE-RELAY a carrier substrate such as ammonia is polarised, which then transfers polarisation to a secondary substrate *via* proton exchange or binding to a secondary metal complex.[86] Notably, the relay approach provides access to many of the common substrates typically examined *via* DNP (e.g. pyruvate, glucose, urea), therefore Duckett *et al.* suggest that this may provide a cost effective route to polarise these substrates.[87] The desired hyperpolarised substrate does not bind to the polarisation transfer catalyst; this has previously been achieved *via* molecular cleavage following polarisation transfer, rendering this approach irreversible compared to the relay method.[88] SABRE-

RELAY has been employed for the hyperpolarisation of $^{19}F$ and $^{31}P$, through a proton exchange mechanism, of 2,2-difluoroethanol and diethyl(hydroxymethyl) phosphonate respectively.[89]

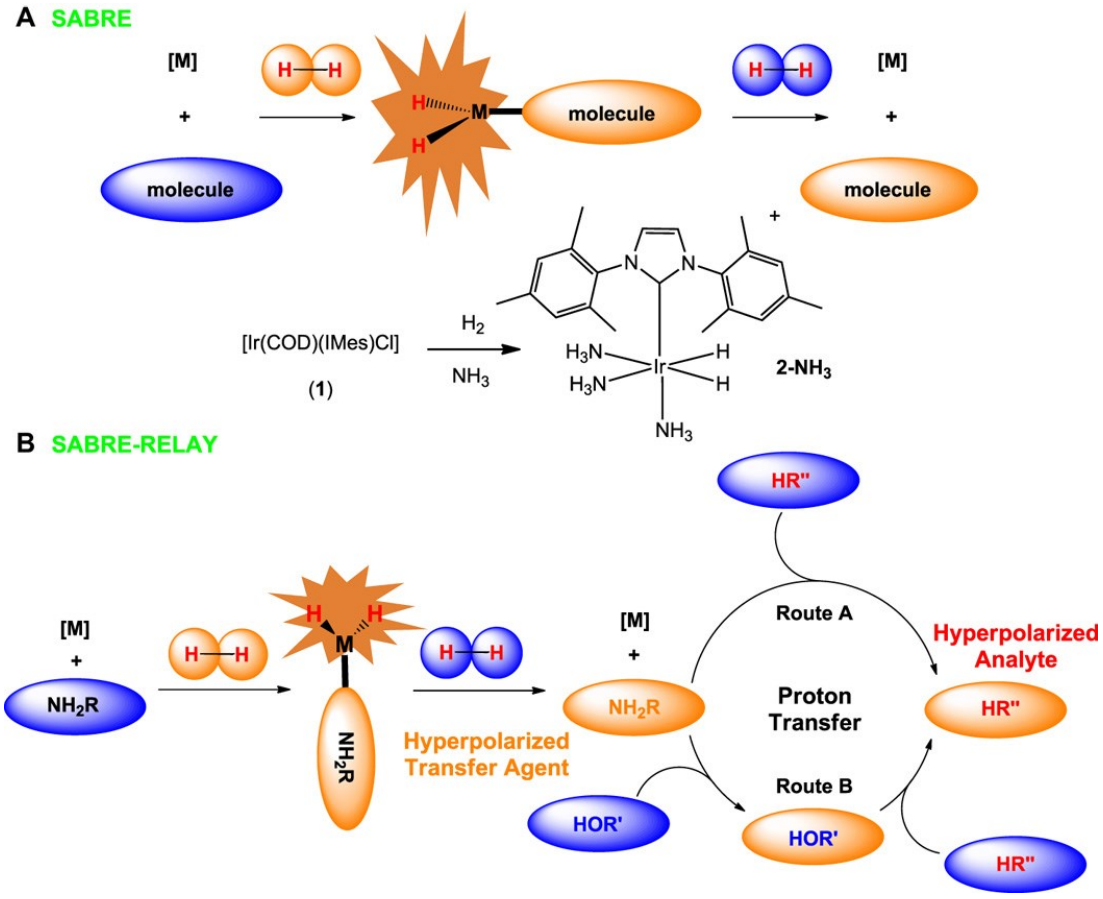


Figure 20. Mechanisms of SABRE (top) and SABRE-RELAY (bottom).[85]

Despite theoretically allowing access to a wider range of biologically relevant molecules such as amino acids, Duckett *et al.* note that a small level of contaminant $H_2O$ may drastically reduce the hyperpolarisation levels attained as proton exchange may then occur with the solvent. A sample of 1-propanol in dichloromethane-$d_2$ (1 µL), [Ir(IMes)(COD)Cl] and a polarisation relay substrate, $d_7$-$BnNH_2$, initially demonstrated an enhancement of 537-fold for $OCH_2$. Addition of 1 and 5 µL of dichloromethane-$d_2$ reduced the polarisation level attained to 48- and 11-fold respectively due to spin dilution and reduced polarisation transfer efficiency between amine and alcohol, suggesting this technique is highly sensitive to small changes in solvent. The author postulates this may potentially be alleviated through the utilisation of a mixed solvent

system such as that employed in catalyst separated hyperpolarisation through SABRE (CASH-SABRE), discussed further in 1.7.5.

### 1.7.4. Catalyst toxicity

Unfortunately, Duckett *et al.* have demonstrated the toxicity of the most common SABRE reaction mixture (utilising the pre-catalyst [Ir(IMes)(COD)Cl]) through cell line studies such as that summarised in Figure 21.[72] This toxicity may be primarily attributed to the iridium complex itself as an evaluation of the solvent system demonstrated that over a 24 hour period no cell viability was lost when a 30:70 mixture of deuterated ethanol and deuterated water respectively was utilised to make up 10% of the solvent within the cell medium. Evaluation of $d_2$-methyl nicotinate demonstrated slight toxicity within a 6 hour timeframe, however, both cell lines remained in excess of 80% viable within this time period, even at 20 mM concentrations. The dramatic loss in viability for the full SABRE reaction mixture may, therefore, be attributed to the iridium species.

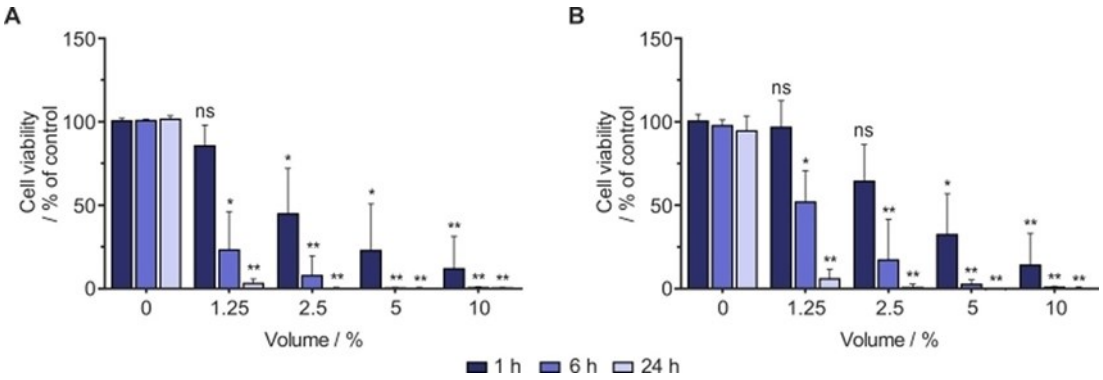


Figure 21. Cell viability of cell lines A549 (A) and MCF7 (B) following exposure to 0, 1.25, 2.5, 5 and 10% bolus volumes of a SABRE reaction mixture containing [Ir(IMes)(COD)Cl] (5 mM), $d_2$-methyl nicotinate (20 mM) in $d_6$-ethanol:$D_2O$ (30:70) after 1, 6 and 24 hours.[72]

Changing the carbene identity associated with the pre-catalyst or utilisation of a significantly different species such as $[Ir(H)_2(Nam)(solv)(mPTA)(tmx)](I)(CF_3SO_3)]$, (Nam = 4,6-nicotinamide, mPTA = methylated 1,3,5-triaza-7-phosphaadamantane, tmx = tetramethylxanthine)

still demonstrated a significant loss of cell viability, suggesting the iridium itself is responsible for the cytotoxicity observed.[79]

Due to the toxicity of the most effective reported polarisation transfer catalyst, [Ir(IMes)(COD)Cl], there has been a recent focus in literature to remove the catalyst from a bolus, be that through phase separation such as CASH-SABRE, heterogeneous SABRE (HET-SABRE) or through catalyst sequestration through heterogeneous scavenging.

### 1.7.5. CASH-SABRE

CASH-SABRE, reported by Duckett *et al.* in 2017, utilises a mixed solvent system such as $CDCl_3/D_2O$ where SABRE occurs within the organic $CDCl_3$ phase and the substrate, for instance pyrazine, resides primarily within the aqueous phase (~77% in aqueous phase under thermal conditions).[90] This approach is similar to a phase separation approach, which has been reported for the preparation of an *in vivo* suitable aqueous bolus for PHIP.[91-93]

Duckett *et al.* note that though chloroform is partially soluble in water, an assessment 10 seconds after phase mixing resulted in 0.08% $CDCl_3$ within the water phase and doping of $D_2O$ with 0.16% w/v NaCl reduces the $CDCl_3$ present to 0.06%. The inclusion of sodium chloride within the aqueous phase also increases the speed of phase separation as previously an emulsion had been formed which did not provide phase separation within the timeframe of the hyperpolarised state. However, utilising the aqueous salt mixture phase separation was achieved in *circa* 10 seconds at which point an enhancement of 790-fold per proton was reported. Cell line studies making use of the aqueous phase did not demonstrate a decrease in cell viability within the 24 hour period measured within the report.[72]

### 1.7.6. Catalyst sequestration

Expanding upon the work done with phase separation to remove the iridium complex from solution, Barskiy *et al.* have demonstrated that a silica or polymer particle may sequester the SABRE catalyst from solution.[73] Barskiy *et al.* demonstrated that CASH-SABRE and sequestration may be combined,

with a bolus containing 81.67 ppm Ir, representative of the iridium content remaining after phase separation, demonstrating that iridium concentrations as low as 4.08 ppb may be attained after 12 hours exposure to 10 mg of a suitable metal scavenger.

Addition of a scavenging agent such as 3-mercaptopropyl and 2-mercaptoethyl ethyl sulfide following bubbling of *para*hydrogen through a metronidazole containing SABRE mixture utilising the pre-catalyst [Ir(IMes)(COD)Cl] has demonstrated that catalyst sequestration may occur on a timescale within the lifetime of the hyperpolarised state.[74] In this instance there was no detectable iridium remaining in solution on this timescale, and attempts to re-hyperpolarise the sample following scavenger addition resulted in no SABRE enhancements being observed. ICP-MS (inductively coupled plasma-mass spectroscopy) of an analogous bolus suggested that ~98.381% iridium removal occurred on average after a scavenger exposure time of several minutes. The addition of unfunctionalised $SiO_2$ was demonstrated to reduce the SABRE enhancements observed, however, hyperpolarisation continued to be observed in measurements following $SiO_2$ addition.

### 1.7.7. Heterogeneous catalysts

The separation of catalytic species and a hyperpolarised bolus offers advantages both in the relaxation time of the hyperpolarised species and in advancement towards *in vivo* applications, as the separation of catalyst means toxicity concerns are reduced in addition to lowering costs if the catalyst can be recycled. To this end a number of heterogeneous SABRE catalysts have been synthesised, the structures of which are shown in Figure 22. These examples make use of a solid support framework bound *trans* to IMes which prevents exchange of the solid support during SABRE, whilst still enabling access to the equatorial plane for polarisation transfer and ligand exchange.

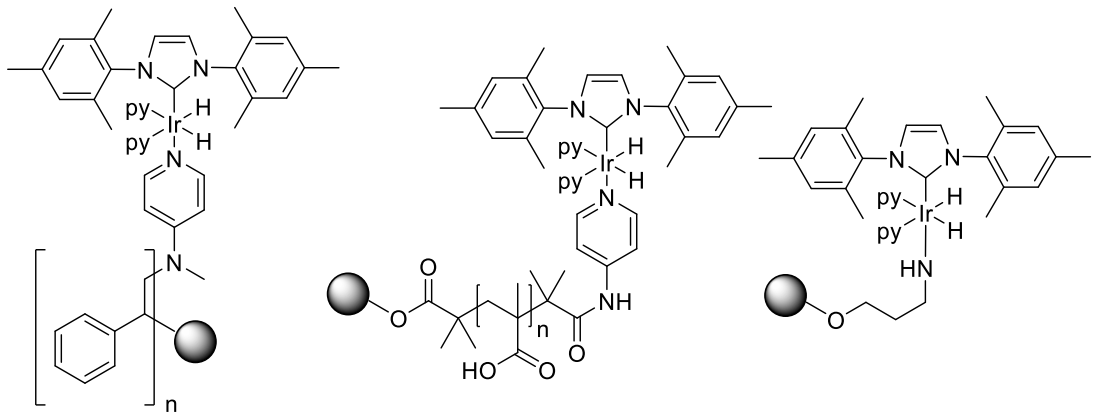


Figure 22. Pyridine activated HET-SABRE catalysts immoblised on polymermicrobeads (left),[94] $TiO_2$/poly(methacrylic acid) (PMAA) nanoparticles (middle)[37] and bound to a silica supported amine linker (right).[95]

The polymer microbead example has demonstrated SABRE activity polarising pyridine to yield an enhancement ~15 times lower than when the homogenous pre-catalyst [Ir(IMes)(COD)Cl] was utilised under the same conditions. No bound signals were observed in the hyperpolarised spectra due to the solid supported catalyst rapidly dropping to the bottom of the NMR tube after shaking. The binding of the catalyst to the solid support was confirmed making use of IR (infrared spectroscopy), MS (mass spectroscopy) and AAS (atomic absorption spectroscopy), with AAS showing that 4% of the total homogenous bulk was the iridium complex. Removal of the supernatant following heterogeneous hyperpolarisation and subsequent testing separated from the solid bulk revealed no SABRE activity, demonstrating that the heterogeneous catalyst was responsible for the polarisation. $^1$H NMR, AAS and MS were also used to interrogate this sample and failed to detect any catalyst leaching into solution.

A further study by Shi *et al.* demonstrated the synthesis of a heterogeneous catalyst on both a $TiO_2$/PMAA nanoparticle and PVP (polyvinylpyridine) polymer. These species were characterised by NMR, AAS and DLS (dynamic light scattering). AAS determined that 25% of the total nanoparticle catalyst by weight was iridium complex; the final filtrate wash following production of the heterogeneous species did not show the presence of iridium when analysed with AAS, indicating a robust heterogeneous catalyst. The enhancements

obtained from the nanoparticle catalyst were *ca*. 2.5 times higher than those obtained from the polymer based catalyst reported by Shi *et al.* making use of a 'shake and drop' method with pyridine as the substrate. When *para*hydrogen was bubbled through the solutions instead for 300 s the nanoparticle based catalyst's enhancements increased from 18-, 17- and 7-fold for each pyridine site respectively to give enhancements of 26-, 39- and 11-fold respectively. This equates to an overall polarisation of *ca.* 0.13%. This study also demonstrated that the heterogeneous catalyst may be recycled for use in further SABRE experiments, though enhancements were slightly reduced following the recovery process.

Kovtunov *et al.* demonstrated the use of a commercially available silica supported amine linker.[95] Though this report demonstrates lower polarisations for pyridine (~2.6 fold) compared to the work of Shi *et al.*,[37, 94] the aim of the publication was to demonstrate HET-SABRE of heteroatoms, specifically $^{15}$N. Therefore, the $^{1}$H polarisation was not optimised. Kovtunov *et al.* successfully demonstrated a $^{15}$N polarisation of ~100 fold under HET-SABRE-SHEATH conditions.[50, 52] The lower gyromagnetic ratio of $^{15}$N compared to $^{1}$H suggests that far greater $^{1}$H polarisation would be feasible using this HET-SABRE system if $^{1}$H polarisation was optimised.[5] The signal has been attributed to solid-supported catalyst through the lack of $^{15}$N bound peaks typically observed for axially and equatorially bound pyridine to [Ir(IMes)(COD)Cl] (**4**). The supernatant was further tested with x-ray photoelectron spectroscopy (XPS) and ICP-MS suggesting no iridium is lost from the surface during the HET-SABRE process and there is minimal leaching into the supernatant.

### 1.7.8. Progress towards applying SABRE to biologically relevant substrates

SABRE has been utilised to hyperpolarise a range of biologically relevant molecules including world health organisation (WHO) essential medicines such as metronidazole,[30, 68, 74] and pyrazinamide,[49, 96] in addition to voriconazole,[97] the polarisation of which is reported in 6.2.

Furthermore, the application of SABRE to hyperpolarise pyridine in the presence of blood, has been examined.[68, 98] Hövener *et al.* added 2 mL fresh human blood to an ethanol solution containing 4 equivalents of pyridine relative to **4**.[98] Continuous SABRE polarisation was attempted making use of *para*hydrogen bubbling through the solution and hyperpolarisation continued to be observed following the addition of blood. However, Hövener *et al.* note that, after a short time, the liquid coagulated and the observed hyperpolarised signal had decreased to approximately a tenth of its initial value.

In a further report, Hövener *et al.* demonstrated that pyridine SABRE may be observed in a $D_2O$ solution containing HL-60 cells and a separate solution containing DPBS, both simulating parts of the blood environment.[68] However, Hövener *et al.* were unable to observe SABRE within a mixture including whole blood, cells and serum when nicotinamide was the substrate. Hövener *et al.* note, however, that in a previous report where pyridine was utilised as the substrate, hyperpolarisation within a blood mixture was observed and attribute this to a higher initial signal enhancement.[98]

Expanding the scope of biologically relevant substrates to which SABRE may be applied remains a key focus of current literature and it is envisaged that these substrates in combination with catalyst removal techniques such as CASH-SABRE and catalyst scavenging may provide a route towards SABRE *in vivo* imaging.

# 2. Aims

The work contained herein aims to develop SABRE towards future biological applications. Several key areas have been identified as gaps within the current literature or areas that require expansion and further development. These are:

- Testing alternative metals, such as rhodium, which may be capable of replacing iridium within the polarisation transfer catalyst required for SABRE.
- Applications of SABRE to a range of biologically relevant substrates such as new psychoactive substances (NPS) and applying $^{19}F$ SABRE to a WHO essential medicine to expand the biological applications of the SABRE technique.
- Extending the scope of $^{19}F$ SABRE as this may be utilised *in vivo* without the water background signal typically associated with $^{1}H$ imaging. Developing HET-SABRE catalysts or catalyst scavengers capable of rapidly producing a metal free bolus so that the toxicity of the catalyst may be circumvented.
- Applications of SABRE to a range of biologically relevant substrates such as new psychoactive substances (NPS) and applying $^{19}F$ SABRE to a WHO essential medicine to expand the biological applications of the SABRE technique

# 3. SABRE active complexes

## 3.1. Introduction

Despite there being numerous reports relating to the SABRE technique since it was first evidenced in 2009, nearly all reports utilise an iridium-based polarisation transfer catalyst similar to that utilised in the first reports.[98, 99] There have been some developments in catalyst design, in that the initially utilised Crabtree's catalyst is now rarely employed to facilitate polarisation transfer. Instead, the current literature standard complex of [Ir(IMes)(COD)Cl], is almost exclusively used.[26, 28, 32]

This chapter aims to investigate the use rhodium complexes for facilitating polarisation transfer in SABRE. These complexes will be compared to analogous, or similar, iridium complexes, to better understand their catalytic potential.

### 3.1.1. Use of non-iridium metals for SABRE

The majority of recent SABRE reports make use of the iridium complex [Ir(IMes)(COD)Cl], however, other metal complexes, such as platinum, cobalt and rhodium, have been used to facilitate *para*hydrogenation-based polarisation transfer. The following sections will detail how these metal complexes have been employed in this regard.

#### 3.1.1.1. Platinum

A platinum complex, [Pt(OTf)(sub)(*bis*-diphenylphosphinopropane)]OTf (where OTf is trifluoromethanesulfonate), has been reported by Duckett *et al.* within SABRE-RELAY to transfer polarisation from a pre-polarised relay substrate onto the substrate of interest.[85] Though, in this instance, the traditional SABRE process does not occur within the platinum containing complex as the *para*hydrogen derived hydrides are still bound to a polarisation transfer catalyst derived from [Ir(IMes)(COD)Cl]. The initially polarised substrate, such as ammonia or nicotinamide,[37] then binds to platinum and

transfers polarisation to a secondary species which would not typically be accessible by SABRE, as shown in Figure 23.

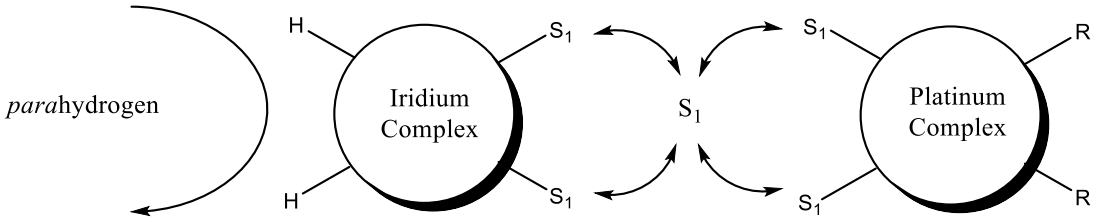


Figure 23. Schematic representation of the application of SABRE-RELAY where R is indirectly polarised.

Though polarisation transfer takes place around the platinum complex, this is not a full SABRE process as a second iridium species is required for initial polarisation transfer from *para*hydrogen derived hydrides in order to facilitate the relaying of polarisation by a substrate, **S1**. Duckett *et al.* have utilised a range of *N*-heterocyclic substrates to fulfil this relay role including nicotinic acid, nicotinamide and pyrazine. Polarisation transfer from **S1** to R was then reported *via* a scalar coupling network formed around the platinum complex in order to polarise the *bis*-diphenylphosphinopropane ligand of the platinum complex, resulting in $^{31}$P hyperpolarisation being observed.

#### 3.1.1.2. Cobalt

As discussed in 1.4, cobalt has been used to facilitate simultaneous SABRE and PHIP polarisation using a [(Mes$^{CCC}$)Co($N_2$)($PPh_3$)] (Mes$^{CCC}$ = (*bis*(mesityl-benzimidazol-2-ylidene)phenyl)) pre-catalyst, shown in Figure 24.[39, 100, 101] The bulky strongly electron donating tridentate ligand means the SABRE active form of this species has been proposed as [(Mes$^{CCC}$)Co($H_2$)(substrate)]. Polarisation transfer efficiency, though not reported within the literature, is likely to be significantly less efficient as only a single ligand may bind simultaneously, resulting in a far slower build-up of hyperpolarised species in solution.

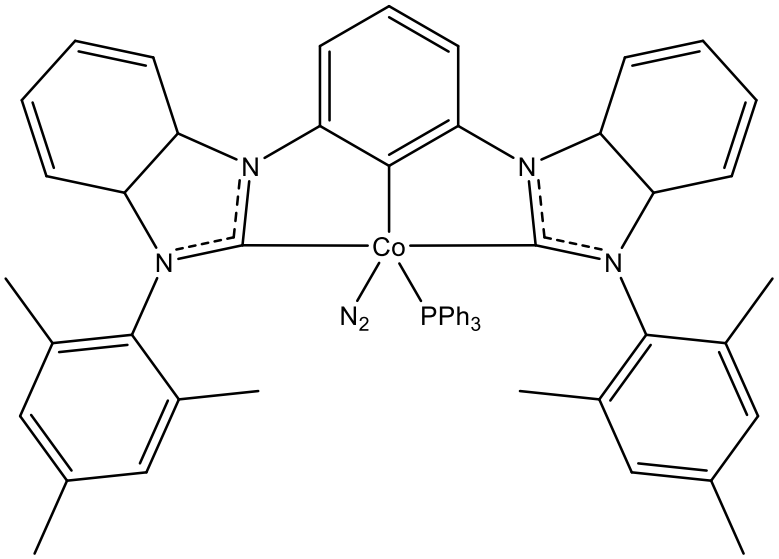


Figure 24. Structure of [(Mes$^{CCC}$)Co($N_2$)($PPh_3$)] pre-catalyst utilised for cobalt SABRE.[100]

### 3.1.1.3. Rhodium

Despite its common use in PHIP,[102] there is only a single literature source for the use of rhodium in SABRE. This report by Koptyug *et al.* comes from a mixed [Rh(DPPB)(COD)]$BF_4$ (DPPB = 1,4-*bis*(diphenylphosphino)butane) and [Ir($PCy_3$)(COD)(Py)]$PF_6$ (Crabtree's catalyst) pre-catalyst system used to achieve $^{31}$P polarisation.[40] However, the authors note that due to a complex equilibrium of multiple species within the sample, they were unable to assign polarisation transfer to a particular species. Crabtree's catalyst has, however, been previously reported as an effective SABRE polarisation transfer species, in that this catalyst was utilised within the first report of SABRE.[98]

Rhodium complexes such as Wilkinson's catalyst, Rh($PPh_3$)$_3$Cl, have been extensively utilised for PHIP for the hydrogenative integration of *para*hydrogen into the target substrate.[102, 103] The substrates polarised included phenylacetylene, styrene, halide containing alkenes and branched alkenes.

Given the reported potential for cobalt to be utilised as an unusual SABRE catalyst, and the report by Koptyug *et al.*, further investigations into the potential of rhodium to facilitate SABRE were undertaken within this work.

### 3.1.2. Rhodium Hydride Species

A key component of forming a SABRE active species from current literature appears to be the necessity to form a dihydride metal species capable of reversible exchange of both hydrides and the desired substrate.

Unfortunately, while there is experimental evidence for rhodium dihydride species, they are known to typically be highly transient at room temperature and, whilst detection is possible, the process is challenging.[103] In the majority of reported cases dihydride species have been observed at lower temperatures, with species stability differences primarily attributed to changes in electron donating properties of the associated ligands.[104] Wilkinson's catalyst has been reported to form a stable dihydride at room temperature,[105] however, other species such as dirhodium tetrahydride degrade above 273 K,[106] with some solvate dihydride species requiring study at temperatures in the range of 183 K – 213 K in order to remain stable during analysis.[107]

An approximation with [Ir(IMes)(COD)Cl] may be found in [Rh(P,SR)(COD)Cl], where R = Ph, Et, $^{t}$Bu, Bz, which has been evaluated for PHIP by Manoury *et al.*[108] This complex utilised a ferrocenyl phosphine thioether ligand, shown in Figure 25, which is bound *trans* to COD in the initial pre-catalyst.

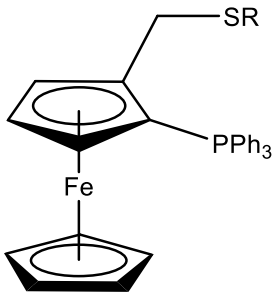


Figure 25. Structure of (P,SR) bidentante ligand utilised by Manoury *et al.*[108]

Addition of $H_2$ over the temperature regime 233 – 298 K did not result in an observable hydride species, however, there was a new set of peaks observed in the $^{1}$H NMR spectrum associated with partial hydrogenation of the COD ligand, suggestive of a slow reaction to form a Rh hydride species followed by rapid reaction with COD. Manoury *et al.* note that this is not

unexpected due to Rh(III) hydride complexes being known to be less stable than the Ir(III) analogues. Manoury *et al.* note that some free cyclooctene is observed in solution at temperatures as low as 253 K, demonstrating that $H_2$ addition occurs at this temperature. The presence of HD scrambling became evident at 273 K, suggestive of exchanging hydrides and solvent adducts. However, whilst direct observation of the hydrides is not reported, Manoury *et al.* note that these sites may exist primarily as deuterium and thus not be observed in the $^1$H NMR spectrum. While hydrides were not visible for reactions conducted within $d_4$-methanol, utilisation of deuterated dichloromethane demonstrated weak hydride species at -9.7 and -23 ppm within a $^1$H spectrum that promptly disappeared upon addition of a low quantity of MeOH.

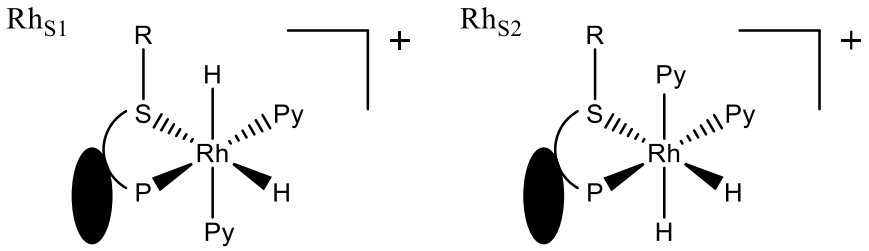


Figure 26. Structural isomers of $[Rh(P,SR)(Py)_2(H)_2]^+$ formed upon addition of $H_2$ and pyridine.[108] Structure of ligand is shown in Figure 25.

Manoury *et al.* note, however, that when an excess of pyridine (initially 75 equivalents relative to the polarisation pre-catalyst) is added alongside *para*hydrogen gas at a low temperature (233 K – 283 K), four hydride peaks are observed at -13.1, -14.3, -17.2 and -17.6 ppm. These are representative of two dihydride species, **Rh$_{S1}$** and **Rh$_{S2}$** as shown in Figure 26. These *para*hydrogen derived hydride peaks disappear when the sample is warmed to 298 K or above. When non-*para* enriched $H_2$ was utilised at room temperature only the thermodynamically favoured complex **Rh$_{S2}$** was observed.

EXSY analysis of hydride exchange at 273 K within this complex yielded rates of 0.29 $s^{-1}$ when 8 equivalents of pyridine were utilised, increasing to 0.39 $s^{-1}$ when 173-fold excess of pyridine was utilised. Manoury *et al.* note

that these transitions were only observed between **Rh$_{S1}$** and **Rh$_{S2}$**, which exist at this temperature however, and no evidence was observed for hydride exchange with free $H_2$, which would be a crucial requirement for SABRE activity.

Despite this, the direct analogue of [Ir(IMes)(COD)Cl], [Rh(IMes)(COD)Cl] has been reported to conduct PHIP when partnered with an additional phosphine,[109] and [Rh(IMes)$_2$(CO)(H)] has been reported,[110] demonstrating that rhodium NHC complexes are capable of forming hydrides. Therefore, the decision was made to evaluate the potential utility of [Rh(IMes)(COD)Cl] as a polarisation transfer pre-catalyst in order to directly compare with [Ir(IMes)(COD)Cl] utilised extensively within extant SABRE reports.

## 3.2. Complex Characterisation

### 3.2.1. [Ir(IMes)(COD)Cl]

Initially both [Ir(IMes)(COD)Cl] and [Rh(IMes)(COD)Cl were synthesised utilising established literature methods for the reaction of the dimer [M(COD)Cl]$_2$ with an NHC.[28]

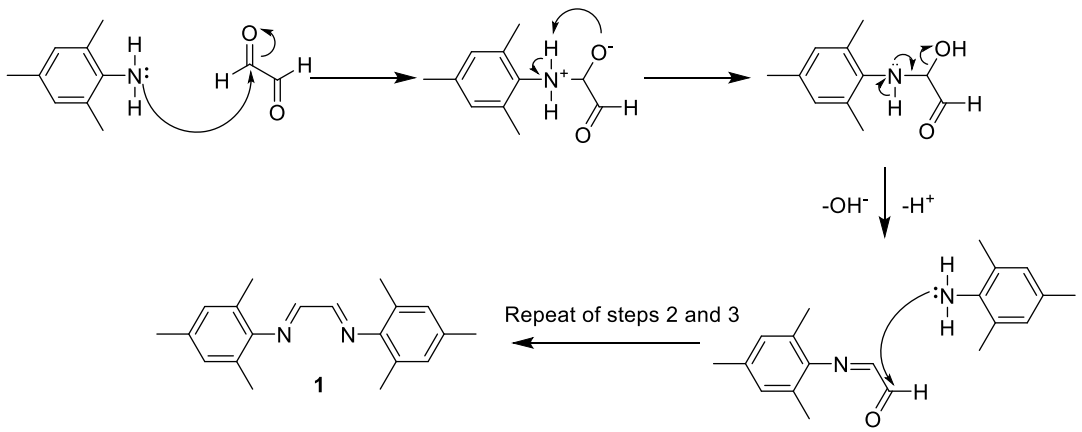


Figure 27. Reaction scheme for the synthesis of *N,N'*-bis(2,4,6-trimethylphenyl)ethanediimine (**1**).

*N,N'*-bis(2,4,6-trimethylphenyl)ethanediimine (**1**) was yielded from the reaction of 2,4,6-trimethyl aniline and glyoxal in a 39% yield, as shown in Figure 27.

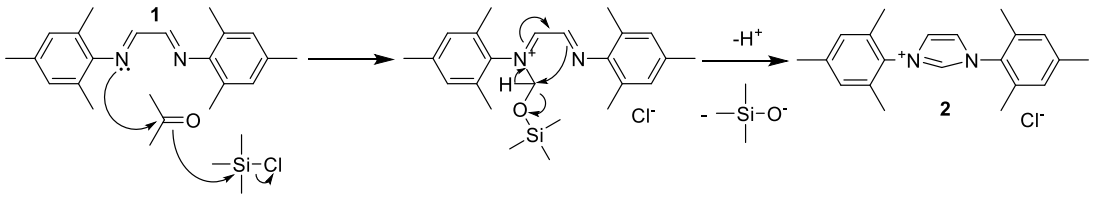

Figure 28. Reaction scheme for the synthesis of 1,3-*bis*(2,4,6-trimethylphenyl)-imidazolium hydrochloride (**2**).

This was then reacted with paraformaldehyde in the presence of trimethylsilyl chloride to form 1,3-*bis*(2,4,6-trimethylphenyl)-imidazolium hydrochloride (**2**) in a 79% yield, as shown in Figure 28. $[Ir(COD)Cl]_2$ (**3**) was formed by the reaction of $IrCl_3.xH_2O$ with cyclooctadiene (COD) in an 18% yield based on anhydrous $IrCl_3$.

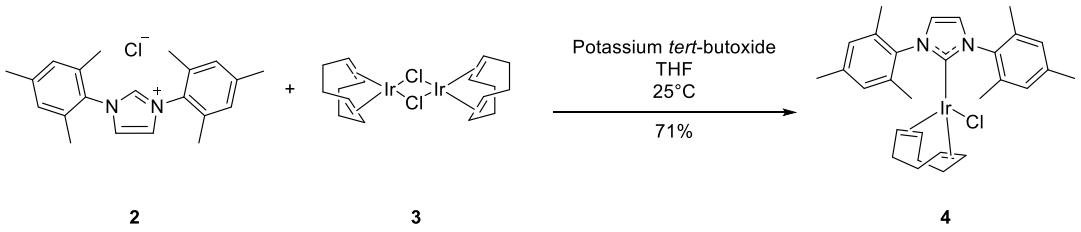


Figure 29. Reaction scheme for the synthesis of [Ir(IMes)(COD)Cl].

As shown in Figure 29, **2** was free based utilising potassium *tert*-butoxide before reaction **3** at room temperature. The reaction mixture was then separated *via* silica gel chromatography and the desired complex isolated in a 71% yield for the iridium complex [Ir(IMes)(COD)Cl] (**4**). These complexes were then characterised, with the $^1H$ NMR data for each complex shown below.

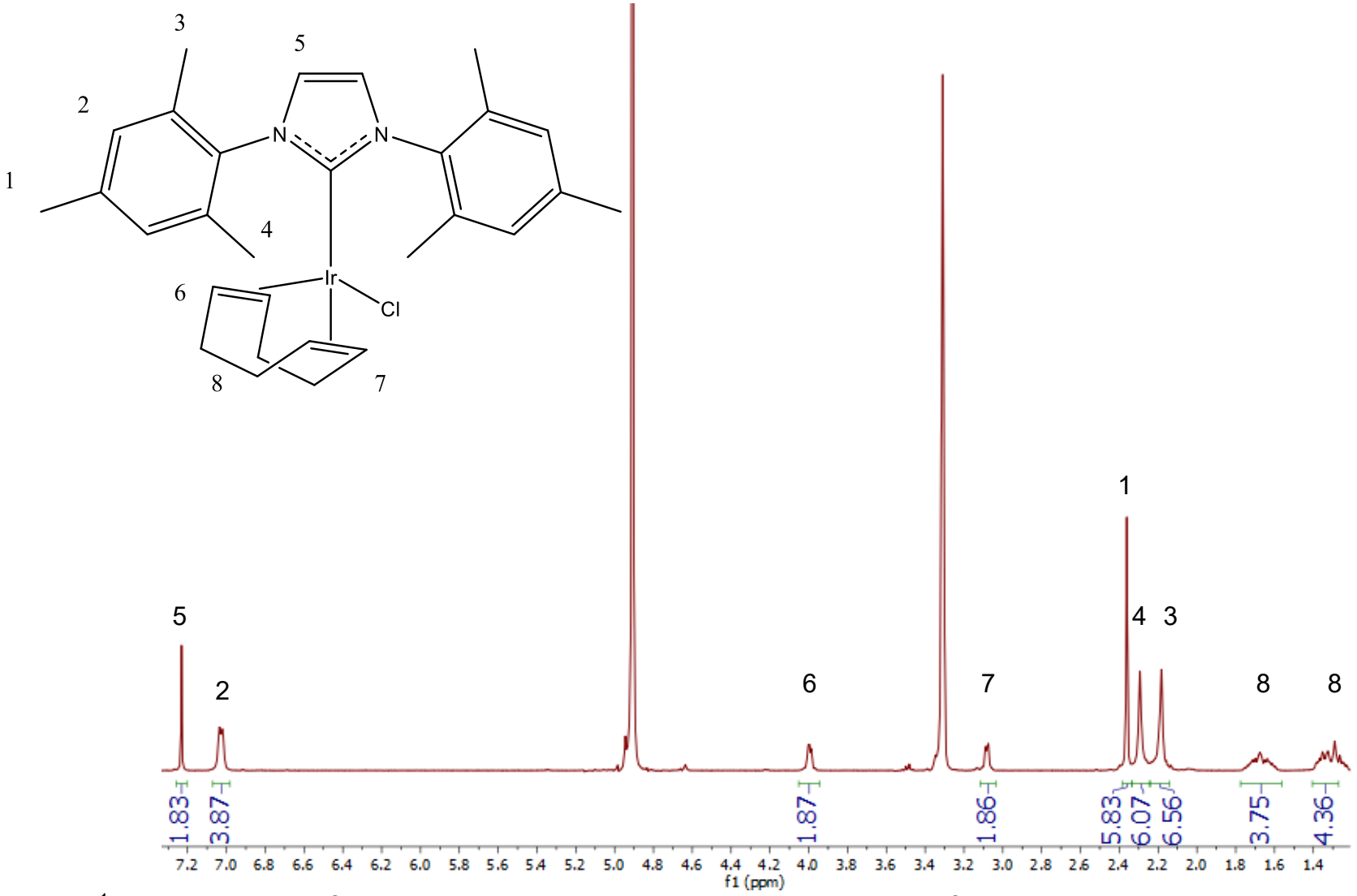


Figure 30. $^{1}$H NMR spectrum of **4** in $d_4$-methanol and species in solution responsible for proton environments.

Table 3. $^{1}$H NMR assignments of **4** from Figure 30.

| $^{1}$H environment | ppm | Multiplicity |
|---|---|---|
| 1 | 2.36 | s |
| 2 | 7.03 | d, *J*= 6.46 Hz |
| 3 | 2.18 | s |
| 4 | 2.29 | s |
| 5 | 7.23 | s |
| 6 | 4.02 - 3.97 | m |
| 7 | 3.11 - 3.05 | m |
| 8 | 1.67 + 1.33 | m |

The $^{1}$H NMR spectrum of the complex **4** in solution is shown in Figure 30. The splitting of environments 3 and 4 suggests that the imidazole N-C bonds may not rotate freely, leading to the methyl environments being in different rotational environments. This rotational difference is represented to a lesser extent by the splitting of environment 2, resulting in a peak that appears as a doublet due to two very similar, but distinct, rotational environments. The cyclooctadiene ligand contributes four peaks in total in the $^{1}$H spectrum, two downfield peaks at 4.00 and 3.08 ppm respectively closest to the iridium $\eta^4$ COD bonds and two up-field aliphatic environments with complex splitting around the cyclooctadiene ring which are present at 1.67 and 1.33 ppm.

### 3.2.2. Rh(IMes)(COD)Cl]

The rhodium analogue, [Rh(IMes)(COD)Cl] (**6**) was then synthesised following the same scheme as shown within Figure 29, however, replacing $[Ir(COD)Cl]_2$ with $[Rh(COD)Cl]_2$ (**5**, 50% yield based on anhydrous mass of $RhCl_3$) to produce [Rh(IMes)(COD)Cl]. This reaction yielded 88% product, which is comparable to the 71% recorded for the iridium analogue and the difference is likely due to losses during purification, making use of silica gel chromatography.

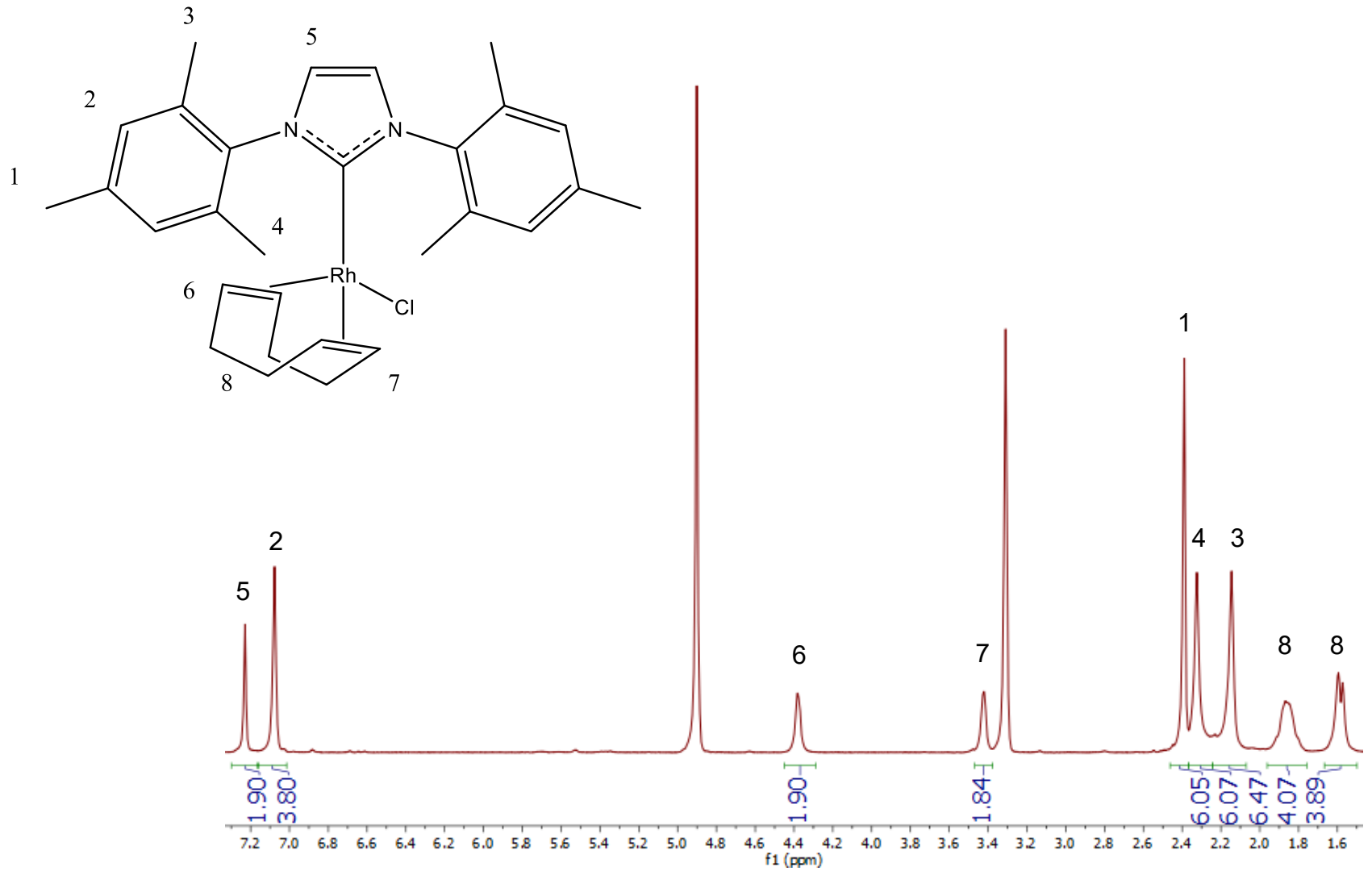


Figure 31. $^{1}$H NMR spectrum of **6** and species in solution responsible for proton environments.

Table 4. $^{1}$H NMR assignments of **6** from Figure 31.

| $^{1}$H environment | ppm | Multiplicity |
|---|---|---|
| 1 | 2.39 | s |
| 2 | 7.08 | s |
| 3 | 2.32 | s |
| 4 | 2.16 | s |
| 5 | 7.23 | s |
| 6 | 4.41 - 4.35 | m |
| 7 | 3.45 – 3.40 | m |
| 8 | 1.86 + 1.58 | m |

The $^{1}$H NMR spectra of **4**, shown in Figure 30, and of **6**, shown in Figure 31, as expected both structures demonstrate similar environments for the carbene backbone. While the spectrum of **6** shown in Figure 31 has the same peaks present as the analogous iridium system shown in Figure 30, the peak locations are generally shifted downfield by between 0.03 and 0.38 ppm, with the greatest shifts being present for the COD environments closest to the metal. The only exception to this trend is environment 4 that has slightly shifted up field, suggesting this methyl is furthest from the rhodium. The general trend of downfield shifting when iridium is replaced with rhodium is due to the latter possessing a higher electronegativity, leading to reduced electron density in the surrounding environments.[111] In general, however, the two complexes are highly comparable, facilitating the testing of **6** as a potential SABRE polarisation transfer pre-catalyst with comparison to the well reported iridium system.

## 3.3. Catalyst Activation

In order to function as a polarisation transfer catalyst for SABRE, the metal complexes must be capable of reversibly binding a substrate of interest. To facilitate this, the substrate must be capable of displacing chlorine within the

complex and have an observable exchange on the NMR timescale. The assessment of these parameters for **4** and **6** is reported within this section.

### 3.3.1. Chlorine displacement

Following the addition of 5 equivalents of pyridine to **6**, displacement of the chloride ion may be observed as bound peaks for pyridine are visible. The integration of these peaks demonstrates they are in a ratio of 4:1 free to bound, which is suggestive of a singular pyridine bound to the rhodium. The displacement of the chlorine is expected as this is the most labile of the previously bound ligands. However, this is further confirmed by minimal changes within the COD and IMes environments which were already present within **6**. The main change is the appearance of a new set of peaks that, upon interrogation by correlation spectroscopy (COSY), are shown to cross correlate. These peaks are due to COD now being in a different environment within the rhodium pyridine complex with Rh $\eta^4$ COD bound peaks now appearing at 3.71 and 3.87 ppm. Interestingly, COD environments for **6** are still present in a ratio of 35:65 suggesting that pyridine has only displaced chlorine in roughly two thirds of potential complexes.

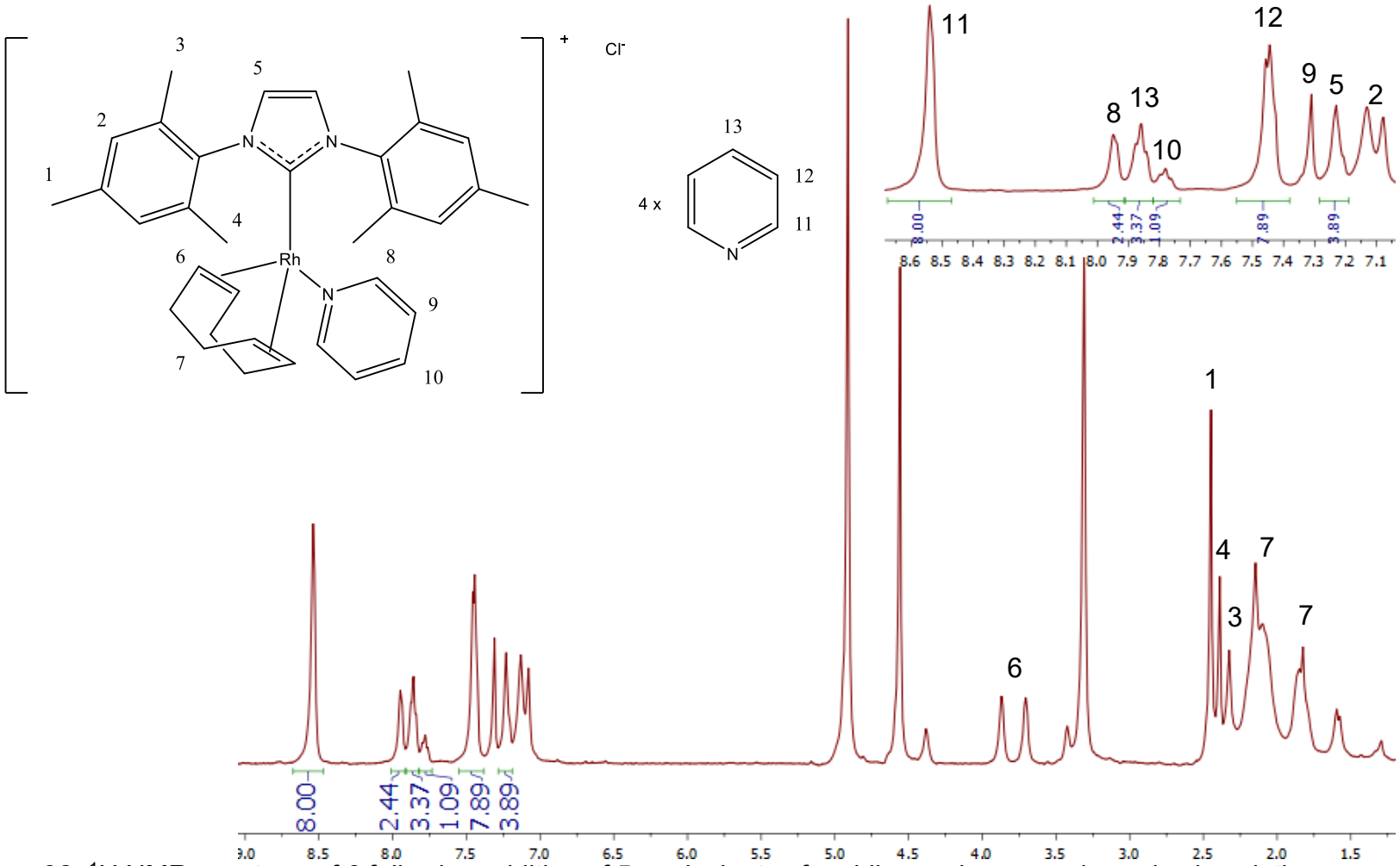


Figure 32. $^{1}$H NMR spectrum of **6** following addition of 5 equivalents of pyridine and proposed species in solution responsible for proton environments.

Table 5. $^{1}$H NMR assignments of **6** and pyridine from Figure 32.

| **$^{1}$H environment** | **ppm** | **Multiplicity** |
|---|---|---|
| 1 | 2.45 | s |
| 2 | 7.08 | s |
| 3 | 2.32 | s |
| 4 | 2.39 | s |
| 5 | 7.31 | s |
| 6 | 3.71 + 3.87 | m |
| 7 | 2.15 + 1.82 | m |
| 8 | 7.94 | d, *J*=4.95 Hz |
| 9 | 7.23 | t, *J*=3.37 Hz |
| 10 | 7.78 | tt, *J*=7.73, 1.55 Hz |
| 11 | 8.53 | d, *J*=4.32 Hz |
| 12 | 7.44 | t, *J*=5.88 Hz |
| 13 | 7.86 | tt, *J*=7.71, 1.71 Hz |

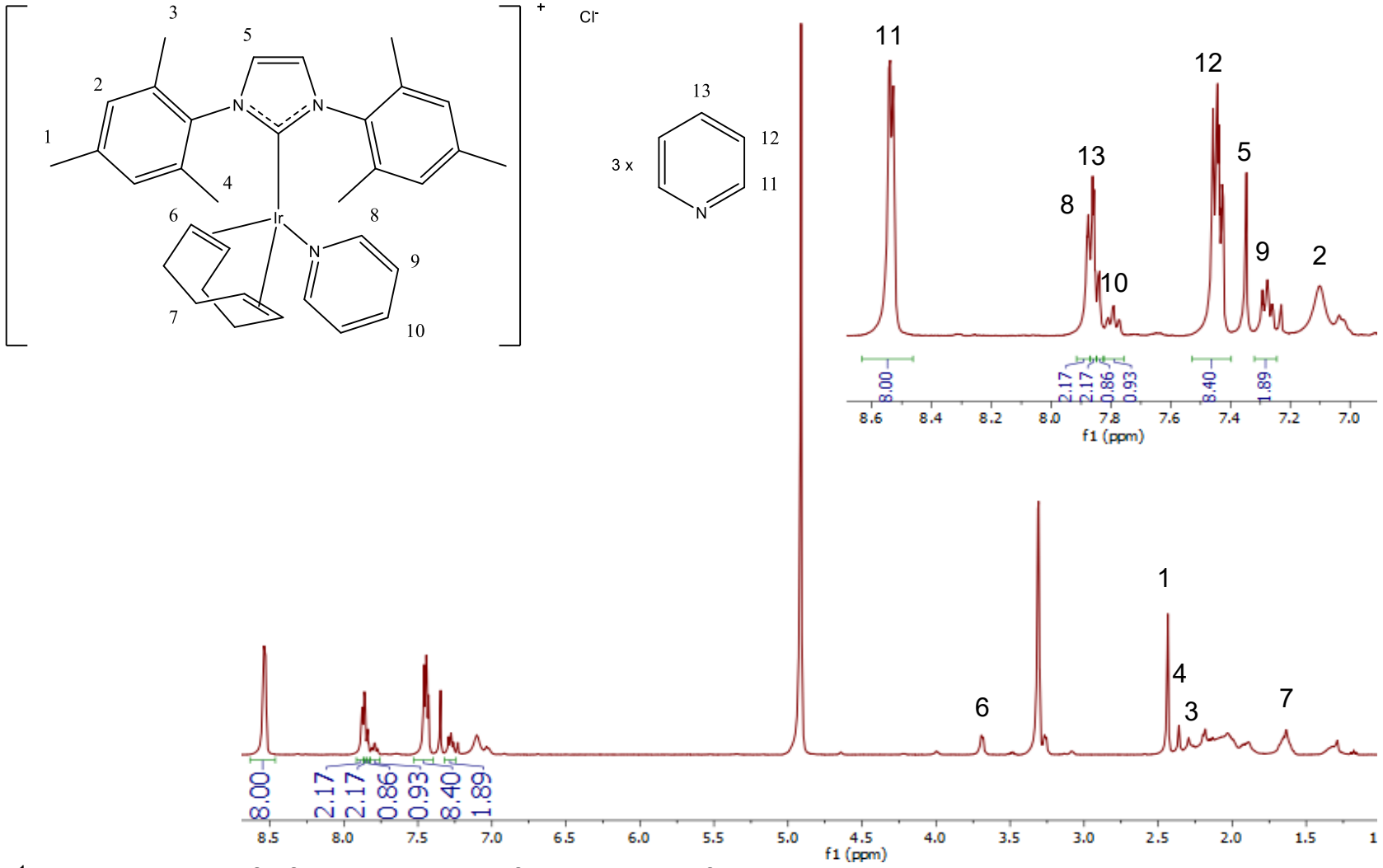


Figure 33. $^{1}$H NMR spectrum of **4** following addition of 4 equivalents of pyridine and proposed species in solution responsible for proton environments.

Table 6. $^{1}$H NMR assignments of **4** and pyridine from Figure 33.

| $^{1}$H environment | ppm | Multiplicity |
|---|---|---|
| 1 | 2.43 | s |
| 2 | 7.07 | s |
| 3 | 2.29 | s |
| 4 | 2.36 | s |
| 5 | 7.35 | s |
| 6 | 3.69 + 3.26 | m |
| 7 | 1.64 | m |
| 8 | 7.88 | m |
| 9 | 7.28 | ddt, *J*=1.57, 4.95, 6.58 Hz |
| 10 | 7.79 | tt, *J*=1.56, 7.69 Hz |
| 11 | 8.53 | dd, *J*=1.87, 4.34 Hz |
| 12 | 7.44 | ddt, *J*=1.54, 4.57, 5.95 Hz |
| 13 | 7.86 | tt, *J*=1.83, 3.51 Hz |

Addition of an excess of pyridine (4 equivalents) to **4** results in displacement of the chloride ion by pyridine similar to that within the analogous rhodium system with 3 equivalents remaining free in solution. The iridium complex demonstrates significantly higher degrees of spectral overlap within the aromatic region that makes accurate peak integration more challenging. However, both free and bound pyridine environments may be assigned both due to chemical shift and splitting patterns. The iridium system appears to possess a weaker metal-chloride bond that results in a higher ratio of iridium possessing a bound pyridine, determined by the COD environment associated with this species. Under the same conditions the pyridine bound proportion has increased from 65% within the rhodium system to 86% within the iridium analogue. This trend of stronger chloride binding is in general agreement with

lower yields obtained when insertion of $SnCl_2$ occurs across a Rh-Cl bond compared to an Ir-Cl bond.[112]

With both the Rh and Ir species demonstrating the ability for a substrate such as pyridine to displace the chloride and form the general species $[M(IMes)(COD)Py]^+$, the first steps towards a SABRE active species have been demonstrated. However, crucially, both complexes need to form hydrides and demonstrate reversible exchange of the substrate and hydrides in order to be viable SABRE polarisation transfer catalysts.

### 3.3.2. Pyridine Exchange

The ability of the complexes $[M(IMes)(COD)Py]^+$ to exchange pyridine at room temperature was investigated as this would be the temperature regime where most practical applications of SABRE would be desirable. EXSY was utilised to interrogate the bound pyridine peaks and observe any transitions from the bound complex to free within solution for a range of mixing times up to 5 seconds.

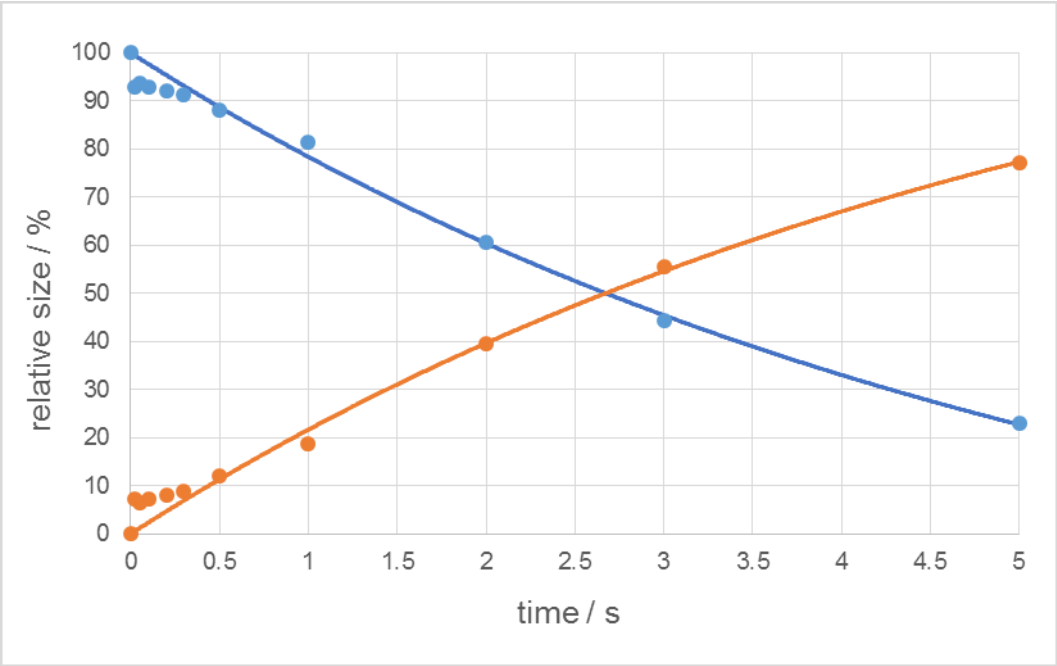


Figure 34. Relative integrals of excited bound (blue) and free (orange) pyridine within $[Rh(IMes)(COD)Py]^+$ over a 5 second period at 295 K, interrogated by EXSY.

Interestingly, no pyridine dissociation was observed for $[Ir(IMes)(COD)Py]^+$ at 295 K, suggesting this complex is more stable than the rhodium analogue which did demonstrate pyridine exchange. Figure 34 demonstrates the conversion of excited bound (blue) and free (orange) pyridine within $[Rh(IMes)(COD)Py]^+$ following selective excitation of the bound *ortho* peak at 7.94 ppm. This determined the rate of pyridine dissociation at 295 K to be 0.2415 ± 0.0056 $s^{-1}$. This demonstrates that pyridine exchange occurs, however, this rate is still exceptionally slow when compared to literature reports of SABRE active species. For comparison, at 295 K, Duckett *et al.* have reported the exchange rate of pyridine within the commonly utilised iridium complex $[Ir(IMes)(Py)_3(H)_2]^+$ to be 23 $s^{-1}$.[28]

## 3.4. Hydride formation

As SABRE requires both substrate and hydride exchange for polarisation transfer from the singlet state of *para*hydrogen, the ability for the complex to form *para*hydrogen derived hydrides is essential. Now $[Rh(IMes)(COD)Py]^+$ has demonstrated the ability to exchange the pyridine substrate, albeit slowly, the ability of this complex to form hydrides was then probed.

### 3.4.1. Hydrogen Addition

As previously discussed in 3.3.1, for SABRE to occur exchangeable metal hydride species must form which are capable of breaking the symmetry of *para*hydrogen and, thus, enabling SABRE hyperpolarisation. To that end, hydrogen was added to the samples characterised within Figure 32 and Figure 33 and the resulting hydride region is shown in Figure 35.

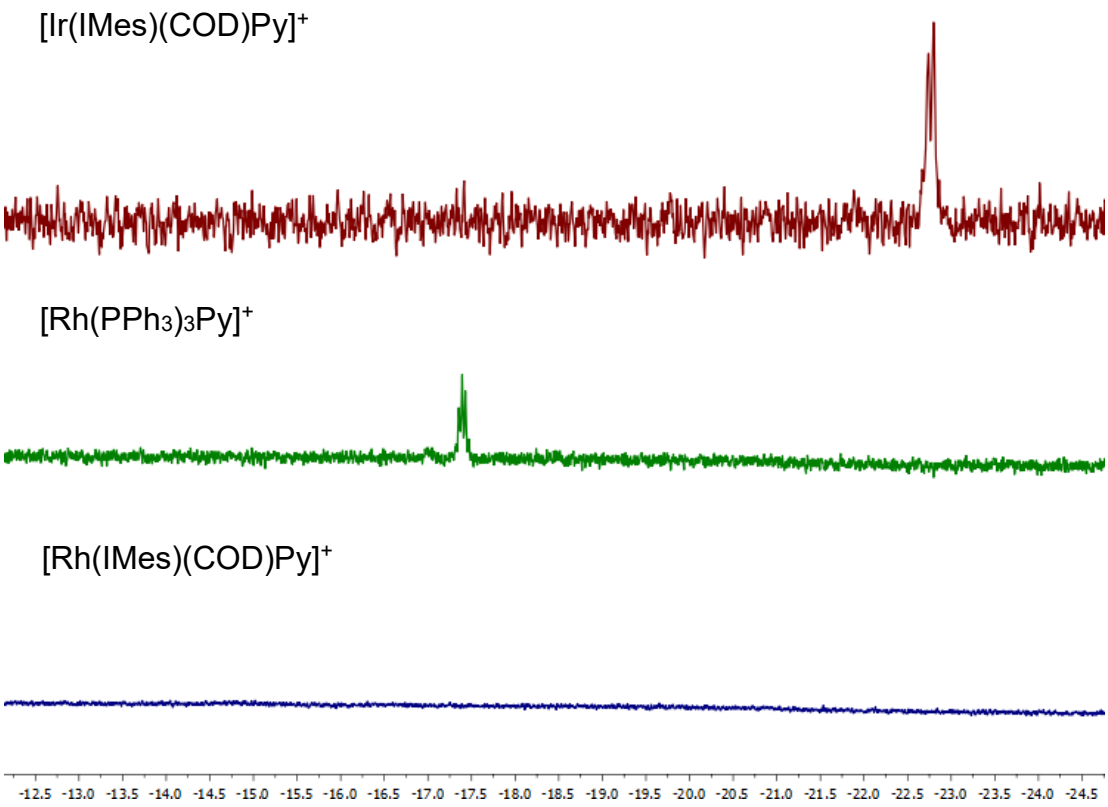


Figure 35. $^{1}H$ NMR spectra of the hydride regions following the addition of $H_2$ to [Ir(IMes)(COD)(Py)], $[Rh(PPh_3)_3Py]$ (Wilkinson's catalyst) and [Rh(IMes)(COD)Py] respectively.

For $[Ir(IMes)(COD)Py]^+$, addition of $H_2$ resulted in the formation of $[Ir(IMes)(Py)_3(H)_2]^+$ for which hydrides are visible at -22.82 ppm in addition to a hydride due to the complex $[Ir(IMes)(Py)_3(H)(D)]^+$ being observed at -22.76 ppm. These are very similar to the values reported by Duckett *et al.* for this complex.[28] Unfortunately, under the same conditions, no hydrides were observed for the rhodium analogue. In addition, while the hydrogenation of COD is visible in the form of transient peaks briefly observed at ~-12 to -17 ppm within the $^{1}H$ NMR spectrum following $H_2$ addition to the iridium system, this is not observed within rhodium. Even varying the ligand identity to 3-fluoropyridine does not yield visible hydrides or evidence of the complex changing upon addition of $H_2$. $^{19}F$ NMR spectra of a sample containing $[Rh(IMes)(COD)3\text{-fluoropyridine}]^+$ do not show variation within the free/bound peaks of 3-fluoropyridine following addition of *para*hydrogen. Additionally, after several days, no evidence of HD scrambling was observed with the rhodium

complex. This is typically observed when both a hydride and solvent adduct are present within the complex and deuterium transfer may occur. This was observed for $[Ir(IMes)(Py)_3(H)_2]^+$ as the complex $[Ir(IMes)(Py)_2(d_4\text{-methanol})(H)_2]^+$ is formed as a minor component which may facilitate HD scrambling.

The formation of rhodium hydrides was not observed following the addition of a reducing agent such as $NaBH_4$, despite HD being observed in solution directly following the addition of sodium borohydride. Subsequent, degassing and refilling the Young's NMR tube with fresh $H_2$ eliminated the presence of HD and it was not regenerated over several days. The initial HD was, therefore, attributed to a reaction of $NaBH_4$ with the deuterated methanol solvent, resulting in the formation of HD and MeONa, rather than activity around the rhodium, particularly in the absence of visible rhodium hydrides.

The formation of hydrides when pyridine (4 equivalents) and $H_2$ were added to Wilkinson's catalyst, $[Rh(PPh_3)_3Cl]$ was also investigated as this was one of the few rhodium species which has been reported to form a dihydride species at room temperature and, therefore, has been utilised for PHIP.[105] This formed a species that demonstrates a hydride at -17.39 ppm with evidence of at least one $PPh_3$ ligand still being within the coordination sphere of rhodium as deduced from the $^{31}P$ coupling of 14.76 Hz within the hydride signal.

### 3.4.2. Temperature study

As no hydride ligands were formed when $H_2$ was added to $[Rh(IMes)(COD)Py]^+$ at room temperature, the potential of this complex being suitable to facilitate polarisation transfer for SABRE is low. Despite low temperatures typically being utilised to form stable rhodium dihydride species, the necessary exchangeable nature of the hydrides for SABRE meant that a transient species potentially obtained at a higher temperature regime may suffice for the lifetime required for polarisation transfer. Further to this, the low substrate exchange speeds measured within 3.3.2 suggested that cooling of the system, even if a hydride was generated, would exclude SABRE activity as substrate exchange would proceed too slowly, if at all. Therefore,

[Rh(IMes)(COD)Py]$^+$ under $H_2$ was heated and the hydride region observed as shown in Figure 36.

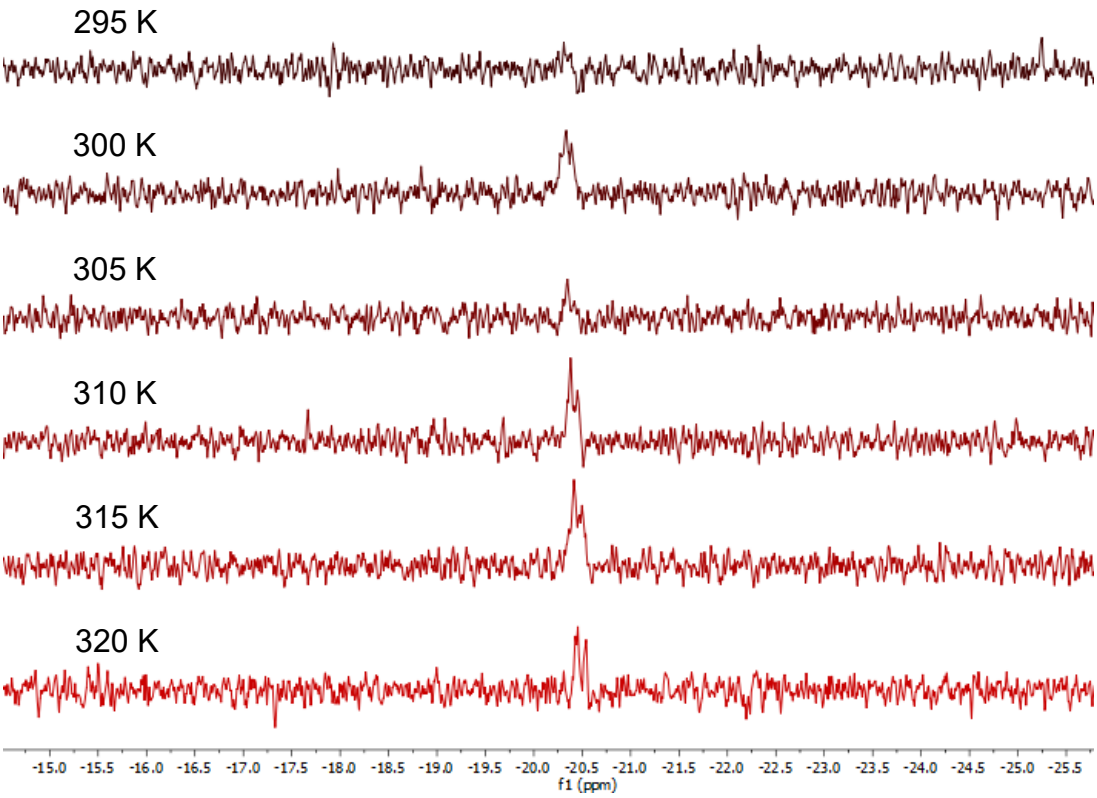


Figure 36. $^1$H NMR spectra of the hydride region of [Rh(IMes)(COD)Py]$^+$ after addition of $H_2$ at the temperatures noted. Spectra are 32 scan collections with a relaxation delay of 5 seconds.

At higher temperatures a minor hydride species was observed, however, a concurrent bound peak in the $^{19}$F NMR spectrum was not observed when [Rh(IMes)(COD)(3-fluoropyridine)]$^+$ was investigated. This is suggests that a transient hydride containing species was present within solution or that the hydride containing complex did not contain the substrate. For instance, this hydride may be due to an exchangeable methanol adduct rather than a substrate containing species. Unfortunately, due to the low concentrations observed it is not practical to fully characterise this hydride species and the associated complex. Examination of [Rh(IMes)(COD)Py]$^+$ was repeated in deuterated toluene, similar to the examination of hydrides within dichloromethane discussed within 3.1.2, in order to access a wider

temperature range. However, no hydride formation was observed in this aprotic solvent, supporting the supposition hydrides may be due to a methanol adduct containing species.

## 3.5. SABRE using rhodium-based catalysts

Rhodium-based catalysts, namely Wilkinson's catalyst and **6**, were investigated as potential SABRE pre-catalysts. These were compared to **4**, an established pre-catalyst for use with SABRE.

When Wilkinson's catalyst was utilised with 4 equivalents of pyridine under *para*hydrogen no SABRE was observed, even when the polarisation transfer field was changed to 65 G from earth's field. Given that Wilkinson's demonstrates room temperature hydrides when in the presence of pyridine this lack of activity suggests that the hydride species or pyridine species do not exchange. Unfortunately, due to the high number of aromatic environments present within $^{1}H$ NMR due to the presence of $PPh_3$, examination of the pyridine binding and exchange is challenging. Therefore, 3-fluoropyridine was utilised so that $^{19}F$ observation may allow insight into substrate binding and exchange. Utilising 3-fluoropyridine as a $^{19}F$ containing probe, chlorine displacement is observed (shown in Figure 37) through the presence of a new bound signal at -122.73 ppm compared to free at -126.48 ppm. This bound signal demonstrates chlorine displacement and subsequent substrate binding has occurred for ~33% of the Wilkinson's complexes within the sample (4 equivalents of 3-fluoropyridine are utilised).

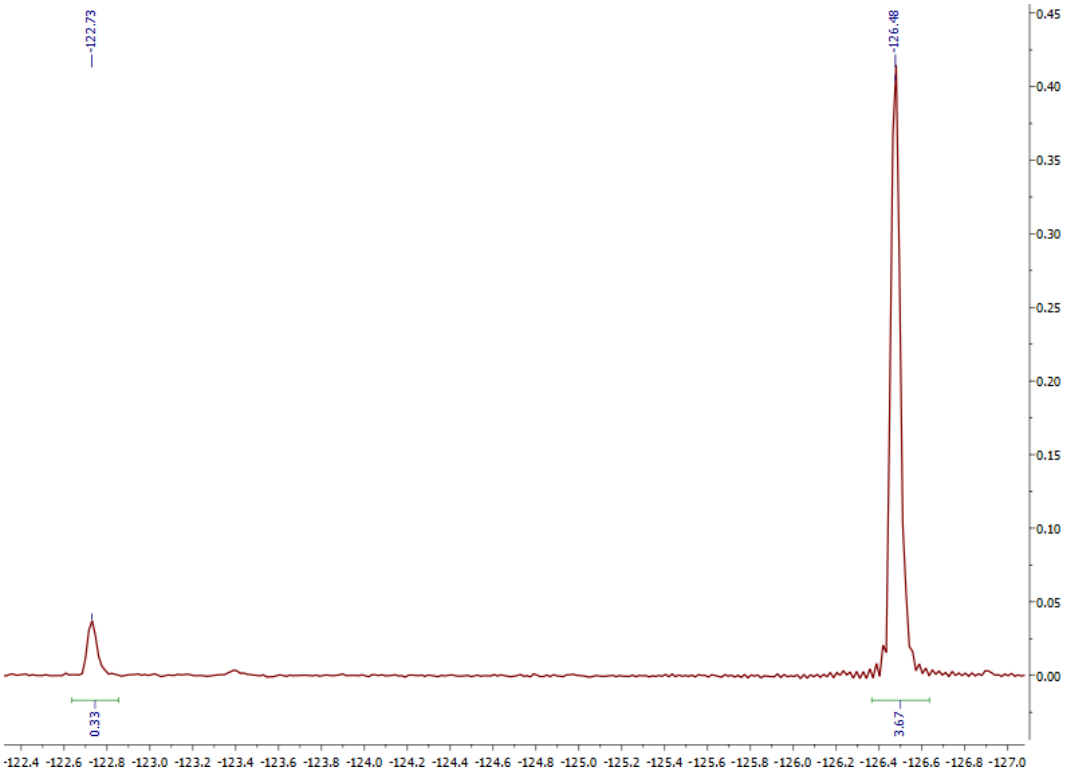


Figure 37. $^{19}F$ NMR spectrum of bound (-122.7 ppm) and free (-126.5 ppm) peaks for Wilkinson's catalyst when 4 equivalents of 3-fluoropyridine were utilised.

When **6** was utilised as a pre-catalyst in combination with *para*hydrogen and pyridine or 3-fluoropyridine this system did not display SABRE activity at room temperature. However, this is unsurprising given the lack of observed hydrides within this temperature regime. Given the low-level (~8% relative to the concentration of $[Rh(IMes)(COD)Py]^+$) hydrides observed at higher temperatures and that the pyridine exchange rate is likely to be increased at higher temperatures, this system was investigated further at higher temperatures. A Young's capped NMR tube containing 4 equivalents of pyridine relative to **6** under 3 bar of *para*hydrogen was heated to 50°C and SABRE attempted. Unfortunately, even at 50°C, no SABRE was observed making use of **6** and pyridine.

Attempts to perform SABRE utilising rhodium complexes with a varied carbene were also attempted to see if a small change in ligand identity may facilitate SABRE through attenuation of the substrate and hydride exchange rates.

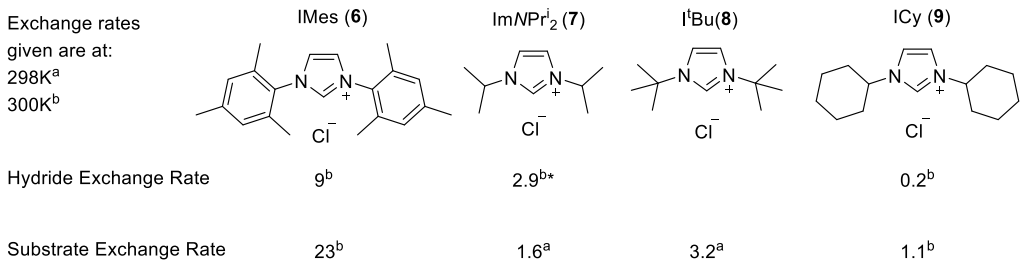


Figure 38. Carbenes utilised in further testing of rhodium complexes. Exchange rates noted are for [Ir(Carbene)(Pyridine)$_3$(H)$_2$] at the temperatures noted.[28, 113] *Hydride data is for ImMe$_2$*N*Pr$^i_2$. Compound numbers are reflective of [Rh(Carbene)(COD)Cl].

It was desired that changing the identity of the carbene may aid stabilisation of the complex as the carbenes utilised have all been reported to result in slower hydride and substrate exchange compared to IMes, as shown in Figure 38, when utilised within an iridium system with pyridine as the substrate. Unfortunately, testing of complexes [Rh(Im*N*Pr$^i_2$)(COD)Cl] (**7**), [Rh(I$^t$Bu)(COD)Cl] (**8**) and [Rh(ICy)(COD)Cl] (**9**) demonstrated the same result with pyridine being capable of displacing chlorine, however, no visible hydrides were observed at room temperature and no SABRE observed when pyridine was utilised as the substrate.

## 3.6. Conclusion

A range of rhodium complexes have been synthesised and **6** has been characterised for direct comparison with the literature standard SABRE catalyst **4**.

For SABRE to occur reversible exchange of both substrate and hydrides must occur. It has been demonstrated that in both IMes-containing complexes chlorine may be displaced by the most commonly utilised SABRE substrate, pyridine, and the exchange rate of pyridine has been measured to be 0.2415 ± 0.0056 s$^{-1}$ for the rhodium complex [Rh(IMes)(COD)Py]$^+$. This exchange rate could feasibly be increased by increasing the pyridine equivalents present as observed by Manoury *et al.* and discussed in 3.1.1.3.[108] However, COD hydrogenation is not observed and hydrides do not readily form for **6**, with variable temperature interrogation demonstrating only trace hydride presence

at elevated temperatures. Attempting to conduct SABRE utilising **6** as the pre-catalyst did not demonstrate SABRE activity at room temperature or 50°C where minor hydrides appear to be present. The disappearance of these transient hydrides and lack of associated polarisation suggests a methanol adduct containing species may be responsible for these hydrides. It was hoped that tuning the system to facilitate slower ligand/hydride exchange through the variation of the carbene present, such as **7**, **8** and **9**, would facilitate SABRE, however no SABRE or hydrides were observed at room temperature for these pre-catalysts.

# 4. Applications of SABRE to $^{19}F$

## 4.1. Introduction

Signal amplification by reversible exchange (SABRE) has previously been applied to heteroneclei such as $^{15}N$ and $^{31}P$ but the high gyromagnetic ratio of $^{19}F$ (94% compared to proton) and its 100% natural abundance means that this nucleus presents an attractive prospect for MR studies.[65] This will be explored in this chapter.

### 4.1.1. Biological relevance of $^{19}F$ from an applications prespective

$^{19}F$ is particularly attractive for *in vivo* imaging applications as there is minimal biological background signal as mobile physiological $^{19}F$ concentrations are typically below the detection limits (typically under $10^{-3}$ μmol/g wet tissue weight).[115] Higher concentrations of $^{19}F$ are present in bones and teeth, however these immobilized phases exhibit very short spin-spin ($T_2$) relaxation times which mean they are not typically visible in clinical MRI. Conveniently, the similar gyromagnetic ratio of $^{19}F$ compared to $^{1}H$ means $^{19}F$ can be measured with most existing MRI instruments after appropriate tuning of the RF coils.[116] The potential advantages of $^{19}F$ MRI has led to an increase in publications within this field in the last decade,[117] within this literature there have been efforts to overcome the inherent insensitivity of magnetic resonance techniques through the incorporation of multiple $^{19}F$ atoms in the same environment, particularly in perfluorocabons.[118-123]

In 2010 it was calculated that 20% of approved drugs contain fluorine, with several structures already suitable for SABRE without modification, such as ripasudil and voriconazole.[124] The advantages of $^{19}F$ for clinical applications has led to the development of a range of $^{19}F$ containing contrast agents, which are already detectable at millimolar levels when thermally polarised.[66] It is hoped that hyperpolarisation techniques such as SABRE could potentially lower this detection limit by an order of magnitude. Indeed, developing the

applications of $^{19}F$ SABRE to biologically relevant molecules has been highlighted in recent reviews of the field as a suggested focus for the field.[5]

### 4.1.2. Literature applications of SABRE to $^{19}F$

The application of SABRE to fluorinated molecules was first demonstrated by Duckett *et al.* in their 2009 initial report of SABRE.[21] This paper demonstrated $^{19}F$ hyperpolarisation of 3-fluoropyridine, with the reported spectrum being characterised by a complicated antiphase multiplet, shown in Figure 39, that is enhanced relative to a thermal spectrum.

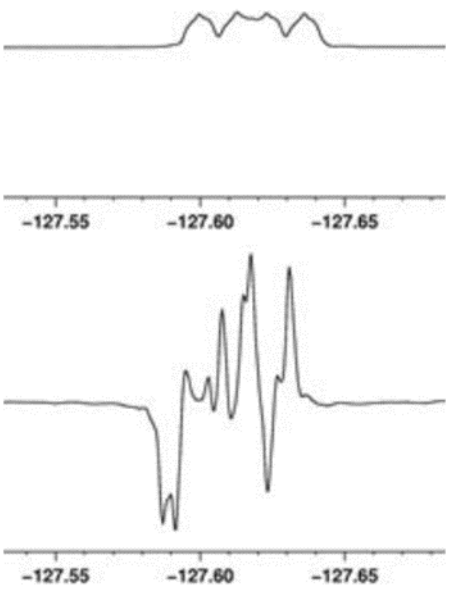


Figure 39. $^{19}F$ NMR spectra of 3-fluoropyridine collected under thermal (top) and SABRE hyperpolarised (bottom) conditions.[21]

This antiphase multiplet was most likely due to $^{19}F$-$^{31}P$ coupling between the substrate and the spin transfer pre-catalyst, in this case [Ir(COD)($PCy_3$)(MeCN)][$BF_4$]. It has been proposed that polarisation transfer occurs *via* a coupling system with $J_{HF}$ being commensurate to $J_{HH}$. If this is the case then it is likely that a range of fluorine containing substrates could be hyperpolarised.

Eshuis *et al.* included 3-fluoropyridine within a mixture of potentially SABRE active substrate species in a 2015 report, however, the SABRE hyperpolarised

spectrum was not sufficiently resolved to observe $^{1}$H hyperpolarisation of this substrate in this report, and no $^{19}$F spectra are included within this paper.[125]

During the course of this work Theis and co-workers have demonstrated $^{19}$F polarisation of 3-fluoropyridine to give a polarisation level of ~0.3% (compared to ~50% demonstrated for proton).[45, 68] Though Theis notes that only 50% *para*hydrogen was used, if 100% had been used this could lead to an effective polarisation of ~0.85%. Recent work, aiming to quantify the effect of *para*hydrogen enrichment on substrate polarisation, supports this estimate as for a range of substrates, catalysts and fields there was a ~3 times increase in signal when 99% enriched *para*hydrogen was used compared to 50%.[37] However, it is worth noting that this report only makes use of $^{1}$H SABRE to quantify the polarisation changes with *para*hydrogen enrichment.

While it is noted this polarisation is significantly lower than $^{1}$H and other heteronuclei, such as $^{15}$N,[51] it is hypothesised that this is due to the significantly lower $T_1$ of $^{19}$F leading to signal loss during sample transfer prior to magnetisation read-out.

The large chemical shift range of $^{19}$F was noted as a further advantage of heteroneuclei SABRE as Theis *et al.* demonstrate the application of hyperpolarised $^{19}$F to pH detection. This is noted to be similar in capability to $^{15}$N while demonstrating a sensitivity >30 times larger than $^{1}$H NMR for changes in local pH and represents another potentially useful application for SABRE hyperpolarised $^{19}$F containing ligands.[68]

In addition to 3-fluoropyridine, pentafluoropyridine and 2-fluoropyridine were also tested as substrates, however, both failed to demonstrated the SABRE effect. Theis *et al.* suggest the lack of activity and observed hydrides indicative of the formation of the spin transfer species $[Ir(IMes)(L)_3(H)_2]^+$ is likely due to the steric effects of a fluorine in the neighbouring position to the nitrogen binding site. Pentafluoropyridine has been previously reported to be SABRE inactive by Rovedo *et al.* who made use of both [Ir(IMes)(COD)Cl] (**4**) and Crabtrees catalyst in testing this substrate.[67]

The lack of activity for substrates with $^{19}F$ neighbouring the SABRE binding site is consistent with previous literature reports in which picolines and lutidines demonstrated that the inclusion of a methyl substituent in the *ortho* position of a pyridine ring leads to no SABRE activity.[126] Though $^{19}F$ is less bulky than a methyl group it has a larger steric effect than $^{1}H$ typically present next to the substrate binding site.[47, 95, 125, 127, 128]

Despite the examples of picolines and lutidines showing no SABRE activity, a methyl substituent next to the binding site in a substrate has been demonstrated in metronidazole.[29, 73] However, this is a 5-membered ring system, and therefore, the higher internal angle will mean the functionality neighbouring the binding site has a lower steric effect on binding.

Buckenmaier *et al.* additionally reported detecting 3-fluoropyridine, 3,5-*bis*(trifuoromethyl)pyridine and ethyl-5-fluoronicotinic acid making use of a superconducting quantum interference device (SQUID) based detector.[129] In this paper a $^{19}F$ enhancement in excess of 2000 times the thermal signal is reported, when the absolute integral of the hyperpolarised signal is used as both emissive and absorptive signals are present. They note that the polarisation of $^{19}F$ appears to be substrate dependent, with 3-fluoropyridine showing the highest enhancement followed by ethyl-5-fluoronicotinic acid and 3,5-*bis*(trifuoromethyl)pyridine respectively. The polarisation of these substrates at a range of mixing fields is demonstrated in Figure 40 for both $^{1}H$ and $^{19}F$ in each substrate.

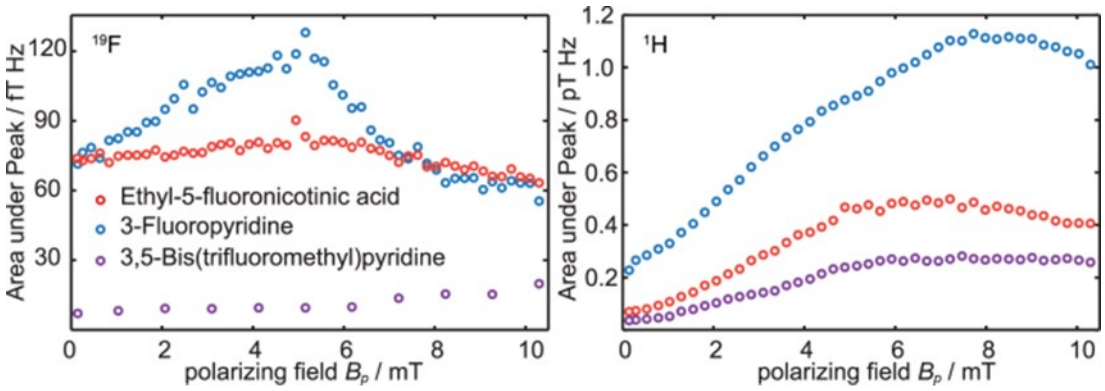


Figure 40. Area under peaks compared to polarisation field for SQUID measurements of ethyl-5-fluoronicotinic acid, 3-fluoropyridine and 3,5-*bis*(trifluoromethyl)pyridine.[129]

The polarisation transfer field is also noted to have an effect on the level of polarisation achieved, with polarisation transfer appearing to favour low fields. Buckenmaier, however, notes that the field dependence effect appears to be far less pronounced for $^{19}$F than $^{1}$H. In particular, the polarisation of 3,5-*bis*(trifuoromethyl)pyridine appears to be independent of the polarisation transfer field – although there is an increase, shown in Figure 40, the authors attribute this to an increase in noise due to the low signal to noise ratio (SNR). Buckenmaier *et al.* also note that the polarisation transfer field yielding the maximum enhancement was different for $^{1}$H and $^{19}$F within the same substrate and field dependent for the monofluorinated substrates even when within a very low polarisation transfer field.[130]

### 4.1.3. SABRE-SHEATH

Theis *et al.* demonstrated that $^{19}$F SABRE of 3-fluoropyridine results in an antiphase signal when conducted at earth's magnetic field. Previous heteronuclei studies have demonstrated this due to intramolecular couplings.[49] An antiphase signal would be less suitable for MR imaging, as a smaller observation window may result in effective observed signal cancellation, partially negating the polarisation gain from SABRE.

Signal amplification by reversible exchange in shield enables alignment transfer to heteronuclei (SABRE-SHEATH) has previously been reported to

optimise polarisation transfer to $^{15}N$, though making use of a very low (μT) polarisation transfer field.[49, 51] This is achieved by introducing *para*hydrogen into the sample within a magnetic shield – Truong *et al.* have presented a theoretical model demonstrating why a near-zero field is effective for polarisation transfer.[51] They note that in a system where $J_{HH}$ dominates the J coupling terms, several resonance conditions are fulfilled simultaneously for a heteronuclear SABRE-SHEATH system and estimate that for a $^{15}N$ system the optimal transfer field will be ~ 0.26 μT (assuming a value of ~9 Hz for $J_{HH}$). Rayner *et al.* agree with this figure, suggesting an approximate transfer field of 0.2 - 0.4 μT is the optimum transfer field when a $^{2}J_{HX}$ scalar coupling is used to optimise polarisation transfer to a hetronucleus bound directly to the spin transfer catalyst.[86] However, Truong *et al.* note that although PHIP requires the spin optimisation conditions to be met precisely, this is not the case for SABRE.[51] They note the exchanging of *para*hydrogen derived hydrides, typically several times a second, means that the optimal transfer field has a reduced effect due to the low residence time of the hydride within the J-coupling network responsible for polarisation transfer around the SABRE catalyst. Truong *et al.* conclude that, so long as the actual transfer field is commensurate in order with that of the optimal field, an effective polarisation transfer will take place.[51]

## 4.2. Results

### 4.2.1. Context of work

When this project was conceived the only literature report at the start of this study was a single spectrum published in 2009 for 3-fluoropyridine,[21] though, during the course of this work, two reports expanded upon this first report before the publication of the work presented in this results section.[68, 129] The work presented in this chapter contributed to the publication 'Extending the scope of $^{19}F$ hyperpolarization through Signal Amplification by Reversible Exchange in MRI and NMR Spectroscopy'.[96]

### 4.2.2. Initial Testing

Pyridine (**L1**) has been used as a benchmark ligand for SABRE testing in previous publications, therefore, several fluorinated pyridine derivatives were chosen as substrates for the initial testing of $^{19}F$ SABRE; these are shown alongside their $pK_a$ in Figure 41 (with pyridine included for reference).

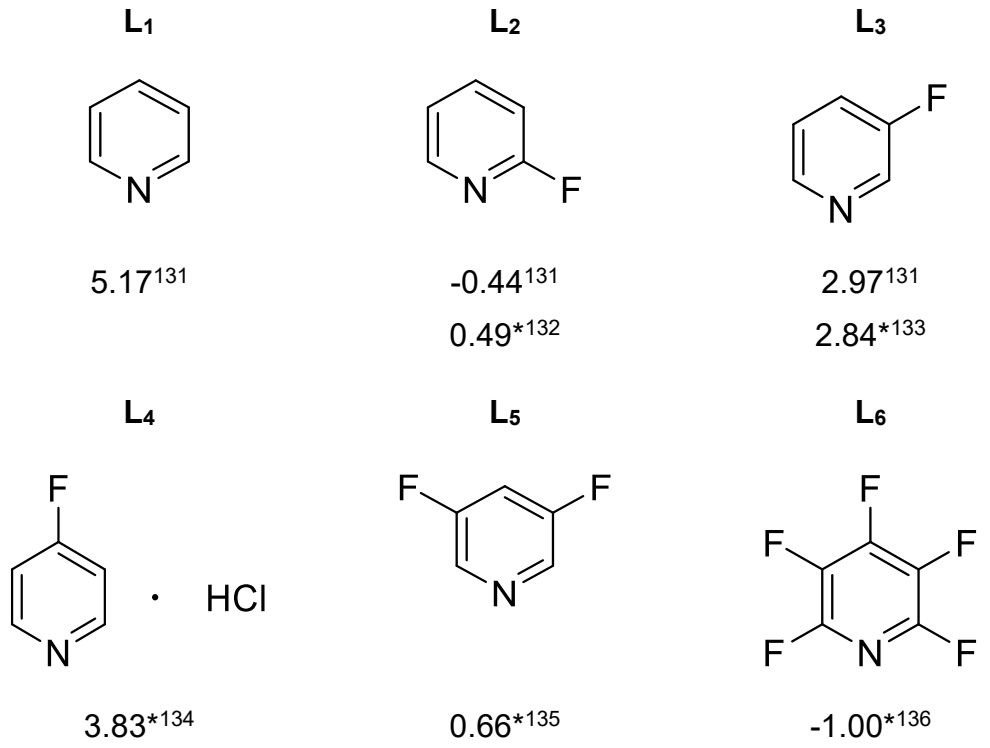


Figure 41. Initial substrate scope for the application of SABRE to $^{19}F$ with $pK_a$ data where available. As $pK_a$ data was not available for all substrates, the chloropyridine analogue $pK_a$ values are shown, denoted by an *.

The substrates were tested in a range of concentrations relative to the pre-catalyst **4** used for all measurements. These concentrations were 4, 10 and 20 equivalents relative to the catalyst in order to provide between a 1 and 17 fold excess due to the formation of $[Ir(IMes)(L)_3(H)_2]^+$.

In the case of **L4** the freebase could not be isolated under conditions suitable for SABRE testing. This is likely due to self reaction to give *N*-(4'-pyridyl)-4-fluoropyridinium fluoride which may hydrolyze to *N*-(4'-pyridyl)-4-pyridone, as shown in Figure 42.[137]

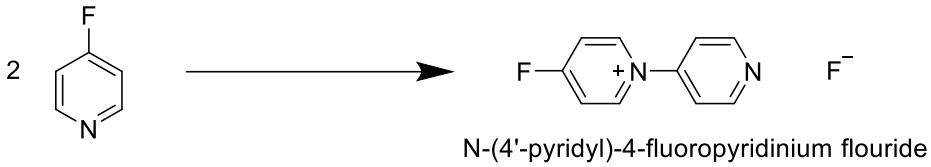


Figure 42. Self reaction of **$L_4$** to form *N*-(4'-pyridyl)-4-fluoropyridinium fluoride.

*N*-(4'-pyridyl)-4-fluoropyridinium fluoride was found not to be suitable for SABRE due to its formation as a salt inhibiting binding to **4** in order to form the SABRE active species. Addition of **$L_4$** to **4** under $H_2$ resulted in no bound signals in the $^{19}F$ NMR spectrum which were observed for other ligands. Therefore, the testing for **$L_4$** was not carried out. All other ligands were tested with an excess of between 1 and 17 times relative to $[Ir(IMes)(L)_3(H)_2]^+$.

In the case of $^1H$ NMR SABRE for substrates **$L_2$** and **$L_3$**, the distinction between *ortho* and *para* environments signal enhancement is difficult to separate due to the collection of NMR spectra on a 1.4 T instrument, therefore this is labelled as 'downfield'.

Enhancements have been calculated as detailed in section 8.3.1. Due to the antiphase nature of some of the resulting spectra, magnitude mode has been used to prevent internal cancellation of the enhancement integral due to mixed phasing. A comparison between unprocessed and magnitude is shown in Figure 43.

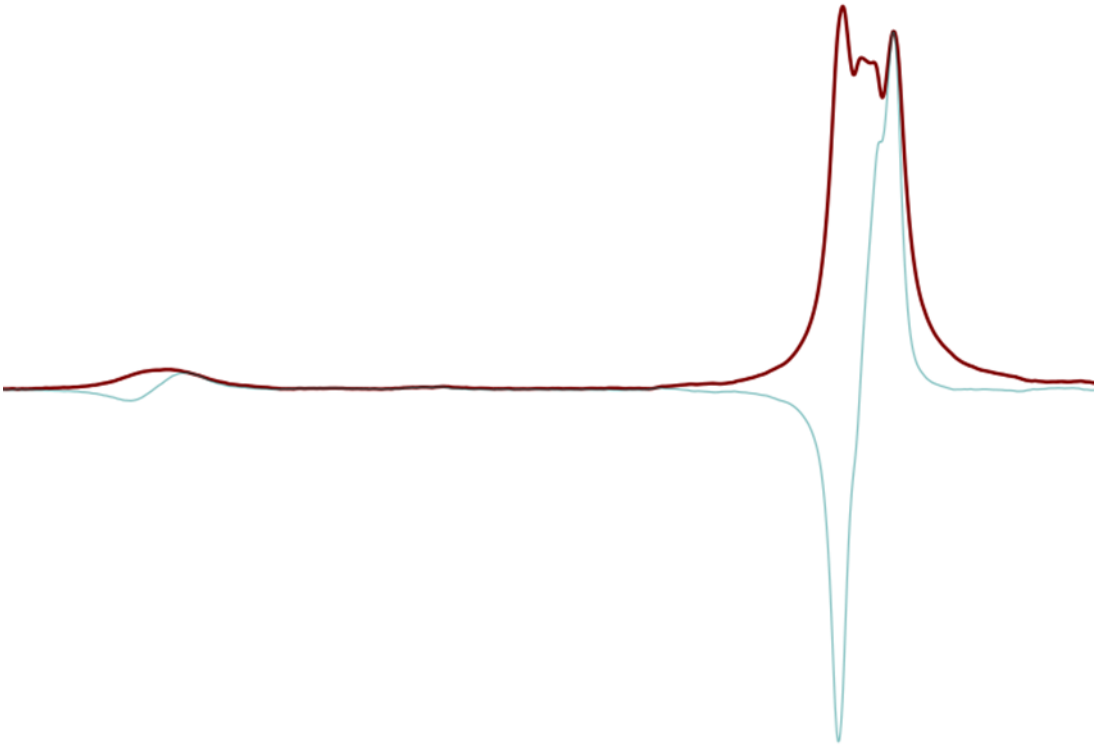

Figure 43. Comparison of $^{19}F$ NMR spectra of **$L_3$** (4 equivalents relative to **4**) with (red) and without (blue) magnitude correction. The bound peak of [Ir(IMes)(**$L_3$**)$_3$(H)$_2$] is shown downfield of the signal for free **$L_3$**.

The anti-phase signal appears to be characteristic to the majority of ligands; this is likely due to interactions between the $^1H$ and $^{19}F$ spins resulting in a coupled $^1H$-$^{19}F$ two spin order which is commensurate with antiphase signals observed from the homonuclear $^1H$-$^1H$ couplings generated when undertaking ALTADENA through substrate hydrogenation with *para*hydrogen.

The results of the SABRE hyperpolarisation of the ligands, shown in Figure 41, is detailed in Table 7 and Table 8 below. Enhancements are quoted both without magnitude processing and with magnitude processing (shown in parentheses).

Table 7. $^{1}$H NMR SABRE substrate enhancements for **$L_2$**, **$L_3$** and **$L_5$**. The value given in parentheses are when the enhancement data has been magnitude corrected. *combination of *ortho* and *para* $^{1}$H NMR sites, indistinct as separate as spectra are collected at 1.4 T.

| **Substrate** | **$L_2$** | | **$L_3$** | | **$L_5$** | |
|---|---|---|---|---|---|---|
| **Environment** | Downfield* | *Meta* | Downfield* | *Meta* | *Ortho* | *Para* |
| **20 Equivalents** | 0.38<br>(0.36) | 0.87<br>(0.67) | 67<br>(56) | 72<br>(45) | 237<br>(131) | 66<br>(69) |
| **10 Equivalents** | 5.53<br>(0.64) | 19.85<br>(0.79) | 133<br>(100) | 85<br>(117) | 81<br>(52) | 146<br>(32) |
| **4 Equivalents** | 1.17<br>(1.4) | 0.59<br>(1.6) | 325<br>(193) | 208<br>(153) | 20<br>(4.65) | 9<br>(1.44) |

Table 8. $^{19}F$ NMR SABRE substrate enhancements for **$L_2$**, **$L_3$** and **$L_5$**. The value given in parentheses are when the enhancement data has been magnitude corrected.

| **Substrate** | **$L_2$** | **$L_3$** | | **$L_5$** | |
|---|---|---|---|---|---|
| **Mixing Field** | Earths | Earths | SABRE-SHEATH | Earths | SABRE-SHEATH |
| **20 Equivalents** | 1.91<br>(1.38) | 8.75<br>(37) | | 43<br>(34) | 8<br>(3.27) |
| **10 Equivalents** | 0.71<br>(0.66) | 9.24<br>(80) | | 71<br>(35) | 4.48<br>(6.62) |
| **4 Equivalents** | 0.11<br>(0.57) | 67.61<br>(166) | 808<br>(243) | 14<br>(3.43) | 14<br>(3.53) |

**L6** is not included as no SABRE was observed for this substrate at any concentration. Following attempts to activate this species through the introduction of hydrogen, no hydride peak was observed in the $^{1}$H NMR spectrum. When **L6** was introduced into the Young's tube with **L1** to ensure catalyst activation, the $^{19}$F NMR spectrum still possessed three 'free' peaks with no 'bound' peak being apparent to suggest **L6** was binding to the iridium catalyst.

The lack of **L6** binding to **4** is likely due to two main factors: the steric bulk of the *ortho* fluorine and the *p*K$_a$ of the substrate. The steric bulk of $^{19}$F at ~1.47 Å is smaller than that of a methyl group in the same position (radius =~2.00 Å)[138, 139] which would not be expected to form a SABRE active complex due to literature reports of picolines and lutidines with a methyl group in the *ortho* position failing to demonstrate SABRE.[126] The radius of fluorine is, however, far closer to the ~1.20 Å of $^{1}$H than that of a methyl group so steric effects would not be expected to be as severe. It is worth noting that the *p*K$_a$ of **L6** shows it is the most acidic of the ligands tested within this study, therefore, may not be as effective a ligand as alternatives also investigated. Though no data could be found in literature for a precise *p*K$_a$ value for **L6**, a value of -1.00 is reported for pentachloropyridine (all *p*K$_a$ values are shown in Figure 41).[136] This lack of SABRE activity is in agreement with previous literature which has reported no hyperpolarisation observed for pentafluoropyridine.[67]

**L2** demonstrated activity, however this was typically below unity and a hydride signal was not observed for [Ir(**L**$_2$)(IMes)(H)]$^+$. The lack of hydride signal did not enable exchange rates for this complex to be interrogated and therefore a detailed mechanistic explanation for the low activity level is not possible. This ligand does suffer from many of the same drawbacks as **L6** discussed above with a fluorine substituent similarly in the *ortho* position and a low *p*K$_a$ (-0.44).[131]

Both **L2** and **L6** have been previously reported to be poor ligands for SABRE hyperpolarisation, with steric effects being cited as one of the limiting factors. The reported use of [Ir(IMe)(COD)Cl] as the polarisation transfer pre-catalyst (as opposed to **4** used here) does not demonstrate an increase in activity for

these two ligands, however.[96] It was hoped the reduced buried volume of this carbene may better facilitate the binding of bulky ligands. The use of asymmetric carbenes within the pre-catalyst has recently been reported to be advantageous for bulky ligands, while reducing the enhancements of simpler substrates such as pyridine due to longer residence times bound to the iridium centre, these may present a potential route to increase the activity of **$L_2$** and **$L_6$**.[34]

**$L_5$** appears to show a reduction in enhancements with reducing excess of substrate, however this trend is partially reversed when SABRE-SHEATH is used. The $^{19}F$ NMR spectra for this substrate are typically either emissive or absorptive with negligible antiphase characteristic. It is thought that this is due to the symmetrical nature of the coupling network around this ligand compared to the other ligands which demonstrate SABRE enhancements. The enhancement values obtained for this ligand system were surprisingly low when compared to **$L_3$**, this is discussed, in section 4.2.5 when considering exchange rate data. Though it is worth noting that the *p*$K_a$ of **$L_5$** is still low (with the chloropyridine value available in literature being 0.66),[135] meaning that this substrate is likely to be a worse ligand than **$L_3$** with its higher *p*$K_a$ value.

**$L_3$** demonstrates the highest enhancements of the substrates tested, with NMR enhancements increasing, when the ratio of substrate : catalyst is decreased to 4:1 respectively, in agreement with prior reports for $^{1}H$ SABRE. The $^{19}F$ NMR spectra for this substrate, however, demonstrate a strong antiphase signal, leading to significantly reduced polarisation values when no phase processing is applied as the majority of the polarisation is cancelled within the integral calculation. The cause for this antiphasing is likely to be due to F-H coupling which doesn't lead to an antiphase signal in **$L_5$** due to the symmetric nature of the substrate.

In addition to being the least sterically bulky of the substrates tested, **$L_3$** has the additional advantage of a higher *p*$K_a$ (2.97) than the other fluoropyridines tested and is the most similar to the reported *p*$K_a$ of pyridine (5.17).[131] In combination with the exchange rates collected for the SABRE active ligands discussed in 4.2.5 this explains the increased enhancements of **$L_3$** compared

to the other ligands tested. However, the antiphase characteristic of the spectra obtained means this signal would have limited *in vivo* use without a method of avoiding internal signal cancellation.

### 4.2.3. SABRE-SHEATH testing

In an attempt to counteract the antiphase nature of the **$L_3$** the magnetisation transfer field (MTF) was varied based on previous $^{15}N$ work by Theis *et al.*[51]

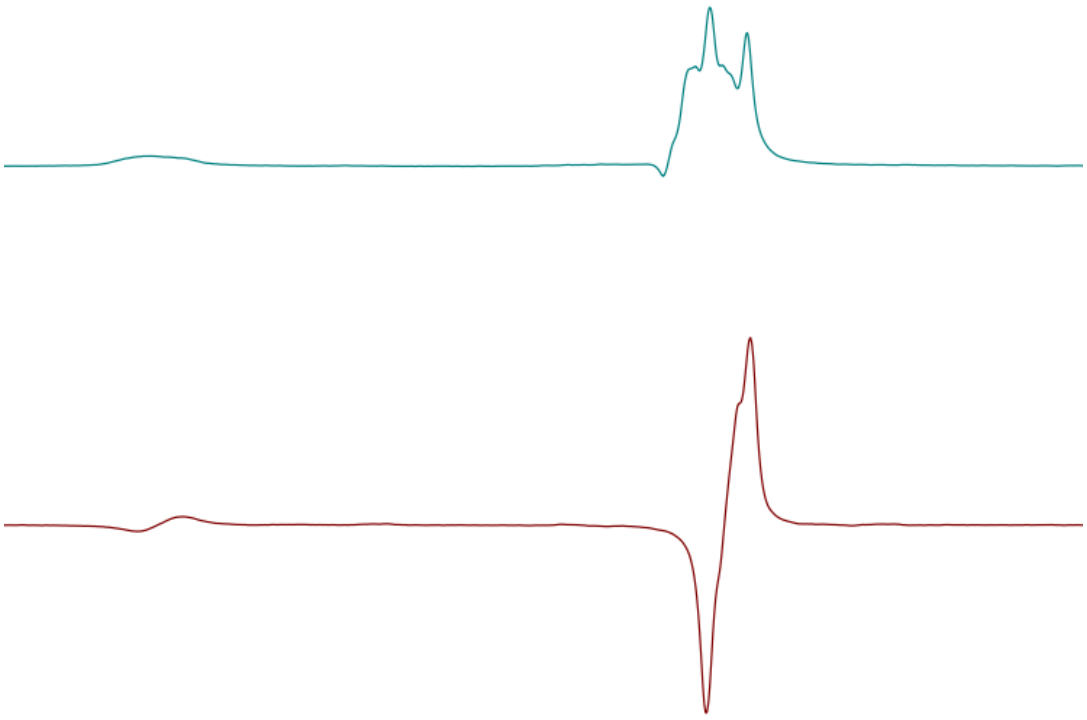

Figure 44. Comparison of $^{19}F$ NMR spectra of **$L_3$** when SABRE-SHEATH is utilised (top) and when polarisation transfer takes place at earth's field (bottom).

The unprocessed signal of **$L_3$** when SABRE-SHEATH was employed is in excess of 95% in phase (as shown in Figure 44) leading to a 12-fold apparent increase in integration (for an overall enhancement of 808) when compared to the unprocessed signal without making use of a μ-magnetic shield due to the reduction in internal signal cancellation. This has important implications when moving towards *in vivo* applications as the smaller collection window of MRI

would lead to significant signal cancellation if the signal contained a large anti-phase characteristic.

This has been reported during the course of this study with **$L_3$** as the only substrate examined and Theis *et al.* demonstrated a 100% in phase signal.[68] The method used for this measurement was the bubbling of *para*hydrogen through the sample, leading to more controlled polarisation transfer while at a reduced magnetic field, whereas the results presented in this thesis involved manually shaking the sample within the μ-shield. This 'shake and drop' method potentially allows polarisation transfer to continue during the non-adiabatic transfer to the measurement field - resulting in an element of polarisation transfer occurring at earth's field during transfer, likely leading to the less than fully emissive spectra collected in this work.

The work presented here, however, demonstrates a 1.6% total polarisation of **$L_3$** at 4 equivalents relative to **4** based on a 808-fold signal increase in a measurement field of 1.4 T, a significant improvement on the 0.3% polarisation reported.

### 4.2.4. SABRE active species

Both **$L_3$** and **$L_5$** demonstrated good enhancements due to the SABRE process. The complex responsible for polarisation transfer was characterised to inform EXSY investigation of the exchange thermodynamics, discussed in section 4.2.5, and to gain insight into the differences, if any, between the two complex's which may affect polarisation transfer efficiency.

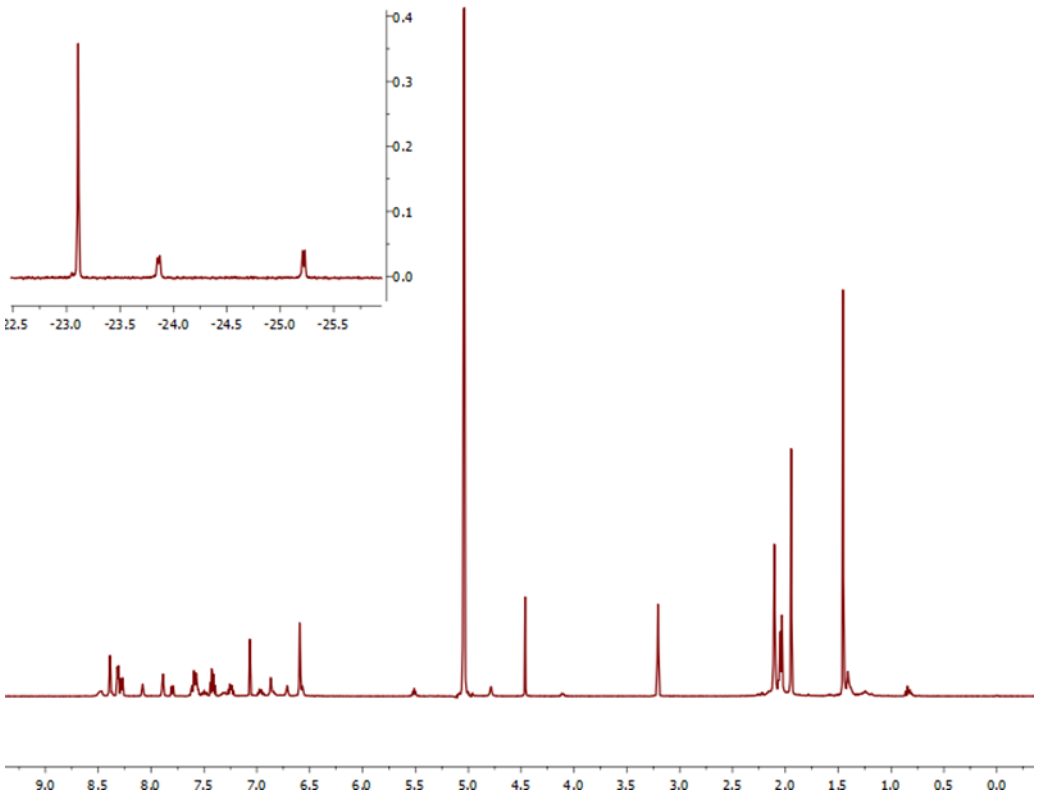


Figure 45. $^{1}$H NMR spectrum of [Ir(IMes)(**L$_3$**)$_3$(H)$_2$]$^+$. Hydride region is shown in expansion.

**L$_3$** forms [Ir(IMes)(**L$_3$**)$_3$(H)$_2$]$^+$ when reacted with **4** in the presence of $H_2$. This is supported by the relative integrals of peaks associated with the *ortho* protons of 3-fluoropyridine at 8.39, 8.31 and 8.28 ppm giving the relative integrals of 1.56:1.53:0.90 respectively when four equivalents of **L$_3$** was added relative to **4**. These three environments demonstrate that with four equivalents of **L$_3$** present three bind, with two *trans* to the hydrides and one substrate *trans* to the carbene which has been shown not to participate in polarisation transfer.[140] The hydride region shows a major hydride at -23.11 ppm; there were also two minor broad hydrides at -23.87 and -25.19 ppm which are diagnostic of a second complex in solution, likely to be [Ir(IMes)(**L$_3$**)$_2$(H)$_2$(MeOH)] with the methanol adduct *cis* and *trans* to the hydrides respectively. Methanol adducts have been previously reported.[35, 128] Enhancement of the solvent OH protons was observed during this study and, again, this has been previously reported.[141] The methanol attributed hydride peaks were too broad for rigorous investigation making use of EXSY, and previous literature has assumed a component two exchange system

(hydrides and the primary substrate *trans* to the hydrides exchanging only). Therefore, for comparisons sake only the major hydride attributed to [Ir(IMes)(**L$_3$**)$_3$(H)$_2$] will be used for EXSY.

**L$_5$** forms [Ir(IMes)(**L$_5$**)$_3$(H)$_2$]$^+$ with peaks for the *ortho* protons being present at 8.48 and 8.32 ppm for free and bound substrate respectively. These peaks are present in a 2.08:1.92 ratio when 4 equivalents of **L$_5$** are present. A similar ratio of free and bound substrate is observed within the *para* proton environments at 7.57 (free) and 7.42 (bound) ppm – though in this instance the ratio is 1.94:2.06 suggesting that not all of the complex in solution exists in the form [Ir(IMes)(**L$_5$**)$_3$(H)$_2$]$^+$ as a ratio of 1:3 would be expected in this instance. This is supported by the presence of a main hydride at -24.02 ppm accompanied by hydrides representative of methanol adducts present at -24.16 and -24.77 ppm.

### 4.2.5. Exchange Rates

The initial SABRE testing revealed that **L$_3$** produced the largest enhancement of the substrates tested; though this may partially be explained through the *p*K$_a$ difference between the two substrates, **L$_5$** would still be expected to have a greater enhancement due to two polarisable $^{19}$F sites. Burns *et al.* report that this is demonstrated for $^{31}$P polarisation when pyridine is *meta* substituted with diethylphosphonate ($^{31}$P enhancement of 860) compared to the singly *meta* substituted substrate with a $^{31}$P enhancement of 336.[63] However, Burns *et al.* do note that the steric bulk of the substituents results in a chlorine adduct being present in the polarisation transfer complex for this substrate.

The exchange rates of the hydride and substrate ligands in these complexes, was examined by exchange rate spectroscopy (EXSY). The exchange rate of pyridine with the pre-catalyst **4** was initially investigated both as method validation, given these values are reported, and as a benchmark for the comparison of the unreported substrates. Eyring-Polanyi plots making use of the exchange data have been used to provide an insight into the thermodynamics of the ligand exchange process. Initially [Ir(IMes)(**L$_1$**)$_3$(H)$_2$]$^+$, shown in Figure 46, was interrogated for literature comparison.

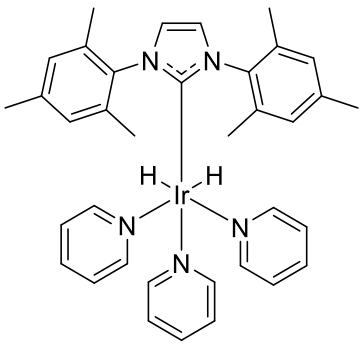


Figure 46. [Ir(IMes)(**L$_1$**)$_3$(H)$_2$]$^+$ complex to be interrogated by EXSY.

Table 9. Hydride exchange rates in the $[Ir(IMes)(\mathbf{L_1})_3(H)_2]^+$ complex.

| Temperature (K) | Exchange Rate ($s^{-1}$) |
|---|---|
| 268 | 0.2181 ± 0.001 |
| 275 | 0.6668 ± 0.010 |
| 280 | 0.9692 ± 0.021 |
| 285 | 1.6962 ± 0.041 |
| 290 | 2.6507 ± 0.091 |
| 300 | 6.1498 ± 0.213 |

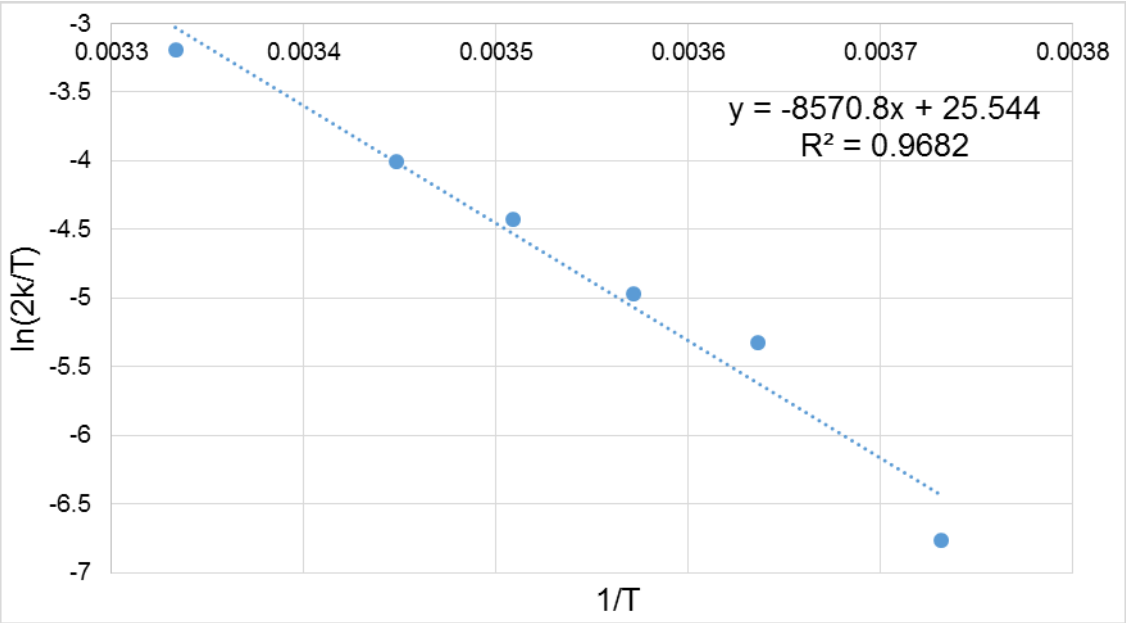


Figure 47. Eyring-Polanyi plot for the hydride exchange rate in the complex $[Ir(IMes)(\mathbf{L_1})_3(H)_2]^+$.

Table 10. Hydride energy values for the exchange rate in $[Ir(IMes)(\mathbf{L_1})_3(H)_2]^+$.

| | ΔH (kJ $mol^{-1}$) | ΔS (J $K^{-1}$ $mol^{-1}$) | $\Delta G_{300}$ ( kJ $mol^{-1}$) |
|---|---|---|---|
| **Literature[26]** | 79 ± 1 | 41 ± 3 | 66.4 ± 0.3 |
| **Experimental** | 71.3 ± 6.2 | 14.83 ± 21.79 | 66.8 ± 0.3 |

Table 11. Pyridine exchange rates in the $[Ir(IMes)(\mathbf{L_1})_3(H)_2]^+$ complex.

| Temperature (K) | Exchange Rate ($s^{-1}$) |
|---|---|
| 268 | 0.3019 ± 0.014 |
| 275 | 0.7788 ± 0.046 |
| 280 | 1.4240 ± 0.040 |
| 285 | 2.0792 ± 0.057 |
| 290 | 3.8554 ± 0.046 |
| 300 | 11.9357 ± 0.215 |

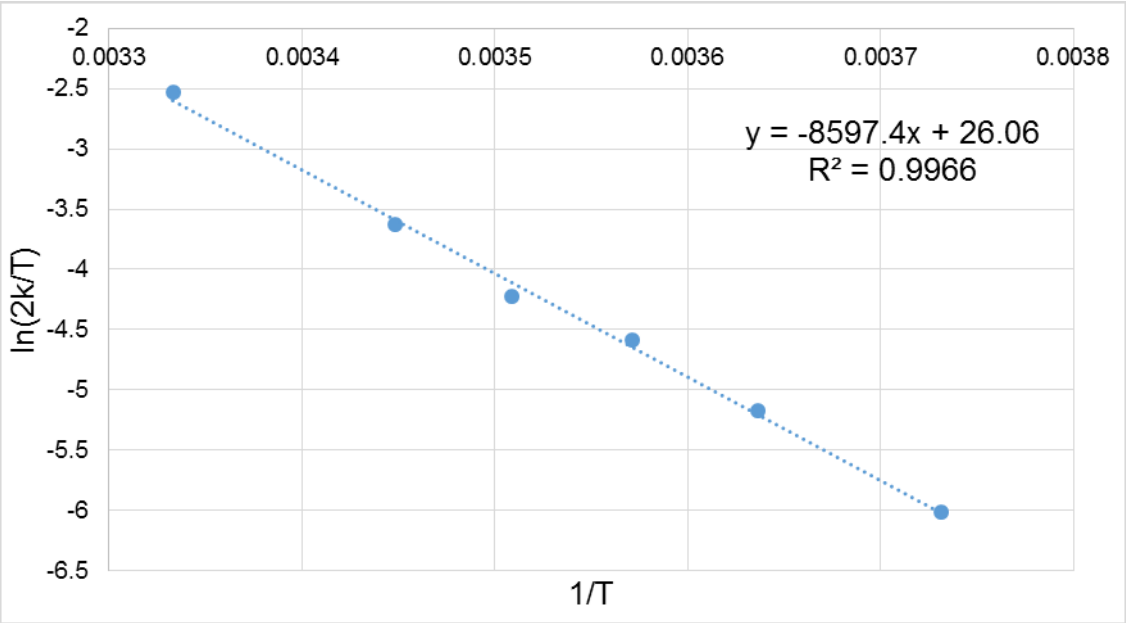


Figure 48. Eyring-Polanyi plot for the pyridine exchange rate in the complex $[Ir(IMes)(\mathbf{L_1})_3(H)_2]^+$.

Table 12. Pyridine energy values for the exchange rate in $[Ir(IMes)(\mathbf{L_1})_3(H)_2]^+$.

| | ΔH (kJ $mol^{-1}$) | ΔS (J $K^{-1}$ $mol^{-1}$) | $\Delta G_{300}$ ( kJ $mol^{-1}$) |
|---|---|---|---|
| **Literature[26]** | 93 ± 3 | 97 ± 9 | 64 ± 2 |
| **Experimental** | 71.5 ± 1.3 | 19.12 ± 4.65 | 65.7 ± 0.1 |

The energy values generated from this data validated the method for application on novel systems. There is a large difference between the experimental and tabulated entropy values, particularly for pyridine exchange, however the contribution of this value to the overall Gibb's energy is minimal and the overall Gibb's free energy for the system shows reasonable literature agreement. Therefore, the system $[Ir(IMes)(\mathbf{L_3})_3(H)_2]^+$, shown in Figure 49, was interrogated.

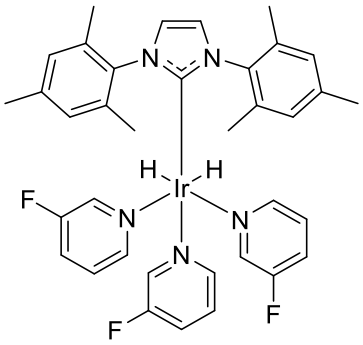


Figure 49. $[Ir(IMes)(\mathbf{L_3})_3(H)_2]^+$ complex to be interrogated by EXSY.

Table 13. Hydride exchange rates in the $[Ir(IMes)(\mathbf{L_3})_3(H)_2]^+$ complex.

| Temperature (K) | Exchange Rate ($s^{-1}$) |
|---|---|
| 275 | 0.5577 ± 0.051 |
| 280 | 1.2001 ± 0.072 |
| 285 | 2.2009 ± 0.073 |
| 290 | 3.9706 ± 0.147 |
| 300 | 11.5417 ± 1.015 |

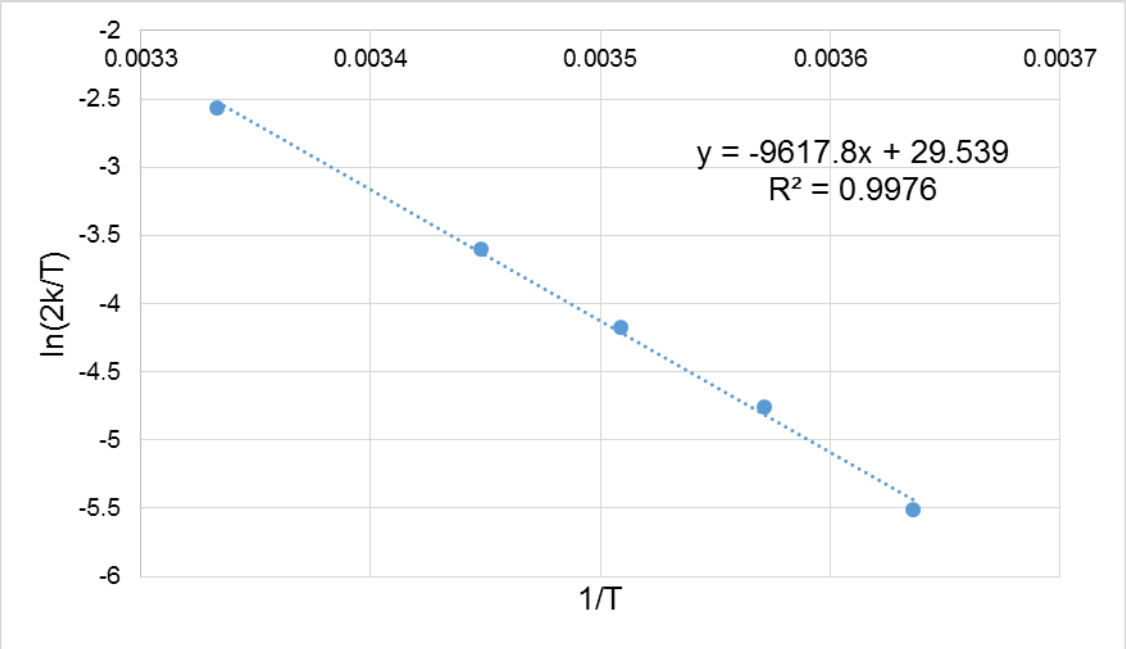


Figure 50. Eyring-Polanyi plot for the hydride exchange rate in the complex $[Ir(IMes)(\mathbf{L_3})_3(H)_2]^+$.

Table 14. Hydride energy values for the exchange rate in $[Ir(IMes)(\mathbf{L_3})_3(H)_2]^+$.

| | ΔH (kJ $mol^{-1}$) | ΔS (J $K^{-1}$ $mol^{-1}$) | $\Delta G_{300}$ ( kJ $mol^{-1}$) |
|---|---|---|---|
| **Literature (for Pyridine)** | 79 ± 1 | 41 ± 3 | 66.4 ± 0.3 |
| **Experimental** | 80.0 ± 2.6 | 48.05 ± 9.05 | 65.6 ± 0.1 |

Table 15. Substrate exchange rates in the $[Ir(IMes)(\mathbf{L_3})_3(H)_2]^+$ complex.

| Temperature (K) | Exchange Rate ($s^{-1}$) |
|---|---|
| 268 | 0.5268 ± 0.008 |
| 275 | 1.7190 ± 0.048 |
| 280 | 2.7007 ± 0.030 |
| 285 | 3.9581 ± 0.046 |
| 290 | 7.3558 ± 0.037 |
| 300 | 18.1232 ± 0.626 |

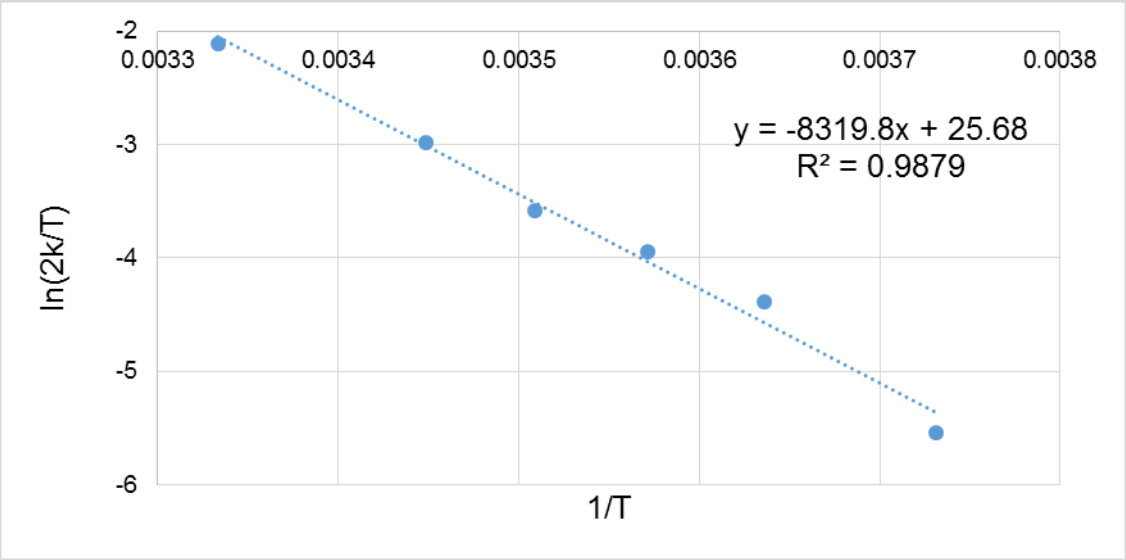


Figure 51. Eyring-Polanyi plot for the 3-fluoropyridine exchange rate in the complex $[Ir(IMes)(\mathbf{L_3})_3(H)_2]^+$.

Table 16. 3-Fluoropyridine energy values for the exchange rate in $[Ir(IMes)(\mathbf{L_3})_3(H)_2]^+$.

| | ΔH (kJ $mol^{-1}$) | ΔS (J $K^{-1}$ $mol^{-1}$) | $\Delta G_{300}$ ( kJ $mol^{-1}$) |
|---|---|---|---|
| **Literature (For Pyridine)** | 93 ± 3 | 97 ± 9 | 64 ± 2 |
| **Experimental** | 69.2 ± 3.2 | 15.96 ± 10.92 | 64.4 ± 0.1 |

In the **L3** system the experimentally observed exchange rates are ~50% faster than those in pyridine. The commensurate exchanges of hydride and substrate in the same order of magnitude as pyridine provide a theoretical basis for the polarisation transfer leading to high SABRE enhancements. When combined with the *p*$K_a$ of **L3** (discussed in section 4.2.2) the observed exchange rates explain why 3-fluoropyridine demonstrates the highest enhancements of substrates tested here. The EXSY interrogation of $[Ir(IMes)(\mathbf{L_5})_3(H)_2]^+$, shown in Figure 52, was then attempted.

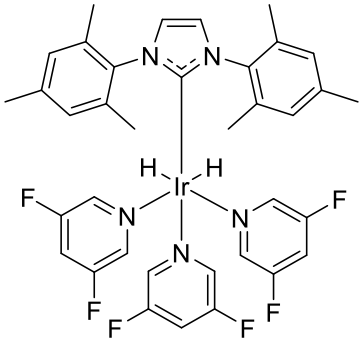


Figure 52. $[Ir(IMes)(\mathbf{L_5})_3(H)_2]^+$ complex to be interrogated by EXSY.

EXSY of $[Ir(IMes)(\mathbf{L_5})_3(H)_2]^+$ was attempted and values obtained at 268 and 280 K, are shown in Table 17 and Table 18 for hydride ligands and **L5** respectively.

Table 17. Hydride exchange rates in the $[Ir(IMes)(\mathbf{L_5})_3(H)_2]^+$ complex.

| **Temperature (K)** | **Exchange Rate ($s^{-1}$)** |
|---|---|
| 268 | 2.1616 ± 0.097 |
| 280 | 11.1510 ± 0.513 |

Table 18. Substrate exchange rates in the $[Ir(IMes)(\mathbf{L_5})_3(H)_2]^+$ complex.

| Temperature (K) | Exchange Rate ($s^{-1}$) |
|---|---|
| 268 | 2.3428 ± 0.039 |
| 280 | 16.9151 ± 1.301 |

EXSY for temperatures above 280 K was attempted, however, exchange rates were too fast to accurately track on the NMR timescale. It is worth noting that one of the closest literature reports available (excluding the publication of this work) notes the hyperpolarisation build up time of 3,5-ditrifluoromethylpyridine is also too short to measure.[129] Hydride exchange at 268 and 280 K was 10 times faster than in a pyridine system at the same temperature, with substrate exchange being 20 times faster at the same temperatures. The speed of these exchanges explains the SABRE enhancement at room temperature being lower than expected for **$L_5$** as exchange is too fast for a J-coupling network to be formed which facilitates polarisation exchange.

The high exchange speed suggested that, if SABRE were to be carried out on **$L_5$** at reduced temperature regime, there may be an increase in enhancement. Therefore, this was tested with the results of the study presented in Table 19.

Table 19. **$L_5$** enhancements at room temperature and after 90s in an ice bath without and (with) magnitude processing of data.

| | **Room Temperature** | | **After 90 s in ice bath** | |
|---|---|---|---|---|
| **$^1$H** | ***Ortho*** | ***Para*** | ***Ortho*** | ***Para*** |
| **20 equivalents** | 237 (131) | 66 (69) | 12 (12) | 7.57 (10) |
| **10 equivalents** | 81 (52) | 146 (32) | 15 (4.13) | 0.94 (2.31) |
| **4 equivalents** | 20 (4.65) | 9 (1.44) | 7.18 (0.76) | 0.04 (0.42) |
| **$^{19}$F** | **Earths** | **Shield** | **Earths** | **Shield** |
| **20 equivalents** | 43 (34) | 8 (3.27) | 3.34 (3.35) | 46 (20.32) |
| **10 equivalents** | 71 (35) | 4.48 (6.62) | 2 (4.5) | 31 (59) |
| **4 equivalents** | 14 (3.43) | 14 (3.53) | 20 (9) | 239 (82) |

Polarisation transfer after 90 seconds in an ice bath at 0 °C appears to reduce the $^1$H enhancement, particularly for the ortho site of the ring. This is likely due to a shortened $T_1$ resulting from prolonged exposure to the polarisation transfer catalyst, particularly for the ortho protons.

$^{19}$F enhancements also show a reduction, again potentially due to relaxation effects. However, when sample shaking was undertaken in the magnetic shield directly after removal from the ice bath, enhancements were noticeably increased – this may be suggestive of an optimal temperature slightly above

0°C as these samples will have had maximum time to warm between removal from the ice bath and transfer to the collection field. This does, however, demonstrate that **L5** may be optimised at a temperature lower than that of the initial measurements for $^{19}F$ polarisation.

### 4.2.6. Signal relaxation

Quick relaxation rates can be a barrier to potential *in vivo* use, as even the collection of MR images following a short (~8 s) transfer time may result in a significant decrease in signal for substrate systems with a low relaxation time ($T_1$).[86, 142] This may be overcome through the bubbling of *para*hydrogen through the sample within the image collection instrument however this would not be viable for clinical applications.

The short $T_1$ values of some substrates is further complicated through the potential mixing of Zeeman values when the SABRE-SHEATH technique is employed.[55] This can lead to drastically reduced $T_1$ values, an order of magnitude smaller than those available at earth's field or higher. This can significantly decrease the potential polarisation build up for SABRE-SHEATH.

Now $^{19}F$ SABRE has been demonstrated, the longevity of the signal was investigated as a high enhancement shortly lived signal may exclude biological applications; methods exist for lengthening of the relaxation time and these are discussed further in 5.2.4.[30]

Table 20. $^{1}H$ $T_1$ relaxation times for the substrates recorded at 9.4 T.

| **Substrate** | **$L_1$ (s)** | | | **$L_2$ (s)** | | | | **$L_3$ (s)** | | | | **$L_5$ (s)** | |
|---|---|---|---|---|---|---|---|---|---|---|---|---|---|
| | ***Ortho*** | ***Meta*** | ***Para*** | ***Meta* 3** | ***Para* 4** | ***Meta* 5** | ***Ortho* 6** | ***Ortho* 2** | ***Para* 4** | ***Meta* 5** | ***Ortho* 6** | ***Ortho*** | ***Para*** |
| **20 eq** | 15.58 | 26.22 | 19.58 | 24.56 | 26.18 | 27.91 | 7.20 | 16.04 | 26.13 | 24.05 | 16.61 | 21.90 | 29.24 |
| **10 eq** | 9.12 | 15.44 | 12.95 | 20.78 | 24.02 | 24.88 | 19.36 | 8.21 | 15.13 | 11.99 | 10.06 | 17.74 | 28.44 |
| **4 eq** | 4.18 | 7.78 | 6.46 | 27.93 | 18.43 | 20.22 | 18.48 | 10.44 | 16.39 | 14.12 | 12.90 | 4.87 | 1.08 |

Table 21. $^{19}F$ $T_1$ relaxation times for the substrates recorded at 1.4 T.

| **Substrate** | **$L_2$ (s)** | **$L_3$ (s)** | **$L_5$ (s)** | **$L_6$ (s)** | | |
|---|---|---|---|---|---|---|
| | | | | *Ortho* | *Para* | *Meta* |
| **20 eq** | 12.52 | 23.56 | 18.21 | 26.36 | 30.55 | 43.05 |
| **10 eq** | 13.13 | 18.63 | 21.67 | 19.94 | 25.52 | 23.10 |
| **4 eq** | 9.59 | 19.23 | 17.95 | 12.57 | 20.10 | 18.05 |

The $^{19}F$ $T_1$ values reported are reasonably short, with relaxation times of ~20 s for four equivalents of **$L_3$** relative to **4** (the optimum for enhancements). It is notable that these relaxation times are lengthened by ~3 times when $^{19}F$ measurements are taken at 1.4 T compared to 9.4 T; suggesting these signals may be useful for low field MRI.[96] A theoretical basis for this is provided by Theis *et al.*[49]

Relaxation times show a trend with shorted $T_1$ durations for lower concentrations of ligand relative to **4**, this is because of increased spin interactions when **L** is bound to the metal centre of the catalyst. The relaxing effect of the polarisation transfer catalyst means that optimisation of a SABRE system requires a balance between high enhancement levels associated with four equivalents of ligand relative to **4** and the shorter relaxation times this leads to. Methods for lengthening $T_1$ have been previously reported,[30] in particular through the deactivation of the SABRE active species following polarisation transfer – attempting to make this process heterogeneous is discussed further in section 5.2.

### 4.2.7. Deuteration Studies

The selective deuteration of a hyperpolarisation ligand of interest has been well established to increase the polarisation levels achieved through preventing 'dilution' of the hyperpolarisation to a range of receiver nuclei.[26, 45, 143, 144] This has been reported in biologically relevant ligands, such as the tuberculosis drug isoniazid and its derivatives,[86, 95] where elongation of $T_1$ values are reported in addition to improved signal enhancements. The use of a fully deuterated carbene has also been reported to lead to higher levels of ligand polarisation, though this can be partially balanced by a reduced relaxation time.[32, 145]

Though deuteration of the SABRE ligand and catalyst bound carbene have both been well established in literature the impact of a selective deuteration strategy SABRE of heteroatoms remains, to the best of the authors knowledge, unreported.

In most reported instances of a selective deuteration strategy reported for $^{1}H$ SABRE a single proton in the *ortho* position of a pyridyl ring was left undeuterated to act as a polarisation receptor. However, as described in section 4.1.2, the polarisation of substrates with a $^{19}F$ atom present in this position has failed to result in SABRE activity. A deuteration strategy for selective labelling of a $^{19}F$ containing substrate for SABRE would therefore likely have to include the $^{19}F$ to be polarised in the *meta* or *para* positions if the 'benchmark' pyridine ring scaffold is to be used, as shown in Figure 53.

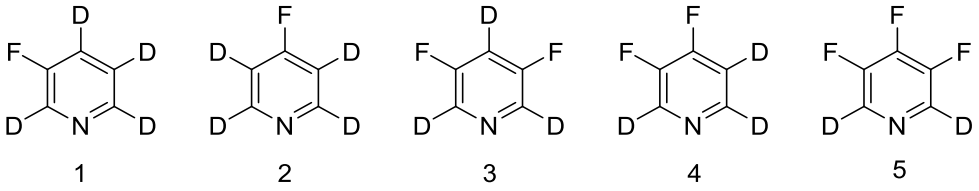


Figure 53. Possible deuterated fluoropyridine structures suitable for SABRE.

However traditional SABRE models suggest that polarisation is relayed to the *meta* and *para* positions *via* a J-coupling network formed with the proton in the *ortho* position.[129] Therefore deuterating this site would mean that polarisation transfer didn't take place to the hetroneuclei. However, in their recent report of 3-fluoropyridine being hyperpolarised using SQUID detection Buckenmaier *et al.* note that if the protons are required to relay polarisation onto the $^{19}F$ present then the field dependencies (shown in Figure 40) would be similar and correlated, which is not the case. They therefore propose that a direct transfer of polarisation from the catalyst-bound *para*hydrogen derived hydrides to the heteroatom may be feasible, as shown in Figure 54.

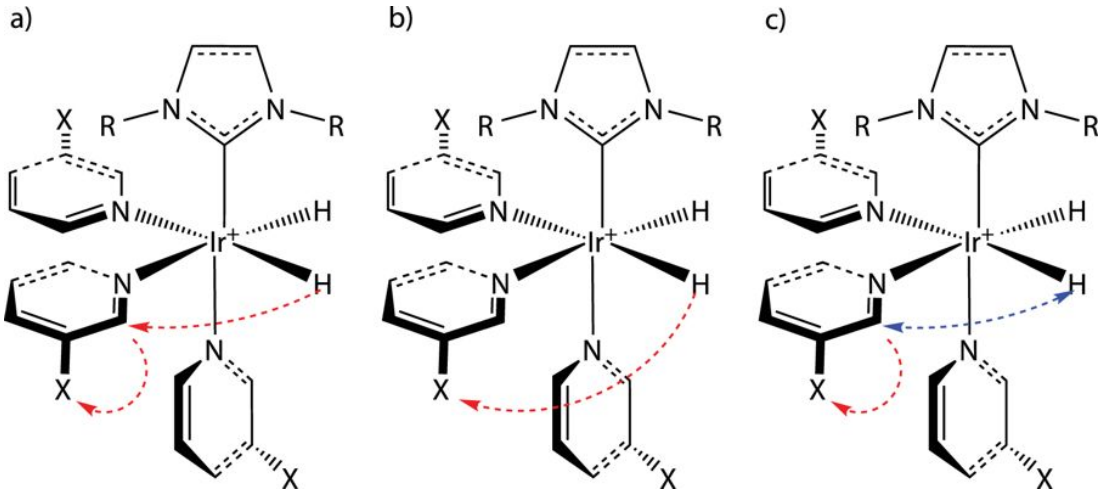


Figure 54. Possible polarisation transfer mechanisms to spin-1/2 heteronuclei (X, eg. $^{19}F$) of pyridine derivatives. (a) Indirect polarisation transfer: the polarisation of hydrogen is transferred to hydrogen of the pyridine derivative and subsequently to X. (b) Direct polarisation transfer: the polarisation is transferred directly to heteronucleus X. (c) Polarisation transfer after H/H exchange reaction. Hydrogens of a pyridine ligand in *ortho*-position can exchange during SABRE polarisation transfer could then relay polarisation to heteronucleus X.[146]

If mechanism B from Figure 54 occurs then the deuteration of other positions, shown in Figure 53, may be an effective strategy to increase the $^{19}F$ polarisation levels obtained and potentially increase the relaxation time, $T_1$. If this is the case then this would represent a novel mechanism for SABRE polarisation transfer to heteronuclei.

As initial substrate tests reported **L3** to demonstrate the highest $^{19}F$ SABRE enhancements, the deuterated analogue of **L3** was synthesised (see section 8.6). Utilising TMS as an internal standard collection of a $^{1}H$ spectrum suggests a *circa* 52% deuteration. However, protonation of the *ortho* site was observed within this $d_4$-methanol sample. Subsequent attempts to perform SABRE with $d_4$-**L3** did not result in an observed hyperpolarised signal for the substrate, suggesting that mechanism A described within Figure 54 may be in effect within this sample. Alternatively, mechanism B may occur, however, the long range J-coupling is not strong enough to effectively transfer polarisation

form the *para*hydrogen derived hydrides directly to the fluorine hetronuclei present in $d_4$-**L**$_3$.

## 4.3. Conclusion

The SABRE hyperpolarisation of a range of $^{19}$F containing substrates is presented. At the time of project commencement the only prior literature for $^{19}$F SABRE was a single spectrum for 3-fluoropyridine without a quoted enhancement factor in the SI of the first report of SABRE.[21] An additional report had found pentafluoropyridine to be SABRE inactive, however, no explanation for this had been presented.[67] During the course of this project there were two additional publications for $^{19}$F SABRE.[68, 129]

The work presented here demonstrates SABRE hyperpolarisation of previously unreported ligands. This work explains the lack of activity in 2-fluoropyridine, 4-fluoropyridine and pentafluoropyridine while demonstrating high enhancement values for 3-fluoropyridine and 3,5-difluoropyridine.

SABRE-SHEATH was applied to the SABRE active ligands demonstrating a route towards phase correction of the hyperpolarised signal for future *in vivo* application.

The species responsible for polarisation transfer were characterised and the binding affinities of the ligands discussed. The characterisation of these species has enabled interrogation of the ligand and hydride exchange rates for the successfully polarised ligands.

Exchange rates of ligand and hydride species provide a basis to explain the higher polarisation levels of 3-fluoropyridine compared to 3,5-difluoropyridine. The results suggest [Ir(IMes)(3,5-difluoropyridine)$_3$(H)$_2$] will better facilitate polarisation transfer at a low temperature regime. Conducting SABRE with 3,5-difluoropyridine at low temperature has then been attempted resulting in increased $^{19}$F SABRE-SHEATH polarisations. However $^{1}$H polarisation has decreased – this was investigated through examination of the ligand relaxation time for the SABRE active species.

The relaxation times of all SABRE active species have been investigated, demonstrating the difficulty in optimising a polarisation transfer system as reduced ligand equivalents relative to the polarisation transfer catalyst result in a higher enhancement, due to a higher efficiency transfer process, but also results in a reduced relaxation time meaning the resulting hyperpolarised signal returns to unity faster. This work also demonstrates that low field applications such as benchtop NMR have an advantage over more traditional high field applications due to longer $T_1$ values for the same sample.[96]

Finally, a deuteration approach has been taken to gain insight into the mechanism of polarisation transfer to $^{19}F$ and to increase the overall levels of polarisation. Testing of $d_4$-**L3** revealed that no hyperpolarised signals were present when this substrate was assessed for SABRE activity. This result suggests that polarisation transfer may require a proton within the *ortho* site for this ligand to facilitate indirect polarisation transfer from the iridium bound *para*hydrogen derived hydrides onto the $^{19}F$ *via* this proton. It may also suggest that long range scalar couplings are simply not strong enough to facilitate direct polarisation transfer to the heteronuclei in this ligand.

This thesis demonstrates the feasibility of using $^{19}F$ SABRE to hyperpolarise a range of ligands, including those demonstrated here, and has been utilised as a basis for the polarisation of biologically relevant $^{19}F$ containing ligands, including a world health organisation (WHO) essential medicine the results of which are presented in section 6.2.

# 5. Studies towards a metal-free SABRE bolus

## 5.1. Introduction

Recent studies have demonstrated that the typically employed SABRE pre-catalyst, [Ir((IMes)(COD)Cl] (**4**), demonstrates cytotoxicity.[71, 78] This chapter details the application of heterogeneous SABRE (HET-SABRE) catalysis to hyperpolarise molecules, and the use of heterogeneous supports as catalyst scavengers. Both of these approaches are viable methods to separate a SABRE catalyst, such as **4**, from solution in order to prepare a bolus suitable for *in vivo* imaging. These methodologies have been explored in direct response to circumventing the cytotoxicity of the SABRE catalyst.

### 5.1.1. Catalyst toxicity

One of the key goals of SABRE hyperpolarisation is the eventual application to *in vivo* imaging, with that in mind any toxicity attributed to the SABRE catalyst, substrate or solvent should be minimised or avoided. Substrate toxicity will have to be tested on an individual basis, however, as the SABRE process doesn't chemically change the substrate, previously approved drugs should be safe to use. Indeed, SABRE has already been demonstrated on several commercially available drugs.[48, 95, 96]

Recent developments towards a biocompatible SABRE solvent system have also been reported through approaches including the use of water-soluble catalysts and pre-activating **4** to endow water solubility.[80-83] However, the highest enhancement levels have been reported when polarisation transfer occurs in a deuterated alcoholic solvent,[28, 45] therefore a simple method suggested to generate a biologically compatible bolus is polarisation transfer in $d_6$-ethanol before dilution with $D_2O$,[71, 78] with lower ethanol concentrations significantly decreasing mortality in mice.[147] Indeed, high ethanol concentrations have been utilised for the euthanasia of laboratory mice and

rats,[148-150] so work to determine a suitable dilution has been conducted by Duckett *et al.*[71, 78]

The remaining, potentially toxic, component of the SABRE process is the (typically) iridium containing polarisation transfer catalyst. Iridium toxicity has been previously reported, however, iridium compounds are, in general, defined as 'practically non-toxic' in a recent review.[151] Iridium and rhodium chloride salts have been reported to inhibit rat fibroblast cell proliferation *in vitro* in addition to inducing DNA damage, though notably iridium(III) chloride hydrate had a reduced effect compared to rhodium(III) chloride hydrate.[152] Hypersensitivity to iridium salts has also been reported to be developed after long term exposure in a factory setting.[153]

Recently, Duckett *et al.* have sought to evaluate the toxicity of the SABRE process, specifically to determine if additional work is required to overcome toxicity barriers before considering progressing SABRE towards clinical applications. This work first sought to establish if a $d_6$-ethanol:$D_2O$ mixture led to loss of cell viability, as shown in Figure 55.

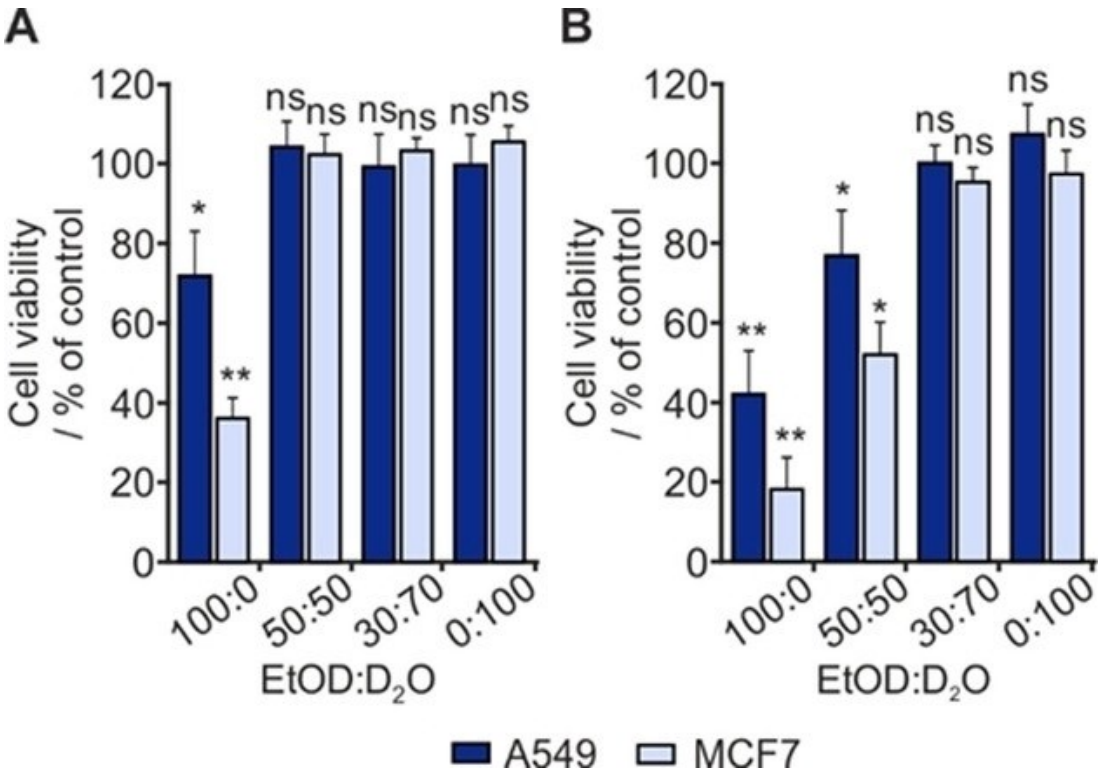


Figure 55. Evaluating the effect of a $d_6$-ethanol:$D_2O$ mixture on cell viability against two different cell lines: A549 (dark blue) and MCF7 (light blue) after 6 hours (A) and 24 hours (B).[71]

This led to the conclusion that a 30% $d_6$-ethanol mixture in $D_2O$ did not lead to a drop in cell viability so would be ideal for potential *in vivo* use. Although $D_2O$ has been reported to induce cell apoptosis, this is typically at higher concentrations or longer timescales than those utilised in by Duckett *et al.*[154, 155]

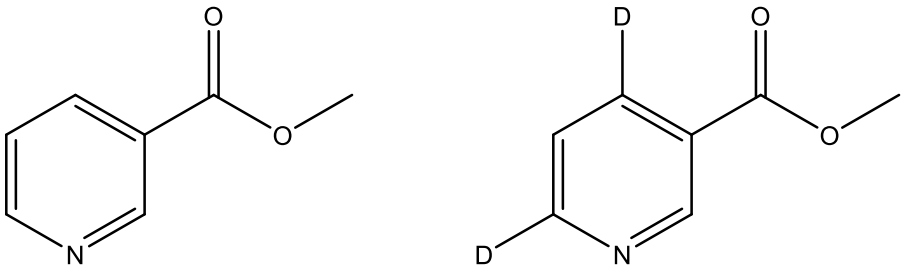


Figure 56. Methyl nicotinate and $d_2$-methyl nicotinate utilised by Duckett *et al.*[71]

Methyl nicotinate and $d_2$-methyl nicotinate, as shown in Figure 56, were the substrates utilised for this study and also did not show a statistically significant

(P<0.05) loss of cell viability over a 6 hour period, even at relatively high (20 mM) concentrations. After 24 hours cell mortality did occur at this concentration, with only the A549 cell line utilising undeuterated methyl nicotinate at a concentration of 5 mM reporting a cell viability in excess of 90% after 24 hours.

The limiting factor for biological hyperpolarisation is likely to be signal relaxation with Roy *et al.* and Theis *et al.* currently reporting substrate $T_1$ values of under half an hour.[50, 156] Given SABRE-focused pharmacokinetic nicotinamide studies have demonstrated a terminal elimination phase half-life of close to an hour in rat studies, even when the lowest dose tested was utilised (20 mg/kg), hyperpolarisation is likely to only be observed for a minor portion of the bolus' *in vivo* residence time.[157]

Duckett *et al.* then prepared a full SABRE reaction mixture consisting of **4** (5 mM) and 20 mM deuterated methyl nicotinate in 30% $d_6$-ethanol:70% $D_2O$ in order to test the cell viability of the full SABRE mixture with the activated catalyst, the results of this assay are shown in Figure 57.

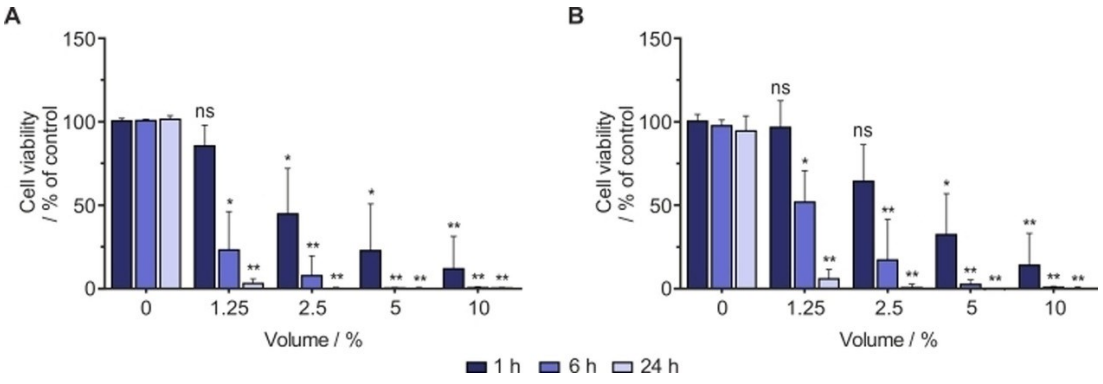


Figure 57. Cell viability of two cell lines A549 (A) and MCF7 (B) after 1, 6 and 24 hours (A) and 24 hours (B) when exposed to several bolus volumes (0, 1.25, 2.5, 5, and 10%) of SABRE reaction mixture.[71]

Figure 57 shows there was no significant loss of cell viability after 1 hour with the lowest bolus volume of SABRE mixture used, 1.25%. However, any higher concentration or longer exposure time led to significant drops in cell viability.

This toxicity was attributed to **4** itself as the toxicity was not present when the solvent and substrates were tested individually. Duckett *et al.* demonstrated in a later extension of this study that changed the identity of **4** to an alternative water soluble iridium containing catalyst, that this improved both aqueous solubility and could potentially increase activity.[35, 78] The water soluble catalyst utilised was $[Ir(H)_2(tmx)(mPTA)](I)(CF_3SO_3)]$, shown in Figure 58, where tmx is tetramethylxanthine and mPTA is the coligand ethylated 1,3,5-triaza-7-phosphaadamantane.

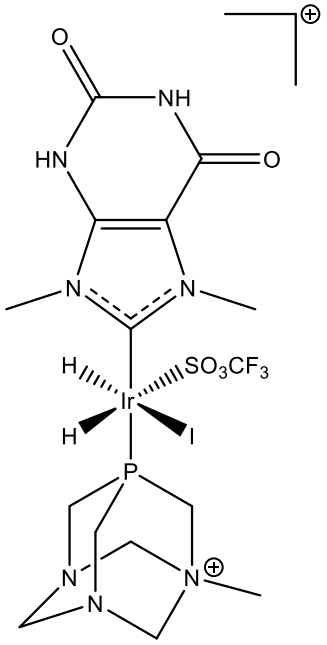


Figure 58. Structure of $[Ir(H)_2(tmx)(mPTA)](I)(CF_3SO_3)]$ water soluble catalyst utilised by Duckett *et al.*[78]

Utilising $[Ir(H)_2(tmx)(mPTA)](I)(CF_3SO_3)]$ or deuterating (either the imidazole ring for $d_2$-IMes, all positions but the imidazole ring for $d_{22}$-IMes or fully deuterated for $d_{24}$-IMes) IMes in **4,** still demonstrated toxicity.[78] Though it was noted that deactivating the catalyst after polarisation transfer may be an effective approach to negate some of the toxicity,[71] in addition to significantly increasing the relaxation times of the substrate,[30] this increase in signal longevity is due to limiting access to the iridium which acts as a relaxing agent.

The associated toxicity of the iridium complex means that techniques such as heterogeneous SABRE (HET-SABRE) catalysis,[36, 93, 94] the use of biphasic

mixtures to separate the catalyst and substrate,[89] or making use of metal scavengers to remove the catalyst from solution are logical progressive steps towards clinical application.[72]

### 5.1.2. HET-SABRE catalyst systems

The separation of the catalytic species, to form a hyperpolarised bolus, offers advantages both in the relaxation time of the hyperpolarised signal and in advancement towards clinical applications, as the removal of the catalyst means toxicity concerns are reduced in addition to lowering costs if the catalyst can be recycled. To this end, four heterogeneous SABRE (HET-SABRE) systems have been reported to date: these have been attached to either polymer microbeads,[93] $TiO_2$/PMAA (poly(methacrylic acid)) nanoparticles,[36] or silica labelled with amine linkers.[94] The structures of these HET-SABRE catalysts are shown in Figure 59.

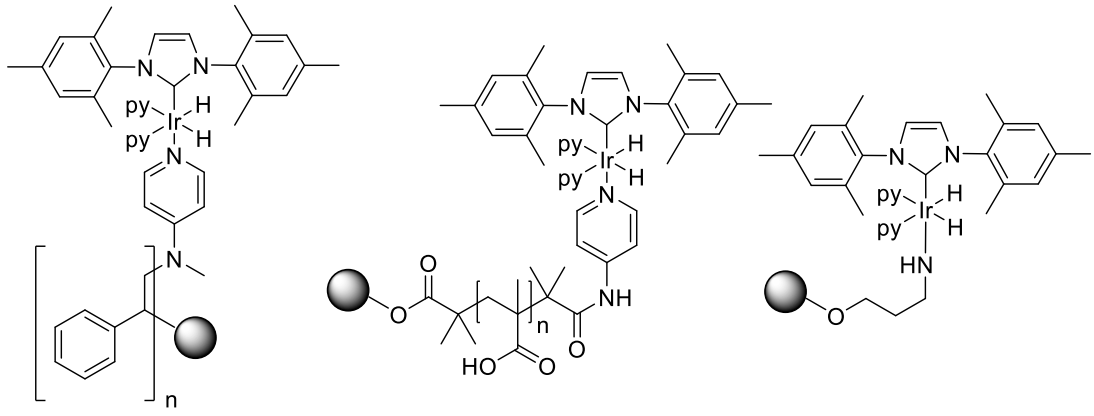


Figure 59. Pyridine activated HET-SABRE catalysts immobilised on polymer microbeads (left),[93] $TiO_2$/PMAA nanoparticles (middle)[36] and bound to a silica supported amine linker (right).[94]

All these HET-SABRE catalysts make use of a solid support axially bound to the iridium; ligands in this position have been reported not to exchange due to its stronger metal bonding interaction.[28]

The polymer microbead example has demonstrated SABRE activity polarising pyridine to yield an enhancement of between 5.2 (*ortho* protons) and 2.7 (*para* proton). No bound signals were observed in the hyperpolarised spectra due to

the solid supported catalyst rapidly settling to the bottom of the NMR tube after shaking, and was, therefore, not excited during the 90° pulse subsequently applied. The binding of the catalyst to the solid support was confirmed making use of IR, MS and AAS, with AAS showing that 4% of the total homogenous bulk was the iridium complex. Removal of the supernatant following heterogeneous hyperpolarisation and subsequent testing separated from the solid bulk revealed no SABRE activity, demonstrating that the heterogeneous catalyst was responsible for polarisation - $^{1}$H NMR, AAS and MS were also applied to this sample and failed to detect any catalyst leaching into solution, within the detection limits of the instrumentation employed.[93]

A further study demonstrated the synthesis of a heterogeneous catalyst on both a $TiO_2$/PMAA nanoparticle and PVP (polyvinylpyridine) polymer.[36] These species were characterised by NMR, AAS and DLS (dynamic light scattering). AAS determined that 25% of the total nanoparticle catalyst by weight was iridium complex and that the final filtrate wash following production of the heterogeneous species did not show the presence of iridium, indicating a robust heterogeneous catalyst. The enhancements obtained from the nanoparticle catalyst were *ca*. 2.5 times higher than those obtained from the polymer based catalyst making use of a 'shake and drop' method with pyridine as the substrate. When *para*hydrogen was bubbled through the solutions instead for 300 s, the nanoparticle based catalyst's enhancements increased from 18-, 17- and 7-fold for *ortho*, *meta* and *para* pyridine environments respectively to give enhancements of 26-, 39- and 11-fold respectively. This equates to an overall polarisation of *ca.* 0.13%. The improved enhancements when a bubbling approach was taken to the introduction of *para*hydrogen to the HET-SABRE solution suggests this may be a more efficient approach given the difficulty of facilitating an interaction between dissolved gas and the HET-SABRE catalysts in solution, particularly given the relatively low $H_2$ solubility in most of the deuterated solvents employed. This study also demonstrated that the heterogeneous catalyst may be recycled for use in further SABRE experiments, though enhancements were slightly reduced following the recovery process.

Kovtunov *et al.* demonstrated the use of a commercially available silica supported amine linker to form a HET-SABRE catalyst.[94] Though this report demonstrates lower polarisations for pyridine (~2.6 fold) compared to the work of Shi *et al.*,[36, 93] the aim of the publication was to demonstrate HET-SABRE of heteroatoms, specifically $^{15}$N. Therefore, the proton polarisation was not optimised. Kovtunov *et al.* successfully demonstrated a $^{15}$N polarisation of ~100 fold under HET-SABRE-SHEATH conditions.[49, 51] The lower gyromagnetic ratio of $^{15}$N compared to $^{1}$H suggests that far greater $^{1}$H polarisation would be feasible using this HET-SABRE system if $^{1}$H polarisation was optimised.[5] The signal has been attributed to solid-supported catalyst through the lack of $^{15}$N bound peaks typically observed for axially and equatorially pyridine to **4**. The supernatant was further tested with XPS and ICP-MS suggesting no iridium is lost from the surface during the HET-SABRE process and there is minimal leaching into the supernatant.

### 5.1.3. Catalyst deactivation

Another alternative approach towards biological SABRE applications would be the employment of scavengers to remove the toxic iridium species following polarisation, but before injection of the hyperpolarised bolus. For this application, catalyst removal would have to proceed within the relaxation time of the substrate in order to produce a non-toxic bolus that still contains hyperpolarised substrate. Recent work has demonstrated $T_1$ values of 9.7±1 min for specifically $^{15}$N enriched metronidazole substrates at 1.4 T. However, the authors noted that the method could be expanded to the FDA approved anti-infective nimorazole,[158] so a catalyst removal time in the order of ~5 mins would be ideal.

The first catalyst deactivation report by Mewis *et al.* polarised nicotinamide making use of pre-catalyst **4** before employing 2,2'-bipyridine (bpy) or 1,10-phenanthroline to homogenously rapidly deactivate the catalyst when the Young's capped NMR tube was opened to air and the deactivating agent added.[30]

Table 22. $T_1$ of nicotinamide (5 equivalents relative to **4**) under $H_2$ for the proton spins shown in Figure 60 when nicotinamide is without SABRE catalyst, with **4** and with **4** and deactivating agent bpy.[30]

| | $T_1$ (free)/s | $T_1$ (with **4**)/s | $T_1$ (with **4** and bpy)/s |
|---|---|---|---|
| a | 43.1 | 7.0 | 38.0 |
| b | 11.3 | 6.1 | 11.5 |
| c | 13.5 | 3.7 | 14.0 |
| d | 6.6 | 4.3 | 6.8 |

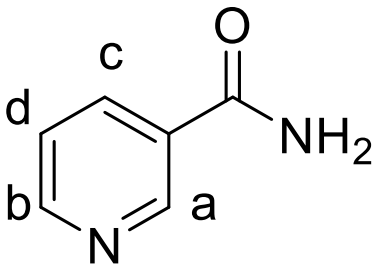


Figure 60. Nicotinamide with proton environments labelled; nomenclature utilised in Table 22.

As shown in Table 22, the deactivation of **4** led to the near total regeneration of the $T_1$ measured when the relaxing agent **4** is not present in solution. The authors had hoped to produce a re-activatable system making use of UV light to dissociate the deactivating agent from the metal, however, this was proven not to be possible. When discussing the potential for heterogeneous scavenging of the metal catalyst, this effect may be helpful in prolonging the hyperpolarisation, through limiting interactions with the iridium catalyst which acts as a relaxing agent of the catalyst-free bolus, in addition to removing the toxic component. [159]

A similar approach has been reported making use of bathophenanthrolinedisulfonic acid disodium salt (BPS).[71] This is structurally similar to 1,10-phenanthroline which had been reported by Mewis *et al.*, with additional steric bulk incorporated away from the iridium binding sites. Once

deactivated the catalyst was then removed to produce a biocompatible bolus, making use of ion exchange chromatography to remove ~98% of the iridium present.

During the course of this work, a range of silica supported scavengers have been assessed as catalyst scavengers by Barskiy *et al*.[72] Barskiy *et al.* began by making use of a biphasic mixture approach, using a mixed aqueous/organic phase to remove >99% of the activated iridium catalyst as the substrate favours the aqueous phase. There was, however, still a measurable quantity of iridium present in the aqueous phase, likely due to the reported water solubility of the catalyst once activated,[80] which may prevent this approach being used in isolation to produce a biocompatible bolus.[160]

| | | Particle Size (µm) | Extent of labelling (mmol/g) |
|---|---|---|---|
| **$S_A$** | 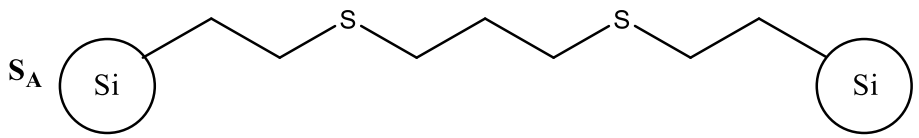 | >45 | 0.7 - 1.1 |
| **$S_B$** | 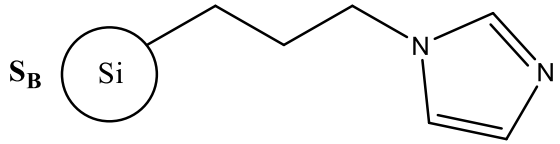 | 400 - 750 | 1.0 - 1.4 |
| **$S_C$** | 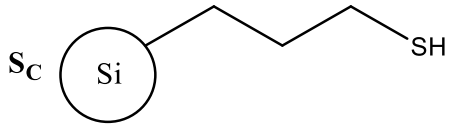 | 20 - 100 | 1.0 - 1.5 |
| **$S_D$** | 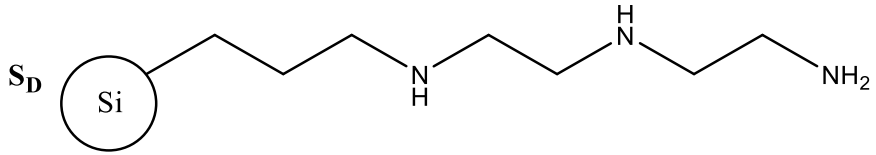 | 20 - 100 | 0.5 - 1.5 |
| **$S_E$** | 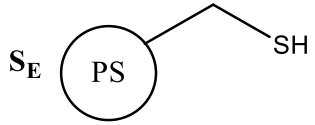 | 37 - 74 | ~2 |
| **$S_F$** | 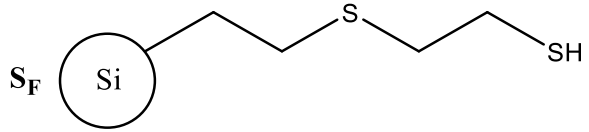 | >45 | 0.7 - 1.3 |

Figure 61. Solids tested by Barskiy *et al.* for scavenging efficacy,[72] **$S_A$-$S_F$** are silica mounted except **$S_E$** which is polystyrene mounted.

Barskiy *et al.* then assessed the metal scavenging efficacy of a range of nitrogen and sulphur containing commercially available scavengers, shown in

Figure 61, which widely ranged in size from ~20 – 750 μm and loadings between 0.5 and ~2 mmol/g. This work demonstrated that solid supported scavengers could be effective at removing low concentrations of iridium over a 12 hour period with 10 mg of the most effective scavenger removing ~95% of ~82 ppb iridium. The most effective scavenger, **S$_C$**, was then assessed for the quantity of iridium that varying quantities of the scavenger could remove and syringes packed with **S$_C$** were assessed as a practical method for the removal of SABRE catalyst and preparation of a bolus. Capture efficiencies >99% were reported when >75 mg of **S$_C$** was used.

In a further report, **S$_C$** and **S$_F$** are added, along with unfunctionalised silica, to a mixed solvent system.[73] This resulted in catalyst capture within the lifetime of the substrate, in this case metronidazole, resulting in an average of >98% catalyst removal (with **S$_C$** removing a higher percentage than **S$_F$**) compared to the theoretical maximum iridium concentration value. Attempts to conduct SABRE following the addition of the scavengers were unsuccessful with the authors noting the previously iridium containing supernatant had become clear and the scavengers taking on a pale yellow colour similar to the catalyst.

## 5.2. Solid Supported HET-SABRE catalyst results

The following section reports the attempts to utilise silica particles for the support of SABRE catalysts and their potential application for the deactivation of homogenous SABRE catalysts.

### 5.2.1. Synthesis of potential HET-SABRE catalysts

The initial aim of this work was to expand upon the initial report in which a silica support functionalised with a primary amine had been utilised (support **$S_1$**).[94] Substrates for testing were therefore chosen (see Figure 62) to examine if this approach was feasible for application in instances where secondary amine binding site(s) were available (supports **$S_2$** and **$S_3$**), heterocyclic rings were present (supports **$S_4$** and **$S_5$**) and the identity of the solid support was varied from silica to a polymer (supports **$S_6$** and **$S_7$**).

Commercially available supports were employed in order to be able to compare and contrast based on a quality controlled particle size and labelling quantity information. The smallest possible range of particle sizes and loadings was desirable as though this limits the validity of direct comparisons with the work of Barskiy *et al.*, particularly when comparing the otherwise structurally analogous pairs **$S_B$**/**$S_4$** and **$S_D$**/**$S_3$**. The approach presented here has the advantage of improved internal comparisons. In the instances where an alternative support is utilised, the binding mode of the functional labelling was as close as feasible to silica supports also being tested – in particular supports **$S_1$** and **$S_2$** being comparable with supports **$S_6$** and **$S_7$**. HET-SABRE catalyst synthesis was attempted making use of supports **$S_1$**-**$S_7$** using a synthetic approach based on the work of Kovtunov *et al.*[94] (see section 8.6.13).

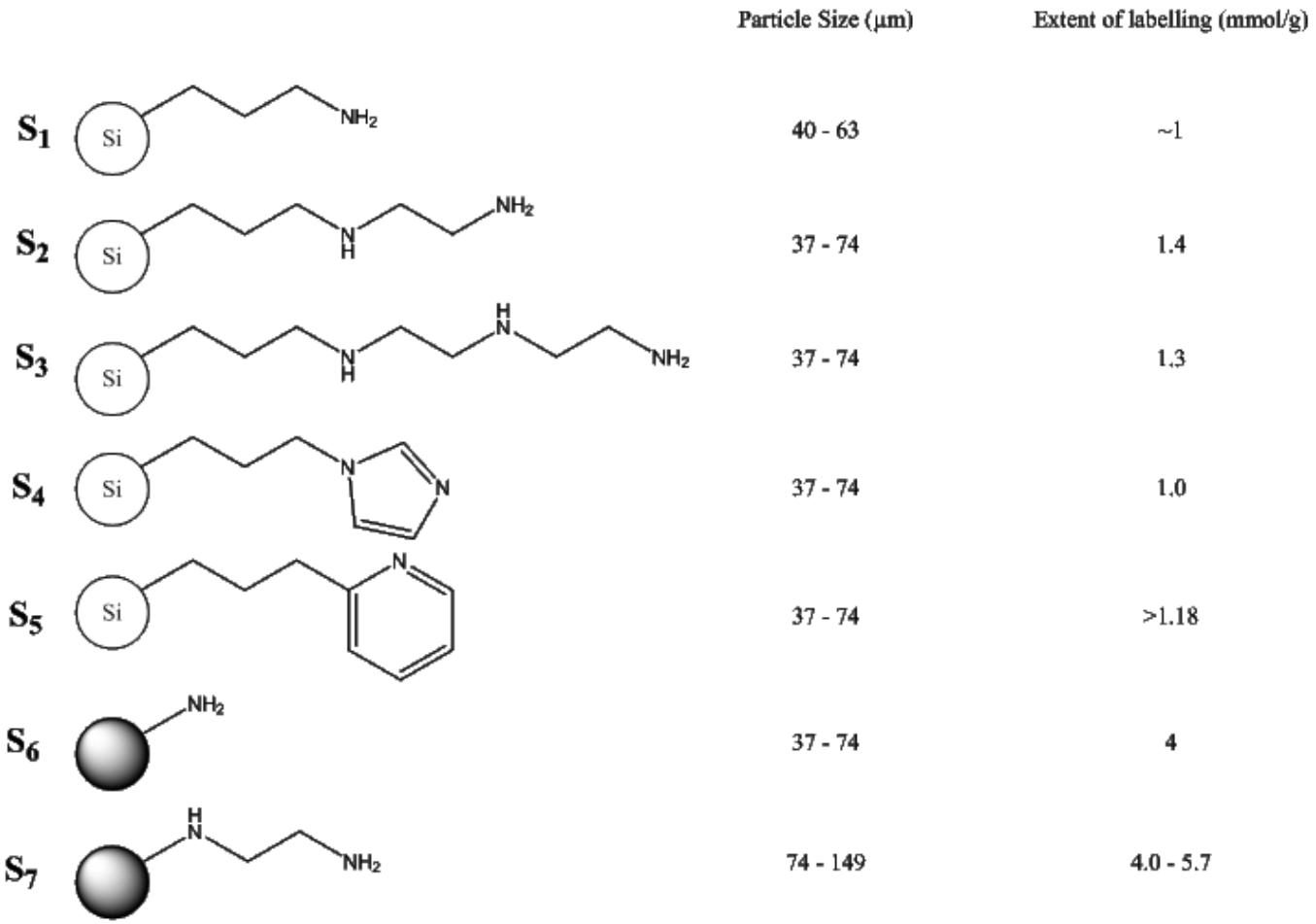


Figure 62. Solid supports tested as HET-SABRE catalyst candidates. Supports **$S_1$-$S_5$** are silica supported, **$S_6$** and **$S_7$** are polystyrene bound.

### 5.2.2. EDX testing of solid supports

Following the exposure of the supports to the SABRE pre-catalyst the species produced were evaluated for iridium content to assess the efficacy of this technique for a wider range of substrates. EDX was utilised to examine the iridium atomic weight percentage on the surface of the silica as the quantities utilised meant that analysis techniques such as XRF were not viable.

EDX is typically utilised to analyse samples with higher (*circa.* >10%) elemental weight loadings and iridium sensitivity, particularly for scavengers **$S_1$-$S_5$**, is hampered by the close proximity of K emission bands for Si and Ir. The iridium loading appeared to be relatively inconsistent across particles with the data shown in Table 23 representing an average from a minimum of 8 replicates. There is still, however, likely to be a large error in the data due to the lack of uniformity between particles – the relatively high deviations shown in Table 23 reflect this.

Table 23. Iridium percentage weight on the surface of the potential HET-SABRE catalysts synthesised with the standard deviation of measurements shown.

| Sample | Average iridium weight % |
|---|---|
| **$S_1$** | 0.459% ± 0.194% |
| **$S_2$** | 0.796% ± 0.267% |
| **$S_3$** | 0.891% ± 0.284% |
| **$S_4$** | 0.693% ± 0.268% |
| **$S_5$** | 0.194% ± 0.102% |
| **$S_6$** | 0.386% ± 0.158% |
| **$S_7$** | 0.422% ± 0.319% |

Table 23 highlights that at such low elemental concentrations there are large errors associated with some samples analysed by EDX. However, this was the most suitable quantitative technique available for the produced sample volumes.

Supports **$S_1$**-**$S_3$** show that, with increased chain length and potential binding sites, more iridium appears to be bound to the silica surface. Though a higher catalyst loading would likely be advantageous for HET-SABRE activity, it is possible that the binding of the iridium to supports **$S_2$** and **$S_3$** is enhanced through a chelate effect that may not be advantageous for catalyst turnover; this is further discussed in section 5.2.4.

Interestingly the relatively high iridium quantities detected for supports **$S_1$** and **$S_2$** aren't reflected in the results for the polymer bound analogues of similar functionality in supports **$S_6$** and **$S_7$**. This may be due to changes in surface area as the polymer particles appeared to demonstrate significantly more uniform shapes compared to the silica which demonstrate a wider range of

particle shapes, potentially increasing surface area, as demonstrated in Figure 63.

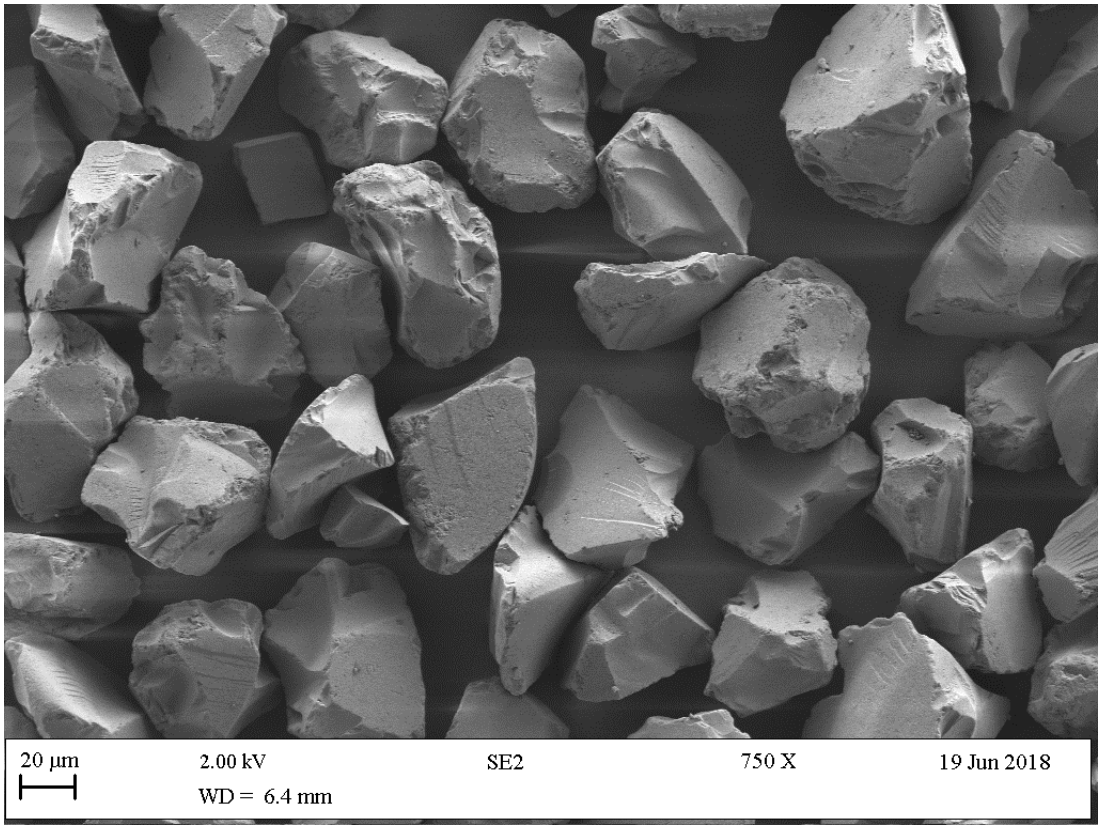


Figure 63. SEM image of **S5** prior to iridium loading.

The quantity of iridium bound to the surface of support **S4** is commensurate with that of support **S1** with a similar binding mode. Support **S4** does show a slight increase in iridium quantity compared to **S1** that may be due to the increased distance between the binding site and the steric bulk of the support. The additional iridium bound to **S4** may also be explained by the higher *p*K$_a$ of the imidazole (*p*K$_a$ of imidazole ~18.6)[161] leading to more favourable metal binding compared to the amine binding site of **S1** (*p*K$_a$ of ethylamine ~10.9).[162]

Support **S5** demonstrates the lowest iridium quantity on the surface which is unsurprising given previous attempts to bind a 2-substituted pyridine ring to the SABRE catalyst utilised have been unsucessful for 2-picoline,[126] for which the steric bulk of the methyl substituent had been blamed. Attemps to hyperpolarise 2-fluoropyridine have also resulted in negligible catalyst binding, as discussed in section 4.2.2, with only hyperpolarisation near unity being

observed, in addition to no hydrides attributable to an activated catalyst species being found, even when an alternative SABRE catalyst with a less bulky carbene was utilised.[96] Notably the less sterically encumbered 2-methylthiophene has reported SABRE hyperpolarisation utilising [Ir(IMes)(COD)Cl].[163]

### 5.2.3. HET-SABRE testing

Following initial analysis, all potential HET-SABRE catalysts were tested for activity making use of a sample containing 15 µL pyridine and 10 mg synthesised potential HET-SABRE catalyst in $d_4$-methanol (see 8.6.13).

Making use of the standard SABRE procedure utilised throughout this work, with a 10 s mixing time, no hyperpolarisation was observed. However, increasing the mixing time led to observable HET-SABRE in the catalyst derived from **S1**, with hyperpolarised signals first observed following a 20 s shake time and 30 s shake yielding the highest signal enhancements, suggesting a slow build-up of polarised species in solution. The proposed structure of this HET-SABRE active species is shown in Figure 22. It is proposed that the increased shake time is required due to the low frequency of triphasic interactions of *para*hydrogen with the catalytic surface within the solvent, likely limiting the availability of replacement *para*hydrogen derived hydrides to enable consistent polarisation transfer. The molecular tumbling effects of the solid support may have additional $T_1$ shortening effects upon the substrate that may compound an already slow polarisation build up. The consistent bubbling of *para*hydrogen through a HET-SABRE solution would likely, therefore, increase the enhancements observed. However, making use of the available equipment, this was not feasible and no HET-SABRE was observed for species derived from the other heterogeneous supports.

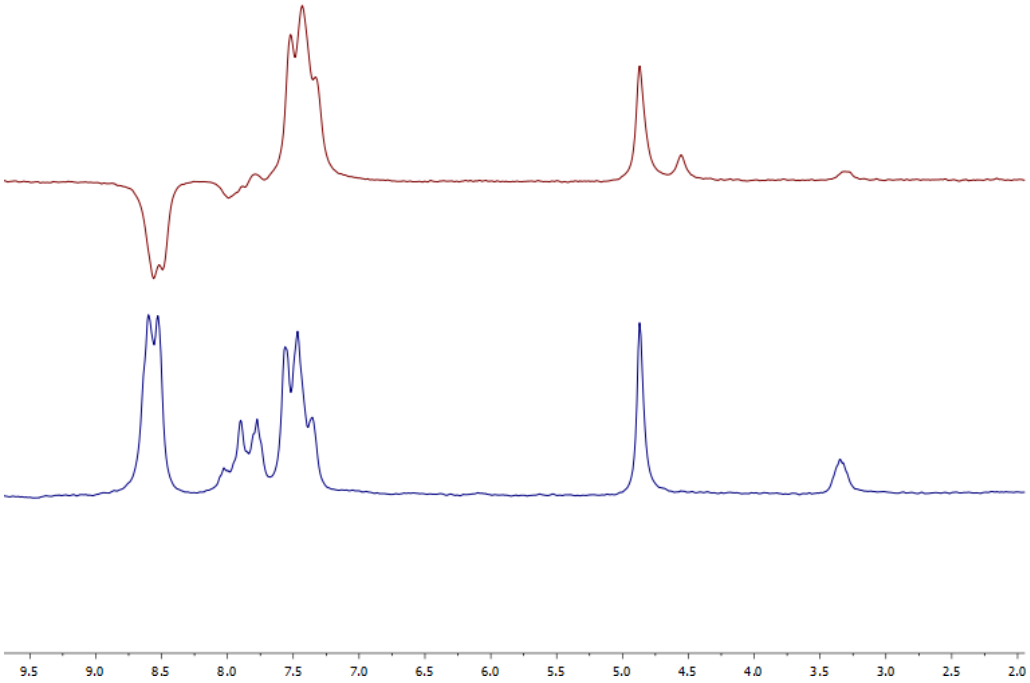


Figure 64. Observed HET-SABRE (top, red) of pyridine utilising catalyst synthesised from **S₁**. The associated thermal spectrum is shown below in blue.

Though HET-SABRE making use of **S₁** and [Ir(IMes)(COD)Cl] has been previously reported,[94] and the enhancements demonstrated in Figure 64 are below unity, the presence of antiphase signals, particularly for the *ortho* environment, demonstrates that a SABRE active species has formed on the support surface. The low enhancements are expected for a HET-SABRE system due to the scarcity of triphasic interactions between the catalytic sites on the support surface, the substrate and *para*hydrogen. The previous report of **S₁** forming a HET-SABRE catalyst sought to overcome this barrier to application through the use of continuous *para*hydrogen bubbling through solution.[94] However, the formation of an active species and subsequent observable SABRE polarisation is the aim of this study.

### 5.2.4. SABRE catalyst deactivation

As no HET-SABRE was observed for the prepared species, with the exception of support **S₁**, it was noted that supports **S₂**/**S₇** and **S₃** could potentially facilitate bidentate or tridentate binding modes respectively. This could therefore deactivate the SABRE catalyst in a similar manner to that previously reported

for bipyridine.[30] This could, therefore, explain the relatively high iridium loadings observed *via* EDX resulting in no observed HET-SABRE.

The characterisation of the support-bound species would be challenging, therefore analogues were sought. The ligands ethylenediamine and diethylenetriamine were utilised to simulate the heterogeneous supports in combination with **4**.

Following the addition of ethylenediamine or diethylenetriamine to a SABRE sample containing four equivalents of pyridine, relative to **4**, a significant reduction in polarisation on average across all environments was observed – 99.04% in the case of ethylenediamine and 99.55% in the case of diethylenetriamine. This result demonstrates that the homogenous equivalent to supports $\mathbf{S_2}$, $\mathbf{S_3}$ and $\mathbf{S_7}$ are effective at catalyst deactivation, which may prevent the formation of a HET-SABRE catalyst though the prevention of substrate binding.

The displacement of pyridine from the activated species $[Ir(IMes)(Pyridine)_3(H)_2]$ may be observed through monitoring the $T_1$ values associated with pyridine before and after the addition of ethylenediamine or diethylenetriamine.

Table 24. Pyridine $T_1$ values demonstrating the effect of changing environment with and without **4**, ethylenediamine and diethylenetriamine present.

| **4 present** | **Condition** | **Additional Ligand Added** | **Pyridine Environment** | **Pyridine Proton Environment $T_1$ (seconds)** | | |
|---|---|---|---|---|---|---|
| | | | | ***ortho*** | ***meta*** | ***para*** |
| No | Vacuum | No | Free | 31.165 | 26.892 | 35.221 |
| No | $H_2$ | No | Free | 30.384 | 26.232 | 35.166 |
| Yes | $H_2$ | No | Free | 4.176 | 6.452 | 7.848 |
| Yes | $H_2$ | No | Equatorially bound | 4.044 | 5.897 | 9.494 |
| Yes | $H_2$ | No | Axially bound | 1.802 | 3.433 | 5.103 |
| Yes | $H_2$ | Ethylenediamine (1.5 eq relative to **4**) | Free | 15.094 | 25.316 | 18.871 |
| Yes | $H_2$ | Diethylenetriamine (1.5 eq relative to **4**) | Free | 30.030 | 25.422 | 33.079 |

Table 24 demonstrates that the relatively long $T_1$ of pyridine is significantly reduced when in the presence of [Ir(IMes)(Pyridine)$_3$(H)$_2$] due to interactions with the extended spin system surrounding the iridium.[159] Notably exchanges are brisk enough, with recorded pyridine exchange speeds of 11.7 $s^{-1}$ at 300 K,[26] that the $T_1$ of the pyridine free in solution and not currently bound to the catalyst is still drastically shortened compared to when the catalyst is not present.

The addition of ethylenediamine reverses much of the decrease in $T_1$ caused by interaction with the iridium species. This is due to a majority complex forming (~90%), as shown in Figure 65, in which ethylenediamine binds *trans* to the *para*hydrogen-derived hydrides. This is analogous with reported orientations for bipyridine deactivation,[30] and prevents pyridine (substrate) exchange. Notably, in this spatial orientation with ethylenediamine bound *trans* to hydride ligands, pyridine would still be bound *trans* to IMes. Ligands bound to this site have been reported not to exchange, so this is unlikely to impact the relaxation time of free pyridine.[30]

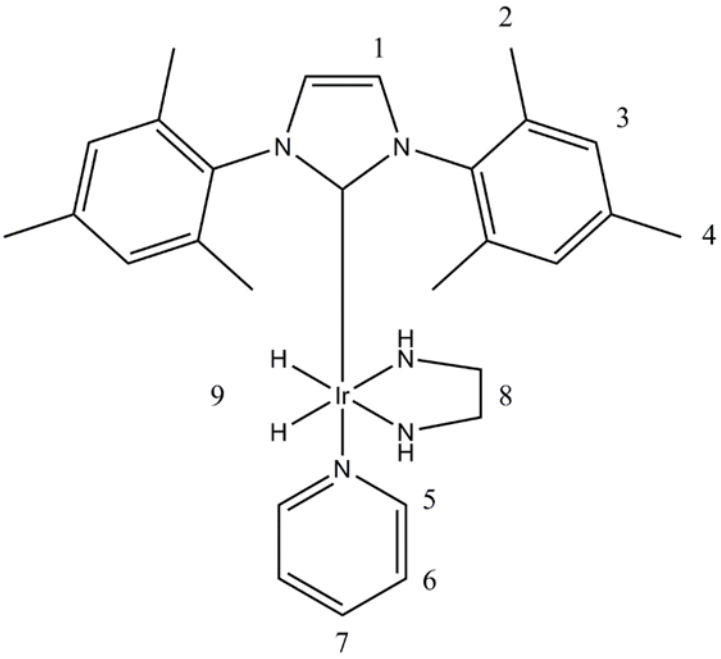


Figure 65. Major species in solution following addition of three equivalents ethylenediamine to [Ir(IMes)(pyridine)$_3$(H)$_2$].

Table 25. $^1$H NMR characterisation data for complex shown in Figure 65.

| Site number | $^1$H chemical shift/ppm |
|---|---|
| 1 | 7.10 |
| 2 | 2.20 |
| 3 | 7.13 |
| 4 | 2.39 |
| 5 | 8.49 |
| 6 | 7.16 |
| 7 | 7.73 |
| 8 | 2.05 |
| 9 | -21.84 |

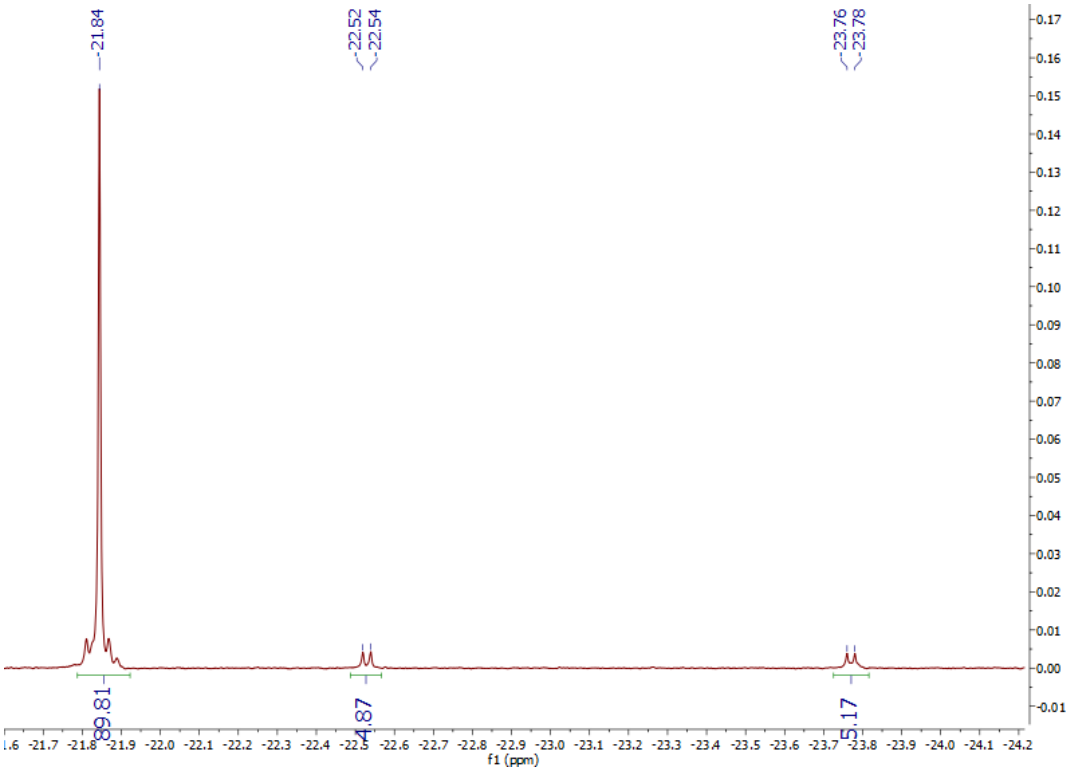


Figure 66. Hydride region demonstrating the major and minor species in solution following addition of three equivalents ethylenediamine to [Ir(IMes)(pyridine)$_3$(H)$_2$].

However, even with 1.5 equivalents of ethylenediamine added relative to the polarisation transfer pre-catalyst [Ir(IMes)(COD)Cl], the deactivation process appears incomplete as demonstrated by the incomplete restoration of relaxation times to levels commensurate with isolated free pyridine and the continued presence of some SABRE signals. Addition of 3 equivalents of ethylenediamine results in near complete catalyst deactivation, however, there are still minor hydride signals present, as shown in Figure 66, at -22.54 and -23.78 ppm at a ratio of ~5% each compared to the major species in solution. These chemical shift values are likely due to pyridine and methanol respectively bound *trans* to the *para*hydrogen derived hydrides. These peaks, however, are present at such concentration that full characterisation of the complexes was not possible.

Addition of diethylenetriamine appears to deactivate the SABRE active species more effectively with an average relaxation time (Table 24) of 96.6% that of isolated pyridine; this is commensurate with the 99.55% decrease in hyperpolarisation observed following diethylenetramine addition. This increase in deactivation efficacy may be due to a chelate effect with the tridentate diethylenetriamine forming a predominantly *fac*-isomer in solution, displacing pyridine from sites both *trans* to hydrides and the IMes ligand as shown in Figure 67. The formation of this isomer is supported though the lack of visible bound signals for pyridine in the $^{1}H$ NMR spectrum, even *trans* to IMes as shown in Figure 68.

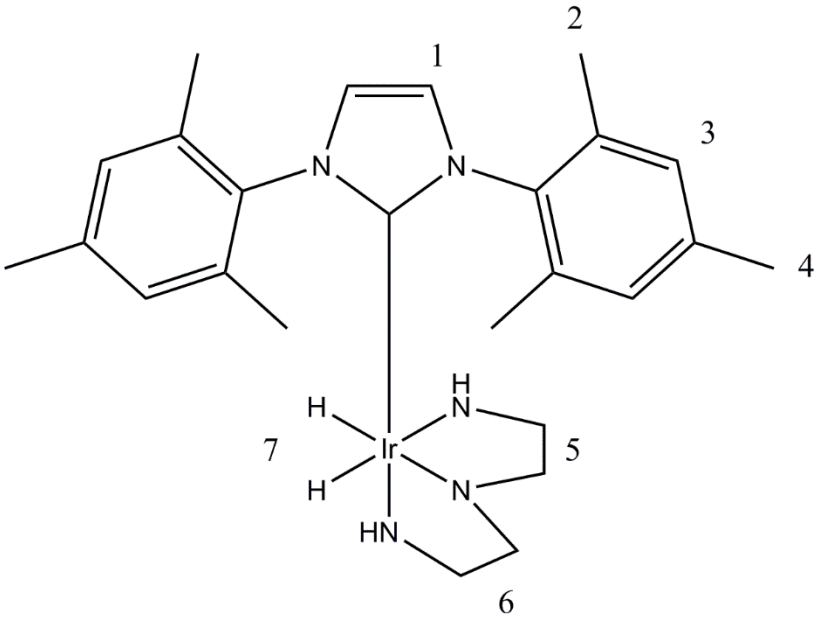


Figure 67. Majority species in solution following addition of 1.5 equivalents diethylenetriamine to $[Ir(IMes)(pyridine)_3(H)_2]$.

Table 26. NMR characterisation data for complex shown in Figure 67.

| Site number | $^{1}$H chemical shift/ppm |
|---|---|
| 1 | 7.03 |
| 2 | 2.11 |
| 3 | 7.07 |
| 4 | 2.36 |
| 5 | 2.16 |
| 6 | |
| 7 | -22.68 |

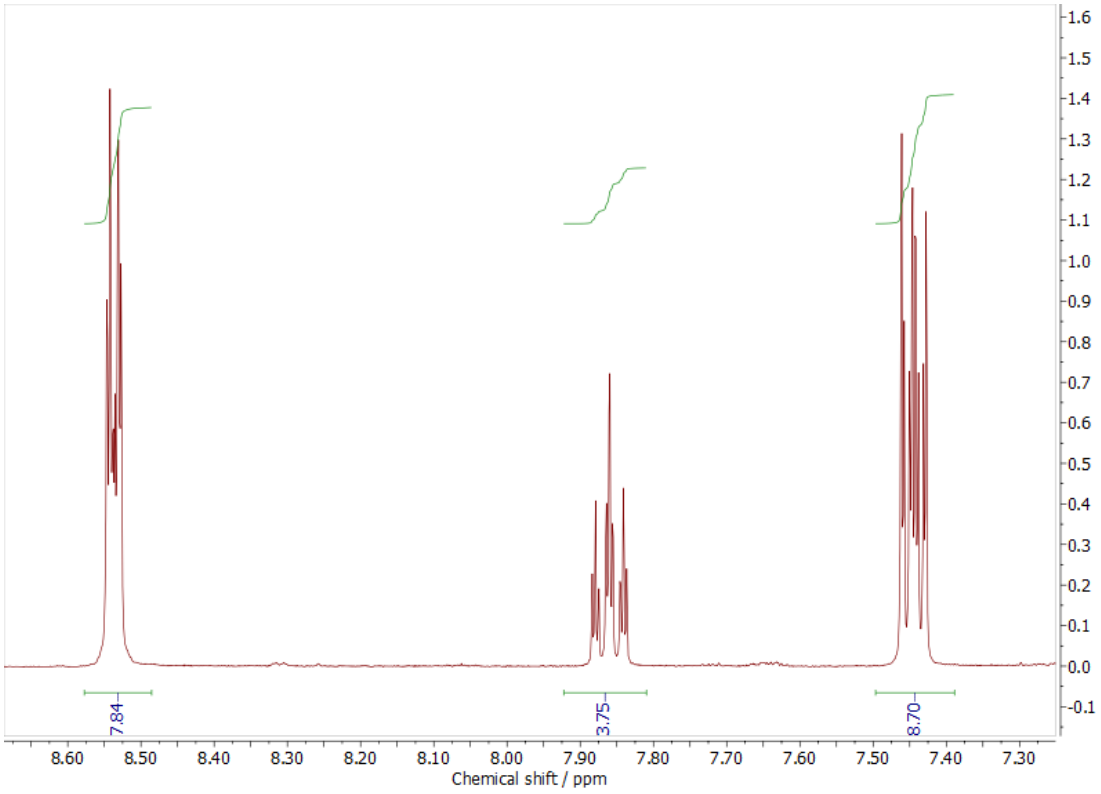


Figure 68. Aromatic region demonstrating the lack of bound pyridine peaks following addition of 3 equivalents diethylenetriamine to [Ir(IMes)(pyridine)$_3$(H)$_2$].

The main hydride occurring at -22.68, as shown in Table 26, is also similar to the reported signal attributed to [Ir(IMes)(ammonia)$_3$(H)$_2$] in which the hydride resonance is present at -23.61.[84]

With the homogenous model demonstrating that supports **S$_2$**, **S$_3$** and **S$_7$** specifically may deactivate the SABRE active species, an assessment was undertaken to consider if these supports may be useful in attempting to progress SABRE towards *in vivo* application through removing the cytotoxic iridium species and aiding in the preparation of a biocompatible bolus.[71]

## 5.3. Solid Supports as catalyst scavengers

The majority of the proposed solid supports **$S_1$-$S_7$** did not show HET-SABRE activity, however, all supports did show that iridium, specifically in the form of **4**, may bind to their surface.

The value of these proposed supports was, therefore, evaluated as a catalyst scavenger in order to remove the toxic iridium component from a homogenous SABRE hyperpolarised bolus that would be required for future *in vivo* application.[71, 78]

### 5.3.1. ICP-OES optimisation

ICP has previously been used for the determination of iridium removal from solution,[72, 73] therefore a method was designed for use with ICP-OES. This method made use of the most sensitive detection line at 224.268 nm with manual inspection of sample data ensuring there were no interferences.[164]

SABRE samples will contain a significant quantity of organic residue due to the catalyst bound carbene, methanol and pyridine used in this work. Though it is not possible to matrix match the iridium-bound organics, it was possible to account for the methanol solvent and pyridine substrate used to activate the polarisation pre-catalyst **4**. To do this, a stock solution containing the quantities of pyridine and methanol representative of a SABRE sample with 4 equivalents of pyridine used relative to **4** was prepared. This organic containing stock was then used to spike a range of iridium standards from 10 ppb to 10 ppm with 0-1% organic spiking. These standards were then analysed in both axial and radial viewing modes to assess which would be most suitable for this work (Figure 69 and Figure 70, respectively).

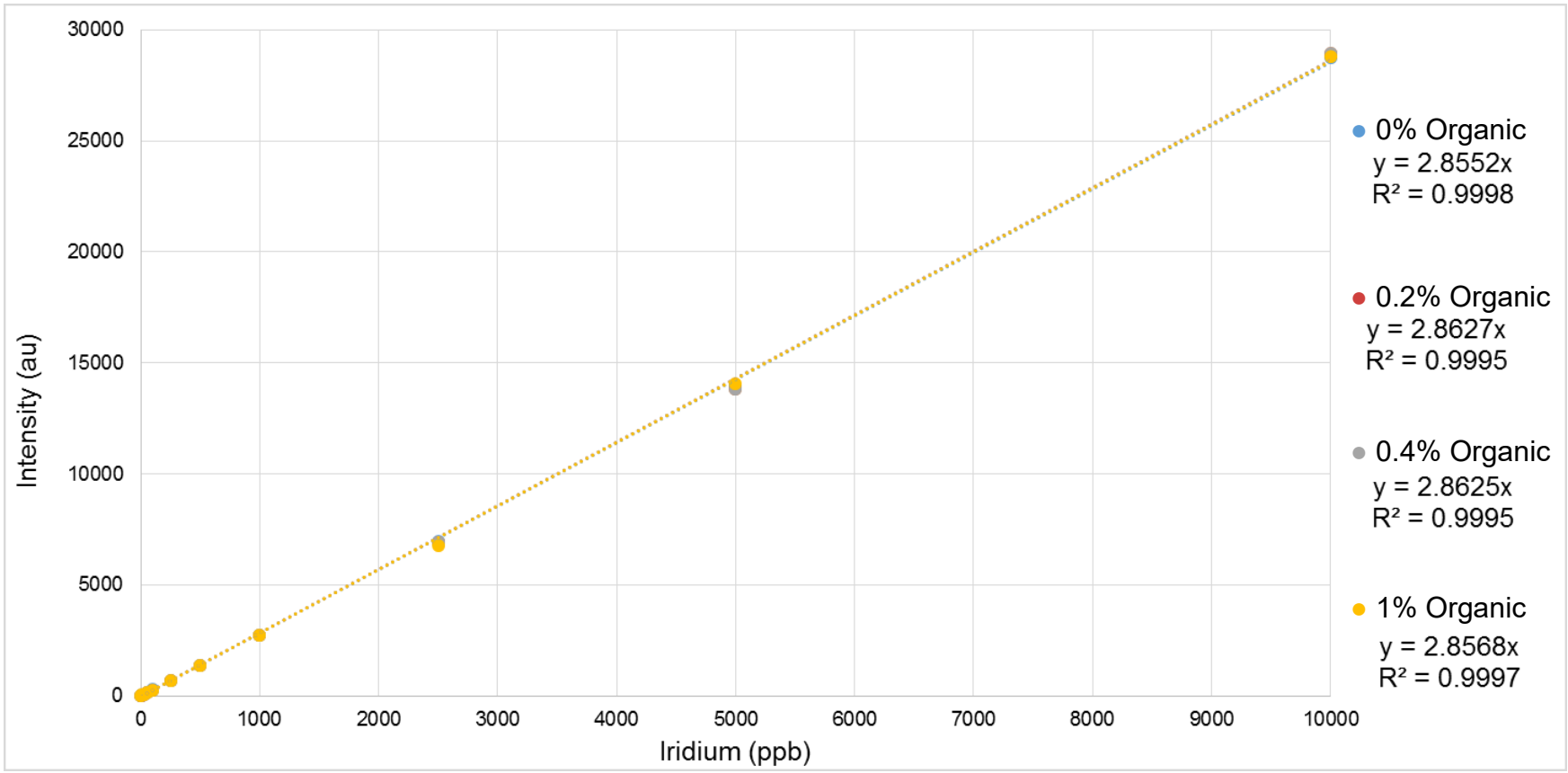


Figure 69. A calibration plot of 0 to 10 ppm iridium making use of the axial viewing mode. The stock solutions had been spiked with between 0 and 1% of an organic stock representative of the organics present in a SABRE sample.

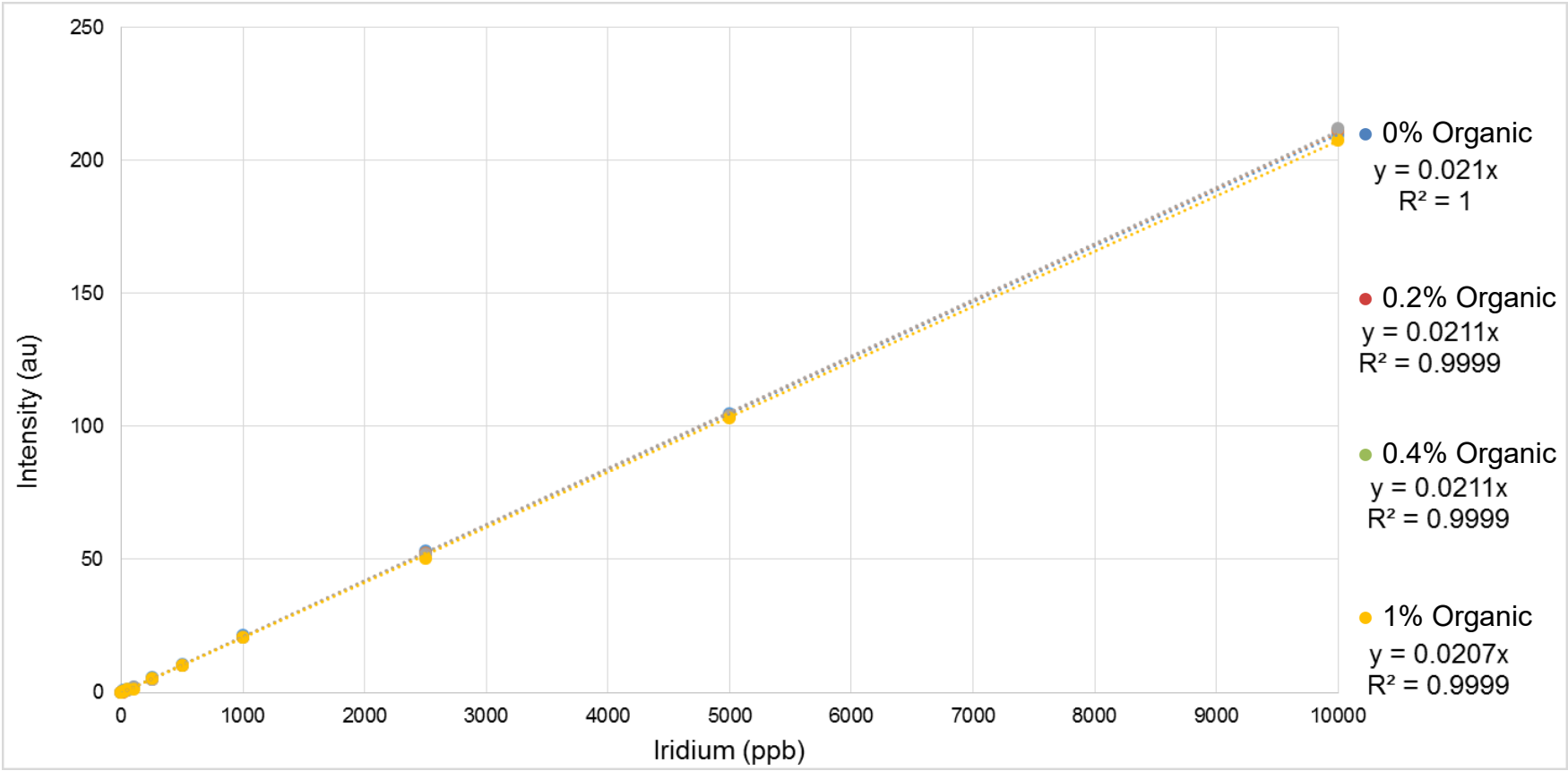


Figure 70. A calibration plot of 0 to 10 ppm iridium making use of the radial viewing mode. The stock solutions had been spiked with between 0 and 1% of an organic stock representative of the organics present in a SABRE sample.

These tests demonstrated that the presence of organics had a minor effect on the signal intensity observed. Changing the radiofrequency (RF) power from which the plasma is induced within the working range between 1050 and 1150 W demonstrated little effect, therefore, the instrument optimised value of 1175 W was used. The axial viewing mode was also utilised for further work as this provided the highest intensity and thus minimised the effect of the organic sample spiking. The standards spiked with 1% organic stock were utilised as standards for the quantitative determination of iridium concentration for the rest of this chapter as this was most representative of the analyte.

### 5.3.2. Effectiveness of heterogeneous catalyst scavengers

With an ICP-OES method established for accurately determining iridium content, the supports shown in Figure 62 were tested for efficacy as catalyst scavengers. 10 mg of each scavenger was vortexed into an iridium stock solution of known concentration in order to determine which support was the most effective scavenger and how much iridium was removed over a temporal range. Scavenger particles could potentially interfere with measurement *via* blockages in the sample injection system. Therefore, it was experimentally challenging to measure the iridium remaining after very short time periods as samples required centrifuging before analysis. The time point labelled t = 0 is therefore the fastest experimentally feasible testing time, with other time points labelled for the total 'wait' time without necessary centrifuge time considered. Further details of this method are included in section 8.8.3, with a flow chart demonstrating the preparation of samples t = 0 and t = 2 shown in Figure 71 and the actual exposure times of each sample summarised in Table 27.

Table 27. Actual exposure times due to experimental limitations of ICP-OES samples. An example of the preperation steps utilised for samples t = 0 and t = 2 is detailed in Figure 71.

| Label | Actual exposure time |
|---|---|
| t = 0 | ~ 2 mins |
| t = 2 | ~ 6 mins |
| t = 5 | ~ 11 mins |
| t = 10 | ~ 18 mins |
| t = 15 | ~ 25 mins |
| t = 20 | ~ 32 mins |

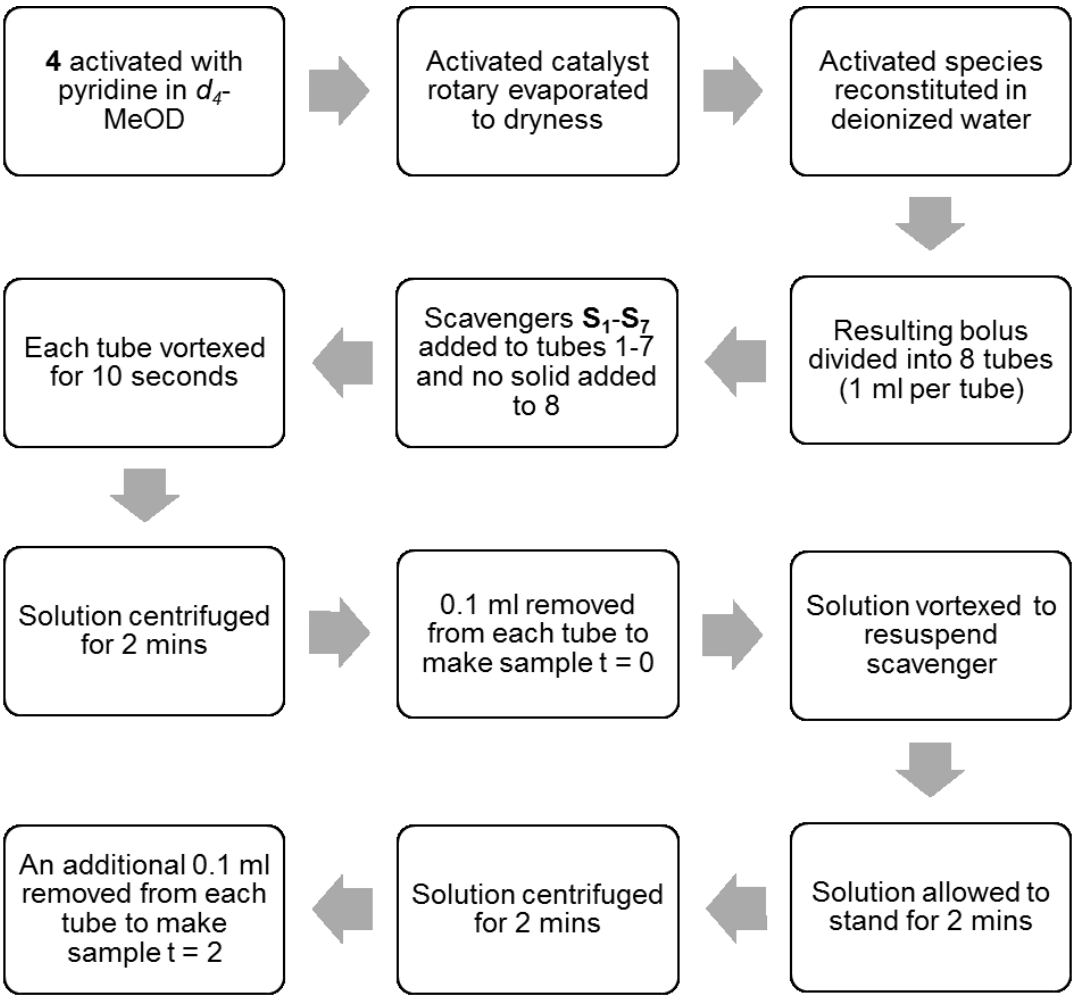


Figure 71. Flow chart demonstrating the preperation steps for ICP-OES samples t = 0 and t = 2. Additional time samples were gathered through the repetition of the vortex, wait, centrifuge, sample steps. This resulted in the actual exposure times shown in Table 27.

.

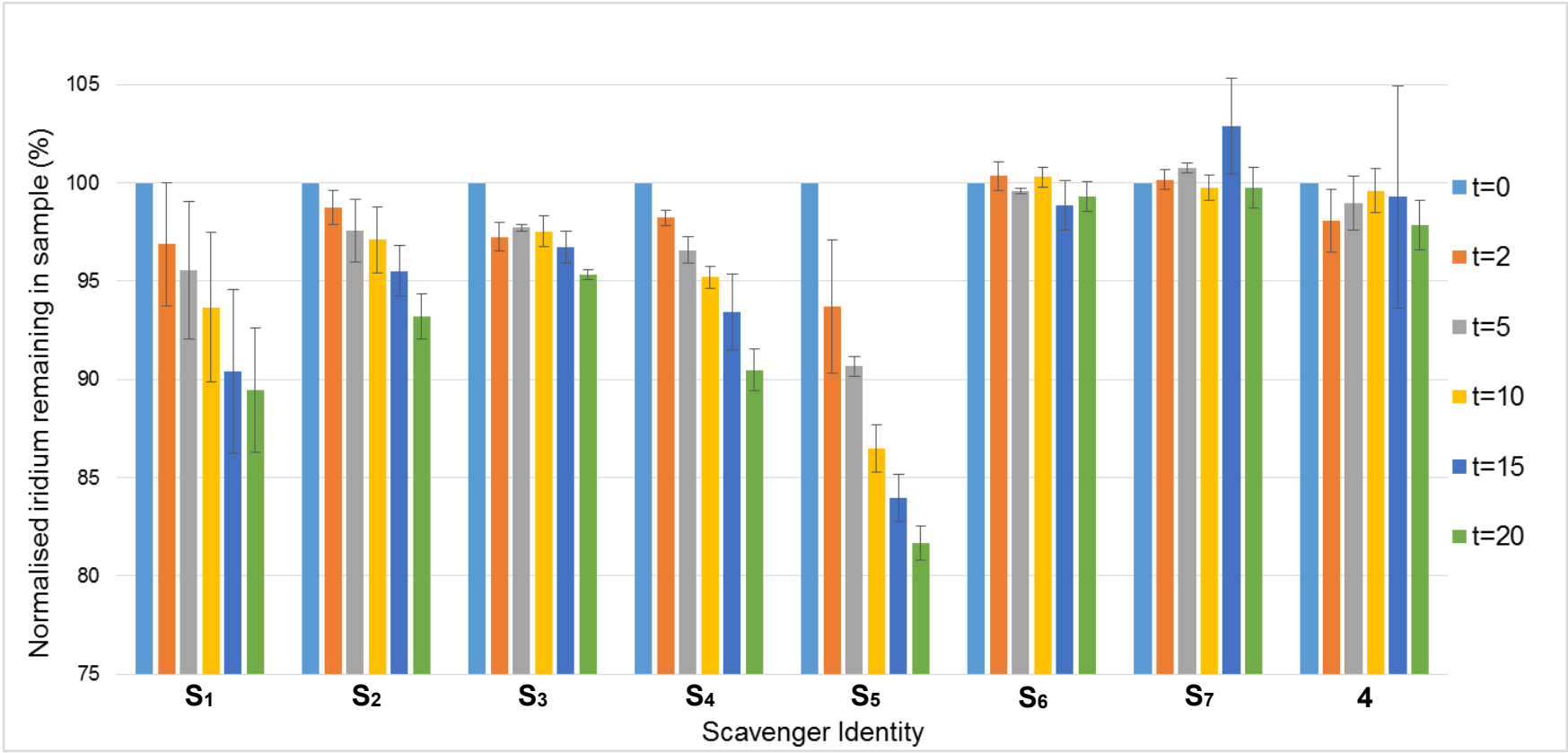


Figure 72. Iridium present in samples following the addition of 10 mg of scavengers **S1-S7** and with no scavenger added (**4**). Aliquots were taken over a range of time points with t = 0 being the fastest experimentally feasible sampling time (see section 8.8.3). Errors are one standard deviation between repeat samples. For ease of comparison, the ordinate has been focused towards the top end of the scale.

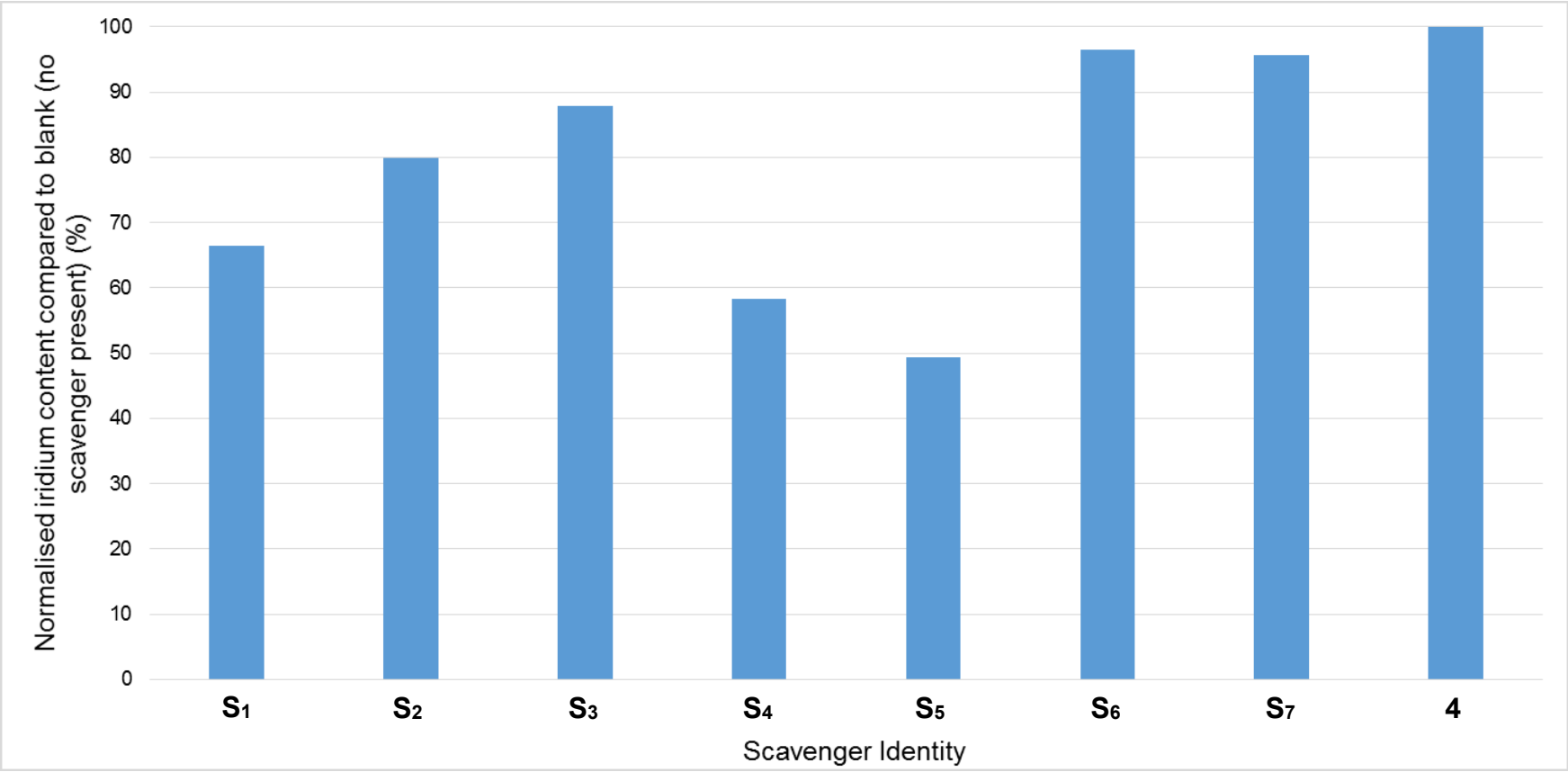


Figure 73. Iridium present in samples following the addition of 10 mg of scavengers **$S_1$-$S_7$** and with no scavenger added (**4**) after 12 days normalised to iridium content of the blank sample with no scavenger added.

Figure 72 and Figure 73 show the results for the testing of the potential catalyst scavengers (shown in Figure 62), thus enabling trends to be examined based on the labelling of the solid support.

Scavengers **$S_1$**, **$S_2$** and **$S_3$** share a common structure with increasing potential binding sites: surprisingly **$S_1$** was shown to be the most effective scavenging agent of these silica based materials. Chelate effects would imply that **$S_2$** and **$S_3$** may form more stable complexes with the iridium SABRE catalyst. This is supported by a previous report by Mewis *et al.* wherein 2,2'-bipyridine and 1, 10-phenanthroline,[30] which share a binding motif with scavenger **$S_2$**, strongly binding to the SABRE active iridium species homogenously to effectively deactivate the catalyst; this has been further discussed in section 5.2.4.[30] However, it is possible that the steric bulk of the silica support prevents multiple binding sites from being favoured. Scavenger **$S_3$** (reported as **$S_D$** by Barskiy *et al.*) has been shown to be capable of scavenging the iridium catalyst from solution, however, it was shown to be largely ineffective.[72] This appears to be in good agreement with the data presented in Figure 72 and Figure 73, however, a direct comparison cannot be made due to the decision to make use of a more uniform range of scavenger particle sizes and loadings than Barskiy *et al.*, this decision is discussed in section 5.2.1. Notably **$S_2$** appears to be a more effective scavenger than **$S_3$** despite diethylenetriamine demonstrating more effective catalyst deactivation in a homogenous model. The reduced efficacy demonstrated here to sequester the catalyst may be due to the local steric bulk of the support preventing the formation of the *fac*-isomer characterised in section 5.2.4. Scavenger **$S_1$** is demonstrated to be the most effective sequestering agent of **$S_1$**-**$S_3$**; the ability of this support to bind iridium has been previously reported in the context of synthesising an HET-SABRE catalyst during which catalyst leaching into solution was not observed.[94]

Scavenger **$S_4$** was also reported as **$S_B$** by Barskiy *et al.* in their 2018 report, however, it was shown to be significantly more effective than that of scavenger **$S_3$** – removing ~81% of the iridium present in solution within 12 hours.[72] Although Figure 73 shows that only ~42% of the iridium was removed in this work, it is worth noting that while the scavenger quantities are the same (10

mg of each), the initial iridium concentrations varied by orders of magnitude with this report's initial concentration being ~3.25 ppm compared to the ~82 ppb in the solution tested by Barskiy *et al.* It is, therefore, likely that this discrepancy is due to a saturation of the available binding sites on the surface of scavenger **S4** in this report.

Scavenger **S5** is novel and the most effective scavenger included in this test, continuing the theme of nitrogen containing heterocyclic binding motifs that began with **S4**. This result represents a novel and potentially highly effective new scavenger that may be used in the preparation of an iridium-depleted bolus. Despite this, previous attempts to hyperpolarise 2-substituted picoline substrates has been unsuccessful.[126] This has been attributed to steric effects, however, 2-substituted pyridine compounds have been shown to bind to **4** through the binding of 2,2'-bipyridine and 1,10-phenanthroline by Mewis *et al.* demonstrating that a sterically hindered pyridine may bind apparently irreversibly.[30] In a separate report, Pravdivtsev notes that SABRE hyperpolarised signals for sites on bound 2,2'-bipyridine may be detected but evidence of this ligand exchanging is not presented.[165]

Attempts to hyperpolarise 2-picoline as a homogenous analogue of scavenger **5** were unsuccessful as reported in literature.[126] However, when a co-ligand is utilised which may activate **4**, such as acetonitrile, then hyperpolarised signals corresponding to the ring of 2-picoline were evident, as shown in Figure 74.

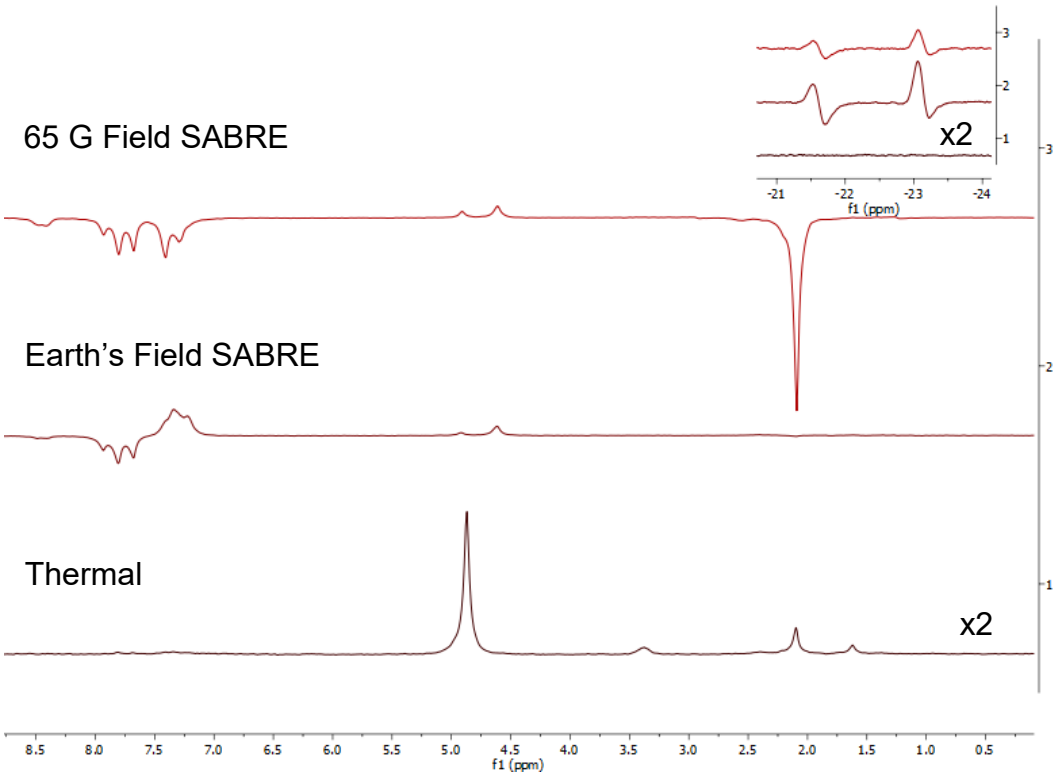


Figure 74. Spectra of 2-picoline (4 equivalents), acetonitrile (10 equivalents) relative to a single equivalent **4**. Hydride region shown as expansion. Thermal spectrum is scaled by 2-fold relative to the other spectra.

Table 28. 2-Picoline SABRE enhancements at earth's field and 65 G when acetonitrile is utilised as a co-ligand.

| Magnetic Field in which hyperpolarisation conducted | Proton Environment Enhancement | | |
|---|---|---|---|
| | *Ortho* | *Meta* | *Para* |
| Earth's Field | 9.28 | 28.14 | 39.35 |
| 65 G | 19.46 | 32.53 | 54.62 |

Utilising acetonitrile as a co-ligand in order to hyperpolarise 2-picoline resulted in SABRE being observed. This novel result shows relatively good enhancements and a pair of hydrides occurring at -21.69 and -23.14 ppm. The first resonance is broadly in agreement with a resonance of -20.56 which has been reported for a hydride *trans* to acetonitrile in the complex

[Ir(IMes)(Acetonitrile)(Pyridine)$_2$(H)$_2$] suggesting this is the acetonitrile adduct within the 2-picoline containing complex.[166] The hydride *trans* to pyridine in the report by Mewis *et al.* is reported at -22.12 ppm and hydrides *trans* to ammonia have been reported at -23.61 ppm,[84] therefore it seems likely the hydride herein present at -23.14 ppm can be attributed to the hydride *trans* to 2-picoline. The polarisation reported here demonstrates that when a co-ligand is present which can pre-activate the metal complex then the functionality present in **S$_5$** is capable of binding to the iridium catalyst. In this instance pyridine pre-activated the complex as this was utilised in the preparation of the ICP-OES bolus due to the need for water solubility.[80]

Interestingly scavengers **S$_6$** and **S$_7$** demonstrated essentially no scavenging effect, with Figure 73 showing <5% iridium removal for both agents after a period of 12 days. As scavengers **S$_1$** and **S$_2$** are directly comparable with scavengers **S$_6$** and **S$_7$** in terms of binding modes, this significant difference in efficacy is likely due to the difference in support identity, polystyrene for scavengers **S$_6$** and **S$_7$** compared to silica for scavengers **S$_1$**-**S$_5$**. This observation is in line with the single polystyrene scavenger reported which was the worst of the scavengers so far assessed in literature with steric effects of the support cited as the likely cause.[72, 93]

From the data presented in Figure 72 and Figure 73, the most effective scavengers appear to be agents **S$_1$**, **S$_4$** and **S$_5$**, having all shown that 10 mg scavenger may remove >1 ppm iridium over a long time period (12 days) and >60 ppb by t = 0 (method in 8.8.3). By t = 5 these three scavengers had removed >115 ppb Ir from solution, notably more than the initial concentration tested by Barskiy *et al.* in their 12 hour assessments of scavenger efficacy.[72]

### 5.3.3. Effect of changing scavenger quantity utilised

Given the performance of scavengers **S$_1$**, **S$_4$** and **S$_5$** examined in 5.3.2, it was decided to increase the concentrations of these scavengers above the 10 mg of each scavenger utilised in 5.3.2. This increase in quantity used was to examine the effect of this on their iridium scavenging efficiency.

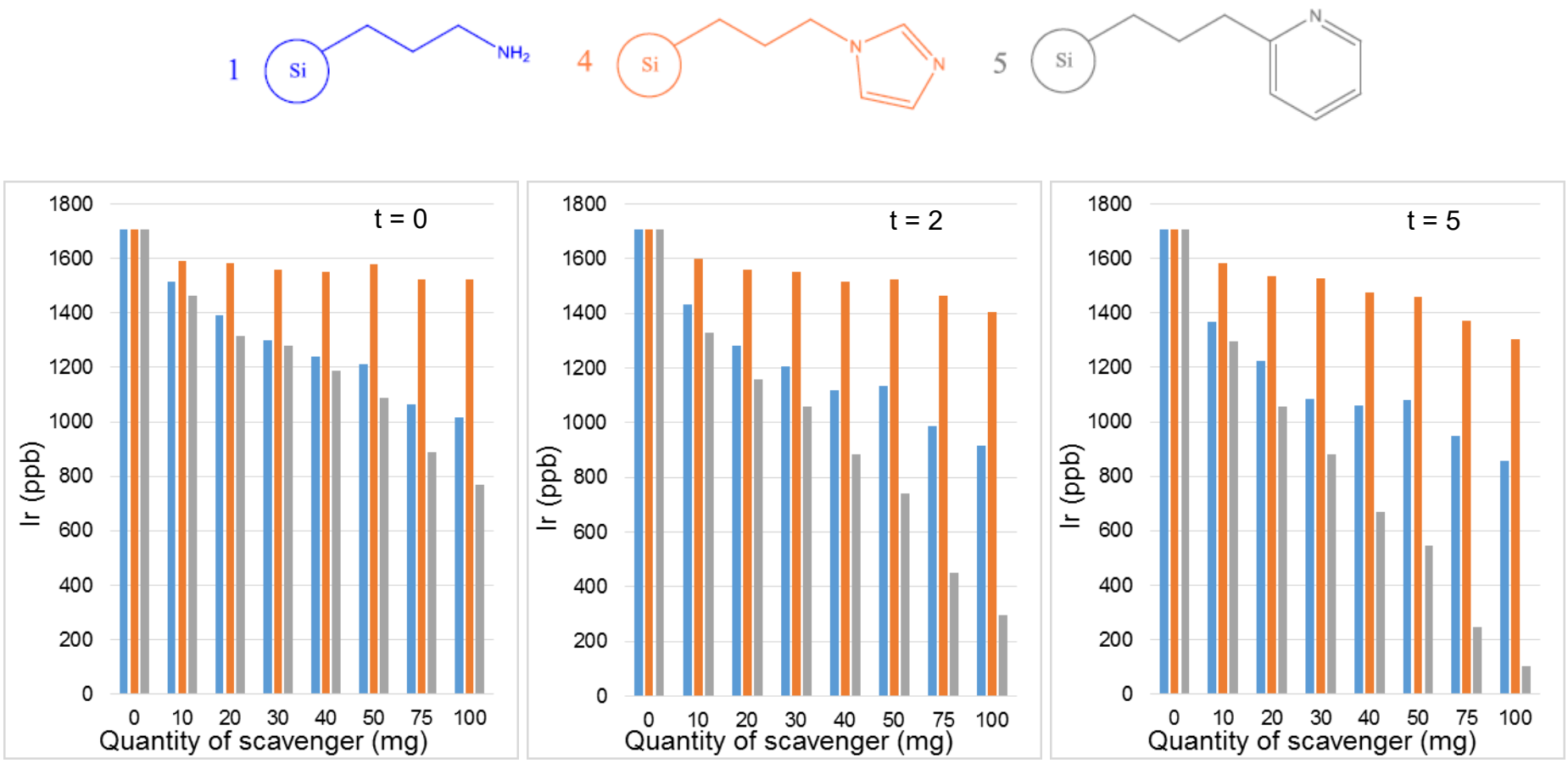


Figure 75. Amount of iridium present in samples following the addition of a variable amount of each scavenger (**S**$_1$ blue, **S**$_4$ orange, **S**$_5$ grey) after t = 0, 2 and 5 as defined in section 8.8.3. Error bars omitted for clarity.

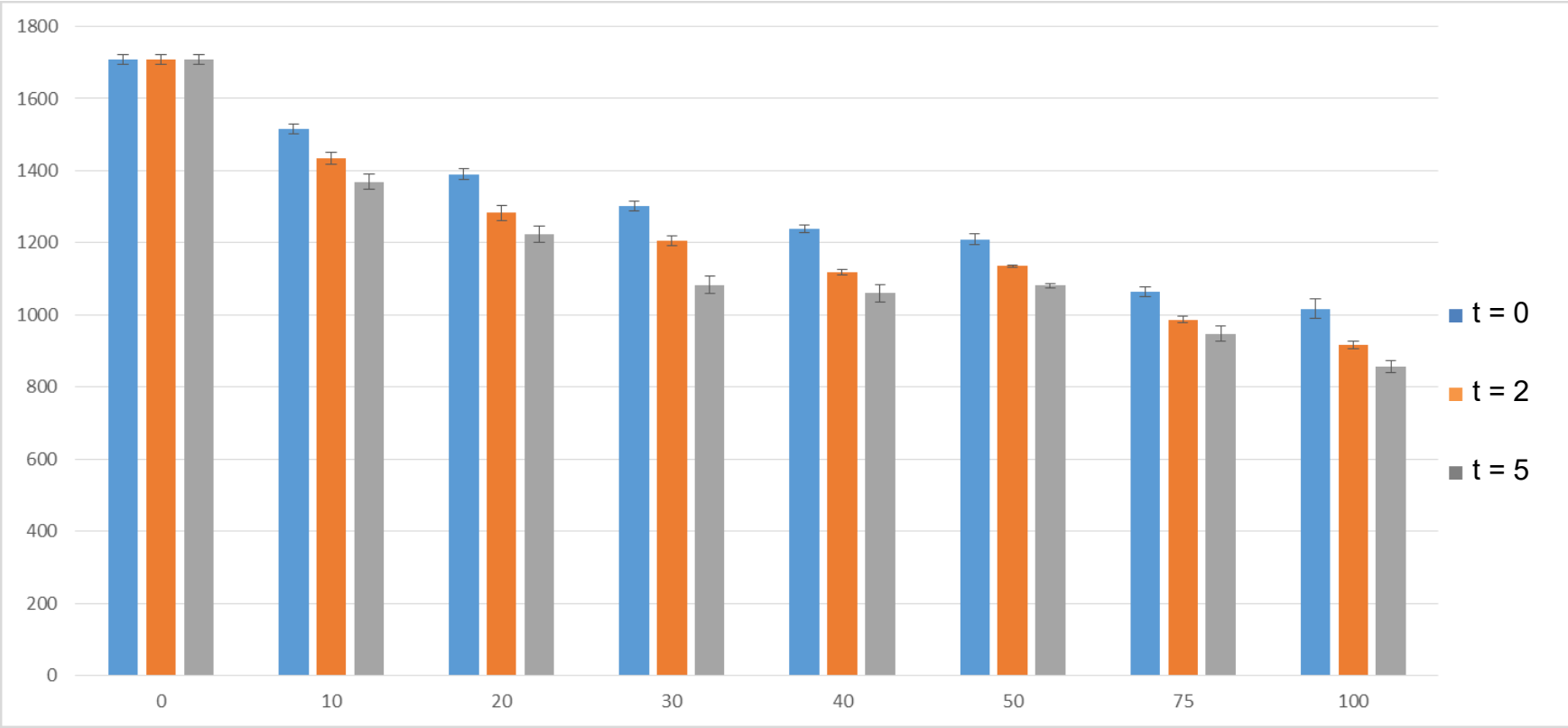


Figure 76. Amount of iridium present in samples following the addition of a variable amount of scavenger **$S_1$** after t = 0, 2 and 5 as defined in section 8.8.3. Error bars show the standard deviation between repeats of the same sample.

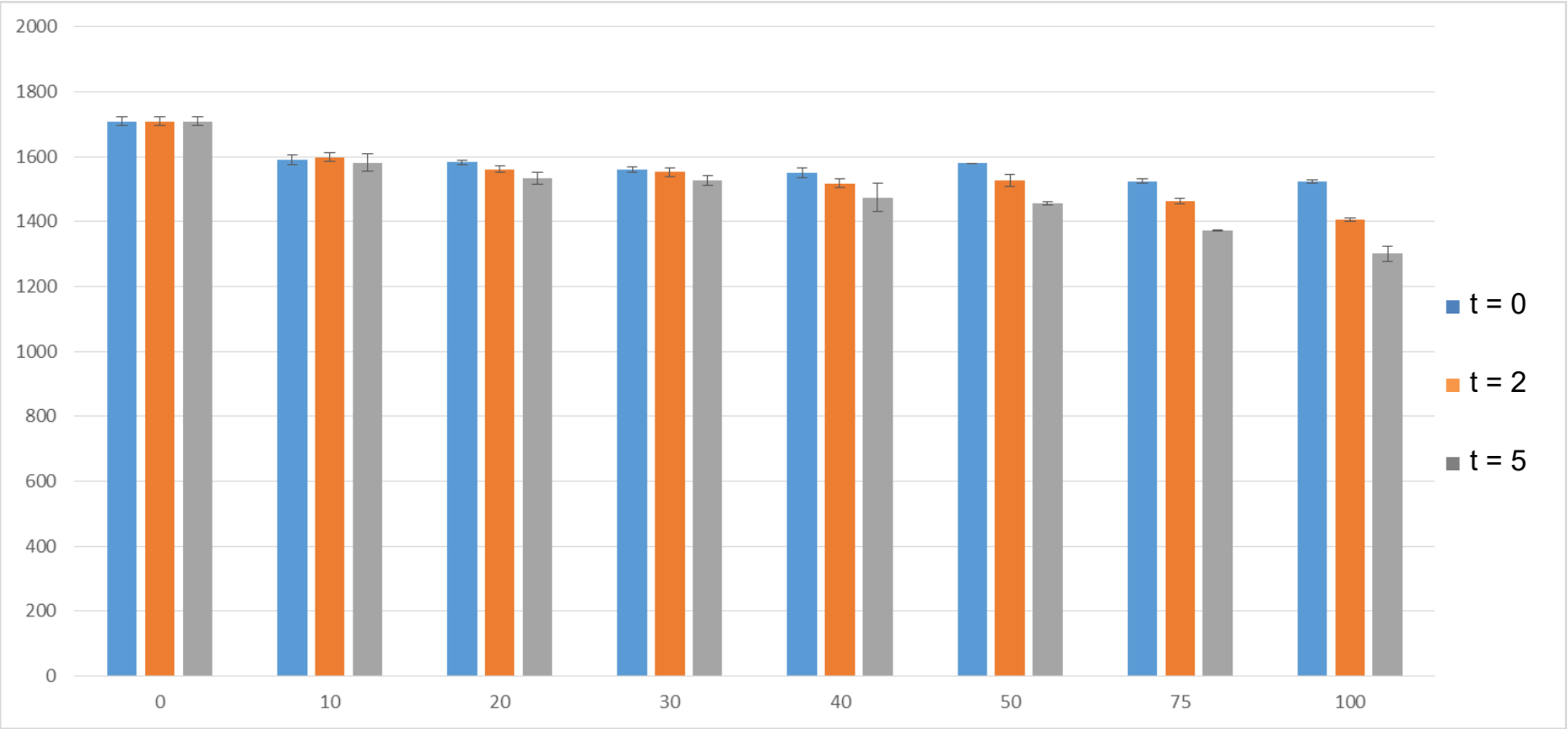


Figure 77. Amount of iridium present in samples following the addition of a variable amount of scavenger **$S_4$** after t = 0, 2 and 5 as defined in section 8.8.3. Error bars show the standard deviation between repeats of the same sample.

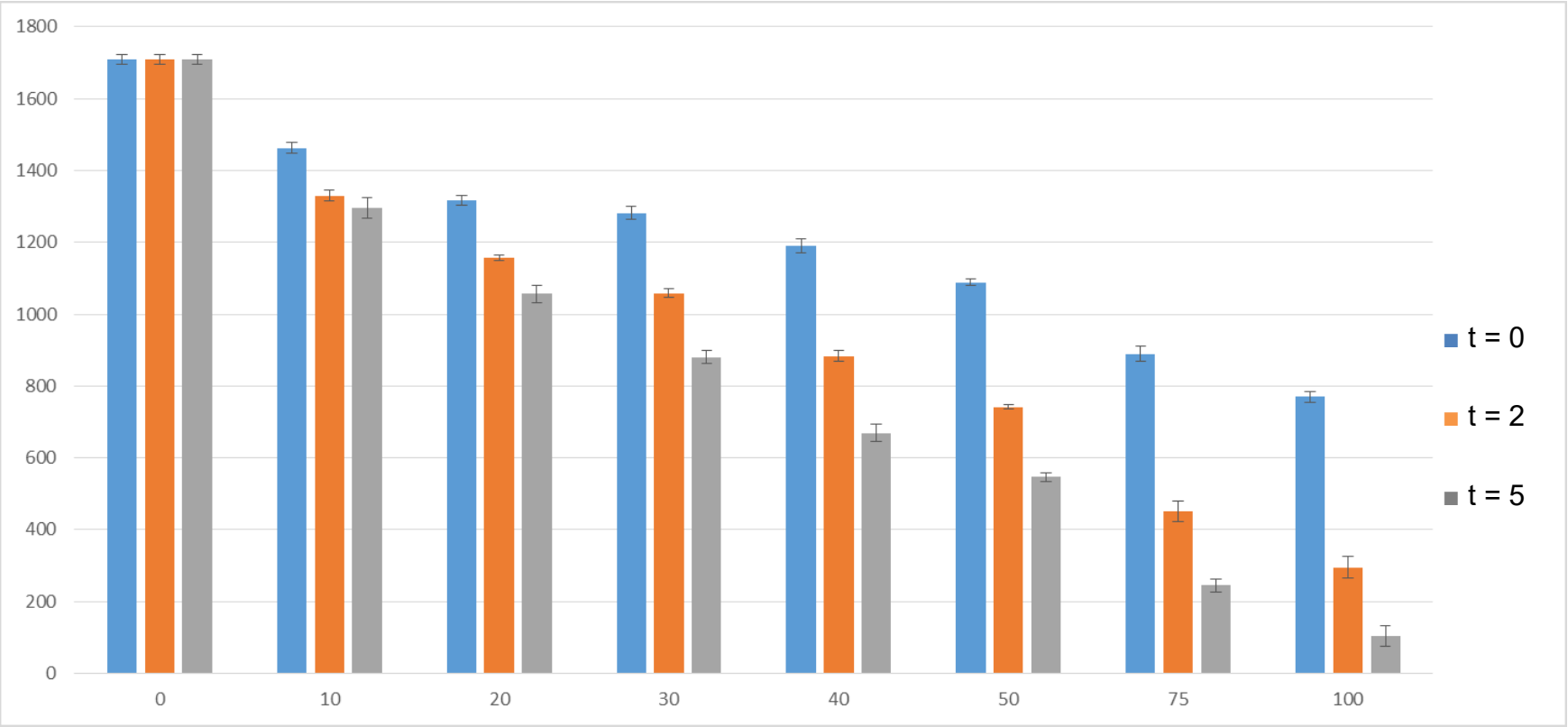


Figure 78. Amount of iridium present in samples following the addition of a variable amount of scavenger **$S_5$** after t = 0, 2 and 5 as defined in section 8.8.3. Error bars show the standard deviation between repeats of the same sample.

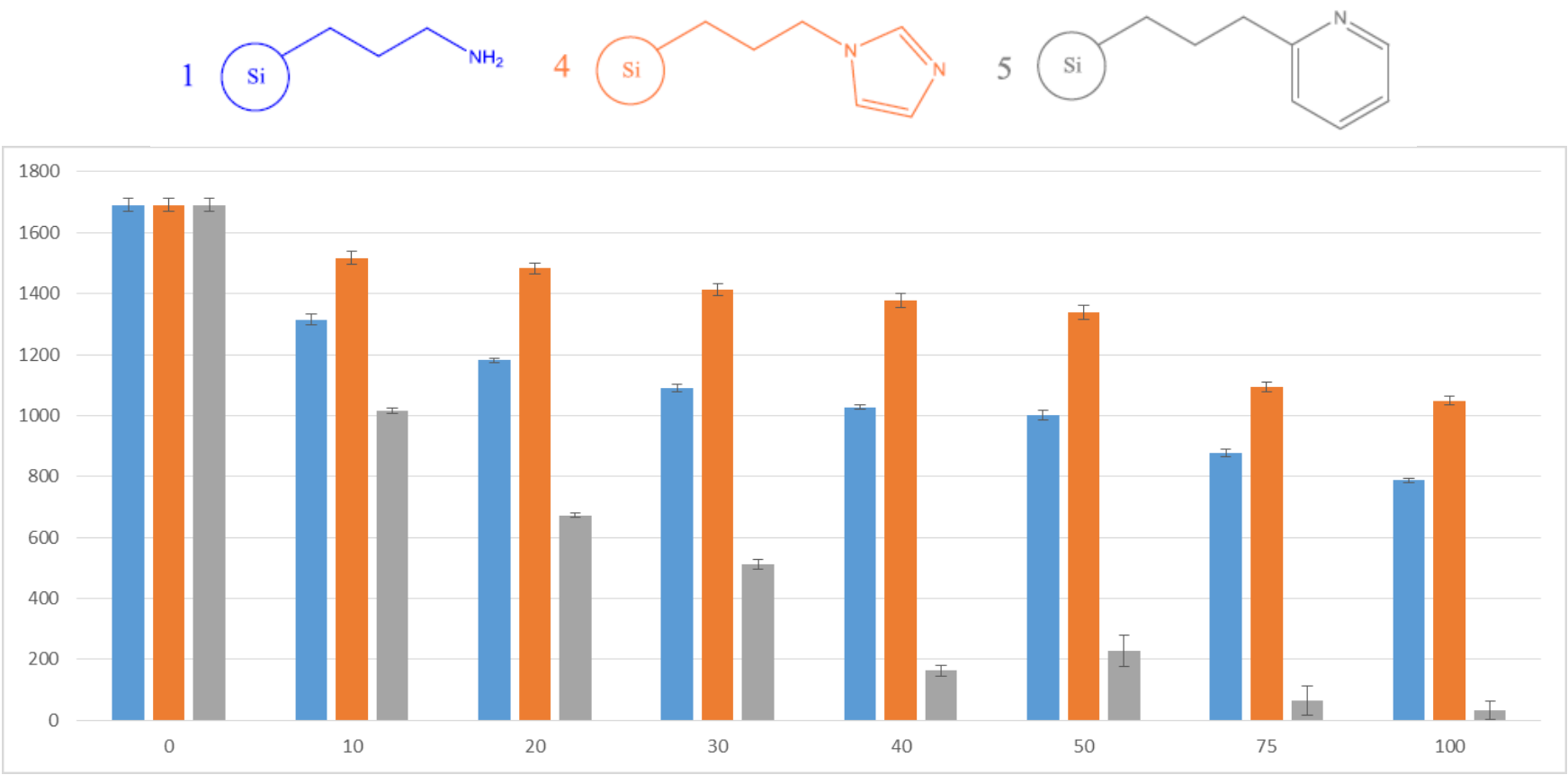


Figure 79. Amount of iridium present in samples following the addition of a variable amount of each scavenger (**$S_1$** blue, **$S_4$** orange, **$S_5$** grey) after one day. Error bars show the standard deviation between repeats of the same sample.

Figure 75 - Figure 79 present an overview of data for varying the scavenger quantities of **$S_1$**, **$S_4$** and **$S_5$**. As expected, increasing the quantity of scavenger and exposure time both resulted in a marked decrease in iridium concentration remaining in solution for all scavengers.

Figure 77 demonstrated that scavenger **$S_4$** resulted in the least iridium being removed from solution of this study, supporting the data shown in Figure 72, that over short time periods both scavengers **$S_1$** and **$S_5$** perform better.

Scavenger **$S_1$** performs well, with Figure 76 demonstrating that 100 mg is able to sequester ~692 ppb of iridium in t = 0 (actual exposure time ~2 min), however, the previously unreported scavenger **$S_5$**, is able to remove ~939 ppb Ir in the same time period, shown in Figure 78. This represents a total removal of ~55% of the iridium present. This may be compared with the results of Barskiy *et al.* whose best scavenger removes ~99.6% of the iridium present under the same conditions.[72] Although a higher percentage removal, the initial concentration reported by Barskiy was 63.7 ppb, meaning the absolute iridium removed was 63.4 ppb, an order of magnitude below that demonstrated herein by scavenger **$S_5$**. It is not possible to directly compare the individual scavenger efficacy beyond overall percentage removal due to the considerations discussed in 5.2.1, however **$S_4$**, the least effective of these three scavengers was employed by Barskiy *et al.* as **$S_B$** (significantly higher particle size, similar loadings) and found to be one of the most effective scavengers previously reported.[72] Comparing the efficacy of **$S_B$** and **$S_4$**, the latter is likely to have a higher surface area due to it's smaller particle size which may increase its scavenging efficacy but it is still outperformed by **$S_1$** and **$S_5$** reported here.

With a longer retention time, as shown in Figure 78, of t = 2 (actual exposure time ~6 mins) a far higher quantity of iridium may be removed by scavenger **$S_5$**, with ~1.4 ppm (~83%) removal. After t = 5 (actual exposure time ~11 mins) this increases to 1.6 ppm (~94%) of the iridium present.

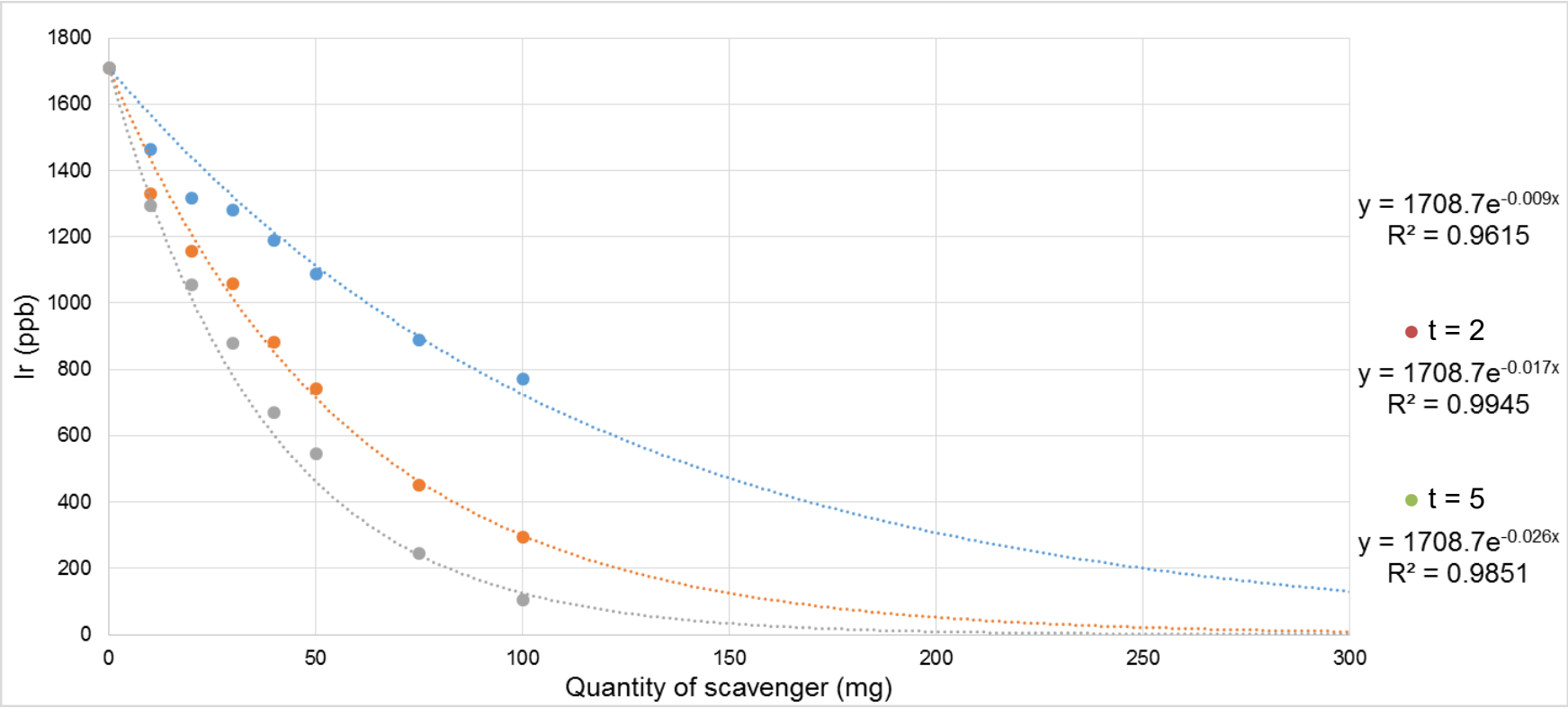


Figure 80. Amount of iridium present in samples following the addition of a variable amount of scavenger **$S_5$** after t = 0, 2 and 5 as defined in section 8.8.3. Quantity of scavenger is extrapolated to demonstrate how much scavenger would be required for near complete iridium removal.

The quantity of scavenger **S5** required to achieve a level of iridium equal to the average value of the deionized water blanks (0.2126 ppb) run at the same time as these samples may be calculated through extrapolation of the data, presented in Figure 80, making use of the calculation detailed in 8.8.4.

Table 29. Calculated quantities of scavenger **S5** required to achieve iridium level equal to the measured blanks.

| Time | Quantity of **S5** Required (mg) |
|---|---|
| T = 0 | 999.1 |
| T = 2 | 528.9 |
| T = 5 | 345.8 |

Calculated (equation shown in 8.8.4, data shown graphically in Figure 80), quantities of scavenger **S5** required to achieve iridium level equal to the average of deionized water blanks are shown in Table 29. This assumes the trends observed over the measured quantities continue.

Table 29 demonstrates that for t = 0 (actual exposure time ~2 mins, see section 8.8.3) about 1 g of scavenger **S5** would be required to remove ~1.7 ppm of iridium from solution under the conditions employed in this report. Recent reports have demonstrated that longer residence times are not necessarily a barrier to application towards an *in vivo* usage as biologically relevant drugs, such as the antibiotic metronidazole,[55] may be hyperpolarised with a $T_1$ of ~10 mins allowing time for iridium removal.[158, 167] This solid scavenging technique could be further integrated with complimentary purification techniques such as catalyst separated SABRE (CASH-SABRE) in order to formulate an efficient approach towards a clinical setting.[89]

It is notable that the experimental method reported here is unlikely to be the most effective approach towards catalyst sequestering as limits on available SABRE pre-catalyst stock meant that samples for different time points were repeatedly vortexed and centrifuged. This centrifugation likely reduced the

scavenging efficiency of the solids due to a reduction in sample homogeneity. It is envisioned that moving towards an automated flow system approach the scavengers may therefore be slightly more effective. The logical approach for preparing a metal free bolus for injection would be packing a column and injecting the iridium rich solution through a plug of the scavenger – this has been reported to have similar efficiency to 'passive' scavenger exposure over a short retention time.[72]

## 5.4. Conclusion

The attempted synthesis of a range of HET-SABRE catalysts is presented and HET-SABRE is demonstrated for **S1**. Though the enhancement attained was reduced compared to a previous report this could likely be improved through the utilisation of *para*hydrogen bubbling through solution, and demonstrated the synthetic approach employed could result in HET-SABRE activity.[94]

Though the majority of supports tested did not show HET-SABRE activity, this was explained utilising a homogenous model for supports **S2**, **S3** and **S7**, which demonstrated they may be effective agents for catalyst deactivation.[30] Removal of [Ir(IMes)(COD)Cl] from solution by a support may be a timely solution as despite its utilisation as the SABRE catalyst resulting in highest enhancement levels attained, in the majority of cases, recent work has demonstrated this iridium species is cytotoxic.[32, 71, 78, 113] Therefore, the potential for the supports to be utilised removing this cytotoxic species from a bolus was examined.

The metal scavenging efficacy of the supports was examined and scavengers **S1**, **S4** and **S5** were shown to be particularly effective. During this work a report was published which meant literature comparisons could be made with scavengers **S3** and **S4**. Though the work reported here represents a lower percentage removal of iridium from a SABRE bolus, the quantity removed was significantly higher making use of an initial iridium concentration closer to that which may be required in a clinical setting.

Extrapolation of the scavenger data suggests that ~1 g of the most effective scavenger, **S5** (which is novel), would render iridium below the level detected

in blanks for the ICP-OES instrument utilised in this study with an initial concentration of ~1.7ppm and an exposure time of ~2 mins. With the quantity required dropping significantly with longer exposure times, the relaxation time of the proposed substrate would have to be considered when designing applications of this approach. It is envisaged that this novel scavenger could, in combination with other approaches, such as CASH-SABRE,[89] enable the rapid preparation of a biocompatible SABRE hyperpolarised bolus. Barskiy *et al.* demonstrated that a biphasic approach could remove 99-99.9% of iridium from a sample.[72] This means utilisation of this approach, combined with ~1g of **S$_5$** should be capable of reducing a sample commensurate with a typical SABRE sample (2 mg of **4** in 0.6 ml, ~1005 ppm) to background levels of iridium present within the hyperpolarised $T_1$ of a suitable substrate.[158, 167]

# 6. Studies towards the application of SABRE to biologically relevant substrates

## 6.1. Introduction

Despite progress towards an *in vivo* application of SABRE through the utilisation of $^{19}F$ to alleviate background signal interference,[68, 96] extending the longevity of the hyperpolarised state,[30, 168] and progress towards a non-toxic bolus,[71, 72, 78] the scope of biologically relevant molecules to which SABRE has been applied remains relatively limited.

This chapter aims to demonstrate the application of SABRE to the study of new psychoactive substances (NPS), specifically fentanyls, in which sensitivity is an issue due to their potency and to a world health organisation (WHO) medicine, voriconazole, which is approved for clinical use.[169]

### 6.1.1. Previous SABRE of biomolecules

SABRE has been applied to a range of biologically relevant molecules within literature. These molecules broadly fall within two categories: those which are clinically relevant and do not require chemical modification to be suitable for SABRE (may reversibly bind to the polarisation transfer catalyst), and those biomolecules, such as peptides, which require chemical modification and labelling, typically with pyridine, in order to be SABRE active.

#### 6.1.1.1. Drugs

Early work by Olaru *et al.* to apply SABRE towards biomolecules focused on applications to vitamin B3 and nicotinic acid.[128] Olaru *et al.* demonstrated that 5 equivalents of nicotinic acid relative to **4** yielded the greatest enhancements (though 4 equivalents was not examined) when measured at a magnetic field of 65 G.

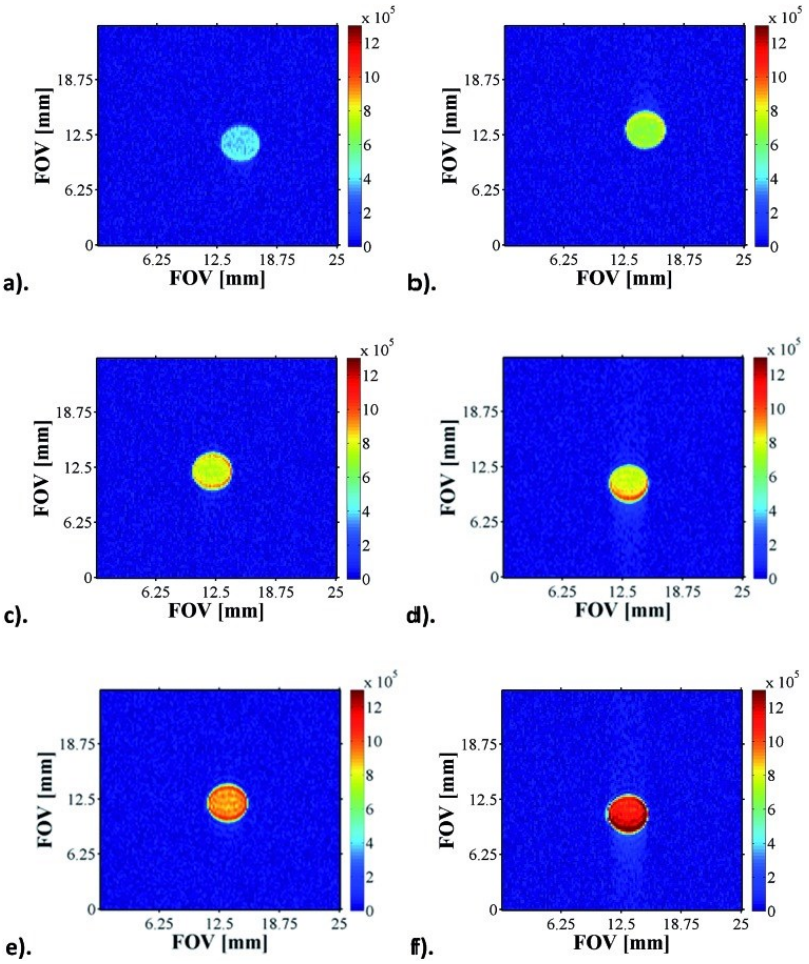


Figure 81. Hyperpolarised nicotinic acid at pH 3.6 (a), 4.6 (b), 5.1 (c), 5.7 (d), 5.9 (e) and 6.9 (f).[128]

This work sought to demonstrate that nicotinic acid may be utilised as a pH probe when combined with SABRE and achieved this, with the pH of the solution directly effecting the observed polarisation due to interconversion between the conjugate acid, uncharged, zwitterion and conjugate base species in solution. The changes in pH may be observed in $^{1}$H MR images of SABRE hyperpolarised nicotinic acid taken at a range of pH values, as shown in Figure 81.

Following this work a further two simple biomolecules suitable for SABRE were identified in the form of the active tuberculosis drugs pyrazinamide and isoniazid – both of these drugs share *N*-heterocycles which are suitable for reversibly binding to **4**; their structures are shown in Figure 82.[48]

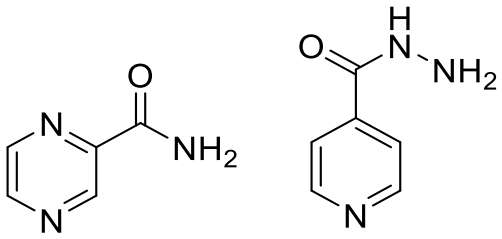

Figure 82. Structures of pyrazinamide (left) and isoniazid (right).

The tuberculosis drugs pyrazinamide and isoniazid have been polarised by SABRE in a range of solvents (methanol, $d_4$-methanol, ethanol and DMSO).[48] With optimal enhancements of up to 1400-fold being observed in $d_4$-methanol, for pyrazinamide at 65 G; this corresponds to a polarisation of ~8%. In the case of isoniazid, polarisation transfer was again optimised in a magnetic field of 65 G, where the *ortho* proton nuclei were enhanced by *ca.* 60-fold. Pyrazinamide and isoniazid have been further examined in an attempt to increase their polarisation levels and lifetimes through a deuteration approach.[95] This report by Duckett *et al.* demonstrated that deuterating IMes in **4** results in significant increases in both ligand $T_1$ and attainable polarisation levels for the substrate as polarisation is not 'diluted'. This deuteration approach is also effective when applied to the substrate itself, though this does mean chemically changing the drug slightly from the currently clinically approved version. In particular, Duckett *et al.* evaluated a series of substrates related to methyl pyrazine-2-carboxylate, which has been shown to be active against tuberculosis.[170-172] The structure of methyl pyrazine-2-carboxylate and a partially deuterated methyl pyrazine-2-carboxylate derivative are shown in Figure 83.

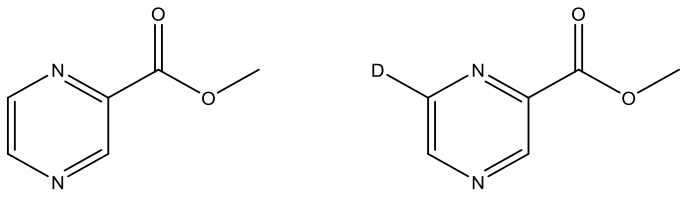

Figure 83. Structures of methyl pyrazine-2-carboxylate (left) and a partially deuterated methyl pyrazine-2-carboxylate (right) derivative.

Utilising the partially deuterated structure shown in Figure 83, polarisation of 11.9 and 9.2% for the 3- and 5- proton environments of the aromatic ring were attained with $T_1$ values of 99.7 and 144.5 seconds respectively.

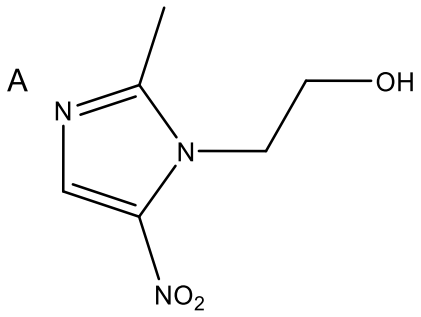


Figure 84. Structure of metronidazole. Available site to bind with **4** is labelled **A**.

In addition to literature reports on currently available tuberculosis medication, several reports have focused on metronidazole (shown in Figure 84), an antibiotic included in the WHO essential medicine's list.[173]

$^{15}$N SABRE-SHEATH of metronidazole has resulted in polarisation levels in excess of 20% for the imidazole nitrogen binding site (labelled **A** in Figure 84) when 80% *para*hydrogen was utilised with nitrogen in all sites at natural abundance.[29] Barskiy *et al.* speculate that utilisation of 100% enriched *para*hydrogen would result in $^{15}$N polarisation levels of *circa* 32% which would be equivalent to a polarisation level of ~100,000 fold within a measurement field of 9.4 T. Though impressive, polarisation build up within this system may be limited by the short $T_1$ relaxation times observed for **A** within the microtesla regime required for SABRE-SHEATH polarisation transfer. Spin lattice relaxation of **A** is highly dependent on external magnetic field with a $T_1$ of 4.5 seconds recorded at microtesla fields compared to 191 seconds within a 0.3 T field. The short relaxation time at low field may limit the polarisation build up, however, once within a suitable measurement field the lengthened $T_1$ may be advantageous to the application of metronidazole to clinical application.

In addition to studies making use of currently available drugs, the application of SABRE to hyperpolarisation in the presence of blood has been examined making use of pyridine as a substrate.[67, 97] In an earlier report, Hövener *et al.*

added 2 mL fresh human blood to an ethanol solution containing 4 equivalents of pyridine relative to **4**.[97] Continuous SABRE polarisation was attempted making use of *para*hydrogen bubbling through the solution and hyperpolarisation continued to be observed following the addition of blood. However, Hövener *et al.* note that after a short time the liquid coagulated and the observed hyperpolarised signal had decreased to approximately a tenth of its initial value.

In a further report, Hövener *et al.* demonstrated that SABRE of pyridine may be observed in a $D_2O$ solution containing HL-60 cells and a separate solution containing DPBS, both simulating parts of the blood environment.[67] Hövener *et al.* attempted the hyperpolarisation of a range of other substrates, including pentafluoropyridine, but pyridine was the only substrate that demonstrated SABRE in these mixtures, likely due to the high polarisation levels that may be obtained with this substrate. Hövener *et al.* report that in this instance, upon addition of blood, the hyperpolarised signal present for pyridine dropped below the limit of detection. They speculate that this may be due to the lower polarisation levels attained in $D_2O$ compared to an ethanol solvent system combined with an increased likelihood that blood components, e.g. salts and proteins, may precipitate from solution in an alcoholic solvent. In conclusion, Hövener *et al.* speculate that blood components may suppress substrate/hydride exchange and reduce substrate $T_1$.

#### 6.1.1.2. Peptides and pyridine labelling

In addition to applications of SABRE to drug molecules, peptides have also been an area of interest with the polarisation of amino acids and some representative small peptides using SABRE first being reported by Appelt *et al*.[46] Appelt *et al*. utilised Crabtree's catalyst (Figure 85) as a polarisation transfer catalyst and SABRE was observed for all of the proteinogenic amino acids.

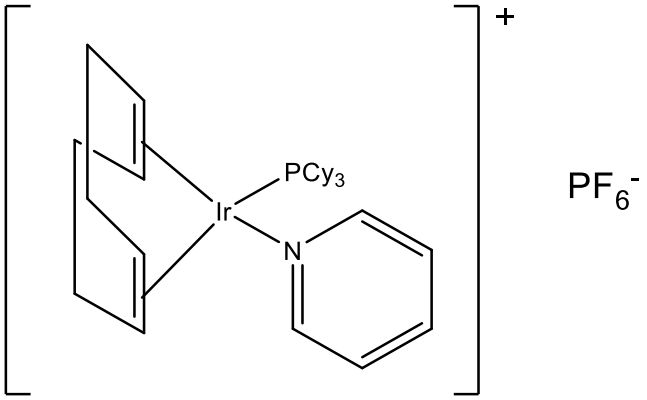


Figure 85. Structure of Crabtree's catalyst, utilised for polarisation transfer by Appelt *et al.*[46]

In addition to singular amino acids, two peptides, GlyGly and ProHisLeu, were also polarised by Appelt *et al.*, but highlighted the need for water-soluble catalysts as their solubility in $d_4$-methanol was poor. Since this report, the water solubility of **4** following activation has been demonstrated so this limitation has now been resolved.[80]

Building on this work, oligopeptides have also been successfully polarised by SABRE.[47] The oligopeptides were effectively SABRE-labelled with nicotinamide or isonicotinamide. The investigated models are shown in Figure 86.

For all the investigated oligopeptides, no signal enhancement was observed for the peptide unit. However, the pyridyl motif did polarise with enhancements of 15- to 25- fold being recorded. These decreased to about 10% of their value from moving from $d_4$-methanol to a 50:50 $d_4$-methanol:$D_2O$ mix.

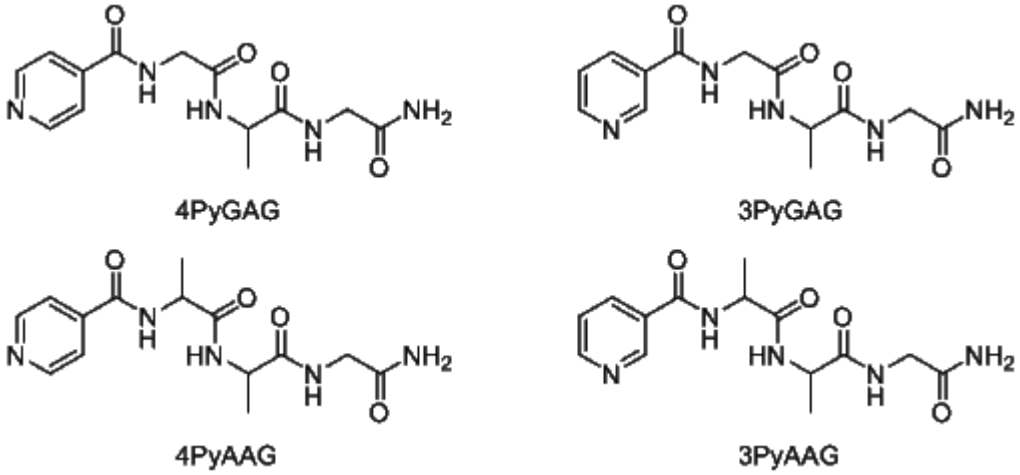


Figure 86. Oligopeptide models investigated by Ratajczyk *et al.*[47]

In a further study, the hyperpolarisation of eNOS (endothelial Nitric Oxide Synthase) substrates were investigated to quantify the production of NO using $^{1}$H NMR spectroscopy.[127] This report continued to develop the utilisation of a pyridyl motif label to facilitate sensitive detection of a substrate that would likely demonstrate minimal SABRE hyperpolarisation. Two generations of eNOS substrates were synthesised; the first generation were focused on the use of a L-arginine carboxylic function to introduce a pyridyl binding group, whereas the second generation made use of $N^{\omega}$–hydroxy-L-arginine (L-NOHA) to incorporate the pyridyl ring.

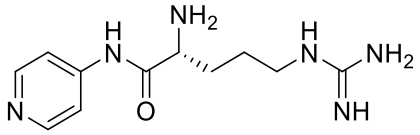

Figure 87. Chemical structure of the pyridyl labelled L-arginine substrate synthesised and polarised by Zanda and co-workers.[127]

The best enhancement obtained was for the derivative shown in Figure 87, which gave an enhancement of 870-fold for the four pyridyl ring protons after polarisation transfer in earth's magnetic field. However, for the dipeptide derivatives, no significant enhancement was observed, most likely due to steric hindrance around the binding site. All of the substrates led to comparable or higher NO production by eNOS than L-arginine. These substrates could, therefore, be potentially used to monitor NO production *in*

*vivo*. However, both the signal enhancement and the longevity of the hyperpolarised signal ($T_1$ values of the pyridyl protons of the substrate in Figure 87 were only 3.2 – 3.3 s at physiological pH) would need to be improved.

The work reported herein aims to extend the scope of SABRE application to higher molecular weight drugs currently available on the market through the application of $^{19}$F SABRE discussed in 4.3. Additionally this study investigates new psychoactive substances (NPS), specifically focusing on fentanyl, and how SABRE may be utilised for the detection of fentanyl derivatives.

## 6.2. Voriconazole

Voriconazole, shown in Figure 88, is a world health organisation (WHO) essential medicine for its activity as an anti-fungal and belongs to the triazole class of drugs.[174] As a broad spectrum fungicidal treatment, voriconazole demonstrates good activity against a range of common and several less common fungi. Voriconazole concentrations *in vivo* have been assessed utilising MRI and metabolites have been identified utilising $^{19}$F NMR following stress testing.[175, 176] The existing literature demonstrating voriconazole may be studied *in vivo* and NMR characterisation of both voriconazole and it's degradation products made it an attractive prospect for SABRE hyperpolarisation.

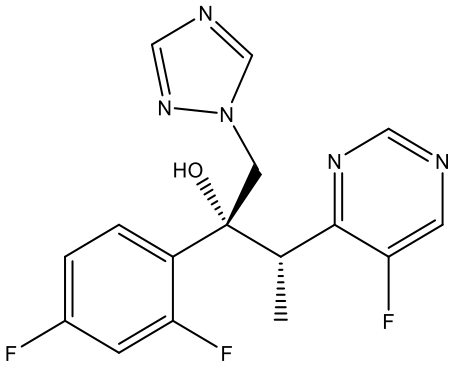


Figure 88. Structure of voriconazole.

This work, reported herein, demonstrates the novel application of $^{19}$F SABRE to a currently utilised drug through the application of the techniques discussed

in section 4.1.3. This work has also been reported by the author in 'Extending the Scope of $^{19}F$ Hyperpolarization through Signal Amplification by Reversible Exchange in MRI and NMR Spectroscopy'.[96]

### 6.2.1. Hyperpolarisation of voriconazole

As discussed in 6.2, voriconazole was identified as an interesting target for the application of SABRE to a commercially available and clinically approved drug. Utilising 4 equivalents of voriconazole relative to **4**, both $^{1}H$ and $^{19}F$ polarisation was attempted.

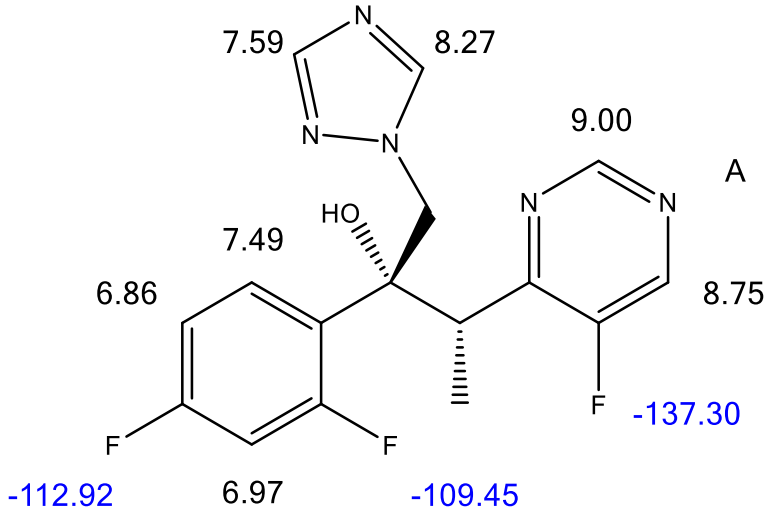


Figure 89. Structure of voriconazole with $^{1}H$ and $^{19}F$ environments labelled.[176]

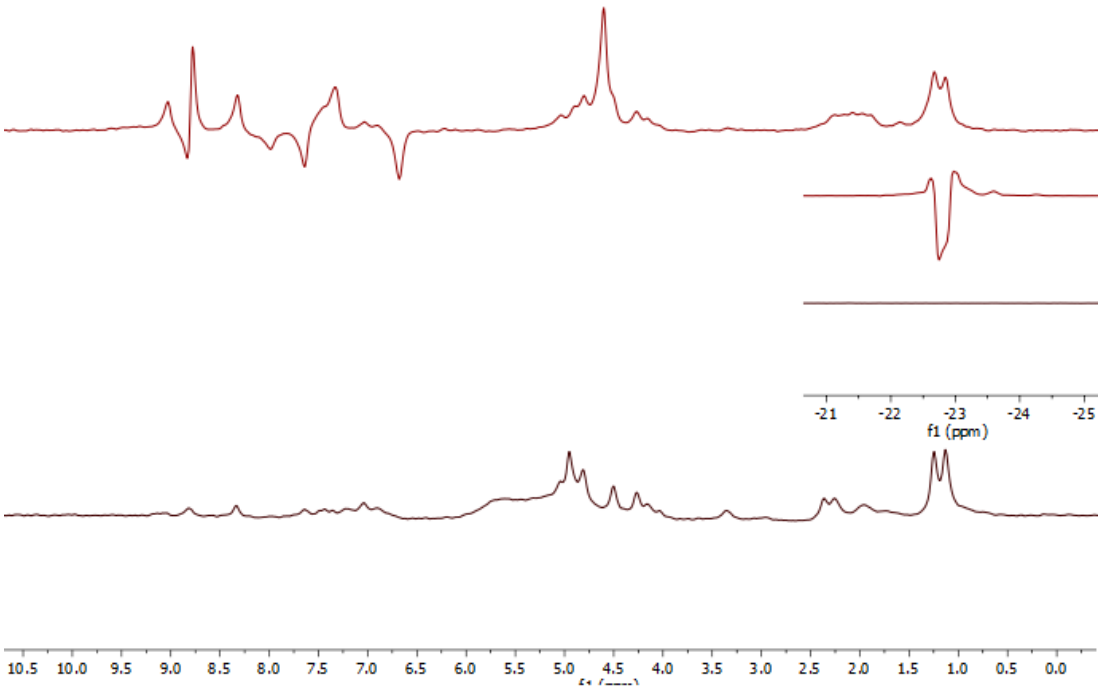


Figure 90. $^{1}$H spectra of voriconazole under thermal (bottom) and SABRE (top) conditions. Hydride region (-21 to -25 ppm) is shown as an expansion.

$^{1}$H SABRE was observed, as shown in Figure 90, with a pair of major hydride resonances forming at -22.72 and -22.91 ppm following the observed hydrogenation of cyclooctadiene. The $^{1}$H environment at 8.75 ppm demonstrated the highest level of $^{1}$H SABRE with an enhancement of ~4-fold. Unfortunately, due to the multiple hydrides present at low intensities, EXSY interrogation of the hydride exchange rate was not feasible. Interestingly, polarisation levels for the environment at 9 ppm demonstrated an enhancement of only ~1.5-fold times under the same conditions, suggesting preferential transfer towards the $^{19}$F environment at -137.3 ppm.

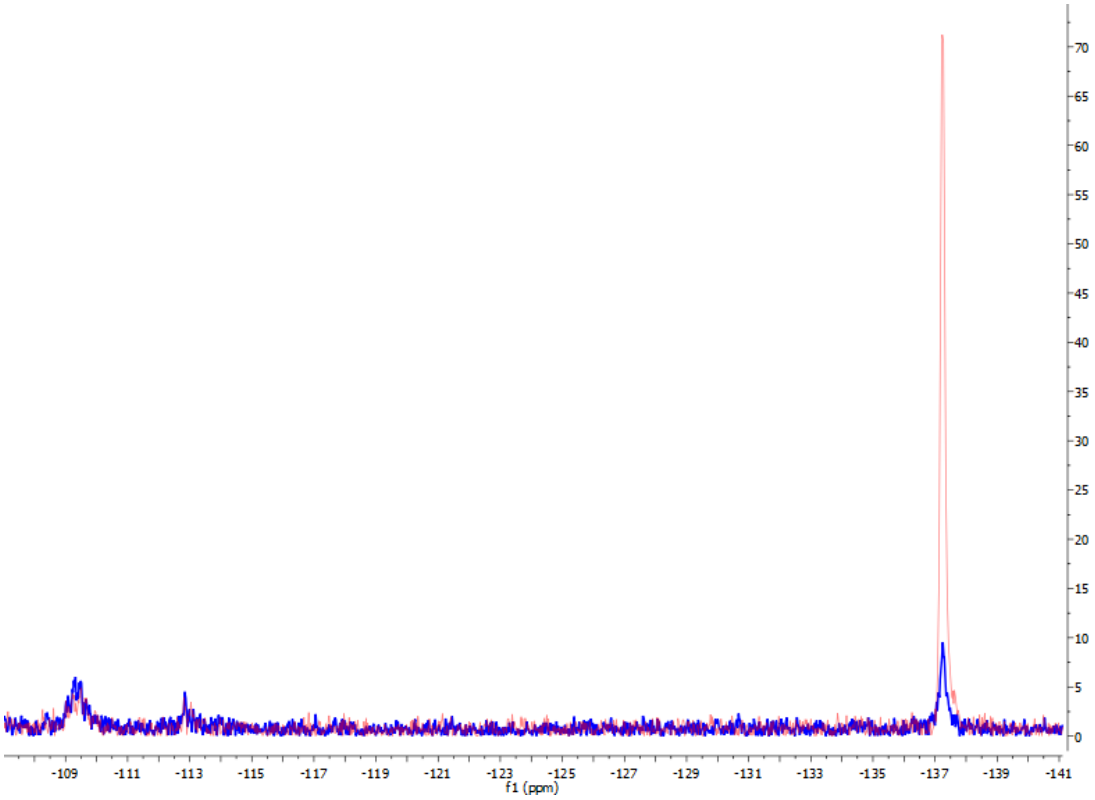


Figure 91. $^{19}F$ spectra of voriconazole, SABRE hyperpolarised trace in red, thermal spectra under the same conditions shown in blue.

$^{19}F$ SABRE was conducted (Figure 91) making use of the same sample and demonstrated selective hyperpolarisation of the $^{19}F$ environment at -137.3 ppm; this is likely due to the other fluorine environments being too far removed from the *para*hydrogen derived hydrides present in the polarisation transfer catalyst for polarisation to be propagated through very long range coupling.

A combination of the $^{19}F$ polarisation only being observed for this environment and the highest $^{1}H$ hyperpolarisation being present in the neighbouring environment, suggests that voriconazole primarily binds to the catalyst making use of nitrogen A in Figure 89. A spectrum of the hydride region at 400 MHz revealed a high number of hydride resonances, in particular the presence of a peak at -23.67 ppm suggests that there is a mixture of species in solution, at least some of which are likely to contain MeOH bound *trans* to *para*hydrogen derived hydrides.[28] The aromatic region also demonstrated low level bound peaks with integrals ~12% that of the free voriconazole in solution. The

combination of the low levels of these bound and hydride peaks made characterisation of the complexes in solution infeasible.

Table 30. Relaxation times for $^{19}F$ environments of voriconazole at 1.4 T.

| $^{19}F$ environment (ppm) | $T_1$ (s) |
|---|---|
| -109.4 | 3.08 |
| -112.9 | 7.73 |
| -137.4 | 5.15 |

The measured relaxation times for the $^{19}F$ environments of voriconazole at 1.4 T are short enough that potential biological application would need to utilise strategies, such as those discussed within section 5.4, for lengthening of $T_1$. The relaxation times within Table 30 also suggest that higher polarisation values than those reported herein are likely accessible as this work has utilised a 'shake and drop' method that necessitates a time delay before measurement for sample transfer to the measurement field. Utilisation of a *para*hydrogen bubbling method would enable SABRE to occur *in situ* within the magnet and partially negate polarisation loss due to relaxation on the sample transfer timescale.

A $^{19}F$ enhancement of 5 times is modest compared to the pyridine substrates, as detailed in section 4.1, however, this substrate contains significant steric bulk in proximity to the binding site which is likely to reduce turnover efficiency. Notably, the quantity used for this enhancement, 13.4 mg, is significantly below the lowest dosage of 50 mg noted in the WHO essential medicines list.[177] This result represents a major step forwards in the SABRE of medicines as voriconazole is significantly more complex than those drugs discussed in section 6.1.1.

## 6.3. Fentanyl

Fentanyl (Figure 92, left), functions as a synthetic opiate, despite the chemical structure differing significantly from morphine, codeine and heroin (Figure 92,

right), which are natural opiates. Fentanyl exhibits a strong affinity towards the μ-opioid receptor, which is found across the central and peripheral nervous system and thus acts in a similar way to naturally occurring opiates. Activation of the μ-opioid receptor leads to analgesia and euphoria, but also physical dependence, constipation and respiratory depression,[178] which can lead to death in the case of an overdose.

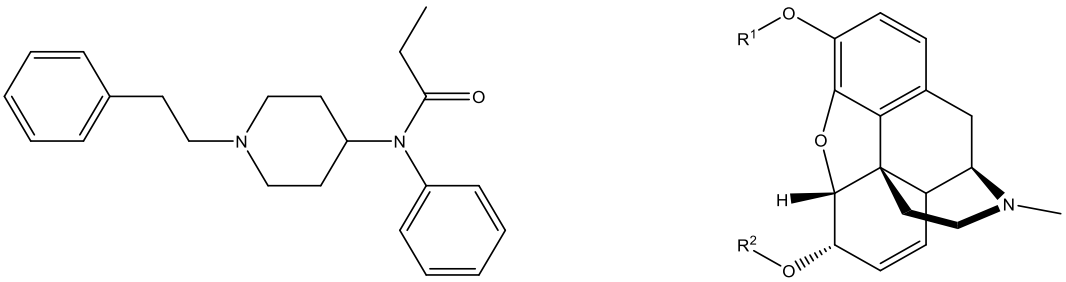


Figure 92. Structure of fentanyl (left) and common natural opiates (right). In morphine $R^1$=$R^2$=H, in codeine $R^1$=$CH_3$, $R^2$=H, in heroin $R^1$=$R^2$=(CO)$CH_3$.

Fentanyl has attained widespread medical use due to its very strong and fast action. In fact, fentanyl is included on the WHO essential medicines list as a painkiller for severe cases. Fentanyl has an estimated potency of 50 to 100 times stronger than morphine.[179] The euphoric effects of fentanyl, resembling those of heroin, have led to recreational use which poses a public health threat as quantities of *circa* 2 mg may induce overdose in the average adult.[180]

Instances where sample purity increases may pose a particular health risk, is due to samples reportedly showing a wide variation within dose sizes (28 – 35 mg) and purity (5.8 – 6.6%).[181] This equates to an active pharmaceutical ingredient (API) of between 1.62 and 2.31 mg, meaning relatively minor increases in purity could push the API of street samples significantly above the estimated lethal dose. An additional issue leading to negative health outcomes is the contamination of heroin samples with fentanyl, often without the users knowledge.[182]

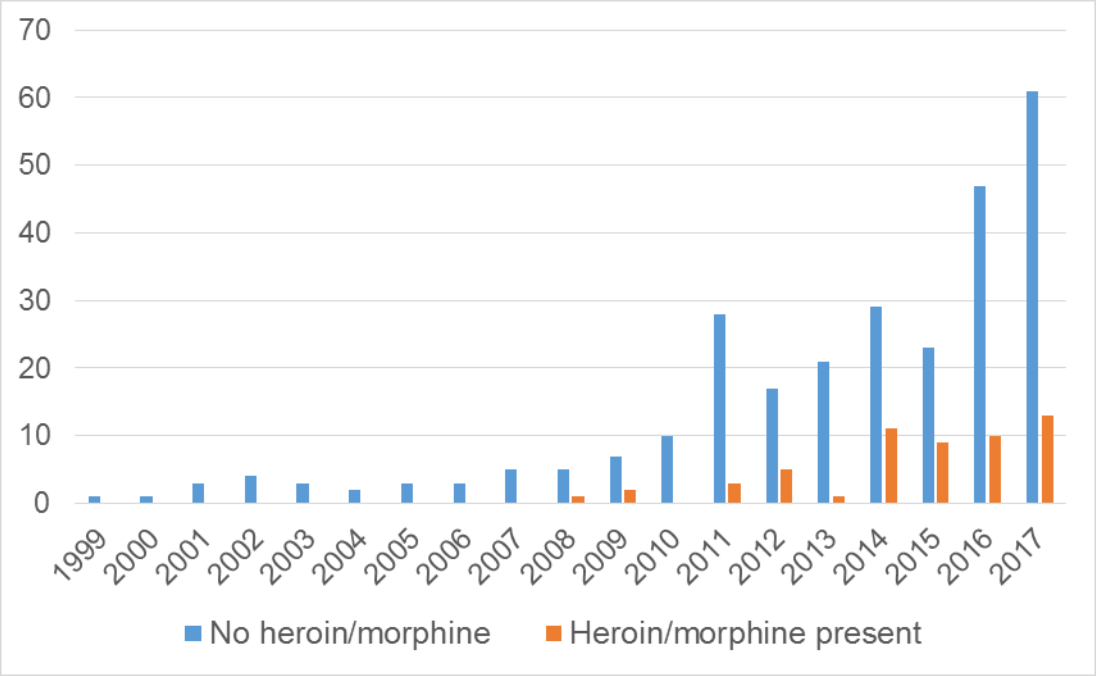


Figure 93. Office of National Statistics data by year in England and Wales for instances where fentanyl is mentioned on death certificate with and without heroin or morphine.[183, 184]

Unfortunately in recent years opiate abuse, including fentanyl and its derivatives, have been responsible for an increasing number of deaths, including 42,249 opioid related deaths in America in 2016.[185] Of these, *circa* 19,400 were attributed to synthetic opioids, representing a 100% increase in synthetic opioid deaths between 2015 and 2016. In Europe, fentanyl has resulted in fewer deaths. However, trends appear to show fatalities increasing year by year, as demonstrated in Figure 93,[183, 184, 186] though Morley *et al.* note that these figures may underestimate the actual numbers. This is because if a cause of death has been established, fentanyl screening is not typically undertaken and many laboratories may be unable to detect fentanyl in low, but potentially lethal, concentrations. This highlights the need for greater sensitivity in detection methods.[186]

Unfortunately, fentanyl derivatives, or fentalogues, such as carfentanil (estimated potency 10,000 times that of morphine), may pose even larger threats to public health and drug detection.[187, 188] Between 2009 and 2017, 18 new fentalogues were detected by the European Monitoring Centre for Drugs

and Drug Addiction (EMCDDA), though 8 of these were reported for the first time in 2016.[189] Fentalogues are already being identified as causes of death with fentanyl present in 56.3% of opioid deaths in the United States and fentalogues present in an additional 14% of cases in July to December 2016.[190]

Given the low-threshold for overdose, it was sought to employ SABRE methodology for detecting pyridyl-labelled fentanyl derivatives in addition to mirfentanyl, which has been assessed for biological activity in rats.[187] Furthermore, it was sought to demonstrate that a fentalogue can be readily detected despite being in a matrix consisting largely of heroin (97% w/w).

### 6.3.1. Hyperpolarisation of fentalogues

**F₁**, as discussed in section 6.3, is a drug that, though it can have significant positive impacts on health when utilised correctly, has recently been becoming a significant concern as a drug of abuse. Given the apparent pharmacological activity of modified fentanyl derivatives, as well as the number of derivatives which are on the market and with more being detected each year, fentanyl was chosen to be the subject of a systematic assessment for SABRE activity.

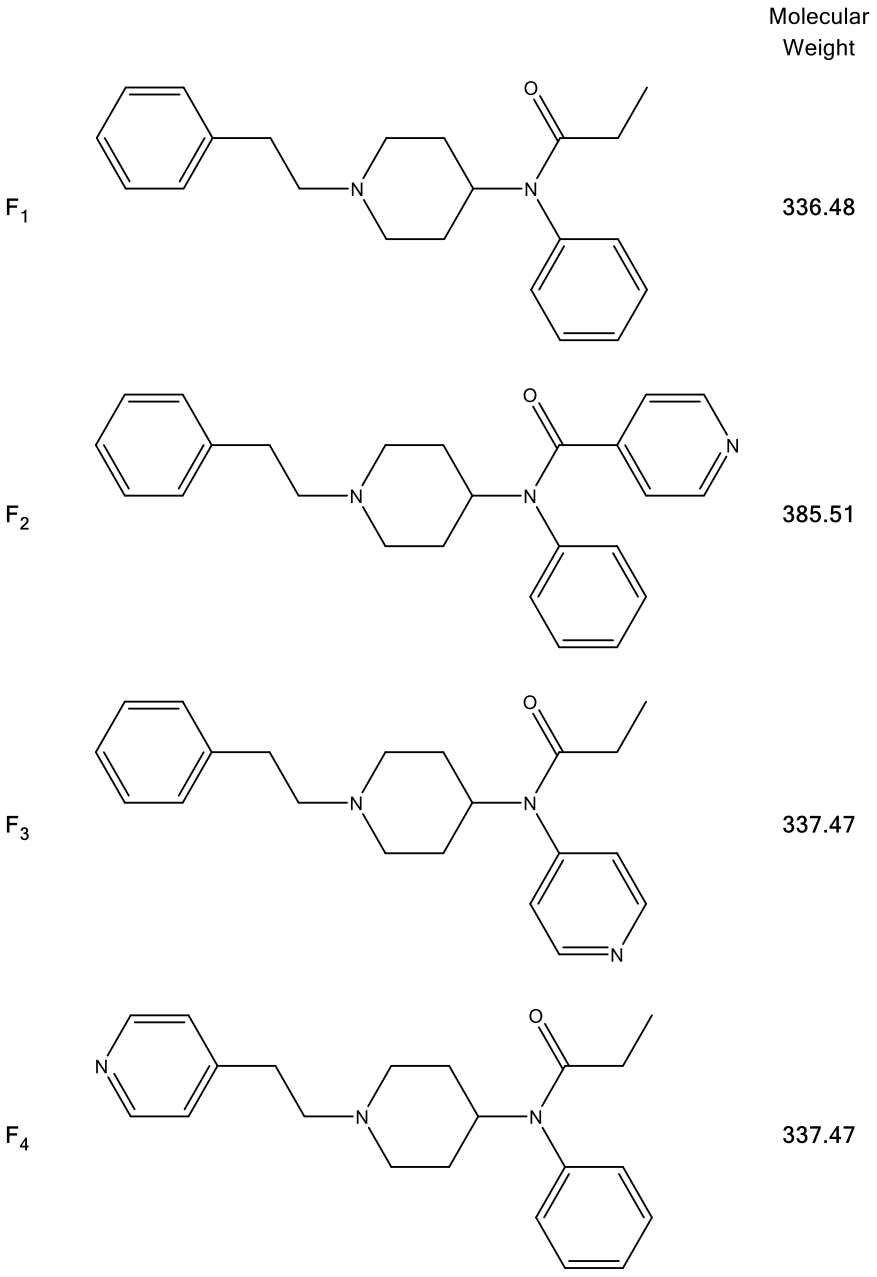


Figure 94. Fentanyl and derivatives (**F₁**- **F₄**) synthesised by the group of Dr Oliver Sutcliffe for evaluation in this work.

In this study a series of fentanyl derivatives, **F2** – **F4**, shown in Figure 94, were synthesised by the Sutcliffe research group. These derivatives aimed to label the fentanyl structure through an existing ring in derivatives **F3** and **F4** or through the addition of a new pyridyl motif in the case of **F2**. Labelling of a substrate for SABRE has been previously reported as an efficient way to enable hyperpolarisation and, in this instance, is commensurate with a feasible modification that may be done, in coming years, to create a new street derivative of fentanyl.[46, 47, 127]

### 6.3.2. Complexes formed

Utilising **4** as the polarisation transfer pre-catalyst, addition of 4 equivalents of **F2** results in the formation of the complex $[Ir(IMes)(\mathbf{F2})_3(H)_2]^+$ with a hydride signal being observed at -23.17 ppm for this species. A smaller pair of hydride resonances representative of hydrides *trans* to methanol are present at -23.52 and -25.56 ppm respectively. The resonance of the hydride *trans* to methanol is in very good agreement with reported values for hydrides *trans* to methanol where pyridine is the substrate, as in this instance these hydrides have been reported at -23.44 and -25.49 ppm.[28]

Relative integrals of the hydrides suggest that $[Ir(IMes)(\mathbf{F2})_3(H)_2]$:$[Ir(IMes)(\mathbf{F2})_2(MeOH)(H)_2]$ are present in the ratio of 98:2 respectively. The low relative size of these hydrides made characterisation of this complex impractical, and it has been ignored for the purposes of exchange rate spectroscopy conducted on this complex.

The analogous complexes, $[Ir(IMes)(\mathbf{F3})_3(H)_2]$ and $[Ir(IMes)(\mathbf{F4})_3(H)_2]$, are formed when **F3** and **F4** are utilised with hydride resonances observed at -22.70 and -22.83 ppm respectively. In both instances only a single hydride is formed, suggesting that **F2** contains the most sterically hindered binding site as this is the only substrate for form methanol adducts.

### 6.3.3. Exchange Rate determination of fentalogues

Using exchange spectroscopy (EXSY), the exchange rates of substrates **F2** - **F4** and hydride in the complex $[Ir(IMes)(\mathbf{F})_3(H)_2]^+$ where **L** is **F2**, **F3** or **F4** were

investigated. This data is tabulated within Table 31 and Table 32, as well as shown graphically within Figure 95 and Figure 96.

Table 31. Exchange rate data for the loss of substrate and hydride from $[Ir(IMes)(\mathbf{F})_3(H)_2]^+$.

| Complex | $[Ir(IMes)(\mathbf{F_2})_3(H)_2]^+$ | | $[Ir(IMes)(\mathbf{F_3})_3(H)_2]^+$ | | $[Ir(IMes)(\mathbf{F_4})_3(H)_2]^+$ | |
|---|---|---|---|---|---|---|
| Gradient | y = -9266x + 27.571 | y = -8370.7x + 24.655 | y = -9114.4x + 26.31 | y = -8385.6x + 24.69 | y = -10235x + 31.042 | y = -9545.6x + 28.156 |
| Data $R^2$ | 0.9949 | 0.9971 | 0.9613 | 0.9973 | 0.9955 | 0.9946 |
| Temperature / K | Loss of hydride / $s^{-1}$ | Loss of $\mathbf{F_2}$ / $s^{-1}$ | Loss of hydride / $s^{-1}$ | Loss of $\mathbf{F_3}$ / $s^{-1}$ | Loss of hydride / $s^{-1}$ | Loss of $\mathbf{F_4}$ / $s^{-1}$ |
| 268 | - | 0.17 | - | - | - | - |
| 275 | - | 0.45 | - | - | - | - |
| 277 | 0.37 | - | - | - | - | - |
| 280 | - | 0.77 | 0.32 | 0.72 | 0.09 | 0.07 |
| 282 | 0.71 | - | 0.39 | 1.22 | 0.28 | 0.22 |
| 285 | 1.14 | 1.29 | 0.74 | 2.23 | 0.68 | 0.39 |
| 290 | 1.82 | 2.04 | 1.88 | 4.05 | 1.17 | 0.72 |
| 295 | 2.92 | 3.88 | 2.99 | 5.52 | 1.94 | 1.28 |
| 300 | 5.59 | 5.43 | 3.69 | 8.61 | 3.62 | 2.24 |

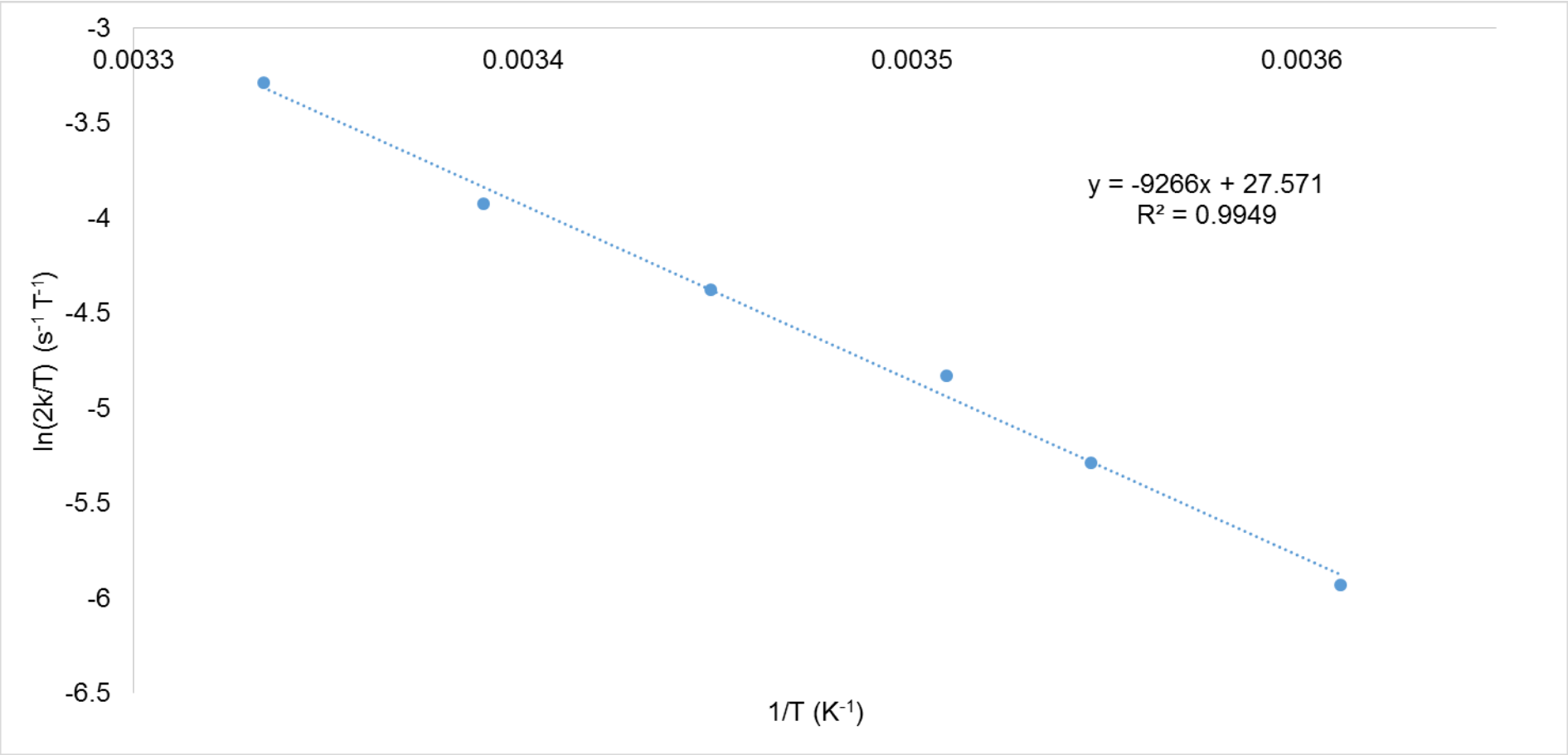


Figure 95. Example Eyring-Polanyi plot for the loss of hydride from the complex $[Ir(IMes)(\mathbf{F_2})_3(H)_2]^+$.

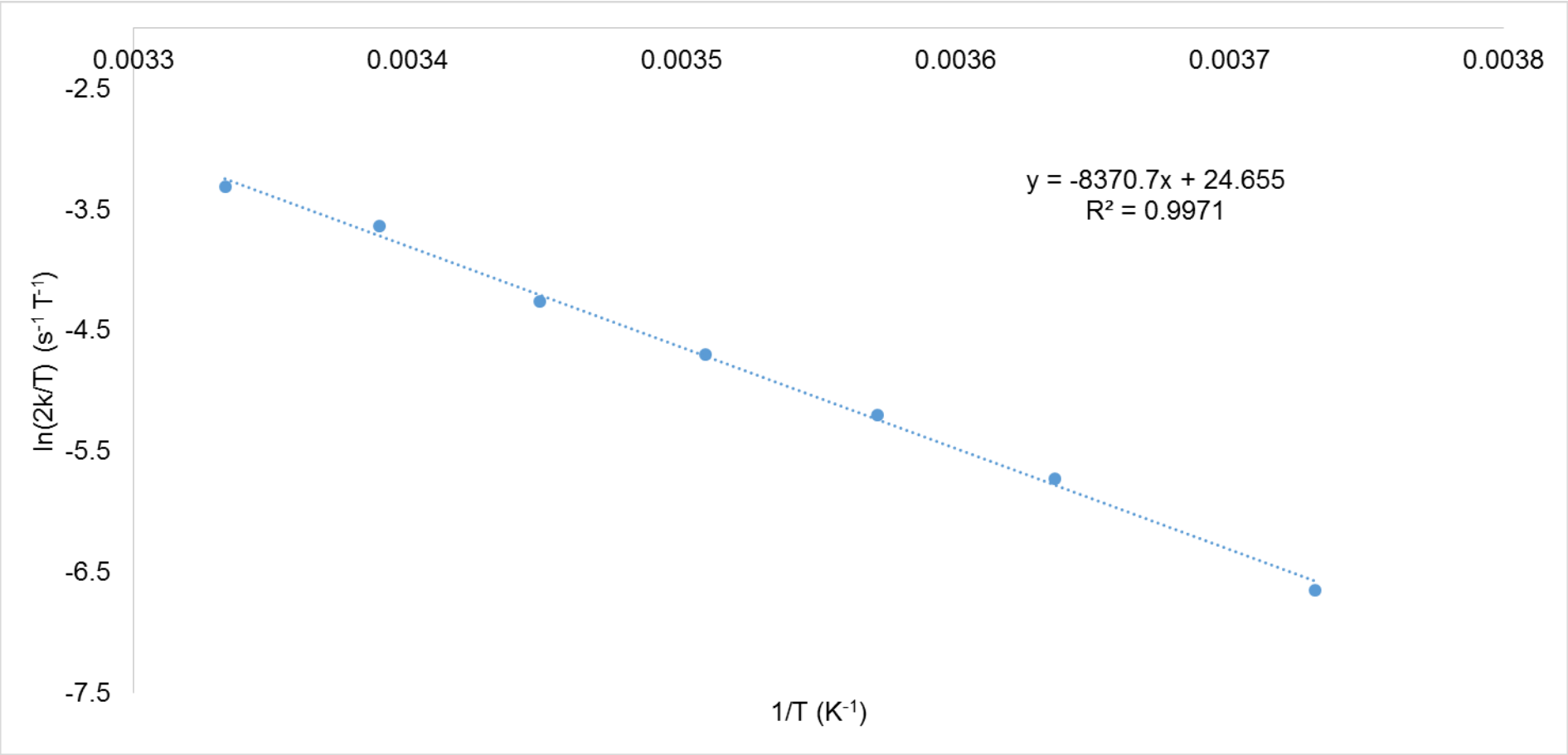


Figure 96. Example Eyring-Polanyi plot for the loss of $\mathbf{F_2}$ from the complex $[Ir(IMes)(\mathbf{F_2})_3(H)_2]^+$.

| | | **$F_2$** | **$F_3$** | **$F_4$** | **Pyridine[26]** |
|---|---|---|---|---|---|
| Hydride loss | $\Delta G_{300}$ / kJ mol$^{-1}$ | 67.6 ± 0.07 | 69.4 ± 0.16 | 66.9 ± 0.06 | 66.4 ± 0.3 |
| | $\Delta H$ / kJ mol$^{-1}$ | 75.8 ± 1.4 | 75.7 ± 4.8 | 85.1 ± 1.5 | 79 ±1 |
| | $\Delta S$ / J mol$^{-1}$ K$^{-1}$ | 27.4 ± 5.0 | 21.0 ± 16.4 | 60.5 ± 5.0 | 41 ± 3 |
| Loss of ligand *trans* to hydride | $\Delta G_{300}$ / kJ mol$^{-1}$ | 67.4 ± 0.07 | 67.4 ± 0.05 | 68.4 ± 0.11 | 64 ± 2 |
| | $\Delta H$ / kJ mol$^{-1}$ | 69.6 ± 1.2 | 69.7 ± 0.6 | 79.4 ± 2.4 | 93 ± 3 |
| | $\Delta S$ / J mol$^{-1}$ K$^{-1}$ | 7.44 ± 4.3 | 7.73 ± 2.2 | 36.6 ± 8.2 | 97 ± 9 |
| Loss of hydride at 300 K / s$^{-1}$ | | 5.6 | 3.0 | 6.8 | 9 |
| Loss of ligand at 300 K / s$^{-1}$ | | 5.4 | 5.5 | 3.5 | 11.7 |

Table 32. Thermodynamic activation parameters and exchange rates at 300 K for complexes [Ir(IMes)(**F**)$_3$(H)$_2$]$^+$ where **L** is **$F_2$**, **$F_3$** or **$F_4$**.

Using EXSY measurements, the loss of hydride and loss of fentanyl ligand *trans* to hydride from the complexes are shown in Table 32. The loss of hydride from $[Ir(IMes)(\mathbf{F_2})_3(H)_2]^+$ proved to be 5.6 $s^{-1}$ at 300 K; this is significantly slower than the previously reported hydride loss in $[Ir(IMes)(Py)_3(H)_2]^+$ which was 9 $s^{-1}$ when probed under the same conditions.[26] An Eyring-Polanyi plot of hydride loss produced a value for $\Delta H$ of 75.8 ± 1.4 kJ $mol^{-1}$; this value of $\Delta H$ suggests that that the Ir-H bond is relatively strong and is similar to the 79 ± 1 kJ $mol^{-1}$ reported when pyridine is utilised.

The loss of $\mathbf{F_2}$ from $[Ir(IMes)(\mathbf{F_2})_3(H)_2]^+$ was found to be 5.4 $s^{-1}$ at 300 K. Similar to the hydride loss rate, this process is much slower than pyridine in the analogous complex $[Ir(IMes)(Py)_3(H)_2]^+$ which has a reported speed of 11.7 $s^{-1}$. The Ir-N bond in $[Ir(IMes)(\mathbf{F_2})_3(H)_2]^+$ is much weaker than in the analogous pyridine complex with $\Delta H$ values of 69.6 ± 1.2 kJ $mol^{-1}$ and 93 ± 3 kJ $mol^{-1}$ respectively. This is the lowest $\Delta H$ value for any of the fentanyl derivatives tested within this study; this appears to support the supposition that this may be the most sterically hindered of the fentalogues and this may account for the presence of methanol adducts discussed in section 6.3.2.

Ligands $\mathbf{F_2}$ and $\mathbf{F_3}$ result in very similar exchange rates for the loss of ligand, whilst hydride loss is quicker for $\mathbf{F_2}$ than $\mathbf{F_3}$ at 300 K. The thermodynamic activation parameters for both $\mathbf{F_2}$ and $\mathbf{F_3}$ show significant similarity, despite the pyridine ring location changing. When $\mathbf{F_4}$ is considered, the loss of $\mathbf{F_4}$ *trans* to hydride from $[Ir(IMes)(\mathbf{F_4})_3(H)_2]^+$ requires a considerable amount of energy. This is reflected in the $\Delta H$ value 85.1 ± 1.5 kJ $mol^{-1}$ which is ~10 kJ $mol^{-1}$ higher than the respective values for $\mathbf{F_2}$ and $\mathbf{F_3}$, implying that the Ir-N bond in $[Ir(IMes)(\mathbf{F_4})_3(H)_2]^+$ is relatively the strongest of the fentalogues investigated. This is likely representative of the relative steric isolation of the pyridyl functionality in ligand $\mathbf{F_4}$. The relatively strong Ir-N bond results in the slowest observed rate of ligand loss and this may have negative effects of the overall SABRE polarisation transfer efficiency of $\mathbf{F_4}$.

### 6.3.4. SABRE of fentalogues

The polarisation of fentanyl and fentanyl hydrochloride was attempted making use of SABRE and the recently reported method SABRE-RELAY, which utilises a polarisation carrier, such as ammonia, for indirect polarisation of the ligand. Utilisation of polarised ammonia, followed by proton exchange in solution, has enabled the transfer of hyperpolarised protons into an alcohol.[37, 85, 86] SABRE of fentanyl proved ineffective due to the lack of suitable ligation groups for reversible binding to the polarisation transfer catalyst. The SABRE-RELAY approach had to be combined with CASH-SABRE (catalyst separated hyperpolarisation-signal amplification by reversible exchange) as, due to the unavailability of facilities for the manipulation of ammonia gas, ammonia (35%) in solution with water was utilised. No SABRE-RELAY signals attributable to fentanyl or fentanyl hydrochloride were observed, however, proton exchange with water would likely have led to dilution of any polarisation successfully transferred to the target analyte. In addition, to the best of the author's knowledge, SABRE- RELAY has only been exemplified for primary and secondary amines; polarisation of tertiary amines such as those present in fentanyl has not been reported.

The fentalogues synthesised by the Sutcliffe group for this project all contain pyridyl moieties which makes them suitable for SABRE. Substrates **F$_2$** – **F$_4$** have therefore been tested for SABRE activity making use of 4 equivalents of **F$_2$** – **F$_4$** relative to the polarisation transfer pre-catalyst **4**.

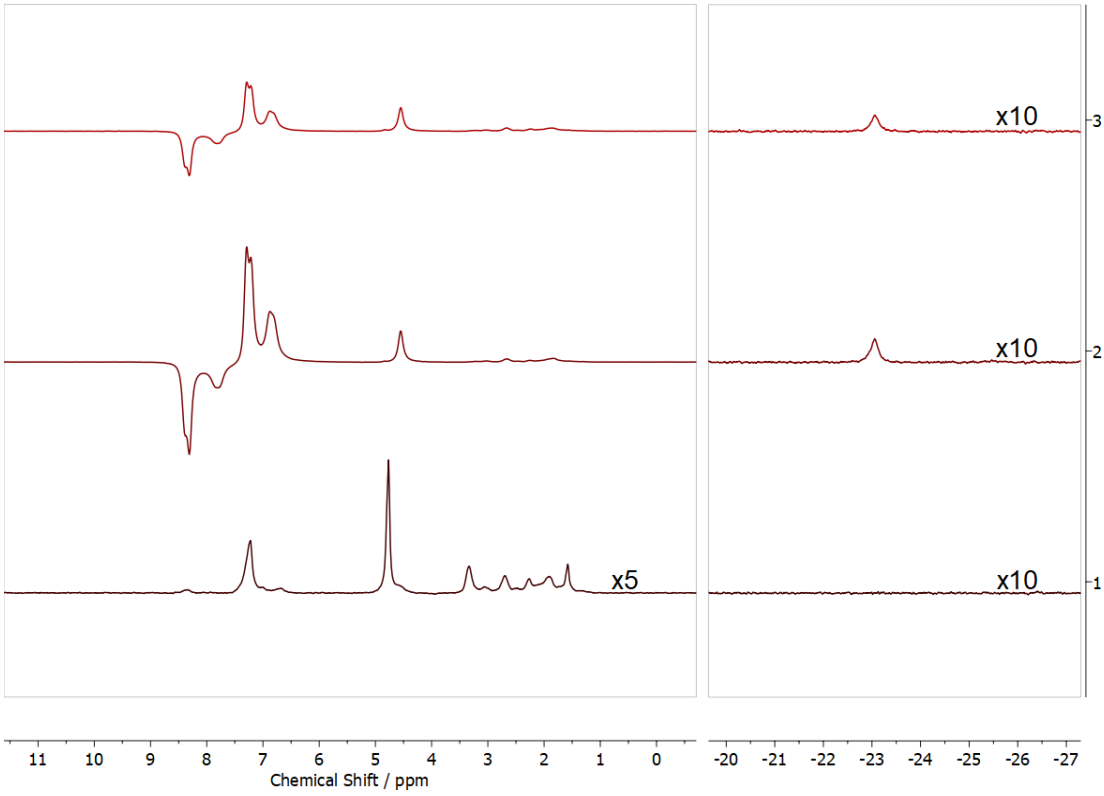


Figure 97. $^{1}$H NMR spectra of **F₂** and **4** in the ratio of 4:1 in the presence of *p*-$H_2$ in $d_4$-methanol. Spectrum 1 is the thermal spectrum whereas spectra 2 and 3 are hyperpolarised following polarisation transfer in earth's magnetic field or at 65 G respectively. Multiplication factors indicate scaling of the vertical axis.

Polarisation is typically observed for just the pyridine ring when a labelling approach is taken. In the cases of ligands **F₂** and **F₃** this is the case, however ligand **F₄** shows a small enhancement in the ethylene chain that connects the pyridine ring to that of the piperidine ring in a small emissive peak at 2.65 ppm. In fentalogues **F₂** – **F₄** polarisation was observed, with SABRE of **F₂** being exemplified in Figure 97. Unfortunately, spectral overlap at a 1.4 T measurement field means that, even though polarisation of *meta* protons is observed, spectral overlap with phenyl protons from elsewhere within the fentalogue means that polarisation cannot be accurately calculated for this environment. The *ortho* and *meta* signals of the pyridyl ring are observed as emission and absorption signals respectively. However, the *ortho* protons are sufficiently resolved that polarisation levels may be calculated for this

environment for all fentalogues; a summary of the enhancements observed is shown in Table 33.

Table 33. $^{1}$H NMR enhancements of the *ortho* proton observed for fentalogues **F$_2$** – **F$_4$** when polarisation transfer is conducted at both earth's field and 65 G.

| | Enhancement value obtained after transfer of polarisation in the field indicated | |
|---|---|---|
| Fentanyl derivative (**F**) | Earth's magnetic field | 65 G |
| **F$_2$** | −168 | −79 |
| **F$_3$** | −38 | −2 |
| **F$_4$** | −50 | −14 |

When polarisation transfer was conducted at 65 G the enhancements dramatically decrease; while this may be due to relaxation associated with increased field cycling time due to additional manual handling required for 65 G measurements, this observation is similar to that made for NOS substrates bearing 4-substituted pyridyl-tethers.[127] In addition, though 65 G has been reported to typically be highly effective for pyridine based substrates,[30, 45, 60, 64, 76, 82, 166] it is possible that this does not optimise the level anti-crossing (LAC) conditions which would optimise polarisation transfer for this system.[130, 191-193]

The enhancements achieved for these substrates are reduced compared to model substrates such as pyridine, however it is worth noting that only 50% *para*-enriched hydrogen has been utilised. Theoretical models suggest that utilising 100% *para*hydrogen would result in ~3 times the polarisation levels observed here.[54]

The highest enhancements at both earth's and 65 G polarisation transfer fields correspond with fentalogue **F$_2$**. This aligns well with the measured exchange rates at 300 K for hydride and ligand loss being 5.6 $s^{-1}$ and 5.4 $s^{-1}$ respectively, as this highly commensurate exchange is likely to result in the most efficient polarisation transfer of the fentalogues tested.

Comparing the polarisation levels obtained for **F2** to those obtained for **F3** and **F4**, demonstrates that **F2** has a significantly more efficient polarisation build-up. This is unsurprising as the exchanges for both **F3** and **F4** at 300 K reveal either loss of hydride or loss of ligand proceeds at approximately twice the speed of the other component. This will lead to ligands reversibly binding to the polarisation transfer catalyst without *para*hydrogen derived hydrides being present for SABRE to occur (as in the case of **F3**) or *para*hydrogen derived hydrides reversibly binding without an unpolarised ligand present due to a slow ligand turnover rate (as in the case of **F4**). Interestingly the polarisation levels for **F4** are higher than **F3**, giving the order **F2**>**F4**>**F3** – this is likely representative of the fact the rate limiting step of polarisation transfer in [Ir(IMes)(**F4**)$_3$(H)$_2$] is the ligand loss at 3.5 $s^{-1}$ compared to hydride loss at 3 $s^{-1}$ in the complex [Ir(IMes)(**F3**)$_3$(H)$_2$].

### 6.3.5. Fentalogue relaxation

The final element in overall polarisation efficiency is the $T_1$ value for the protons, in order to examine if relaxation is occurring on the timescale of the SABRE experiment.

Table 34. $T_1$ values for **F₂** – **F₄** in different environments at 298 K.

| | $T_1$ in the presence of [Ir(IMes)(**F**)$_3$(H)$_2$] and $H_2$ (s) | | $T_1$ in the presence of air (s) | | $T_1$ in the presence of vacuum (s) | |
|---|---|---|---|---|---|---|
| Ligand | *Ortho* proton | *Meta* proton | *Ortho* proton | *Meta* proton | *Ortho* proton | *Meta* proton |
| **F₂** | 3.1 | 3.5 | 2.6 | 1.5 | 2.9 | 2.0 |
| **F₃** | 2.9 | 3.2 | 2.0 | 2.1 | 4.3 | 2.9 |
| **F₄** | 3.3 | 2.1 | 2.3 | 2.0 | 3.2 | 2.5 |

The relaxation times are largely commensurate between fentalogues with only minor deviations. This reinforces the conclusion in section 6.3.4 that the exchange rate is the primary factor determining the polarisation build up efficiency and thus the enhancements levels observed. Despite several *meta* protons, particularly for **F₃**, being part of multiplets, the $T_1$ noted in Table 34 is the overall value for these superimposed environments.

The $T_1$ values here are very short, with multiple $T_1$'s occurring within the polarisation transfer timeframe as shaking was carried out for ~10 seconds before transfer to the 1.4 T measurement field. This means that techniques which may extend the signal relaxation time such as catalyst deactivation,[30] or flow techniques in which there is a continuous build-up of a hyperpolarised bolus, may be effective in increasing the enhancements observed for these fentalogues.[194]

### 6.3.6. Hyperpolarisation of a fentalogue in a heroin mixture

The fentanyl work reported thus far within this chapter has utilised fentalogues that have been specifically synthesised with pyridine labelling in order to make them suitable for SABRE without modification. Though an increasing number of fentalogues are being detected within street samples, and it is not unreasonable to see the incorporation of a pyridine ring being a logical step

towards derivatising the fentanyl pharmacophore, these structures have no extant reports from street samples or medical testing.

However, mirfentanil (**F5**), shown in Figure 98, has been demonstrated to possess analgesic effects alongside respiratory depression in animal models.[195] Although, **F5** appears to be highly selective for μ-opioid receptors, it does not interfere with the immune system through suppression of natural killer (NK) cells that is a known side-effect of morphine and fentanyl. To the best of the authors knowledge, **F5** has not been identified as responsible for deaths. However, the structurally similar analogue furanyl fentanyl, frequently found in combination with heroin, has been found responsible for at least 8 deaths.[196]

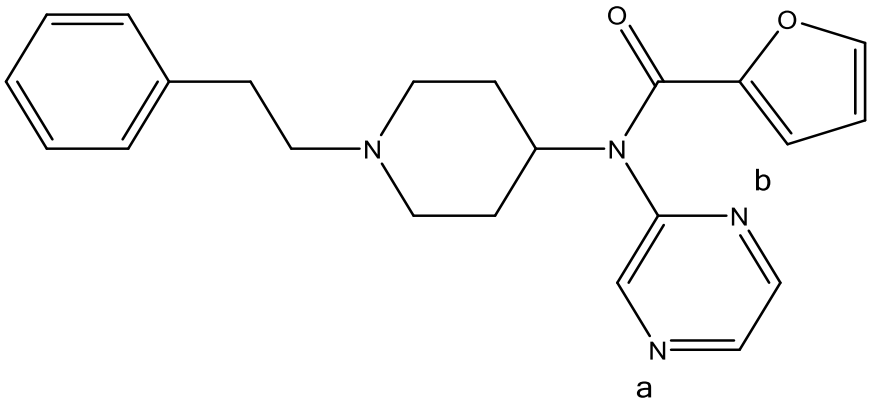


Figure 98. Chemical structure of mirfentanil (**F5**).

As **F5** has known biological activity and is far more likely to be found in street samples and cause negative health outcomes compared to fentalogues **F2** – **F4**, the SABRE hyperpolarisation of this fentanyl derivative was attempted.

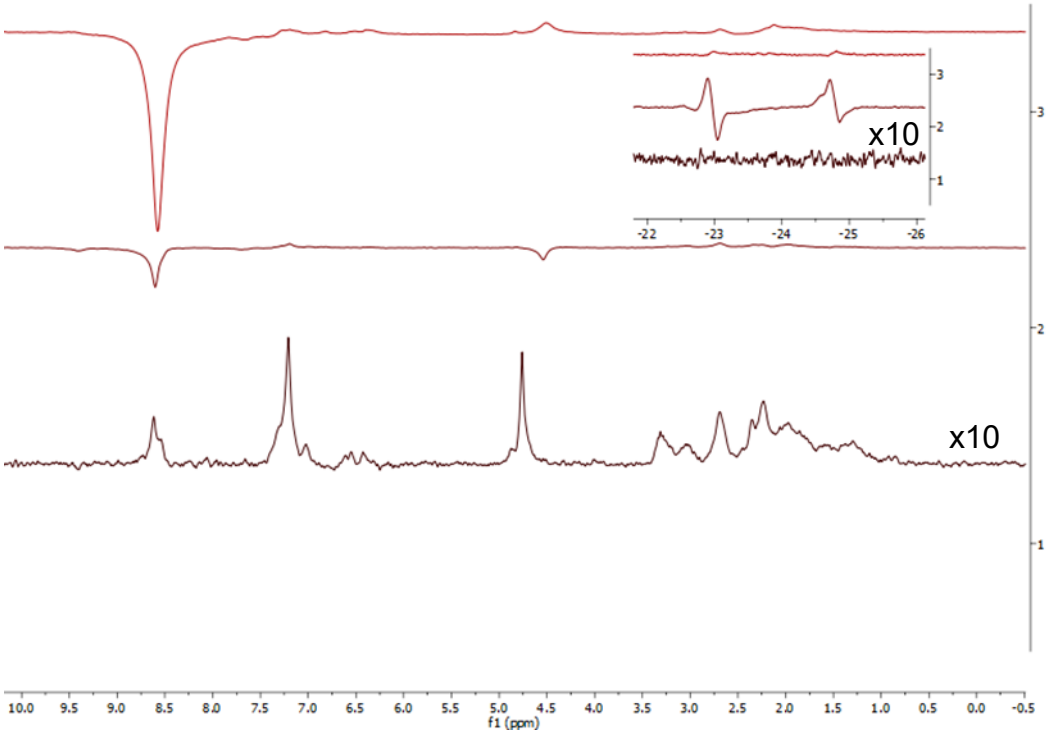


Figure 99. $^{1}$H NMR spectra of **F$_5$** and **4** in the ratio of 4:1 (4.7 mg mirfentanil) in the presence of *p*-$H_2$ in *d*$_4$-methanol. Spectrum 1 is the thermal spectrum whereas spectra 2 and 3 are hyperpolarised following polarisation transfer in earth's magnetic field or at 65 G respectively. Multiplication factors indicate scaling of the vertical axis. Expansion showcases hydride region.

SABRE of **F$_5$** resulted in successful hyperpolarisation being observed. Enhancements for the peak at 8.59 ppm of 11- and 78-fold were attained at a polarisation transfer field of earths and 65 G respectively. Interestingly, though the binding site is now a pyrazine ring, this result demonstrates a higher polarisation transfer at 65 G, unlike the fentalogues discussed in section 6.3.4 and previously reported NOS substrates bearing 4-substituted pyridyl-tethers.[127]

Hydrides are observed for the polarisation transfer species at -22.64 ppm and -24.41 ppm. Though there are two potential binding sites within the pyrazine ring for the polarisation pre-catalyst **4** to form a SABRE active species, it is highly unlikely that there is a species in solution with the iridium bound to nitrogen b in Figure 98. This is due to the reported inability of 2-picoline to form a SABRE active species,[126] though in section 5.2.3 it was demonstrated that

2-picoline may form a SABRE active complex, albeit this did require the presence of a co-ligand which was not utilised here. Therefore, the hydrides are likely representative of **F5** bound through nitrogen a in Figure 98 to form [Ir(IMes)(**F5**)$_3$(H)$_2$] leading to hydride signals for hydrides *trans* to **F5** at -22.64 ppm. The second hydride species at -24.41 ppm may be representative of **F5** bound *trans* to a methanol adduct.

As SABRE of **F5**, a known biologically relevant fentalogue, has been demonstrated it was decided to examine a system where heroin was also present as literature reports suggest heroin containing street samples are often contaminated with fentanyl.[182]

A mock, street-like sample was produced which contained between 0.63% and 3.80% mirfentanil in heroin (w/w). This was then solvated in 3.6 ml of $d_4$-methanol and a 0.6 ml aliquot taken for SABRE. Therefore, between 0.183 mg and 1.15 mg of mirfentanil (81 – 509 μM) was present within the NMR tube utilised for SABRE. This value is far below the estimated lethal dose of ~2 mg.

Conducting SABRE on these mirfentanil containing heroin mixtures resulted in enhancements for the pyrazine ring of between 2-fold and 4-fold for the lowest and highest concentrations respectively. However, conducting polarisation transfer within a 65 G field followed by rapid transfer to the 1.4 T measurement field resulted in a significant increase in hyperpolarisation, with enhancements of between 18- and 44-fold respectively recorded. The SABRE of these samples is shown in Figure 100 and Figure 101 respectively.

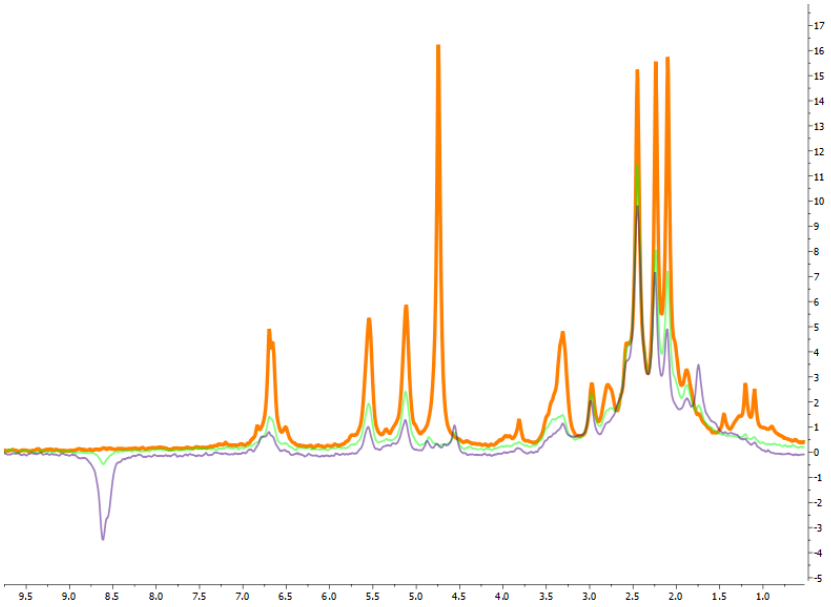

Figure 100. $^{1}$H NMR spectra of **F$_5$** and **4** in the ratio of 4:1 (0.183 mg mirfentanil) in the presence of heroin (43.7 mg) and *p*-$H_2$ in $d_4$-methanol. Orange spectrum is the thermal spectrum whereas the green and blue spectra are hyperpolarised following polarisation transfer in earth's magnetic field or at 65 G respectively.

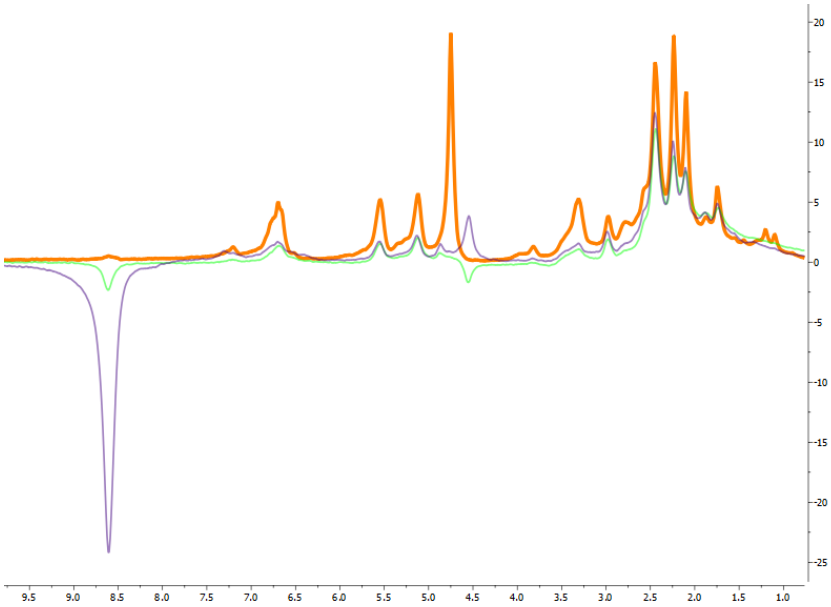

Figure 101. $^{1}$H NMR spectra of **F$_5$** and **4** in the ratio of 4:1 (1.15 mg mirfentanil) in the presence of heroin (43.7 mg) and *p*-$H_2$ in $d_4$-methanol. Orange spectrum is the thermal spectrum whereas the green and blue spectra are hyperpolarised following polarisation transfer in earth's magnetic field or at 65 G respectively.

This result demonstrates for the first time that SABRE could be utilised for the selective hyperpolarisation of a fentalogue within a heroin mixture representative of a street sample within seconds. Despite the lower enhancements present at 81 μM, the presence of mirfentanil is still clearly distinguishable through the presence of an emissive peak within the NMR spectrum. Even for the highest dose tested here, the quantity of mirfentanil within the Young's tube is below the lethal dose and could not be detected by casual inspection at thermal polarisation, making use of 128 scans (collection time ~15 mins) as shown in Figure 102.

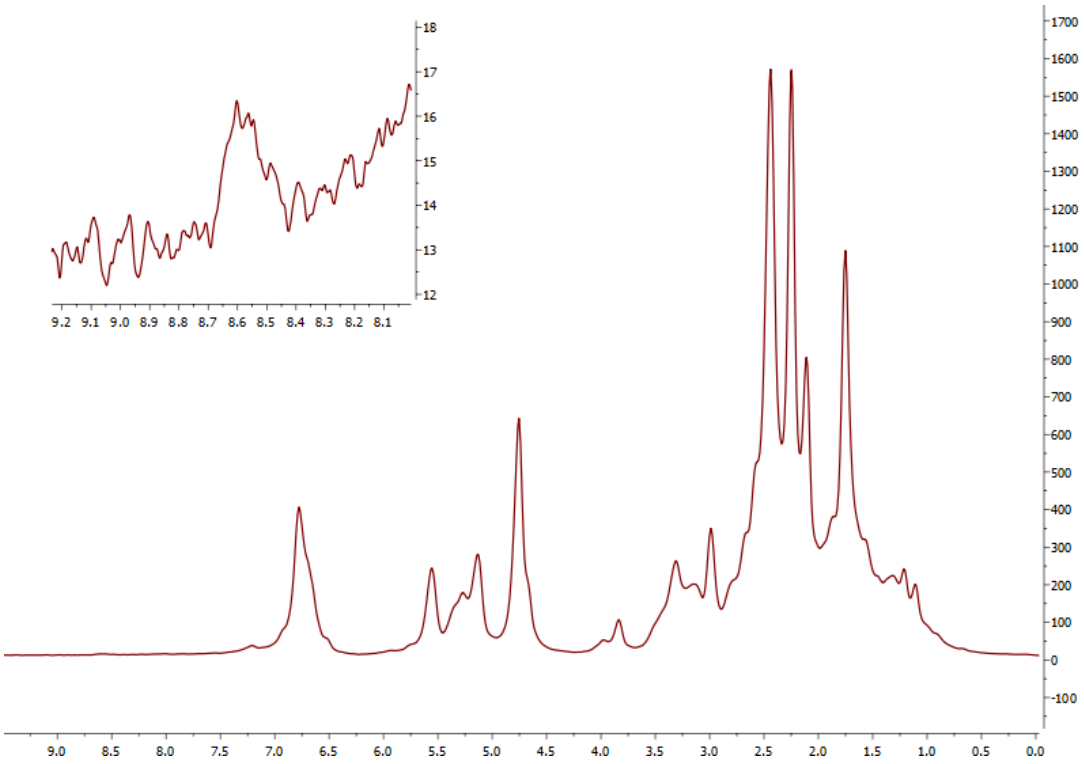


Figure 102. $^{1}$H NMR spectrum of **F$_5$** and **4** in the ratio of 4:1 (0.183 mg mirfentanil) in the presence of heroin (43.7 mg) and *p*-$H_2$ in $d_4$-methanol. Spectrum collected under thermal conditions for 128 scans at 1.4 T.

## 6.4. Conclusion

The $^{19}$F SABRE of a WHO medicine is presented for the first time with hyperpolarisation present even when a quantity of voriconazole significantly below the current dosing guidelines was utilised. This represents the first time a $^{19}$F containing molecule has been SABRE hyperpolarised which is currently

approved for clinical use. It is envisaged that, in combination with techniques for catalyst scavenging discussed in section 5.4, the foundation work for the *in vivo* application of $^{19}$F SABRE are presented here.

The hyperpolarisation of a range of fentalogues has also been presented. This work started with investigating the activity of a range of fentalogues **F₂** – **F₄** specifically synthesised for this work. These ligands all demonstrated SABRE activity that was investigated through the examination of exchange rates making use of EXSY interrogation and relaxation times. It was found the relaxation rates for these fentalogues were similar, so likely didn't have a significant effect upon the variation within polarisation values reported. However, the short $T_1$ values of 2.9 – 3.3 s did mean that multiple $T_1$s will have occurred within the ~10 s shaking time.

The thermodynamic activation parameters of ligand loss *trans* to hydride, where **F**= **F₂**, **F₃** or **F₄**, and hydride loss from $[Ir(IMes)(\mathbf{F})_3(H)_2]^+$ were obtained. Polarisation levels demonstrated that enhancements followed the trend **F₂**> **F₄**>**F₃**. The enhancements for **F₂** were highest and also possessed the most commensurate rates for loss of ligand and hydride. The slowest transfer process of ligand or hydride loss was ligand loss of 3.5 $s^{-1}$ for **F₄** compared to hydride loss at 3 $s^{-1}$ for **F₃**.

Enhancements were consistently lower at 65 G than earth's magnetic field, which is in agreement with previously reported NOS substrates bearing 4-substituted pyridyl-tethers.[127] In addition, the time to field cycle the samples will have impacted negatively on the enhancements obtained given that the time taken to transfer is of the same magnitude as the $T_1$ values measured (*ca.* 3 s).

**F₅** demonstrated that a fentalogue of known biological activity may be hyperpolarised utilising SABRE. SABRE on a mixture containing 81 μM of **F₅**, below the lethal dose, and an excess of heroin has been demonstrated to reveale the presence of the fentalogue within seconds. This represents the selective detection of mirfentanil in a street-like sample where an NMR spectrum of the same sample could not visibly detect its presence, even after

15 mins collection time. It is envisaged that if the SABRE approach may be expanded to a wider range of fentalogues (e.g. thiofentanyl), and remains resilient to mixture content, SABRE may be utilised as a forensic tool for the qualitative detection of fentalogue contaminated drug samples.

# 7. Conclusions

The use of iridium based pre-catalysts for SABRE has been well established within the literature,[1-4] with several reports also demonstrating cobalt SABRE.[5-7] However, there is only a single report of potential rhodium SABRE, which made use of a mixed iridium/rhodium system.[8] Therefore it was prudent to assess if rhodium complexes may be effectively utilised for SABRE polarisation transfer.

A range of rhodium complexes were synthesised and [Rh(IMes)(COD)Cl] was characterised for direct comparison with the literature standard SABRE catalyst [Ir(IMes)(COD)Cl].

For SABRE to occur reversible exchange of both substrate and hydrides must occur. It has been demonstrated that in both IMes-containing complexes chlorine may be displaced by the most commonly utilised SABRE substrate, pyridine. This was further observed for the complexes [Rh(Im*N*Pr$^{i}_{2}$)(COD)Cl], [Rh(I$^{t}$Bu)(COD)Cl] and [Rh(ICy)(COD)Cl]. However, COD hydrogenation is not observed and hydrides do not readily form for the rhodium complexes, with variable temperature interrogation of [Rh(IMes)(COD)Cl] demonstrating only transient hydrides at elevated temperatures. However, the disappearance of these transient hydrides when a non-methanol solvent is utilised suggests that an adduct containing species may be responsible for these hydrides.

Wilkinson's catalyst was evaluated for SABRE due to the clear formation of hydrides upon addition of $H_2$ and its previous utilisation within PHIP.[9] When 3-fluoropyridine was utilised, $^{19}$F NMR spectroscopy provided evidence for substrate binding to ~33% of the Wilkinson complexes in solution. Unfortunately, for both substrates, no SABRE was observed suggesting there was no reversible substrate binding despite the potential presence of *para*hydrogen derived hydrides. Therefore, [Ir(IMes)(COD)Cl] was utilised in this thesis as the SABRE pre-catalyst.

At the start of this work the only report of $^{19}$F SABRE was the initial 2009 report of SABRE itself, which contained a single spectrum for 3-fluoropyridine (**L$_3$**)

without a quoted enhancement factor.[10] Though an additional report had found pentafluoropyridine (**$L_6$**) to be SABRE inactive, no explanation for this was presented.[11] Therefore, a desired goal was to expand the substrate scope to which $^{19}F$ SABRE could be applied. As pyridine is the benchmark substrate for SABRE a range of fluorinated pyridine substrates were identified as initial ligands to be evaluated for SABRE activity.

The work presented here demonstrates SABRE hyperpolarisation of novel ligands. While **$L_2$**, **$L_4$** and **$L_6$** did not demonstrate SABRE explanations for this could be found in the lack of formation of a complex capable of polarisation transfer or self-reaction in the case of **$L_4$**. However, $^{19}F$ SABRE was demonstrated for **$L_3$** and **$L_5$**, with **$L_3$** being the better SABRE ligand, with $^{19}F$ enhancements of up to 166-fold being demonstrated under thermal conditions.

SABRE-SHEATH was applied to **$L_3$** and **$L_5$**. This approach demonstrated significantly increased polarisation levels of ~4-fold greater than polarisation transfer in earth's field for **$L_3$**. SABRE-RELAY also produced an in-phase spectrum, avoiding potential internal signal cancelation for MRI applications.

The polarisation transfer species $[Ir(IMes)(L)_3(H)_2]$ responsible for the SABRE of **$L_3$** and **$L_5$** was interrogated making use of EXSY. This provided a theoretical basis for the improved polarisation levels demonstrated by **$L_3$** over **$L_5$** as the complex formed by the later had a non-commensurate rapid exchange of ligand and hydride. However, this insight meant that subsequent cooling of **$L_5$** demonstrated improved levels of $^{19}F$ polarisation as the polarisation transfer process was optimised at lower temperatures due to more commensurate ligand and hydride exchange speeds.

The relaxation times of **$L_1$** - **$L_6$** have been investigated, demonstrating the difficulty in optimising a polarisation transfer system as reduced ligand equivalents relative to the polarisation transfer catalyst result in a higher enhancement due to a higher efficiency transfer process but also results in a reduced relaxation time meaning the resulting hyperpolarised signal returns to unity faster. This work also demonstrated that low field applications such as

benchtop NMR have an advantage over more traditional high field applications due to longer $T_1$ values for the same sample.[12]

A deuteration approach was taken to gain insight into the mechanism of polarisation transfer to $^{19}F$ and to increase the overall levels of polarisation. Testing of $d_4$-**L3** did not result in SABRE, suggesting that polarisation transfer may require a proton within the *ortho* site for this ligand to facilitate indirect polarisation transfer from the iridium-bound *para*hydrogen-derived hydrides to $^{19}F$ *via* this proton. It may also suggest that long-range scalar couplings are simply not strong enough to facilitate direct polarisation transfer to the heteronuclei in this ligand.

An investigation was conducted to evaluate a range of functionalised solids for the potential formation of HET-SABRE catalysts as this would negate the toxicity concerns associated with [Ir(IMes)(COD)Cl] through simple phase separation of catalyst and hyperpolarised substrate. A HET-SABRE catalyst was produced which was capable of hyperpolarising pyridine, although this structure has been previously reported.[13]

Though the majority of supports tested did not show HET-SABRE activity, this was explained utilising a homogenous model for supports **S2**, **S3** and **S7**, which demonstrated they may be effective agents for catalyst deactivation.[3] Removal of [Ir(IMes)(COD)Cl] from solution by a support may be a timely solution as despite its utilisation as the SABRE catalyst resulting in the highest enhancement levels attained, in the majority of cases, recent work has demonstrated this iridium species is cytotoxic.[14-17] Therefore, the potential for the supports to be utilised removing this cytotoxic species from a bolus was examined.

The metal scavenging efficacy of the supports was examined and scavengers **S1**, **S4** and **S5** were shown to be particularly effective. During this work a report was published which meant literature comparisons could be made with scavengers **S3** and **S4**. Though the work reported here represents a lower percentage removal of iridium from a SABRE bolus, the quantity removed was

significantly higher making use of an initial iridium concentration closer to that which may be required in a clinical setting.

Extrapolation of the scavenger data suggests that ~1 g of the most effective novel scavenger, **S5**, would render iridium below the level detected in blanks for the ICP-OES instrument utilised in this study with an initial concentration of ~1.7ppm and an exposure time of ~2 mins, with the quantity required dropping significantly with longer exposure times. It is envisaged that this novel scavenger could, in combination with other approaches such as CASH-SABRE,[18] enable the rapid preparation of a biocompatible SABRE hyperpolarised bolus. Utilisation of this approach combined with ~1g of **S5** should be capable of reducing a sample commensurate with a typical SABRE sample (2 mg of **4** in 0.6 ml, ~1005 ppm) to background levels of iridium present within the hyperpolarised $T_1$ of a suitable substrate.[19, 20]

As a route to potential biological application has been identified a range of biologically relevant substrates were investigated. Initially the hyperpolarisation of a range of fentalogues was presented. This work started with investigating the activity of a range of fentalogues **F2** – **F4** specifically synthesised for this work by the Sutcliffe research group. These ligands all demonstrated SABRE activity that was investigated through the examination of exchange rates making use of EXSY interrogation and relaxation times. The thermodynamic activation parameters of ligand loss *trans* to hydride, where **F** = **F2**, **F3** or **F4**, and hydride loss from $[Ir(IMes)(\mathbf{F})_3(H)_2]^+$ were obtained. Polarisation levels demonstrated that enhancements followed the trend **F2**>**F4**>**F3**. The enhancements for **F2** were highest and also possessed the most commensurate rates for loss of ligand and hydride. The slowest transfer process of ligand or hydride loss was ligand loss of 3.5 $s^{-1}$ for **F4** compared to hydride loss at 3 $s^{-1}$ for **F3**.

Enhancements were consistently lower at 65 G than earth's magnetic field, which is in agreement with previously reported NOS substrates bearing 4-substituted pyridyl-tethers.[21] In addition, the time to field cycle the samples will have impacted negatively on the enhancements obtained given that the time

taken to transfer is of the same magnitude as the $T_1$ values measured (*ca.* 3 s).

**F5** demonstrated that a fentalogue of known biological activity may be hyperpolarised utilising SABRE. SABRE on a mixture containing 81 μM of **F5**, a concentration below the lethal dose, and an excess of heroin has been demonstrated, revealing the presence of the fentalogue within seconds. This represents the selective detection of mirfentanil in a street-like sample where a $^{1}$H NMR spectrum of the same sample could not visibly detect its presence, even after 15 mins collection time.

The $^{19}$F SABRE of a WHO medicine, voriconazole, was presented and hyperpolarisation observed, even when a quantity of voriconazole ~4 times below the current dosing guidelines was utilised. This represents the first time a $^{19}$F containing molecule has been SABRE hyperpolarised that is currently approved for clinical use. As voriconazole has previously been studied using MRI to obtain brain images, it is envisaged that in combination with techniques for catalyst scavenging discussed in section 5.4, the foundation work for the *in vivo* application of $^{19}$F SABRE are presented herein.

The work presented in this thesis has contributed to the publications:

'*Perspective on the Hyperpolarisation Technique Signal Amplification By Reversible Exchange (SABRE) in NMR and MR Imaging*', T. B. R. Robertson, R. E. Mewis, *Annu. Rep. NMR Spectrosc.*, 2018, **93**, 145-212.

'*Extending the Scope of $^{19}$F Hyperpolarization through Signal Amplification by Reversible Exchange in MRI and NMR Spectroscopy*', A. M. Olaru, T. B. R. Robertson, J. S. Lewis, A. Anthony, W. Iali, R. E. Mewis, S. B. Duckett, *ChemistryOpen*, 2018, **7**, 97-105.

'*Hyperpolarization of Pyridyl Fentalogues by Signal Amplification By Reversible Exchange (SABRE)*', T. B. R. Robertson, L. H. Antonides, N. Gilbert, S. L. Benjamin, S. K. Langley, L. J. Munro, O. B. Sutcliffe, R. E. Mewis, *ChemistryOpen*, 2019, **8**, 1375-1382.

## 7.1. Future Work

A range of rhodium complexes have been evaluated as part of this work for comparison with the commonly utilised iridium based polarisation transfer catalysts. While these have not demonstrated the capability to perform SABRE, it is possible that utilising a tridentate ligand system similar to that utilised within the limited cobalt examples of SABRE may enable polarisation transfer, as although this complex requires the formation of a dihydride species, the change in ligand may serve to stabilise the complex. The investigation of a mixed iridium/rhodium system would also prove useful to confirming the source of SABRE currently reported by Koptug *et al.*, though they state it was hard to differentiate which species was responsible for polarisation transfer. The utilisation of $^{13}C$ SABRE should enable differentiation of the polarisation transfer species as there is a characteristic $J_{RhC}$ coupling observed within the rhodium complexes synthesised here which would only be visible in rhodium-mediated $^{13}C$ SABRE.

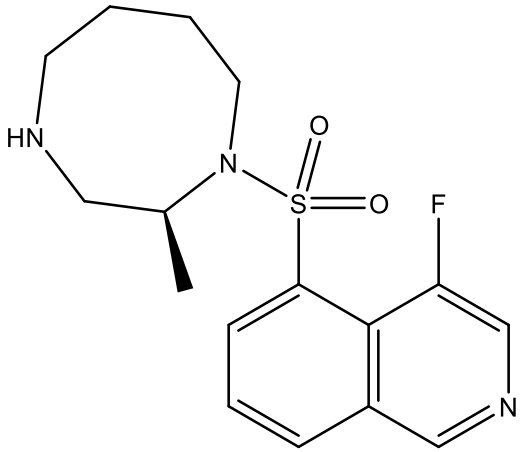


Figure 103. Structure of Rapasudil.

This work has demonstrated the potential for $^{19}F$ SABRE, however, a range of other potential ligands would be of interest, including other clinically approved medication with structures potentially amenable to SABRE such as Rapasudil, the structure of which is shown in Figure 103. The high chemical shift sensitivity of $^{19}F$ may also enable a range of potential applications of utilising fluorinated pyridyl tags for the hyperpolarisation, and detection, of complex molecules. For instance previously reported tagging of oxytocin with

perfluorohetroaromatic groups may enable a hyperpolarisation based detection method for a range of polypeptides.[22]

The capacity for silica-based scavenging of the metal components from solution has been demonstrated herein. However, the scope of scavengers utilised was limited by the initial project design focusing on the formation of a HET-SABRE catalyst. Within literature, the utilisation of sulphur-based scavengers has proven to be advantageous over nitrogen based analogues.[23] Therefore, the combination of the most successful scavengers tested within this work with sulphur containing heterocycles represents a promising avenue for future work. The implementation of a solid-based metal scavenger into an automated system for the production of a metal depleted bolus, from which a hyperpolarised signal may still be measured, would demonstrate a significant step towards production of a clinically relevant technique developing from the work reported here.

# 8. Experimental

## 8.1. Chemicals

All materials for experimental synthesis were sourced from Acros Organics, Sigma-Aldrich, Fisher Scientific or Apollo chemicals. ICP standards were purchased from SCP science. Iridium and rhodium chloride salts were sourced from Precious Metals Online, www.precmet.com.au. All materials were used as received unless stated within the experimental procedure. Solvents were purchased from Fisher Scientific and were of general use or HPLC grade unless specifically stated. Where the use of dry ethyl acetate is stated this was dried over anhydrous potassium carbonate. TLC analysis made use of aluminium backed silica gel 60 $F_{254}$ plates (Merck Millipore). Silica gel chromatography was performed with geduran silica gel 60 (Merck Millipore). Deuterated solvents were sourced from Sigma Aldrich with ≥99.8% deuterium labelling.

## 8.2. Instrumentation

All NMR spectra for characterisation of synthesised compounds were collected on a JEOL ECS-400 FT NMR in the solvent described with chemical shifts (δ) quoted in ppm and coupling constants (J) quoted in hertz (Hz). Spectra were collected at a frequency of 400.14 MHz for $^{1}$H spectra, 101 MHz for $^{13}$C spectra and 376 MHz for $^{19}$F spectra. SABRE NMR spectra were collected on an Oxford Instruments Pulsar benchtop at a frequency of 59.8 MHz for $^{1}$H spectra and 56 MHz for $^{19}$F spectra. NMR analysis was carried out making use of MestReNova version 11.0.4. Measurements making use of a μ-magnetic shield utilised a LakeShore cryogenics model 4065 zero gauss chamber. Measurements making use of a mixing field outside of the spectrometer above earth's field made use of a custom electromagnet produced by Siga Transformers (sigatransformers.co.uk) within which a vertical magnetic field of up to 150 G could be generated. A Hirst Magnetic Instruments Ltd GM07 gaussmeter with transverse (Hirst magnetic instruments ltd, serial #10620) and axial (RS components ltd, stock number 212-736) hall probes were used to determine the exact magnetic field for

measurements which involved polarisation transfer occurring under SABRE conditions.

Hydrogen was generated using a Peak scientific PH200 hydrogen generator set to 3.5 bar. Where *para*hydrogen was required this was generated through the immersion of a charcoal packed coil into liquid nitrogen to generate ~50% enriched *para*hydrogen. SABRE measurements were made utilising GPE scientific, 5mm, 7'' long, 400 MHz, Norell select series Young's tubes.

Mass spectrometry was performed using an Agilent technologies 6540 UHD Accurate-Mass Q-TOF LC/MS system. Where needed, LC separation prior to MS was performed on an Agilent technologies 1260 infinity series LC system.

EDX measurements were acquired on a ZEISS GeminiSEM system equipped with an Ametek EDX attachment. Data was analysed utilising SmartSEM and EDX genesis software.

Microwave reactions made use of an Anton Parr monowave 300 microwave reactor.

Samples requiring sonication made use of a 475H Langford Sonomatic ultrasonic cleaner.

ICP-OES samples were prepared where stated making use of a VWR Microstar12 centrifuge and VWR digital vortex mixer. Deionised water was purified with a Merck Millipore gradient A10 water purification system or a Merck Millipore Milli-Q Integral water purification system. Deionised water was stored after purification in a Merck Millipore polyethylene storage tank. Analysis was performed using a Thermo Scientific iCAP 6000 series ICP-OES utilising Qtegra software.

## 8.3. SABRE hyperpolarisation

### 8.3.1. Enhancement calculations

The calculation of enhancement factors made use of Equation 3

$$Enhancement\ (\varepsilon) = \frac{S_{hyp}}{S_{thermal}}$$

Equation 3. Equation for the calculation of enhancement factors where $S_{hyp}$ is the integral of a set region after hyperpolarisation and $S_{thermal}$ is the integral of the same region without hyperpolarisation.

The same sample was used for the collection of $S_{thermal}$ and $S_{hyp}$, however, $S_{thermal}$ was allowed to fully relax in the measurement field (typically 1.4 T, see section 8.2) before data acquisition. Reference and polarised spectra were collected using identical acquisition parameters, including the use of heating and cooling of the sample prior to acquisition where specified. The raw integrals of the relevant resonances in the polarised and unpolarised spectra were used to determine the enhancement level. The same chemical shift region was selected for integrals to ensure a fair comparison – in all cases each spectrum was properly referenced to the solvent used.

Where stated in the results, some enhancements were calculated making use of signal magnitude. These were collected as described above but made use of Equation 4.

$$Enhancement\ (\varepsilon) = \frac{|S_{hyp}|}{|S_{thermal}|}$$

Equation 4. Equation for the calculation of enhancement factors where $|S_{hyp}|$ is the integral of a set region after hyperpolarisation and $|S_{thermal}|$ is the integral of the same region without hyperpolarisation.

### 8.3.2. Sample preparation

#### 8.3.2.1. SABRE sample preparation

Unless otherwise specified, a sample of ligand (L) was solvated in 600 μL of deuterated solvent with 2 mg of the SABRE pre-catalyst, [Ir(IMes)(COD)Cl]. The ratio of ligand to pre-catalyst was, as specified, typically within the range of 4-20 equivalents ligand:pre-catalyst. The sample was shaken to ensure full ligand and pre-catalyst solvation before transfer into a Young's capped NMR tube. The sample was then freeze-thaw degassed making use of the procedure outlined in section 8.3.3 for the solvent used. The sample was then activated by shaking for 30 seconds following the introduction of *para*hydrogen into the head space of the tube.

#### 8.3.2.2. SABRE-RELAY sample preparation

Unless otherwise specified a sample of ligand (L) was solvated in 500 μL $D_2O$ (Sigma Aldrich, 99.9% deuterated) and 100 μL ammonia (Fisher scientific, 35% in $H_2O$) with 2 mg of the SABRE pre-catalyst, [Ir(IMes)(COD)Cl]. The ratio of ligand to pre-catalyst was 4 equivalents ligand:pre-catalyst. The sample was shaken to ensure full ligand and pre-catalyst solvation before transfer into a Young's capped NMR tube. The sample was then freeze-thaw degassed making use of the procedure outlined in section 8.3.3 for the solvent used. The sample was then activated by shaking for 30 seconds following the introduction of *para*hydrogen into the head space of the tube.

#### 8.3.2.3. Mirfentanil-heroin mix SABRE sample preparation

174.9 mg of heroin, was dissolved in 3.6 mL of $d_4$-methanol and sonicated for ~30 seconds. For the lowest concentration (81.2 μM) 1.1 mg of mirfentanil and 0.5 mg of the SABRE pre-catalyst, [Ir(IMes)(COD)Cl] were added to this stock and sonicated for 30 seconds. Following this a 0.6 mL aliquot was transferred to a Young's capped NMR. The sample was then freeze-thaw degassed making use of the procedure outlined in section 8.3.3 for $d_4$-methanol before *para*hydrogen was introduced into the head space of the tube. SABRE was

then performed with polarisation transfer at both earth's magnetic field and 65 G by shaking the tube for 10 seconds in the polarisation transfer field before rapid transfer and acquisition at 1.4 T. *Para*hydrogen within the headspace of the tube was then replenished prior to additional measurements.

The aliquot was then returned to the stock solution and additional mirfentanil added in steps of 1.1 mg, 2.3 mg and 2.4 mg respectively to give four total concentrations. Alongside these mirfentanil additions 1.0 mg of [Ir(IMes)(COD)Cl] was added at each concentration step up. Following the addition of more mirfentanil and [Ir(IMes)(COD)Cl], the stock was sonicated for 30 seconds before removal of a fresh aliquot and acquisition repeated in this way for the total four concentrations (81.2, 162.3, 332.0 and 509.1 μM mirfentanil).

### 8.3.3. Freeze-thaw degassing methods

#### 8.3.3.1. $d_4$-methanol

The Young's capped NMR tube was submerged in an acetone/dry ice bath before a vacuum was applied to the head space until the pressure was below 6 mbar. The tube was then removed from the acetone/dry ice bath and shaken for a minimum of 20 seconds before repeating the degassing step a further twice.

#### 8.3.3.2. $D_2O$

The Young's capped NMR tube was submerged in a liquid nitrogen bath before a vacuum was applied to the head space until the pressure was below 6 mbar. The tube was then carefully removed from the liquid nitrogen, while acetone was run down the length of the tube, and shaken for a minimum of 20 seconds before repeating the degassing step a further twice.

### 8.3.4. Magnetic Field Measurements

Where SABRE measurements were carried out at a field above Earth's magnetic field, a Siga Transformers hollow tube coil was utilised within which a vertical magnetic field of up to 150 G could be generated (Figure 104). The

sample was then rapidly inserted in to the NMR spectrometer and a $^{1}H$ NMR spectrum acquired.

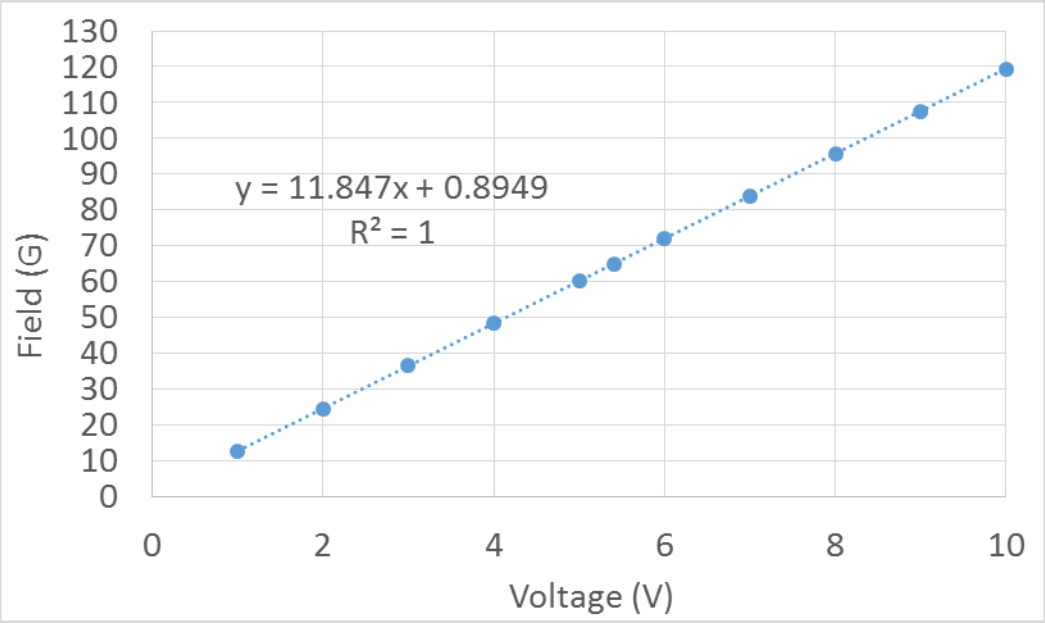


Figure 104. Magnetic field produced in response to voltage applied to the hollow tube coil used for SABRE hyperpolarisation transfer.

### 8.3.5. Variable temperature SABRE

All SABRE measurements were conducted at room temperature unless otherwise specified. Where specified *para*hydrogen was added to the headspace of the Young's capped NMR tube and not shaken until after being submerged within a water bath heated or cooled to the specified temperature for 2 minutes prior to rapid transfer into the measurement field and sample interrogation. Where SABRE occurred the specified enhancements are compared with a thermal spectrum acquired at the same temperature following the same procedure.

## 8.4. Exchange Rate Spectroscopy

A sample of ligand (L) was solvated in 600 µL of deuterated solvent with between 6-10 mg of the SABRE pre-catalyst, [Ir(IMes)(COD)Cl]. The ratio of ligand to pre-catalyst was 4:1. The sample was shaken to ensure full ligand and pre-catalyst solvation before transfer into a Young's capped NMR tube.

The sample was then freeze-thaw degassed making use of the procedure outlined in section 8.3.3 for the solvent used.

Exchange data was collected by running a series of NOESY experiments at temperatures between 268 – 305 K. Data was collected at six temperatures. At each temperature a series of mixing values typically ranging from 0.005 s to 1 s were used to establish the rate constants for hydride and bound-ligand loss. These values were then used to create Eyring-Polanyi plots in order to obtain $\Delta G_{300\,K}$, $\Delta H$ and $\Delta S$ for each exchange process.

## 8.5. Use of controlled substances

All controlled drug standards were either prepared in-house or obtained, under UK Home Office licence (No. 550460), by authorised personnel and in compliance with both the UK Misuse of Drugs Act (1971) and UK Misuse of Drugs Regulations (2001). Test samples (street samples) were provided by Greater Manchester Police (GMP) personnel, in accordance with the legislation and under the approved protocol operating between the MANchester DRug Analysis and Knowledge Exchange (MANDRAKE) and GMP. All controlled/restricted materials were stored, transferred, used and destroyed in compliance with the UK Misuse of Drugs Act (1971) and UK Misuse of Drugs Regulations (2001).

## 8.6. Chemical Synthesis

A range of compounds were synthesised over the course of this work, specifics are detailed below.

### 8.6.1. *N,N'*-bis(2,4,6-trimethylphenyl)ethanediimine, 1

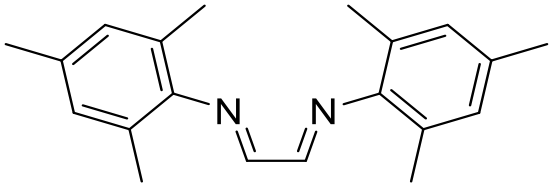


A solution of glyoxal (7.3 mL, 40% in water, 64 mmol) in methanol (25 mL) was added with stirring to a warmed (50°C) solution of 2,4,6-trimethylaniline (13.79 g, 100 mmol), acetic acid (0.05 mL, 1 mmol) and methanol (25 mL). Upon addition of the glyoxal, the desired material began to crystallise out of solution. The mixture was left to stir o/n and the resulting orange suspension filtered. The solid was washed with methanol (20 mL) before drying overnight (o/n) under reduced atmosphere. This yielded **1** as a yellow solid (11.88 g, 39%); $^{1}$H NMR (400 MHz, $CDCl_3$) δ 8.19 (s, 2H, ArH), 6.90 (s, 4H, Mes), 2.28 (s, 6H, Me), 2.15 (s, 12H, Me). $^{13}$C NMR (101 MHz, $CDCl_3$) δ 147.50, 136.65, 136.57, 134.36, 129.07 ($C_{aromatic}$), 20.87, 18.31 ($C_{Me}$). HRMS expected for $C_{20}H_{24}N_2$ m/z=293.2012, found m/z=293.2009.

### 8.6.2.1,3-*bis*(2,4,6-trimethylphenyl)-imidazolium hydrochloride, 2

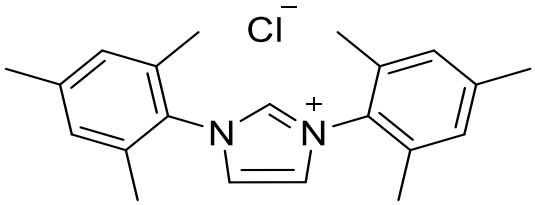


**1** (1.00 g, 3.42 mmol) and paraformaldehyde (115.4 mg, 3.8 mmol) were dissolved in dry ethyl acetate (10 mL) and heated to 70 °C. Trimethylsilyl chloride (0.52 mL, 4 mmol) was added dropwise over 45 mins and the reaction was stirred o/n. The reaction was then cooled to 5 °C. After an hour of stirring at low temperature the solution was filtered and a cream solid obtained. This was washed with ethyl acetate (30 mL) and left to dry o/n under reduced atmosphere. This yielded **2** as a cream solid (0.83 g, 79%); $^{1}$H NMR (400 MHz, $CDCl_3$) δ 10.89 (s, 1H, NC<u>H</u>N), 7.51(s, 2H, Imidazole), 6.97 (s, 4H, Mes), 2.28 (s, 6H, Me), 2.13 (s, 12H, Me). $^{13}$C NMR (101 MHz, $CDCl_3$) δ 141.50, 140.16, 134.17, 130.68, 130.06, 124.25($C_{aromatic}$), 21.26, 17.80($C_{Me}$). HRMS expected for $C_{21}H_{24}N_2$ m/z=305.2017, found m/z=305.2018.

### 8.6.3. $[Ir(COD)Cl]_2$, 3

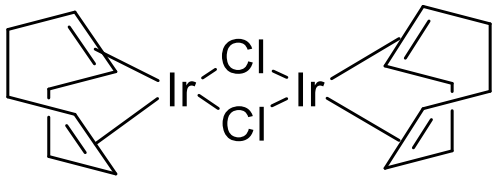


Argon was bubbled through a solution of $IrCl_3.xH_2O$ (0.50 g, 1.6 mmol anhydrous) in distilled water (8 mL) and propan-2-ol (12 mL). After 30 min, cyclooctadiene (COD), (2.7 mL, 20.4 mmol) was added and the mixture was heated to 90°C under argon. After 2-3 h, a brick red solution was formed and the reaction was cooled to room temperature. The precipitate was then filtered and washed with cold methanol (20 mL) and dried under reduced pressure to yield **3** as an orange solid (0.21 g, 18% based on anhydrous $IrCl_3$); $^1H$ NMR (400 MHz, $CDCl_3$) δ 5.59 (s, 8H, CH), 2.37 (s, 16H, $CH_2$). $^{13}C$ NMR (101 MHz, $CDCl_3$) 128.76 (CH), 28.10 ($CH_2$).

### 8.6.4. [Ir(IMes)(COD)Cl], 4

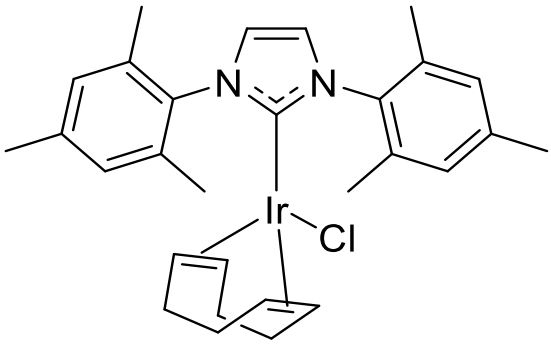


A solution of **2** (0.20 g, 66 mmol) and potassium *tert*-butoxide (0.08 g, 0.71 mmol) in dry tetrahydrofuran (8 mL) was stirred under argon for 30 mins. A solution of **3** (0.2 g, 0.30 mmol) in dry tetrahydrofuran (8 mL) was added to this solution. The reaction was then left to stir o/n. The solution was then concentrated under reduced pressure before purifying with silica gel chromatography (8:1 DCM:acetone). The yellow fraction was collected and dried under vacuum. The product was triturated with diethyl ether (5 mL), and after removal of the solvent under reduced pressure, this yielded **4** as a golden solid (0.27 g, 71%); $^{1}$H NMR (400 MHz, $d_4$-MeOD) δ 7.23 (s, 2H, Imidazole), 7.03 (d, 4H, $J_{HH}$= 6.46, ArH), 4.00 (m, 2H, CH of COD), 3.08 (m, 2H, CH of COD), 2.36 (s, 6H, $CH_3$), 2.29 (s, 6H, $CH_3$), 2.18 (s, 6H, $CH_3$), 1.67 (m, 4H, COD), 1.33 (m, 4H, COD). $^{13}$C NMR (101 MHz, $d_4$-MeOD) 180.65, 139.93 ($C_{Ar}$), 138.24 ($C_{Ar}$), 137.58, 135.94, 130.34, 129.35, 125.28, 82.82, 53.21, 34.38, 29.81, 21.17, 19.98, 18.56. HRMS expected for $IrClN_2C_{29}H_{36}$ m/z=639.2246, found m/z (M-Cl)= 603.2484, found m/z=603.2460.

### 8.6.5. $[Rh(COD)Cl]_2$, 5

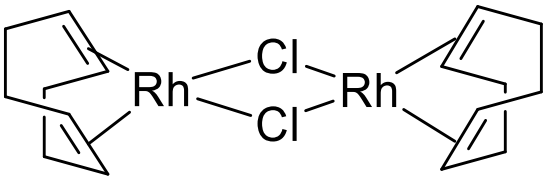


Argon was bubbled through a solution of $RhCl_3.xH_2O$ (0.5068 g, 2.4 mmol) in propan-2-ol (20 mL). After 30 min, cyclooctadiene (COD) (1.1 mL, 9 mmol) was added and the mixture was heated to 80°C under argon. After 2-3 h the reaction was cooled to room temperature, then the solution is left to stand o/n. The precipitate was then filtered and washed with cold methanol and dried under reduced pressure to yield compound **8** as an orange solid $[Rh(COD)Cl]_2$ (0.2972 g, 50% yield based on anhydrous mass of $RhCl_3$); $^1H$ NMR (400 MHz, $CDCl_3$) δ 4.21 (s, 4H), 2.48 (m, 4H), 1.74 (q, 4H, $J_{HH}$= 7.90). $^{13}C$ NMR (101 MHz, $CDCl_3$) 78.79 (d, $J_{CRh}$= 14.40 Hz, CH), 30.96 ($CH_2$). HRMS expected for $C_{16}H_{24}Cl_2Rh_2$ m/z=491.9365, found m/z=252.0258, HRMS expected for [Rh(COD)(MeCN)]= 252.0215.

### 8.6.6. [Rh(IMes)(COD)Cl], 6

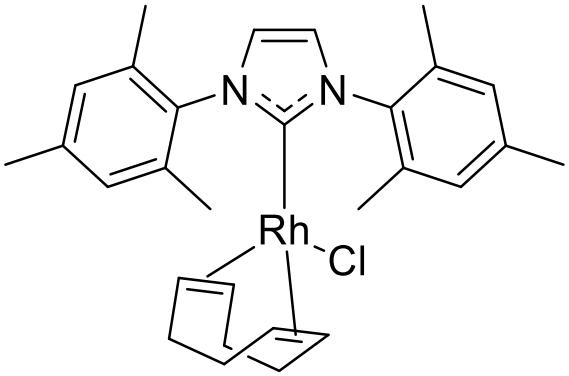


A solution of **2** (277 mg, 0.9 mmol) and potassium *tert*-butoxide (100 mg, 0.9 mmol) in dry tetrahydrofuran (7 mL) was stirred under argon for 30 mins. A solution of **8** (248 mg, 0.5 mmol) in dry tetrahydrofuran (5 mL) was added to this solution. The reaction was then left to stir o/n. The solution was then concentrated under reduced pressure before purifying with silica gel chromatography (8:1 DCM:acetone). The yellow fraction was collected and dried under vacuum. The product was triturated with diethyl ether, and after removal of the solvent under reduced pressure, **9** was obtained as a golden solid (374.4 mg, 88%); $^{1}$H NMR (400 MHz, $CDCl_3$) δ 7.23 (s, 2H, Imidazole), 7.08 (s, 4H, ArH), 4.38 (m, 4H, COD), 3.42 (m, 4H, COD), 2.39 (s, 6H, Mes), 2.32 (s, 3H, Mes), 2.16 (s, 2H, Mes), 1.86 (s, 4H, COD), 1.58 (s, 4H, COD). $^{13}$C NMR (101 MHz, $d_4$-MeOD) 181.48, 140.03 ($C_{Ar}$), 138.40 ($C_{Ar}$), 137.77, 135.93, 130.51, 129.45, 125.54, 96.89 (d, $J_{CRh}$= 7.95), 69.79 (d, $J_{CRh}$= 14.61), 33.62, 29.27, 29.04, 21.19, 20.11, 18.50. HRMS expected for $RhClN_2C_{29}H_{36}$ m/z=550.1622, found m/z (M-Cl)=515.1934.

### 8.6.7. [Rh(Im*N*Pr$^{i}_{2}$)(COD)Cl], 7

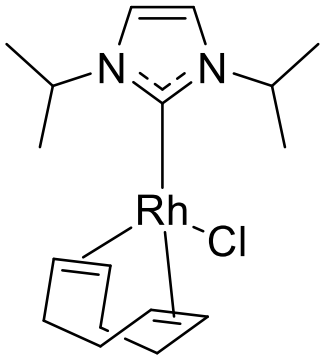


A solution of Im*N*Pr$^{i}_{2}$.Cl (152 mg, 0.80 mmol) and potassium *tert*-butoxide (126 mg, 11.2 mmol) in dry tetrahydrofuran (10 mL) was stirred under argon for 1 hour. A solution of **8** (197 mg, 0.4 mmol) in dry tetrahydrofuran (10 mL) was added to this solution. The reaction was then left to stir o/n. The solution was then concentrated under reduced pressure before purifying with silica gel chromatography (8:1 DCM:acetone). The yellow fraction was collected and dried under vacuum. The product was triturated with diethyl ether, and after removal of the solvent under reduced pressure, **10** was obtained as a bright yellow solid (253.9 mg, 79%); $^{1}$H NMR (400 MHz, $CDCl_3$) δ 6.87 (s, 2H, Imidazole), 5.79-5.68 (septet, J=6.85, 2H, aliphatic CH), 4.98 (s, 2H, COD), 3.31 (s, 2H, COD), 2.39 (m, 4H, COD), 1.93 (d, J= 9.02, 4H, COD). $^{13}$C NMR (101 MHz, $CDCl_3$) 181.54, 116.87, 98.09 (d, $J_{CRh}$= 7.38), 67.55 (d, $J_{CRh}$= 14.43), 52.64, 33.09, 28.99, 24.36, 23.42. HRMS expected for $RhClN_2C_{17}H_{28}$ m/z=398.0997, found m/z (M-Cl)=363.1300.

### 8.6.8. [Rh(I$^t$Bu)(COD)Cl], 8

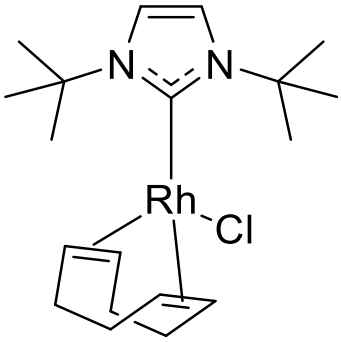


A solution of I$^t$Bu $BF_4$ (111 mg, 0.41 mmol) and potassium *tert*-butoxide (105 mg, 0.94 mmol) in dry tetrahydrofuran (5 mL) was stirred under argon for 2 hours. A solution of **8** (101 mg, 0.2 mmol) in dry tetrahydrofuran (5 mL) was added to this solution. The reaction was then left to stir o/n. The solution was then concentrated under reduced pressure before purifying with silica gel chromatography (8:1 DCM:acetone). The yellow fraction was collected and dried under vacuum. The product was triturated with diethyl ether, and after removal of the solvent under reduced pressure, **11** was obtained as a bright yellow solid (72.8 mg, 37.8%); $^1$H NMR (400 MHz, $CDCl_3$) δ 7.11 (s, 2H, Imidazole), 4.91 (m, 2H, COD), 3.15 (s, 2H, COD), 2.38 (s, 4H, COD), 2.08 (s, 18H, Me), 1.75 (m, 4H, COD). $^{13}$C NMR (101 MHz, $CDCl_3$) 179.93, 119.97, 67.87, 33.01, 32.25, 28.74. $^{19}$F NMR demonstrated no $BF_4$ starting material was still present within the product. HRMS expected for $RhClN_2C_{19}H_{32}$ m/z=428.1461, found m/z (M-Cl)=391.1614.

### 8.6.9. [Rh(ICy)(COD)Cl], 9

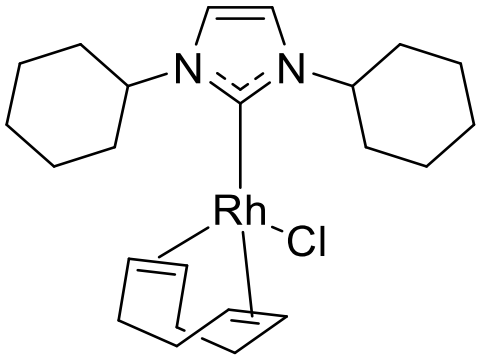


A solution of ICy $BF_4$ (140 mg, 0.44 mmol) and potassium *tert*-butoxide (108 mg, 0.96 mmol) in dry tetrahydrofuran (5 mL) was stirred under argon for 2 hours. A solution of **8** (103 mg, 0.2 mmol) in dry tetrahydrofuran (5 mL) was added to this solution. The reaction was then left to stir o/n. The solution was then concentrated under reduced pressure before purifying with silica gel chromatography (8:1 DCM:Acetone). The yellow fraction was collected and dried under vacuum. The product was triturated with diethyl ether, and after removal of the solvent under reduced pressure, **11** was obtained as a bright yellow solid (77.1 mg, 38.6%); $^{1}$H NMR (400 MHz, $CDCl_3$) δ 6.82 (s, 2H, Imidazole), 5.33 (ddt, J= 11.9, 7.7, 3.7, 2H, ICy), 4.99 (s, 2H, COD), 3.28 (s, 2H, COD), 2.36 (m, 4H, COD), 2.00 (m, 4H, ICy), 1.94 (d, J= 8.00, 4H, COD), 1.62 (m, 4H), 1.36 (td, J= 12.3, 3.8, 2H, ICy). $^{13}$C NMR (101 MHz, $CDCl_3$) 182.96, 117.31, 97.80 (d, $J_{CRh}$= 7.23), 67.31 (d, $J_{CRh}$= 14.51), 60.39, 34.39 (d, $J_{CRh}$= 5.51), 33.25, 29.11, 26.30, 26.00, 25.60. $^{19}$F NMR demonstrated no $BF_4$ starting material was still present within the product. HRMS expected for $RhClN_2C_{23}H_{36}$ m/z=478.1617, found m/z (M-Cl)=443.1931.

### 8.6.10. 3-Fluoropyridine-*N*-oxide, 10

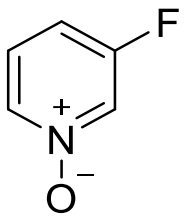

3-fluoropyridine (1.34 mL, 13.65 mmol), hydrogen peroxide (30%, 2.7 mL, 46 mmol) and acetic acid (8.1 mL, 141.6 mmol) were heated to 80°C. The solution was left to stir for 26 hours before being reduced to a small volume (5 mL) under vacuum. The resulting solution was neutralised with potassium carbonate and dried with sodium sulfate before chloroform (30 mL) was added. The solution was then filtered and the filtrate concentrated under reduced pressure to yield **5** as a pale yellow solid (1.46 g, 83%); $^{1}$H NMR (400 MHz, $D_2O$) δ 8.27-8.20 (m, 1H), 8.08-8.01 (m, 1H), 7.49-7.40 (m, 2H). $^{13}$C NMR (101 MHz, $D_2O$) δ 160.36 (d, $J_{CF}$= 252.31, $C_F$), 135.93 ($C_{ortho}$), 129.67 (d, $J_{CF}$= 36.99, $C_{ortho}$), 127.39 (d, $J_{CF}$= 9.51, $C_{meta}$), 119.78 (d, $J_{CF}$= 19.16, $C_{para}$). $^{19}$F NMR (376 MHz, $CDCl_3$) δ -119.86. HRMS expected for $C_5H_4NFO$ m/z=114.0350, found m/z=114.0353.

### 8.6.11. 3-Fluoropyridine-*N*-oxide-$d_4$, 11

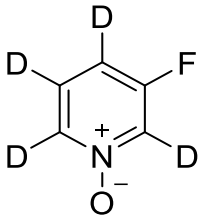


**5** (8, 0.2571 g, 2.27 mmol), potassium carbonate (0.1682 g, 1.22 mmol) and $D_2O$ (1.7 mL) were reacted in a microwave for 3 hours at 190 °C. The volume of the reaction mixture was reduced, additional $D_2O$ added (5 mL) and microwaved at 190 °C, this was repeated 9 times, until >98% deuteration was obtained through $^1H$ NMR monitoring. The solution was then concentrated under reduced pressure to yield **6** as a yellow solid (0.24 g, 90%); $^{13}C$ NMR (101 MHz, $D_2O$) δ 165.49 (d, $J_{CF}$= 252.31, $C_F$), 135.93 ($C_{ortho}$), 129.67 (d, $J_{CF}$= 36.99, $C_{ortho}$), 127.39 (d, $J_{CF}$= 9.51, $C_{meta}$), 119.78 (d, $J_{CF}$= 19.16, $C_{para}$). $^{19}F$ NMR (376 MHz, $CDCl_3$) δ -121.95. HRMS expected for $C_5D_4NFO$ m/z=117.0528, found m/z=117.0534.

### 8.6.12. 3-Fluoropyridine-$d_4$, 12

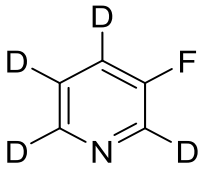


**6** (0.12 g, 1.02 mmol) was dissolved in dichloromethane (25 mL) before addition to $PCl_3$ (0.2 mL, 2.3 mmol) at 0℃. The solution was then heated to 45℃ for 2 hours before cooling and the addition of 10 ml deionised water *at* 0℃. The resulting solution was neutralised with a saturated potassium carbonate solution (15 mL) before separation and the organic layer being concentrated under reduced pressure to yield **7** as a white solid (0.05 g, 48%); $^{13}C$ NMR (101 MHz, $D_2O$) δ 165.48, 135.58 (t, $J_{CF}$= 26.45), 129.43 (t, $J_{CF}$= 27.55), 127.11 (d, $J_{CF}$= 8.32), 119.50. $^{19}F$ NMR (376 MHz, $CDCl_3$) δ -121.99. HRMS expected for $C_5D_4NFO$ m/z=117.0528, found m/z=117.0534.

### 8.6.13. Potential HET-SABRE Catalysts

#### 8.6.13.1. 3-Aminopropyl-functionalised silica gel ($S_1$)

A dry flask was charged with **4** (34.5 mg, 0.05 mmol) and 3-aminopropyl functionalised silica gel (199 mg). A vacuum was applied for 30 mins before addition of dry toluene (5 mL) and TEA (3 drops). The reaction was left o/n before filtering and washing with methanol until the eluent ran clear. 183 mg of the pale yellow product was collected.

#### 8.6.13.2. 3-(ethylenediamino)propyl-functionalised silica gel ($S_2$)

A dry flask was charged with **4** (34.1 mg, 0.05 mmol) and 3-(ethylenediamino)propyl functionalised silica gel (199 mg). A vacuum was applied for 30 mins before addition of dry toluene (5 mL) and TEA (3 drops). The reaction was left o/n before filtering and washing with methanol until the eluent ran clear. 168 mg of the pale yellow product was collected.

#### 8.6.13.3. 3-(diethylenetriamino)propyl-functionalised silica gel ($S_3$)

A dry flask was charged with **4** (34.2 mg, 0.05 mmol) and 3-(diethylenediamino)propyl functionalised silica gel (199 mg). A vacuum was applied for 30 mins before addition of dry toluene (5 mL) and TEA (3 drops). The reaction was left o/n before filtering and washing with methanol until the eluent ran clear. 185 mg of the pale yellow product was collected.

#### 8.6.13.4. 3-(Imidazole-1-yl)propyl-functionalised silica gel ($S_4$)

A dry flask was charged with **4** (34.4 mg, 0.05 mmol) and 3-(imidazole-1-yl)propyl functionalised silica gel (200 mg). A vacuum was applied for 30 mins before addition of dry toluene (5 mL) and TEA (3 drops). The reaction was left o/n before filtering and washing with methanol until the eluent ran clear. 181 mg of the pale yellow product was collected.

#### 8.6.13.5. 2-(2-pyridyl)ethyl - functionalised silica gel ($S_5$)

A dry flask was charged with **4** (34.8 mg, 0.05 mmol) and 2-(2-pyridyl)ethyl functionalised silica gel (200 mg). A vacuum was applied for 30 mins before addition of dry toluene (5 mL) and TEA (3 drops). The reaction was left o/n before filtering and washing with methanol until the eluent ran clear. 58 mg of the pale yellow product was collected.

#### 8.6.13.6. Ethylenediamine, polymer-bound ($S_6$)

A dry flask was charged with **4** (34.9 mg, 0.05 mmol) and polymer bound ethylenediamine (201 mg). A vacuum was applied for 30 mins before addition of dry toluene (5 mL) and TEA (3 drops). The reaction was left o/n before filtering and washing with methanol until the eluent ran clear. 192 mg of the yellow product was collected.

#### 8.6.13.7. (Aminomethyl)polystyrene ($S_7$)

A dry flask was charged with **4** (2.9 mg, 0.005 mmol) and polymer bound ethylenediamine (17 mg). A vacuum was applied for 30 mins before addition of dry toluene (5 mL) and TEA (3 drops). The reaction was left o/n before filtering and washing with methanol until the eluent ran clear. 5 mg of the yellow product was collected.

## 8.7. Characterisation of SABRE complexes

### 8.7.1. NMR characterisation data for $[Ir(IMes)(H)_2(L_3)_3]Cl$ (17-fold excess to 5 mM of 1 in MeOD) at 245 K.

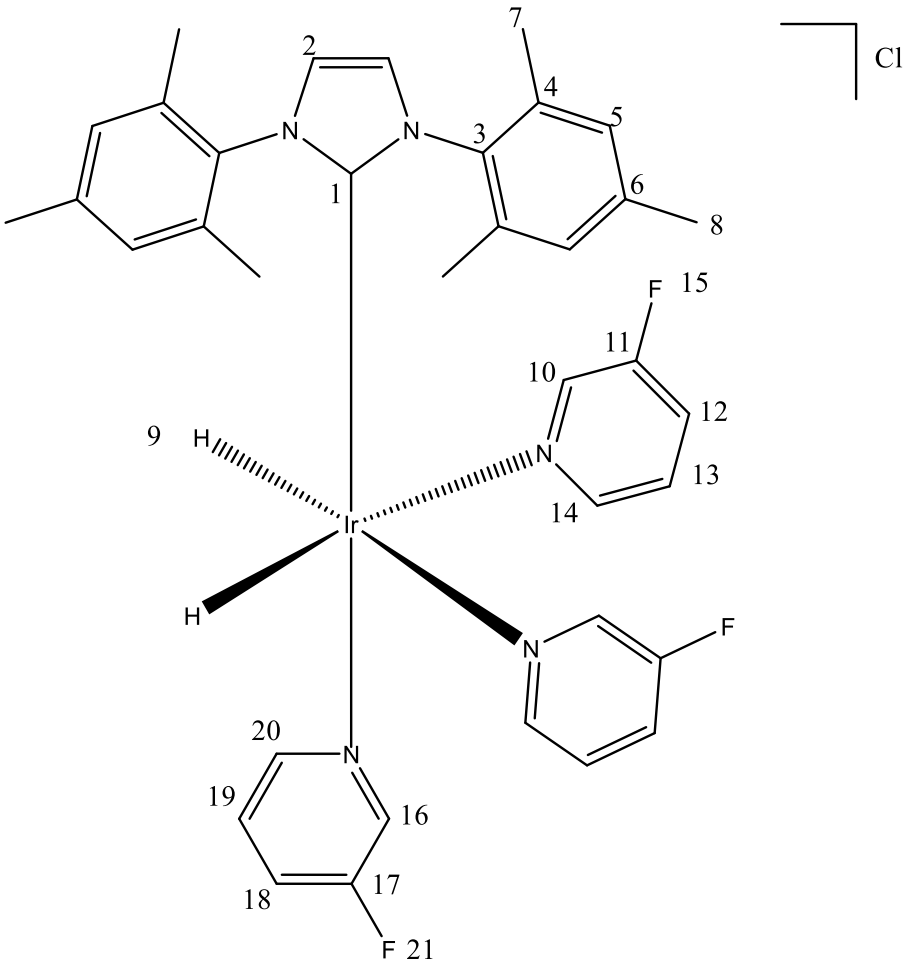


| Resonance number | $^{1}H$ (ppm) | $^{13}C$ (ppm) | $^{19}F$ (ppm) |
|---|---|---|---|
| 1 | | 180.65 | |
| 2 | 7.23 | 122.71 | |
| 3 | | 137.00 | |
| 4 | | 135.00 | |
| 5 | 6.62 | 128.32 | |
| 6 | | 138.45 | |

| | | | |
|---|---|---|---|
| 7 | 2.07 | 17.62 | |
| 8 | 2.22 | 19.60 | |
| 9 | -22.85 | | |
| 10 | 8.42 | 149.13 | |
| 11 | | | |
| 12 | 7.38 | 126.23 | |
| 13 | 7.72 | 123.74 | |
| 14 | 8.00 | 144.22 | |
| 15 | | | -124.2 |
| 16 | 7.94 | 151.38 | |
| 17 | | | |
| 18 | 7.08 | 126.67 | |
| 19 | 7.64 | 123.93 | |
| 20 | 8.25 | 144.51 | |
| 21 | | | -124.5 |

## 8.7.2. NMR characterisation data for $[Ir(IMes)(H)_2(L_5)_3]Cl$ (17-fold excess to 5 mM of 1 in MeOD) at 245 K.

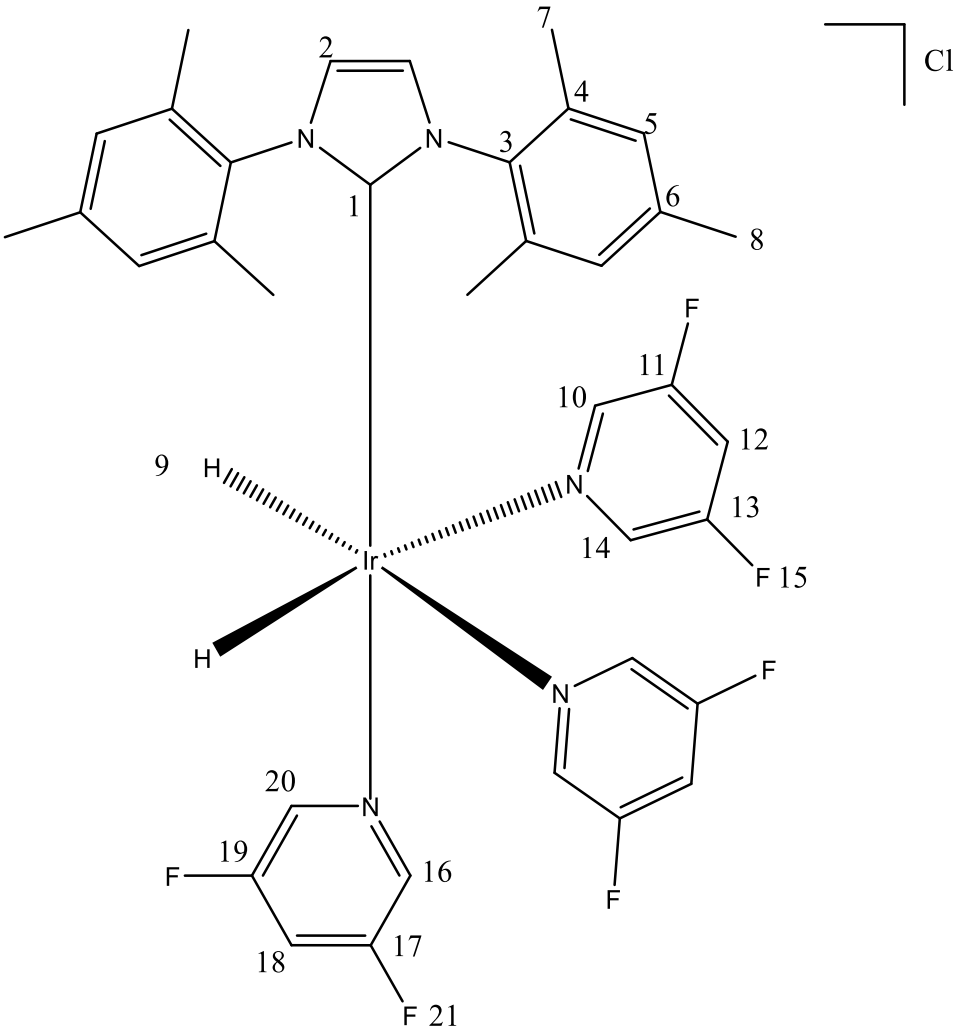


| Resonance number | $^{1}H$ (ppm) | $^{13}C$ (ppm) | $^{19}F$ (ppm) |
|---|---|---|---|
| 1 | | 148.3 | |
| 2 | 7.27 | 122.94 | |
| 3 | | 136.8 | |
| 4 | | 135.1 | |
| 5 | 6.78 | 128.4 | |
| 6 | | | |
| 7 | 2.09 | 17.59 | |

| | | | |
|---|---|---|---|
| 8 | 2.25 | 19.67 | |
| 9 | -23.22 | | |
| 10,14 | 8.19 | | |
| 11,13 | | 159.6 | |
| 12 | 7.88 | 112.72 | |
| 15 | | | -124.35 |
| 16,20 | 8.21 | 141.48 | |
| 17,19 | | | |
| 18 | 7.77 | 112.02 | |
| 21 | | | -124.77 |

NMR characterisation data for [Ir(IMes)$(H)_2$($\mathbf{L_5}$)$_2$(MeOD)]Cl (17-fold excess to 5 mM of 1 in MeOD) at 245 K.

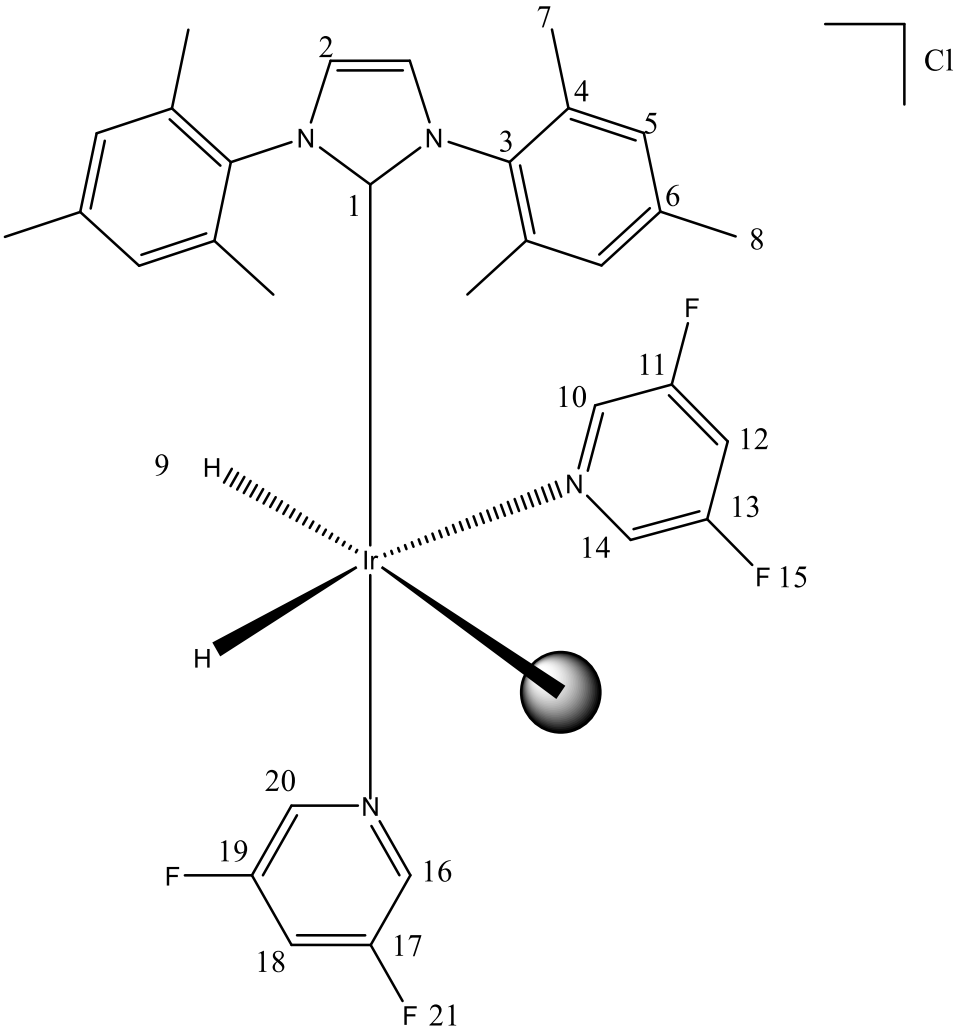


| Resonance number | $^{1}$H (ppm) | $^{13}$C (ppm) | $^{19}$F (ppm) |
|---|---|---|---|
| 1 | | 150.05 | |
| 2 | 7.06 | 121.92 | |
| 3 | | 138.33 | |
| 4 | | 135.5, 135.9 | |
| 5 | 6.86, 6.77 | 128.18, 128.25 | |
| 6 | | | |
| 7 | 2.25 | 17.84 | |

| | | | |
|---|---|---|---|
| 8 | 2.22, 2.20 | 17.68, 17.50 | |
| 9 | -23.94, d 8.3 Hz | | |
| 10,14 | 8.18 | 139.65 | |
| 11,13 | | 159.0, 159.3 | |
| 12 | 7.60 | 110.2 | |
| 15 | | | -124.16 |
| 16,20 | 8.66 | 140.53 | |
| 17,19 | | 159.0 | |
| 19 | 7.62 | 111.8 | |
| 21 | | | -124.9 |

## 8.8. ICP-OES methodology

### 8.8.1. Calibration series

A commercially available 1000 ppm iridium stock solution was diluted with deionised water to produce a 10 ppm standard which was then diluted further to produce a range of standards ranging from 10 ppb to 10 ppm, all standards were stabilised with 3% HCl.

### 8.8.2. Organic content testing

For monitoring the effect of organic species present in solution, an organic stock of 160 µL pyridine in 100 mL MeOH was produced to simulate the organic mixture present in a typical SABRE sample (4 eq pyridine relative to **4**). The iridium standard solutions were prepared a further three times In which the level of the organic stock was varied to give 1%, 0.4% and 0.2% organics.

All four sets of standards were tested making use of the iridium 224.268 nm line in both axial and radial view.

A further test varying the radio frequency utilised to induce the plasma made use of axial view with radio frequency values of 1050 W and 1150 W.

### 8.8.3. Iridium capture with solid supports

2.4 mL of $d_4$-methanol was added to a 7 mL sample vial (non-sterile) containing 45.3 mg of **4** and 0.25 mL pyridine. This was repeated without iridium added for method blanks (A, B and C) and with iridium for triplicate measurements (D, E and F). This gave two stock vials. Both vials were sonicated for ~1 min to ensure homogeneity.

0.8 mL stock blank and 0.8 mL iridium stock were added to new Young's tubes and degassed as in section 8.3.3.1 – though due to the high liquid quantities in the tubes each was degassed 4 times. This was repeated for the three blank (A-C) and three iridium (D-F) containing samples.

Hydrogen (3 bar) was added to the tube before 1.5 mins manual shaking commenced. Hydrogen was refilled 20 mins later and shaken for a further 1 min. Tubes were then left o/n.

Tubes were then shaken for a further 1 min each before being reduced to dryness under reduced pressure (an additional ~0.3 mL methanol was used to wash out Young's tubes and ensure complete sample transfer). The resulting residue was reconstituted with 8.5 mL deionised water and this bolus was divided into 8 centrifuge tubes (1 mL per tube). 10 mg of scavengers $\mathbf{S_1}$ – $\mathbf{S_1}$ was added to tubes 1 – 7 and no solid was added to tube 8. Subsequently this each tube was vortexed for 10 seconds at a speed setting of 1500 rpm.

This produced a series of samples A-F 1-8, as shown in Table 35.

Table 35. Tabular representation of the ICP-OES samples examined for the assessment of support iridium sequestering.

| | 1 | 2 | 3 | 4 | 5 | 6 | 7 | 8 |
|---|---|---|---|---|---|---|---|---|
| A | A1 | A2 | A3 | A4 | A5 | A6 | A7 | A8 |
| B | B1 | B2 | B3 | B4 | B5 | B6 | B7 | B8 |
| C | C1 | C2 | C3 | C4 | C5 | C6 | C7 | C8 |
| D | D1 | D2 | D3 | D4 | D5 | D6 | D7 | D8 |
| E | E1 | E2 | E3 | E4 | E5 | E6 | E7 | E8 |
| F | F1 | F2 | F3 | F4 | F5 | F6 | F7 | F8 |

The solutions were then centrifuged for 2 minutes at 4000 RPM. 0.1 mL of each filtered solution was diluted with 9.9 mL of 3% HCl in de-ionised water to give a total volume of 10 mL for each sample.

Following the removal of an aliquot, the tube was then vortexed again for 10 seconds as above and a wait time *t* was applied before centrifuging again and removal of another aliquot.

### 8.8.4. Calculation of iridium remaining from data extrapolation

Iridium remaining in the sample was calculated *via* extrapolation of data in 5.3.3 using the formula below:

$$y = me^{-nx}$$

$$\frac{Ln\left(\frac{y}{m}\right)}{-n} = x$$

Equation 5 Equation utilised for the extrapolation of scavenger quantity needed to remove enough iridium to match the value measured for deionised water *x*.

The average iridium concentration detected in n=5 deionised water blanks run before the experiments described in section 8.8.3 was 0.2126 ppb.

For all time points y = $1708.7e^{-nx}$ therefore the value of $Ln\left(\frac{y}{m}\right)$ does not change from -8.99194.

# References


1. I. I. Rabi, J. R. Zacharias, S. Millman and P. Kusch, *Phys. Rev.*, 1938, **53**, 318.
2. J. T. Arnold, S. S. Dharmatti and M. E. Packard, *J. Chem. Phys.*, 1951, **19**, 507.
3. E. M. Purcell, H. C. Torrey and R. V. Pound, *Phys. Rev.*, 1946, **69**, 37-38.
4. W. D. Knight, *Phys. Rev.*, 1949, **78**, 1259-1260.
5. T. B. R. Robertson and R. E. Mewis, in *Annual Reports on Nmr Spectroscopy, Vol 93*, ed. G. A. Webb, Elsevier Academic Press Inc, San Diego, Editon edn., 2018, vol. 93, pp. 145-212.
6. A. Abragam and W. G. Proctor, *Phys. Rev.*, 1958, **109**, 1441.
7. D. G. Gadian, K. S. Panesar, A. J. P. Linde, A. J. Horsewill, W. Köckenberger and J. R. Owers-Bradley, *PCCP*, 2012, **14**, 5397-5402.
8. A. W. Overhauser, *Phys. Rev.*, 1953, **92**, 411-415.
9. V. A. Atsarkin, *J. Phys. Conf. Ser.*, 2011, **324**, 012003.
10. K. V. Kovtunov, E. V. Pokochueva, O. G. Salnikov, S. F. Cousin, D. Kurzbach, B. Vuichoud, S. Jannin, E. Y. Chekmenev, B. M. Goodson, D. A. Barskiy and I. V. Koptyug, *Chem.: Asian J.*, 2018, **13**, 1857-1871.
11. E. M. M. Weber, G. Sicoli, H. Vezin, G. Frébourg, D. Abergel, G. Bodenhausen and D. Kurzbach, *Angew. Chem. Int. Ed.*, 2018, **57**, 5171-5175.
12. S. B. Duckett and C. J. Sleigh, *Prog. Nucl. Magn. Reson. Spectrosc.*, 1999, **34**, 71-92.
13. J. B. Hövenera, S. Bära, J. Leupolda, K. Jenneb, D. Leibfritza, J. Henniga, S. B. Duckett and D. V. Elverfeldt, *NMR Biomed.*, 2012, **26**, 124-131.
14. D. Blazina, S. B. Duckett, J. P. Dunne and C. Godard, *Dalton Trans.*, 2004, 2601-2609.
15. S. B. Duckett and N. J. Wood, *Coord. Chem. Rev.*, 2008, **252**, 2278-2291.
16. A. J. Parrott, P. Dallin, J. Andrews, P. M. Richardson, O. Semenova, M. E. Halse, S. B. Duckett and A. Nordon, *Appl. Spectrosc.*, 2018, **73**, 88-97.
17. S. Wagner, *Magn. Reson. Mater. Phys., Biol. Med.*, 2014, **27**, 195-199.
18. C. R. Bowers and D. P. Weitekamp, *Phys. Rev. Lett.*, 1986, **57**, 2645-2648.
19. C. R. Bowers and D. P. Weitekamp, *J. Am. Chem. Soc.*, 1987, **109**, 5541-5542.

20. V. V. Zhivonitko, I. V. Skovpin, M. Crespo-Quesada, L. Kiwi-Minsker and I. V. Koptyug, *J. Phys. Chem. C*, 2016, **120**, 4945-4953.

21. R. W. Adams, A. J. Aguilar, K. D. Atkinson, M. J. Cowley, P. I. P. Elliott, S. B. Duckett, G. G. R. Green, I. G. Khazal, J. López-Serrano and D. C. Williamson, *Science*, 2009, **323**, 1708-1711.

22. D. A. Barskiy, S. Knecht, A. V. Yurkovskaya and K. L. Ivanov, *Prog. Nucl. Magn. Reson. Spectrosc.*, 2019, **114-115**, 33-70.

23. M. J. Cowley, R. W. Adams, K. D. Atkinson, M. C. Cockett, S. B. Duckett, G. G. Green, J. A. Lohman, R. Kerssebaum, D. Kilgour and R. E. Mewis, *J. Am. Chem. Soc.*, 2011, **133**, 6134-6137.

24. K. D. Atkinson, M. J. Cowley, P. I. P. Elliott, S. B. Duckett, G. G. R. Green, J. López-Serrano and A. C. Whitwood, *J. Am. Chem. Soc.*, 2009, **131**, 13362-13368.

25. K. M. Appleby, R. E. Mewis, A. M. Olaru, G. G. R. Green, I. J. S. Fairlamb and S. B. Duckett, *Chem. Sci.*, 2015, **6**, 3981-3993.

26. M. J. Cowley, R. W. Adams, K. D. Atkinson, M. C. R. Cockett, S. B. Duckett, G. G. R. Green, J. A. B. Lohman, R. Kerssebaum, D. Kilgour and R. E. Mewis, *J. Am. Chem. Soc.*, 2011, **133**, 6134-6137.

27. K. D. Atkinson, M. J. Cowley, S. B. Duckett, P. I. P. Elliott, G. G. R. Green, J. López-Serrano, I. G. Khazal and A. C. Whitwood, *Inorg. Chem.*, 2009, **48**, 663-670.

28. L. S. Lloyd, A. Asghar, M. J. Burns, A. Charlton, S. Coombes, M. J. Cowley, G. J. Dear, S. B. Duckett, G. R. Genov, G. G. R. Green, L. A. R. Highton, A. J. J. Hooper, M. Khan, I. G. Khazal, R. J. Lewis, R. E. Mewis, A. D. Roberts and A. J. Ruddlesden, *Catal. Sci. Technol.*, 2014, **4**, 3544-3554.

29. D. A. Barskiy, R. V. Shchepin, A. M. Coffey, T. Theis, W. S. Warren, B. M. Goodson and E. Y. Chekmenev, *J. Am. Chem. Soc.*, 2016, **138**, 8080-8083.

30. R. E. Mewis, M. Fekete, G. G. R. Green, A. C. Whitwood and S. B. Duckett, *Chem. Commun.*, 2015, **51**, 9857-9859.

31. B. A. V. Weerdenburg, S. Glöggler, N. Eshuis, A. J. J. Engwerda, J. M. M. Smits, R. d. Gelder, S. Appelt, S. S. Wymenga, M. Tessari, M. C. Feiters, B. Blümich and F. P. J. T. Rutjes, *Chem. Commun.*, 2013, **49**, 7388-7390.

32. P. J. Rayner, P. Norcott, K. M. Appleby, W. Iali, R. O. John, S. J. Hart, A. C. Whitwood and S. B. Duckett, *Nat. Commun.*, 2018, **9**, 4251.

33. S. Hadjiali, R. Savka, M. Plaumann, U. Bommerich, S. Bothe, T. Gutmann, T. Ratajczyk, J. Bernarding, H.-H. Limbach, H. Plenio and G. Buntkowsky, *Appl. Magn. Reson.*, 2019, **50**, 895-902.

34. C. M. Wong, M. Fekete, R. Nelson-Forde, M. R. D. Gatus, P. J. Rayner, A. C. Whitwood, S. B. Duckett and B. A. Messerle, *Catal. Sci. Technol.*, 2018, **8**, 4925-4933.

35. M. Fekete, O. Bayfield, S. B. Duckett, S. Hart, R. E. Mewis, N. Pridmore, P. J. Rayner and A. Whitwood, *Inorg. Chem.*, 2013, **52**, 13453-13461.

36. F. Shi, A. M. Coffey, K. W. Waddell, E. Y. Chekmenev and B. M. Goodson, *J. Phys. Chem. C*, 2015, **119**, 7525-7533.

37. P. M. Richardson, R. O. John, A. J. Parrott, P. J. Rayner, W. Iali, A. Nordon, M. E. Halse and S. B. Duckett, *PCCP*, 2018, **20**, 26362-26371.

38. K. Tokmic and A. R. Fout, *J. Am. Chem. Soc.*, 2016, **138**, 13700−13705.

39. K. Tokmic, C. R. Markus, L. Zhu and A. R. Fout, *J. Am. Chem. Soc.*, 2016, **138**, 11907−11913.

40. V. V. Zhivonitko, I. V. Skovpin and I. V. Koptyug, *Chem. Commun.*, 2014, **51**, 2506-2509.

41. N. Eshuis, N. Hermkens, B. J. A. van Weerdenburg, M. C. Feiters, F. Rutjes, S. S. Wijmenga and M. Tessari, *J. Am. Chem. Soc.*, 2014, **136**, 2695-2698.

42. O. Semenova, P. M. Richardson, A. J. Parrott, A. Nordon, M. E. Halse and S. B. Duckett, *Anal. Chem.*, 2019, **91**, 6695-6701.

43. P. M. Richardson, A. J. Parrott, O. Semenova, A. Nordon, S. B. Duckett and M. E. Halse, *Analyst*, 2018, **143**, 3442-3450.

44. D. A. Robinson, M. P. Richardson and E. M. Halse, *Appl. Sci.*, 2019, **9**.

45. P. J. Rayner, M. J. Burns, A. M. Olaru, P. Norcott, M. Fekete, G. G. R. Green, L. A. R. Highton, R. E. Mewis and S. B. Duckett, *Proc. Natl. Acad. Sci. U.S.A.*, 2017, **114**, E3188-E3194.

46. S. Gloggler, R. Muller, J. Colell, M. Emondts, M. Dabrowski, B. Blumich and S. Appelt, *PCCP*, 2011, **13**, 13759-13764.

47. T. Ratajczyk, T. Gutmann, P. Bernatowicz, G. Buntkowsky, J. Frydel and B. Fedorczyk, *Chem.Eur. J.*, 2015, **21**, 12616-12619.

48. H. F. Zeng, J. D. Xu, J. Gillen, M. T. McMahon, D. Artemov, J. M. Tyburn, J. A. B. Lohman, R. E. Mewis, K. D. Atkinson, G. G. R. Green, S. B. Duckett and P. C. M. van Zijl, *J. Magn. Reson.*, 2013, **237**, 73-78.

49. T. Theis, M. L. Truong, A. M. Coffey, R. V. Shchepin, K. W. Waddell, F. Shi, B. M. Goodson, W. S. Warren and E. Y. Chekmenev, *J. Am. Chem. Soc.*, 2015, **137**, 1404-1407.

50. T. Theis, G. X. Ortiz, A. W. J. Logan, K. E. Claytor, Y. Feng, W. P. Huhn, V. Blum, S. J. Malcolmson, E. Y. Chekmenev, Q. Wang and W. S. Warren, *Sci. Adv.*, 2016, **2**, 7.

51. M. L. Truong, T. Theis, A. M. Coffey, R. V. Shchepin, K. W. Waddell, F. Shi, B. M. Goodson, W. S. Warren and E. Y. Chekmenev, *J. Phys. Chem. C*, 2015, **119**, 8786-8797.

52. J. F. P. Colell, M. Emondts, A. W. J. Logan, K. Shen, J. Bae, R. V. Shchepin, G. X. Ortiz, P. Spannring, Q. Wang, S. J. Malcolmson, E. Y. Chekmenev, M. C. Feiters, F. Rutjes, B. Blumich, T. Theis and W. S. Warren, *J. Am. Chem. Soc.*, 2017, **139**, 7761-7767.

53. J. F. P. Colell, A. W. J. Logan, Z. Zhou, R. V. Shchepin, D. A. Barskiy, G. X. Ortiz, Q. Wang, S. J. Malcolmson, E. Y. Chekmenev, W. S. Warren and T. Theis, *J. Phys. Chem. C.*, 2017, **121**, 6626-6634.

54. R. V. Shchepin, D. A. Barskiy, A. M. Coffey, T. Theis, F. Shi, W. S. Warren, B. M. Goodson and E. Y. Chekmenev, *ACS Sensors*, 2016, **1**, 640-644.

55. R. V. Shchepin, L. Jaigirdar and E. Y. Chekmenev, *J. Phys. Chem. C*, 2018, **122**, 4984-4996.

56. Z. Zhou, J. Yu, J. F. P. Colell, R. Laasner, A. Logan, D. A. Barskiy, R. V. Shchepin, E. Y. Chekmenev, V. Blum, W. S. Warren and T. Theis, *J. Phys. Chem. Lett.*, 2017, **8**, 3008-3014.

57. T. Glachet, H. Marzag, N. Saraiva Rosa, J. F. P. Colell, G. Zhang, W. S. Warren, X. Franck, T. Theis and V. Reboul, *J. Am. Chem. Soc.*, 2019, **141**, 13689-13696.

58. T. Theis, N. M. Ariyasingha, R. V. Shchepin, J. R. Lindale, W. S. Warren and E. Y. Chekmenev, *J. Phys. Chem. Lett.*, 2018, **9**, 6136-6142.

59. D. A. Barskiy, R. V. Shchepin, C. P. N. Tanner, J. F. P. Colell, B. M. Goodson, T. Theis, W. S. Warren and E. Y. Chekmenev, *ChemPhysChem*, 2017, **18**, 1493-1498.

60. R. E. Mewis, K. D. Atkinson, M. J. Cowley, S. B. Duckett, G. G. R. Green, R. A. Green, L. A. R. Highton, D. Kilgour, L. S. Lloyd, J. A. B. Lohman and D. C. Williamson, *Magn. Reson. Chem.*, 2014, **52**, 358-369.

61. S. S. Roy, P. Norcott, P. J. Rayner, G. G. R. Green and S. B. Duckett, *Chemistry*, 2017, **23**, 10496-10500.

62. V. V. Zhivonitko, I. V. Skovpin and I. V. Koptyug, *Chem. Commun.*, 2015, **51**, 2506-2509.

63. M. J. Burns, P. J. Rayner, G. G. R. Green, L. A. R. Highton, R. E. Mewis and S. B. Duckett, *J. Phys. Chem. B*, 2015, **119**, 5020-5027.

64. A. M. Olaru, A. Burt, P. J. Rayner, S. J. Hart, A. C. Whitwood, G. G. R. Green and S. B. Duckett, *Chem. Commun.*, 2016, **52**, 14482-14485.

65. D. I. Hoult and R. E. Richards, *J. Magn. Reson.*, 1976, **24**, 71-85.

66. B. P. Barnett, J. Ruiz-Cabello, P. Hota, R. Ouwerkerk, M. J. Shamblott, C. Lauzon, P. Walczak, W. D. Gilson, V. P. Chacko, D. L. Kraitchman, A. Arepally and J. W. M. Bulte, *Contrast Media Mol. Imaging*, 2011, **6**, 251-259.

67. P. Rovedo, S. Knecht, T. Baumlisberger, A. L. Cremer, S. B. Duckett, R. E. Mewis, G. G. R. Green, M. Burns, P. J. Rayner, D. Leibfritz, J. G. Korvink, J. Hennig, G. Putz, D. von Elverfeldt and J. B. Hovener, *J. Phys. Chem. B*, 2016, **120**, 5670-5677.

68. R. V. Shchepin, B. M. Goodson, T. Theis, W. S. Warren and E. Y. Chekmenev, *Chemphyschem*, 2017, **18**, 1961-1965.

69. Y. Zhou, J. Wang, Z. N. Gu, S. N. Wang, W. Zhu, J. L. Acena, V. A. Soloshonok, K. Izawa and H. Liu, *Chem. Rev.*, 2016, **116**, 422-518.

70. V. Daniele, F. X. Legrand, P. Berthault, J. N. Dumez and G. Huber, *Chemphyschem*, 2015, **16**, 3413-3417.

71. A. Manoharan, P. J. Rayner, W. Iali, M. J. Burns, V. H. Perry and S. B. Duckett, *Chemmedchem*, 2018, **13**, 352-359.

72. D. A. Barskiy, L. A. Ke, X. Li, V. Stevenson, N. Widarman, H. Zhang, A. Truxal and A. Pines, *J. Phys. Chem. Lett.*, 2018, 2721-2724.

73. B. E. Kidd, J. L. Gesiorski, M. E. Gemeinhardt, R. V. Shchepin, K. V. Kovtunov, I. V. Koptyug, E. Y. Chekmenev and B. M. Goodson, *J. Phys. Chem. C.*, 2018, **122**, 16848-16852.

74. S. Lehmkuhl, M. Wiese, L. Schubert, M. Held, M. Küppers, M. Wessling and B. Blümich, *J. Magn. Reson.*, 2018, **291**, 8-13.

75. P. Štěpánek, C. Sanchez-Perez, V.-V. Telkki, V. V. Zhivonitko and A. M. Kantola, *J. Magn. Reson.*, 2019, **300**, 8-17.

76. P. M. Richardson, S. Jackson, A. J. Parrott, A. Nordon, S. B. Duckett and M. E. Halse, *Magn. Reson. Chem.*, 2018, **56**, 641-650.

77. O. G. Salnikov, R. V. Shchepin, N. V. Chukanov, L. Jaigirdar, W. Pham, K. V. Kovtunov, I. V. Koptyug and E. Y. Chekmenev, *J. Phys. Chem. C.*, 2018, **122**, 24740-24749.

78. A. Manoharan, P. J. Rayner, M. Fekete, W. Iali, P. Norcott, V. Hugh Perry and S. B. Duckett, *ChemPhysChem*, 2019, **20**, 285-294.

79. H. F. Zeng, J. D. Xu, M. T. McMahon, J. A. B. Lohman and P. C. M. van Zijl, *J. Magn. Reson.*, 2014, **246**, 119-121.

80. M. L. Truong, F. Shi, P. He, B. X. Yuan, K. N. Plunkett, A. M. Coffey, R. V. Shchepin, D. A. Barskiy, K. V. Kovtunov, I. V. Koptyug, K. W. Waddell, B. M. Goodson and E. Y. Chekmenev, *J. Phys. Chem. B*, 2014, **118**, 13882-13889.

81. M. Fekete, C. Gibard, G. J. Dear, G. G. R. Green, A. J. J. Hooper, A. D. Roberts, F. Cisnetti and S. B. Duckett, *Dalton Trans.*, 2015, **44**, 7870-7880.

82. P. Spannring, I. Reile, M. Emondts, P. P. M. Schleker, N. K. J. Hermkens, N. G. J. van der Zwaluw, B. J. A. van Weerdenburg, P. Tinnemans, M. Tessari, B. Blumich, F. Rutjes and M. C. Feiters, *Chem.Eur. J.*, 2016, **22**, 9277-9282.

83. F. Shi, P. He, Q. A. Best, K. Groome, M. L. Truong, A. M. Coffey, G. Zimay, R. V. Shchepin, K. W. Waddell, E. Y. Chekmenev and B. M. Goodson, *J. Phys. Chem. C*, 2016, **120**, 12149-12156.

84. W. Iali, P. J. Rayner and S. B. Duckett, *Sci. Adv.*, 2018, **4**.

85. S. S. Roy, K. M. Appleby, E. J. Fear and S. B. Duckett, *J. Phys. Chem. Lett.*, 2018, **9**, 1112-1117.

86. P. J. Rayner and S. B. Duckett, *Angew. Chem. Int. Ed.*, 2018, **57**, 6742-6753.

87. B. E. Kidd, J. A. Mashni, M. N. Limbach, F. Shi, E. Y. Chekmenev, Y. Hou and B. M. Goodson, *Chemistry*, 2018, **24**, 10641-10645.

88. P. J. Rayner, B. J. Tickner, W. Iali, M. Fekete, A. D. Robinson and S. B. Duckett, *Chem. Sci.*, 2019.

89. W. Iali, A. M. Olaru, G. G. R. Green and S. B. Duckett, *Chemistry*, 2017, **23**, 10491-10495.

90. F. Reineri, T. Boi and S. Aime, *Nat. Commun.*, 2015, **6**, 5858.

91. E. Cavallari, C. Carrera, S. Aime and F. Reineri, *Chem. Eur. J.*, 2017, **23**, 1200-1204.

92. F. Reineri, A. Viale, G. Giovenzana, D. Santelia, W. Dastrù, R. Gobetto and S. Aime, *J. Am. Chem. Soc.*, 2008, **130**, 15047-15053.

93. F. Shi, A. M. Coffey, K. W. Waddell, E. Y. Chekmenev and B. M. Goodson, *Angew. Chem.-Int. Edit.*, 2014, **53**, 7495-7498.

94. K. V. Kovtunov, L. M. Kovtunova, M. E. Gemeinhardt, A. V. Bukhtiyarov, J. Gesiorski, V. I. Bukhtiyarov, E. Y. Chekmenev, I. V. Koptyug and B. M. Goodson, *Angew. Chem. Int. Ed.*, 2017, **56**, 10433-10437.

95. P. Norcott, P. J. Rayner, G. G. R. Green and S. B. Duckett, *Chem. Eur. J.*, 2017, **23**, 16990-16997.

96. A. M. Olaru, T. B. R. Robertson, J. S. Lewis, A. Antony, W. Iali, R. E. Mewis and S. B. Duckett, *ChemistryOpen*, 2018, **7**, 97-105.

97. J. B. Hovener, N. Schwaderlapp, T. Lickert, S. B. Duckett, R. E. Mewis, L. A. R. Highton, S. M. Kenny, G. G. R. Green, D. Leibfritz, J. G. Korvink, J. Hennig and D. von Elverfeldt, *Nat. Commun.*, 2013, **4**.

98. R. W. Adams, J. A. Aguilar, K. D. Atkinson, M. J. Cowley, P. I. P. Elliott, S. B. Duckett, G. G. R. Green, I. G. Khazal, J. Lopez-Serrano and D. C. Williamson, *Science*, 2009, **323**, 1708-1711.

99. K. D. Atkinson, M. J. Cowley, S. B. Duckett, P. I. P. Elliott, G. G. R. Green, J. Lopez-Serrano, I. G. Khazal and A. C. Whitwood, *Inorg. Chem.*, 2009, **48**, 663-670.

100. K. Tokmic and A. R. Fout, *J. Am. Chem. Soc.*, 2016, **138**, 13700-13705.

101. K. Tokmic, R. B. Greer, L. Zhu and A. R. Fout, *J. Am. Chem. Soc.*, 2018, **140**, 14844-14850.

102. M. M. Sebeika and D. J. Fox, *J. Chem. Educ.*, 2013, **90**, 1239-1243.

103. S. B. Duckett, C. L. Newell and R. Eisenberg, *J. Am. Chem. Soc.*, 1994, **116**, 10548-10556.

104. C. Fischer, C. Kohrt, H. J. Drexler, W. Baumann and D. Heller, *Dalton Trans*, 2011, **40**, 4162-4166.

105. I. D. Gridnev and T. Imamoto, *Chem. Commun.*, 2009, 7447-7464.

106. T. Imamoto, K. Yashio, K. V. L. Crépy, K. Katagiri, H. Takahashi, M. Kouchi and I. D. Gridnev, *Organometallics*, 2006, **25**, 908-914.

107. I. D. Gridnev, Y. Yamanoi, N. Higashi, H. Tsuruta, M. Yasutake and T. Imamoto, *Adv. Synth. Catal.*, 2001, **343**, 118-136.

108. E. M. Kozinets, M. Fekete, O. A. Filippov, N. V. Belkova, E. S. Shubina, R. Poli, S. B. Duckett and E. Manoury, *Dalton Trans.*, 2013, **42**, 11720-11730.

109. G. Papp, H. Horváth and F. Joó, *ChemCatChem*, 2019, **11**, 3000-3003.

110. S. Douglas, J. P. Lowe, M. F. Mahon, J. E. Warren and M. K. Whittlesey, *J. Organomet. Chem.*, 2005, **690**, 5027-5035.

111. K. Li and D. Xue, *J. Phys. Chem. A*, 2006, **110**, 11332-11337.

112. A. K. Maity, M. Bhattacharjee and S. Roy, *J. Organomet. Chem.*, 2014, **768**, 42-49.

113. B. J. A. van Weerdenburg, S. Gloggler, N. Eshuis, A. H. J. Engwerda, J. M. M. Smits, R. de Gelder, S. Appelt, S. S. Wymenga, M. Tessari, M. C. Feiters, B. Blumich and F. Rutjes, *Chem. Commun.*, 2013, **49**, 7388-7390.

114. I. V. Koptyug, K. V. Kovtunov, S. R. Burt, M. S. Anwar, C. Hilty, S. I. Han, A. Pines and R. Z. Sagdeev, *J. Am. Chem. Soc.*, 2007, **129**, 5580-5586.

115. J. Ruiz-Cabello, B. P. Barnett, P. A. Bottomley and J. W. M. Bulte, *NMR Biomed.*, 2011, **24**, 114-129.

116. S. Mizukami, R. Takikawa, F. Sugihara, Y. Hori, H. Tochio, M. Wälchli, M. Shirakawa and K. Kikuchi, *J. Am. Chem. Soc.*, 2008, **130**, 794-795.

117. M. S. Fox, J. M. Gaudet and P. J. Foster, *Magn. Reson. Insights*, 2016, **8**, 53-67.

118. S. Waiczies, J. T. Rosenberg, A. Kuehne, L. Starke, P. R. Delgado, J. M. Millward, C. Prinz, J. dos Santos Periquito, A. Pohlmann, H. Waiczies and T. Niendorf, *Magn. Reson. Mater. Phys., Biol. Med.*, 2018.

119. A. V. Makela and P. J. Foster, *Magn. Reson. Mater. Phys., Biol. Med.*, 2018.

120. K. Akazawa, F. Sugihara, T. Nakamura, H. Matsushita, H. Mukai, R. Akimoto, M. Minoshima, S. Mizukami and K. Kikuchi, *Angew. Chem. Int. Ed.*, **0**.

121. F. Chapelin, C. M. Capitini and E. T. Ahrens, *J. Immunother. Cancer.*, 2018, **6**, 105-105.

122. X. Liu, Z.-X. Jiang, B. Y. Yu and E.-K. Jeong, *Magn. Reson. Mater. Phys., Biol. Med.*, 2018.

123. M. Plaumann, U. Bommerich, T. Trantzschel, D. Lego, S. Dillenberger, G. Sauer, J. Bargon, G. Buntkowsky and J. Bernarding, *Chem.Eur. J.*, 2013, **19**, 6334-6339.

124. Y. Zhou, J. Wang, Z. Gu, S. Wang, W. Zhu, J. L. Aceña, V. A. Soloshonok, K. Izawa and H. Liu, *Chem. Rev.*, 2016, **116**, 422-518.

125. N. Eshuis, B. J. A. van Weerdenburg, M. C. Feiters, F. Rutjes, S. S. Wijmenga and M. Tessari, *Angew. Chem.-Int. Edit.*, 2015, **54**, 1481-1484.

126. R. V. Shchepin, M. L. Truong, T. Theis, A. M. Coffey, F. Shi, K. W. Waddell, W. S. Warren, B. M. Goodson and E. Y. Chekmenev, *J. Phys. Chem. Lett.*, 2015, **6**, 1961-1967.

127. F. F. Diaz-Rullo, F. Zamberlan, R. E. Mewis, M. Fekete, L. Broche, L. A. Cheyne, S. Dall'Angelo, S. B. Duckett, D. Dawson and M. Zanda, *Biorg. Med. Chem.*, 2017, **25**, 2730-2742.

128. A. M. Olaru, M. J. Burns, G. G. R. Green and S. B. Duckett, *Chem. Sci.*, 2017, **8**, 2257-2266.

129. K. Buckenmaier, M. Rudolph, C. Back, T. Misztal, U. Bommerich, P. Fehling, D. Koelle, R. Kleiner, H. A. Mayer, K. Scheffler, J. Bernarding and M. Plaumann, *Sci Rep*, 2017, **7**, 9.

130. A. N. Pravdivtsev, A. V. Yurkovskaya, H. Zimmermann, H. M. Vieth and K. L. Ivanov, *RSC Adv.*, 2015, **5**, 63615-63623.

131. N. A. Meanwell, K. J. Eastman and E. P. Gillis, *Tactical Applications of Fluorine in Drug Design and Development*, Springer, 2014.

132. R. Linnell, *J. Org. Chem.*, 1960, **25**, 290-290.

133. *Dissociation Constants of Organic Acids and Bases*, https://labs.chem.ucsb.edu/zhang/liming/pdf/pKas_of_Organic_Acids_and_Bases.pdf, Accessed January, 2019.

134. *Dissociation constants of organic acids and bases*, http://sites.chem.colostate.edu/diverdi/all_courses/CRC%20reference%20data/dissociation%20constants%20of%20organic%20acids%20and%20bases.pdf, Accessed September 2017.

135. *Pentachloropyridine*, https://pubchem.ncbi.nlm.nih.gov/compound/pentachloropyridine#section=Dissociation-Constants, Accessed September, 2017.

136. H. Y. Yu, R. Kuhne, R. U. Ebert and G. Schuurmann, *J. Chem Inf. Model.*, 2010, **50**, 1949-1960.

137. J. Iskra, *Halogenated Heterocycles: Synthesis, Application and Environment*, Springer Berlin Heidelberg, 2012.

138. *Van der Waal's radii*, http://ursula.chem.yale.edu/~chem220/chem220js/STUDYAIDS/vanderwaalsradius.html, Accessed July, 2018.

139. S. S. Batsanov, *Inorg. Mater.*, 2001, **37**, 871-885.

140. R. Nelson-Forde, University of York, 2017.

141. K. X. Moreno, K. Nasr, M. Milne, A. D. Sherry and W. J. Goux, *J. Magn. Reson.*, 2015, **257**, 15-23.

142. D. A. Barskiy, K. V. Kovtunov, I. V. Koptyug, P. He, K. A. Groome, Q. A. Best, F. Shi, B. M. Goodson, R. V. Shchepin, M. L. Truong, A. M.

Coffey, K. W. Waddell and E. Y. Chekmenev, *Chemphyschem*, 2014, **15**, 4100-4107.

143. H. Allouche-Arnon, M. H. Lerche, M. Karlsson, R. E. Lenkinski and R. Katz-Brull, *Contrast Media Mol. Imaging*, 2011, **6**, 499-506.

144. J. B. Hovener, N. Schwaderlapp, R. Borowiak, T. Lickert, S. B. Duckett, R. E. Mewis, R. W. Adams, M. J. Burns, L. A. R. Highton, G. G. R. Green, A. Olaru, J. Hennig and D. von Elverfeldtt, *Anal. Chem.*, 2014, **86**, 1767-1774.

145. M. Fekete, P. J. Rayner, G. G. R. Green and S. B. Duckett, *Magn. Reson. Chem.*, 2017, **55**, 944-957.

146. D. A. Barskiy, K. V. Kovtunov, I. V. Koptyug, P. He, K. A. Groome, Q. A. Best, F. Shi, B. M. Goodson, R. V. Shchepin, A. M. Coffey, K. W. Waddell and E. Y. Chekmenev, *J. Am. Chem. Soc.*, 2014, **136**, 3322-3325.

147. J. G. Linakis and C. L. Cunningham, *J. Psychopharmacol.*, 1979, **64**, 61-65.

148. K. H. Allen-Worthington, A. K. Brice, J. O. Marx and F. C. Hankenson, *J Am Assoc Lab Anim Sci*, 2015, **54**, 769-778.

149. R. Lord, *Aust Vet J*, 1989, **66**, 268.

150. B. Close, K. Banister, V. Baumans, E. M. Bernoth, N. Bromage, J. Bunyan, W. Erhardt, P. Flecknell, N. Gregory, H. Hackbarth, D. Morton and W. C., *Lab. Anim.*, 1996, **30**, 293-316.

151. K. S. Egorova and V. P. Ananikov, *Organometallics*, 2017, **36**, 4071-4090.

152. I. Iavicoli, V. Cufino, M. Corbi, M. Goracci, E. Caredda, A. Cittadini, A. Bergamaschi and A. Sgambato, *Toxicol In Vitro*, 2012, **26**, 963-969.

153. A. Bergman, U. Svedberg and E. Nilsson, *Contact. Derm.*, 1995, **32**, 14-17.

154. N. Kumar, P. Attri, D. K. Yadav, J. Choi, E. H. Choi and H. S. Uhm, *Sci Rep*, 2014, **4**, 7589.

155. J. Hartmann, Y. Bader, Z. Horvath, P. Saiko, M. Grusch, C. Illmer, S. Madlener, M. Fritzer-Szekeres, N. Heller, R. G. Alken and T. Szekeres, *Anticancer Res.*, 2005, **25**, 3407-3411.

156. S. S. Roy, P. Norcott, P. J. Rayner, G. G. R. Green and S. B. Duckett, *Angew. Chem.-Int. Edit.*, 2016, **55**, 15642-15645.

157. I. V. Linnik, P. J. Rayner, R. A. Stow, S. B. Duckett and G. M. T. Cheetham, *Eur J Pharm Sci*, 2019, **135**, 32-37.

158. R. V. Shchepin, J. R. Birchall, N. V. Chukanov, K. V. Kovtunov, I. V. Koptyug, T. Theis, W. S. Warren, J. G. Gelovani, B. M. Goodson, S. Shokouhi, M. S. Rosen, Y.-F. Yen, W. Pham and E. Y. Chekmenev, *Chem. Eur. J.*, 2019, **25**, 8829-8836.

159. P. Norcott, M. J. Burns, P. J. Rayner, R. E. Mewis and S. B. Duckett, *Magn. Reson. Chem.*, 2018, **56**, 663-671.

160. F. Reineri, A. Viale, S. Ellena, T. Boi, V. Daniele, R. Gobetto and S. Aime, *Angew. Chem. Int. Ed. Engl.*, 2011, **50**, 7350-7353.

161. F. G. Bordwell, *Acc. Chem. Res.*, 1988, **21**, 456-463.

162. D. D. Perrin, *J. Chem. Educ.*, 1983, **60**, A151.

163. R. V. Shchepin, D. A. Barskiy, A. M. Coffey, B. M. Goodson and E. Y. Chekmenev, *ChemistrySelect*, 2016, **1**, 2552-2555.

164. *Iridium ICP Data*, https://www.inorganicventures.com/element/iridium, Accessed April, 2019.

165. A. N. Pravdivtsev, *Z. Phys. Chem.*, 2017, **231**, 497.

166. R. E. Mewis, R. A. Green, M. C. R. Cockett, M. J. Cowley, S. B. Duckett, G. G. R. Green, R. O. John, P. J. Rayner and D. C. Williamson, *J. Phys. Chem. B*, 2015, **119**, 1416-1424.

167. W. Iali, S. S. Roy, B. J. Tickner, F. Ahwal, A. J. Kennerley and S. B. Duckett, *Angew. Chem. Int. Ed.*, 2019, **58**, 10271-10275.

168. S. S. Roy, P. J. Rayner, P. Norcott, G. G. R. Green and S. B. Duckett, *PCCP*, 2016, **18**, 24905-24911.

169. L. D. Saravolatz, L. B. Johnson and C. A. Kauffman, *Clin. Infect. Dis.*, 2003, **36**, 630-637.

170. S. C. Ngo, O. Zimhony, W. J. Chung, H. Sayahi, W. R. Jacobs and J. T. Welch, *Antimicrob. Agents Chemother.*, 2007, **51**, 2430.

171. M. H. Cynamon, R. Gimi, F. Gyenes, C. A. Sharpe, K. E. Bergmann, H. J. Han, L. B. Gregor, R. Rapolu, G. Luciano and J. T. Welch, *J. Med. Chem.*, 1995, **38**, 3902-3907.

172. K. E. Bergmann, M. H. Cynamon and J. T. Welch, *J. Med. Chem.*, 1996, **39**, 3394-3400.

173. P. Upcroft and J. A. Upcroft, *Clin Microbiol Rev*, 2001, **14**, 150-164.

174. J. P. Donnelly and B. E. De Pauw, *Clin. Microbiol. Infect.*, 2004, **10**, 107-117.

175. M. E. Henry, N. R. Bolo, C. S. Zuo, R. A. Villafuerte, K. Cayetano, P. Glue, B. D. Damle, E. Andrews, T. L. Lauriat, N. S. Rana, J. H. Churchill and P. F. Renshaw, *Antimicrob. Agents Chemother.*, 2013, **57**, 5271-5276.

176. T. M. Barbosa, G. A. Morris, M. Nilsson, R. Rittner and C. F. Tormena, *RSC Adv.*, 2017, **7**, 34000-34004.

177. *The Selection and Use of Essential Medicines*, World Health Organisation, 2017.

178. V. Spahn, G. Del Vecchio, D. Labuz, A. Rodriguez-Gaztelumendi, N. Massaly, J. Temp, V. Durmaz, P. Sabri, M. Reidelbach, H. Machelska, M. Weber and C. Stein, *Science*, 2017, **355**, 966.

179. C. A. Valdez, R. N. Leif and B. P. Mayer, *PLOS ONE*, 2014, **9**, e108250.

180. *Fentanyl drug profile*, http://www.emcdda.europa.eu/publications/drug-profiles/fentanyl#pharmacology, Accessed September, 2017.

181. J. Mounteney, I. Giraudon, G. Denissov and P. Griffiths, *Int. J. Drug Policy*, 2015, **26**, 626-631.

182. P. Bijral, K. P. Hayhurst, S. M. Bird and T. Millar, *Clinical Toxicology*, 2019, **57**, 368-371.

183. *Deaths involving fentanyl with and without heroin/morphine, Regions in England and Wales, 1999 to 2016*, https://www.ons.gov.uk/peoplepopulationandcommunity/birthsdeathsandmarriages/deaths/adhocs/007411deathsinvolvingfentanylwithandwithoutheroinmorphineregionsinenglandandwales1999to2016, Accessed July, 2019.

184. *Deaths involving fentanyl with and without heroin or morphine, regions in England and Wales, 2017*, https://www.ons.gov.uk/peoplepopulationandcommunity/healthandsocialcare/drugusealcoholandsmoking/adhocs/010215deathsinvolvingfentanylwithandwithoutheroinormorphineregionsinenglandandwales2017, Accessed July, 2019.

185. P. Seth, L. Scholl, R. A. Rudd and S. Bacon, *MMWR Morb Mortal Wkly Rep*, 2018, **67**, 349-358.

186. L. Hikin, P. R. Smith, E. Ringland, S. Hudson and S. R. Morley, *Forensic Sci. Int.*, 2018, **282**, 179-183.

187. R. S. Vardanyan and V. J. Hruby, *Future Med Chem*, 2014, **6**, 385-412.

188. *Carfentanil: Report on the risk assessment of methyl 1-(2-phenylethyl)-4-[phenyl(propanoyl) amino]piperidine-4-carboxylate in the framework of the Council Decision on new psychoactive substances*, European Monitoring Centre for Drugs and Drug Addiciton.

189. *European Drug Report: Trends and Developments*, European Monitoring Centre for Drugs and Drug Addiction, 2017.

190. J. K. O'Donnell, J. Halpin, C. L. Mattson, B. A. Goldberger and R. M. Gladden, *MMWR Morb Mortal Wkly Rep*, 2017, **66**, 1197-1202.

191. A. N. Pravdivtsev, A. V. Yurkovskaya, H. M. Vieth, K. L. Ivanov and R. Kaptein, *Chemphyschem*, 2013, **14**, 3327-3331.

192. K. L. Ivanov, A. N. Pravdivtsev, A. V. Yurkovskaya, H.-M. Vieth and R. Kaptein, *Prog. Nucl. Magn. Reson. Spectrosc.*, 2014, **81**, 1-36.

193. A. N. Pravdivtsev, A. V. Yurkovskaya, N. N. Lukzen, K. L. Ivanov and H.-M. Vieth, *J. Phys. Chem. Lett.*, 2014, **5**, 3421-3426.

194. N. Eshuis, R. Aspers, B. J. A. van Weerdenburg, M. C. Feiters, F. Rutjes, S. S. Wijmenga and M. Tessari, *Angew. Chem.-Int. Edit.*, 2015, **54**, 14527-14530.

195. C. P. France, G. Winger, F. Medzihradsky, M. R. Seggel, K. C. Rice and J. H. Woods, *J. Pharmacol. Exp. Ther.*, 1991, **258**, 502.

196. A. L. A. Mohr, M. Friscia, D. Papsun, S. L. Kacinko, D. Buzby and B. K. Logan, *J. Anal. Toxicol.*, 2016, **40**, 709-717.

197. L. S. Lloyd, R. W. Adams, M. Bernstein, S. Coombes, S. B. Duckett, G. G. R. Green, R. J. Lewis, R. E. Mewis and C. J. Sleigh, *J. Am. Chem. Soc.*, 2012, **134**, 12904-12907.

198. D. Gimenez, C. A. Mooney, A. Dose, G. Sandford, C. R. Coxon and S. L. Cobb, *Org. Biomol. Chem.*, 2017, **15**, 4086-4095.

199. M. L. Nolan, S. Shamasunder, C. Colon-Berezin, H. V. Kunins and D. Paone, *J. Urban Health*, 2019, **96**, 49-54.

200. L. H. Antonides, R. M. Brignall, A. Costello, J. Ellison, S. E. Firth, N. Gilbert, B. J. Groom, S. J. Hudson, M. C. Hulme, J. Marron, Z. A. Pullen, T. B. R. Robertson, C. J. Schofield, D. C. Williamson, E. K. Kemsley, O. B. Sutcliffe and R. E. Mewis, *ACS Omega*, 2019, **4**, 7103-7112.